escaled

PROTON-CONDUCTING MEMBRANES FOR THE ARTIFICIAL LEAF

Thesis submitted by

Karell Naomi BOSSON

In partial fulfilment of the requirements for the degree of *Dr. rer. nat.* from the University of Stuttgart

Dissertation approved by the Faculty 4: Energy-, Process- and Bio-Engineering of the University of Stuttgart – Published in 2023

Under the supervision of
Prof. Laurent BILLON, Dr. Vladimir ATANASOV, and Prof. Günter E. M. TOVAR
Defended in Pau, on September 13th 2022

Jury composition:

Dr. Didier GIGMES	Institut de chimie radicalaire – University of Aix Marseille
Dr. David MECERREYES	Polymat – University of the Basque Country UPV/EHU
Prof. Dr.-Ing. Ulrich NIEKEN	ICVT – University of Stuttgart
Dr. Antoine BOUSQUET	IPREM – University of Pau and Adour countries
Dr. Stéphanie REYNAUD	IPREM – University of Pau and Adour countries
Dr. Vladimir ATANASOV	ICVT – University of Stuttgart
Prof. Dr. Günter TOVAR	IGVP – University of Stuttgart
Prof. Dr. Laurent BILLON	IPREM – University of Pau and Pays de l'Adour

University of Stuttgart: Institute for Interfacial Process Engineering & Plasma Technology (IGVP) and Institute of Chemical Process Engineering (ICVT)

University of Pau and Pays de l'Adour: Institute of Analytical Sciences and Physico-Chemistry for Environment and Materials (IPREM)

Abstract

With the aim of producing proton conducting membranes with improved proton conductivity and mechanical properties, the poly(pentafluorostyrene)-*b*-(butyl acrylate) (PPFS-*b*-PBuA) system was investigated. The study mainly focuses on the influence of the forming polymer nanostructures on the conductivity properties of the membranes.

A series of well-defined PPFS-*b*-PBuA block copolymers (BCPs) were synthesized via nitroxide-mediated controlled radical polymerization (NMP). Spontaneous self-assembly of the BCP element was induced via a targeted change in polymer composition. Moreover, by adjusting the molar composition via enrichment of one of the blocks after synthesis, controlled self-assembly of the BCPs was realized. This was done by combining the corresponding homopolymer with the block copolymer to form a polymer blend - one of the blocks mixed to the BCP. Forming such polymer blends expanded the range of available techniques for tailoring the morphology for desired applications.

Sulfonation of BCPs for the preparation of proton-conducting membranes was carried out by a para-fluoro thiol "click" reaction using sodium 3-mercapto-1-propanesulfonate (SMPS). The accessibility of fluorine in the *para* position of the phenylene group of PPFS provides countless opportunities for polymer functionalization by nucleophilic substitution. After modification of BCP, the self-assembly ability was retained, and higher conductivities were obtained compared to random copolymers.

In addition, complementary studies were conducted on the use of printing techniques for membrane upscaling and evaluation of their life cycle.

Résumé

Dans le but de produire des membranes conductrices de protons présentant des propriétés mécaniques et de conduction améliorées, le système poly(pentafluorostyrène)-*b*-(butyle acrylate) (PPFS-*b*-PBuA) a été étudié. L'étude se concentre principalement sur l'influence de la nano-structuration du copolymère sur les propriétés de conduction de la membrane.

Une série de copolymères diblock PPFS-*b*-PBuA bien définis a été synthétisée par polymérisation radicalaire contrôlée par les nitroxides (NMP). L'auto-assemblage spontané de ce copolymère di-bloc a été induit par un changement ciblé de la composition du polymère. De plus, en ajustant la composition molaire par l'enrichissement d'un des blocs après la synthèse, l'auto-assemblage contrôlé des BPCs a été réalisé. Cela s'est fait en combinant l'homopolymère correspondant au copolymère d'origine pour former un mélange de polymères – mélange d'un des blocs au BCP. La formation de tels mélanges de polymères a élargi la gamme des techniques disponibles pour adapter la morphologie aux applications souhaitées.

La sulfonation des BCPs pour la préparation des membranes conductrices de protons a été réalisée par une réaction « click » para-fluoro thiol en utilisant le 3-mercapto-1-propanesulfonate de sodium (SMPS). L'accessibilité du fluor en position *para* du groupe phényle du PPFS offre d'innombrables possibilités de fonctionnalisation du polymère par substitution nucléophile. Après modification du PPFS, la capacité d'auto-assemblage a été conservée, et des conductivités plus élevées ont été obtenues par rapport aux copolymères statistiques.

Des études complémentaires ont été menées sur l'utilisation de techniques d'impression pour l'*upscaling* des membranes et l'évaluation de leur impact environnemental par analyse du cycle de vie.

Mots-clés : Nitroxide Mediated Polymerization NMP, Pentafluorostyrene, Copolymères diblock, Autoassemblage, Sulfonation, Modification Para-fluoro thiol, Membranes conductrices de protons, Analyse du cycle de vie

Kurzzusammenfassung

Mit dem Ziel, protonenleitende Membranen mit verbesserter Protonenleitfähigkeit und verbesserten mechanischen Eigenschaften herzustellen, wurde das System Poly(pentafluorstyrol)-*b*-(butylacrylat) (PPFS-*b*-PBuA) untersucht. Die Studie konzentriert sich hauptsächlich auf den Einfluss der sich dabei ausbildenden Polymer-Nanostrukturen auf die Leitfähigkeits-Eigenschaften der Membranen.

Eine Reihe wohldefinierter PPFS-b-PBuA-Blockcopolymere (BCPs) wurde mittels Nitroxid-vermittelter kontrollierter radikalischer Polymerisation (NMP) synthetisiert. Eine spontane Selbstorganisation des BCP-Elements wurde insbesondere über eine zielgerichtete Veränderung der Polymerzusammensetzung ausgelöst. Darüber hinaus wurde durch die Einstellung der molaren Zusammensetzung mittels Anreicherung eines der Blöcke nach der Synthese eine gesteuerte Selbstorganisation der BCPs realisiert , indem das entsprechende Homopolymer mit dem Blockcopolymer zu einem Polymerblend-zusammengefügt wurde. Durch das Bilden solcher Polymerblends wurde die Palette verfügbarer Techniken zur Anpassung der Morphologie für die gewünschten Anwendungen erweitert.

Die Sulfonierung von BCPs zur Herstellung protonenleitender Membranen erfolgte durch eine para-Fluorthiol-„Klick"-Reaktion unter Verwendung von Natrium-3-mercapto-1-propansulfonat (SMPS). Die Zugänglichkeit des Fluors in der para-Position der Phenylengruppe von PPFS bietet zahllose Möglichkeiten für die Polymerfunktionalisierung durch nukleophile Substitution. Nach der Modifizierung von BCP blieb die Fähigkeit zur Selbstorganisation erhalten und es wurden im Vergleich zu statistischen Copolymeren höhere Leitfähigkeiten erzielt.

Zudem wurden ergänzende Studien zum Einsatz von Drucktechniken für das Upscaling von Membranen und zur Bewertung ihres Lebenszyklus durchgeführt.

Schlüsselwörter: Nitroxid-vermittelte Polymerization (NMP), Pentafluorostyren, Diblockcopolymer, Selbstmontage, Sulfonierung, Para-fluorothiolierung, Protonenleitende Membran, Lebenzyklusanalyse

Acknowledgements

I would like to begin this acknowledgment section by expressing my gratitude to my supervisors, Prof. Laurent Billon, Dr. Vladimir Atanasov, for allowing me to join their labs. I thank you for trusting me and rightly guiding me during those years. I would also like to thank Prof. Günter Tovar for his great discussion about the work, collaboration, and guidance throughout the writing process of my thesis. I am also thankful to Dr. Antoine Bousquet, Dr. Ana Moya, Dr. Claudia Delgado Simao, Jose Espí Gallart, and Frederic Clarens Blanco for their priceless supervision.

To all the eSCALED project supervisors and to every person involved that took the time to provide us with quality trainings and guidance throughout the PhD, thank you.

Thank you to Dr. Laia Francesch for being an amazing support throughout my PhD. Thank you for the quality discussions and guidance both concerning the PhD and out. I am forever grateful to you.

To the PhD fellow of the eSCALED project: Andrew Howe, Ludovico Riccardi, Andrew Bagnall, Afridi Zamader, Silvia Pugliese, Domenico Grammatico, Ignasi De Azpiazu Nadal, Olivera Vukovic, Saeed Sadeghi, Diogo Garcia, Van Nguyen, Robin Dürr and Bruno Branco, I am glad to have participated in the eSCALED project with all of you. It was nice working and sharing this experience with you. I wish you all the best for the future and we will hopefully meet again someday.

I would like to thank Pierre Marcasuzaa for his spot-on comments and remarks, daily great mood, and great energy. I couldn't have made all of this without your support.

To the people I have met throughout my stays in the different countries that have made my journey enjoyable both at work and in life, whether it was just as simple as a discussion, a good laugh or a meal shared together, thank you: Johannes, Hyeongrae, Inna, Galina, Robert, Tunga, the Grabowskis, Alejandra, Ana, Marc, Nuria, David, Joan, Joris, Nicolas, Axelle, Laurence, Christopher, Barbara, Tik, Hisham, Grégoire, Leïla, Antoine, Tibor, François, Alexandre, Prithwiraj, Laurie, Aurélien, Léonard, Fabio.

To my amazing friends all over the world, Yacine, Fatim, Julia, Alexia, Natalie, Amandine, Pauline, Mathilde, Sophie A., Sophie M., Alexandre, Arouj, Coste, Milagros, Steven, you have made those three years easier for me in many ways you can't even imagine. Thank you for your unconditional support.

Tonton John, tatie George, Kemi & James Afilaka, I am beyond blessed to have you as my family. Without you none of this would have been possible. Thank you for everything that you have done for us. To the family friends around the globe thank you for the kind words of encouragement and support – The Pucheu & Cebollada families, the Mamvura family, Muntsa.

Finally, dad, mum, Audrey & Yann, no words can express how much I am grateful for you. You've been there since the beginning and have always believed in me. Thank you for sticking with me through the moments of joy, and despair. Thanks for being my family, my friends, and my psychologists. I am happy that I get to continue this adventure that is life by your side. This PhD is for you.

Abbreviations

AEC	Alkaline electrolyser
AFC	Alkaline Fuel Cell
AFM	Atomic Force Microscopy
AIBN	Azobisisobutyronitrile
ATRP	Atom Transfer Radical Polymerization
BCC	Body centered cubic
BCP	Block-copolymer
BuA	Butyl Acrylate
CCL	Covalent cross-linking
$CDCl_3$	Deuterated chloroform
CRP	Control Radical Polymerization
D	Dispersity
DBU	1,8-Diazabicyclo[5.4.0]undec-7-ene
DMF	N,N-Dimethylformamide
DMFC	Direct Methanol Fuel Cell
DMSO	Dimethylsulfoxide
DMSO-d_6	Deuterated dimethylsulfoxide
DOSY	Diffusion-ordered spectroscopy
DP_n	Degree of polymerization
DS	Degree of sulfonation
DSC	Differential Scanning Calorimetry
EIS	Electrochemical Impedance Spectroscopy
eSCALED	European School on Artificial Leaf: Electrodes and Devices
ETFE	poly(ethylene-*alt*-tretrafluoroethylene)
FRP	Free Radical Polymerization
FU	Functional Unit
fv or Φ	Volume fraction
GWP	Global Warming Potential

H_2SO_4	Sulfuric acid
HCC	Hexagonal closed-packed cylinders
HCl	Chlorhydric acid
HER	Hydrogen Evolution Reaction
HPL	Hexagonally perforated lamellae
HT	1-hexanethiol
ICL	Ionic crosslinking
IEC	Ion Exchange Capacity
$K_2S_2O_8$	Potassium persulfate
KOH	Potassium hydroxide
LAM	Lamella
LCA	Life Cycle Analysis
LCC	Life Cycle Cost
LCI	Life Cycle Inventory
LCIA	Life Cycle Impact Assessment
MA	Menthyl Acrylate
MBM	PMMA-*b*-PnBA-*b*-PMMA: Poly(methyl methacrylate-*b*-butyl acrylate-*b*-methyl methacrylate)
MCFC	Molten Carbonate Fuel Cell
MEA	Membrane Electrode Assembly
MeOH	Methanol
M_n	Number average molar mass
M_w	Weight average molar mass
MW	Molar mass
NMP	Nitroxide Mediated Polymerization
NMR	Nuclear Magnetic Resonance
OER	Oxygen Evolution Reaction
P_4VF	Poly(4-vynilpyridine)
PAFC	Phosphoric Acid Fuel Cell
PBI	Poly(benzimidazole)

|	
PBuA	Poly(butyl acrylate)
PE	Poly(ethylene)
PEEK	Poly(ether ether ketone)
PEM	Polymer Electrolyte Membrane
PEMFC	Polymer Electrolyte Membrane Fuel Cell
PEMWE	Polymer Electrolyte Membrane Water Electrolyser
PET	Poly(ethylene terephthalate)
PFA	Poly(tetrafluoroethylene-*co*-perfluorovinylether)
PFS	2,3,4,5,6-pentafluorostyrene
PFSA	Perfluorinated sulfonic acid
PGMEA	Propylene Glycol Methyl Ether Acetate
PMA	Poly(menthyl acrylate)
PMMA	Poly(methyl methacrylate)
PPFS	Poly(pentafluorostyrene)
PPFS-*b*-PBuA	Poly(pentafluorostyrene-*b*-butyl acrylate)
PPFS-*stat*-PBuA or PPFS-*s*-PBuA	Poly(pentafluorostyrene-*s*-butyl acrylate)
PS	Polystyrene
PTFE	Poly(tetrafluoroethylene)
PU	Polyuretane
PVDF	Poly(vinylidene fluoride)
PVF	Poly(vinyl fluoride)
q	Scattering vector
RAFT	Reversible Addition-Fragmentation chain Transfer
RH	Relative humidity
SAXS	Small-angle X-ray scattering
SDS	Sodium dodecyl sulfate
SEC	Size Exclusion Chromatography
SMPS	Sodium 3-mercapto propane sulfonate
SO_3H	Sulfonic acid

Abbreviations

SOE	Solid Oxide Electrolyser
SOFC	Solid Oxide Fuel Cell
sPEEK	Sulfonated poly(ether ether ketone)
sPPFS	Sulfonated poly(pentafluorostyrene)
sPPFS-*b*-PBuA	Sulfonated poly(pentafluorostyrene-*b*-butyl acrylate)
sPPFS-*stat*-PBuA or PPFS-*s*-PBuA	Sulfonated poly(pentafluorostyrene-*s*-butyl acrylate)
sPSU	Sulfonated polysulfone
s-SIBS	Sulfonated poly(styrene-*b*-isobutylene-*b*-styrene)
Tg	Glass transition temperature
TGA	Thermogravimetric analysis
THF	Tetrahydrofuran
χ	Flory-Huggins parameter
χN	Segregation product
δ	Solubility parameter
ρ	Resistivity
σ	Conductivity
ΔCp	Heat capacity

General introduction and eSCALED project ambition

One of the biggest challenges of our century is energy. Indeed, in our day-to-day life, we are highly dependent on it for our homes, business, transportation, and industries. Although the resources we need to provide this energy are present in nature, most of them are not renewable. This aspect makes it unsustainable for the earth balance. Moreover, producing fuels from those non-renewable sources involves complex steps that result in high greenhouse gases emissions, impacting our climate.

The European eSCALED project is aiming to provide an answer to that issue by seeking a sustainable solution taking nature as the inspiration. Indeed, plants by the photosynthesis process combine CO_2 and water to transform solar energy and store it into chemical energy for their own feeding. The idea is so to mimic this natural photosynthesis to transform solar energy, which is a renewable energy source, and store it in the form of hydrogen or solar fuels, an artificial leaf. The approach to perform this is to make a water splitting device. This device will be connected to a solar cell that will capture solar energy and convert it into electricity. The solar fuel will help split the water into oxygen and hydrogen that will be stored for energy purposes, the process is called water electrolysis. The eSCALED technology will aim to help reduce greenhouse gases emissions in a sustainable way.
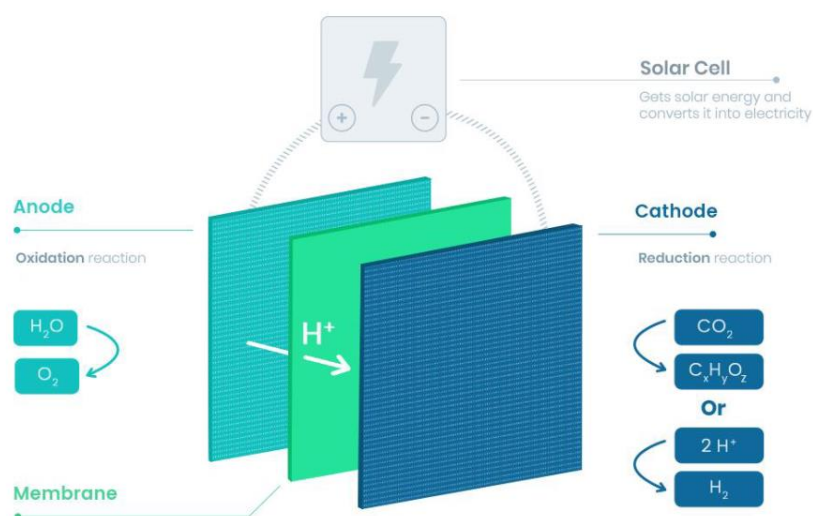
Alongside the research aspect, the eSCALED project is a multidisciplinary project bringing together researchers from different backgrounds coming from various European universities, and research centres. In this sense 14 PhD students (ESR – Early-Stage Researchers) from different backgrounds were recruited and are collaborating on the project. All of us working on the different challenges of the device. My PhD is focused of the development of the proton-conducting membrane of the device. During my PhD, I spent 1 year in ICVT (Institut für Chemische Verfahrenstechnik) of the university Stuttgart (Germany) specialist in polymer engineering and membrane technology; 3 months in Eurecat Mataró (Spain) in the functional printing and embedded devices unit; 2 months in Eurecat Manresa (Spain) in the sustainability unit; and 1 year and 8 months in IPREM (UMR 5254 UPPA-CNRS - Institut des sciences analytiques et de physico-chimie pour l'environnement et les matériaux) of the university of Pau (France).

The **first chapter** of this manuscript is the literature state-of-the-art on the proton-conducting membranes for water electrolysers. In it are described the water electrolysis process and existing technologies, the breakthroughs concerning the membranes development and specificities in term of materials and conduction performances. In this chapter, are also described existing membranes synthetic methods, from the synthesis of polymers to the sulfonation of the latter producing the proton conduction and some specific aspects that are to consider improving the transport properties in the membranes such as the materials structuration.

The **second chapter** of this manuscript describes the challenges of the upscaling of the membrane electrode assembly (MEA). The MEA was made by printing in Eurecat technological centre in Catalunya using commercially available materials. Nafion® was used for the membrane. The upscaling challenges of the membrane manufacture are presented in this chapter.

The **third chapter** of this manuscript is focused on the polymer nano-structuration. Indeed, having a structured material with preferential pathway could help with the conduction properties of the membranes. In this chapter are described the synthesis of block-copolymers of pentafluorostyrene (PFS) and butyl acrylate (BuA) by Nitroxide-

Mediated Polymerization (NMP). The phase separation at the nanometer scale was observed both by AFM and SAXS.

In addition to the block-copolymers BCPs, statistical copolymers were synthetized by controlled radical polymerization CRP (NMP) and free radical polymerization FRP in emulsion. This led to a low molar mass polymer in the first case and a high molar mass polymer in the case of the free radical polymerization. Moreover, a waterborne polymer is obtained *via* the polymerization by emulsion. In the **fourth chapter** are described the synthesis and an original sulfonation of the copolymers. The sulfonation was indeed performed by the para-thiol modification, for a first time. With this highly effective technique, the sulfonation degrees could be tailored and the self-assembly of the block-copolymers is still present after modification and can be tuned. Both AFM and SAXS experiments were used to characterize the nano-phase segregation of the BCPs. Finally, membranes of the PFS/BuA polymer system were made, and their mechanical stability was enhanced by cross-linking them with PBI. Their proton-conductivity was also displayed.

The **fifth** chapter of this manuscript discusses the Life Cycle Assessment of the production of the membranes, providing a study on their impact on the environment. These studies were made in collaboration with Eurecat technological centre in Catalunya.

General table of contents

Chapter 4. *Para* fluoro-thiol clicked diblock-copolymer self-assembly: Towards a new paradigm for highly proton-conductive membranes

Chapter 1. State-of-the-art on proton-conducting membranes for PEM electrolysis

Table of contents Chapter 1

1. Proton conductive membranes in water electrolysis

1.1. Introduction

Energy is widely used and necessary nowadays. The needs go from the use of modern technologies, to heating, to food preparation, and more. Resources for energy purposes are found in nature. Among them are wood/charcoal, coal, crude oil/petroleum, natural gases, and agro fuels (see **Figure 1**).[1] Although they are available in Nature, these resources present some considerable downside. Those downside include the overuse of wood, the toxic contaminants that can be found in the atmosphere after the burning of coal, the costs of extraction, refinement and transportation of petroleum and its non-renewable aspect. Indeed, it takes in average over hundred millions of years for the fossil fuels (coal, petroleum, and natural gases) to regenerate, making it an unsustainable solution.[2] Nuclear energy also used for electricity supply shows a real dangerousness regarding the disposal of the radioactive waste and the danger of the nuclear facilities. Some notable nuclear accidents prove this point: Chernobyl (1986) and more recently Fukushima (2011) where contaminations of water, food, oceans, and very important health issues were to deplore.[1]
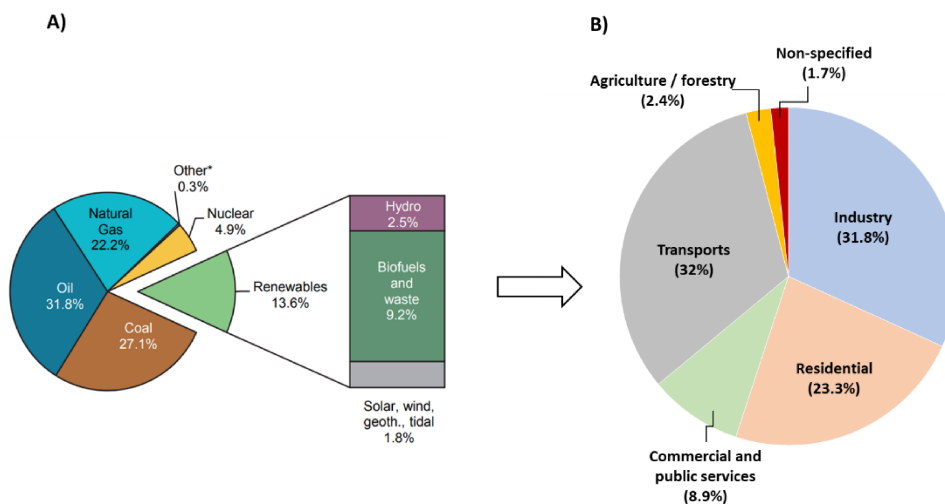
Figure 1. (A) World fuel shares in total primary energy supply, (B) Total final energy consumption by sector, from the International Energy Agency (IEA), data from 2019.[3]

In this sense, fundings have been gradually dedicated over the years to the development of more sustainable alternatives such as renewable energy sources (solar or wind energy or geothermal sources), **Figure 2**. However, those energies are time and weather dependent and developing effective energy storage methods for the different needs are necessary. Several storage techniques were developed such as electromechanical, thermal, and chemical storages. For example, there are batteries that allow the transformation of chemical energy into electrical energy.[1]

Million USD (2017 prices, PPP)

Nuclear ■ Unallocated ■ Hydrogen and fuel cells ■ Other power and storage ■ Other cross-cutting
Renewables ■ Energy efficiency ■ Fossil fuels (CCS) ■ Fossil fuels (coal, oil, gas)
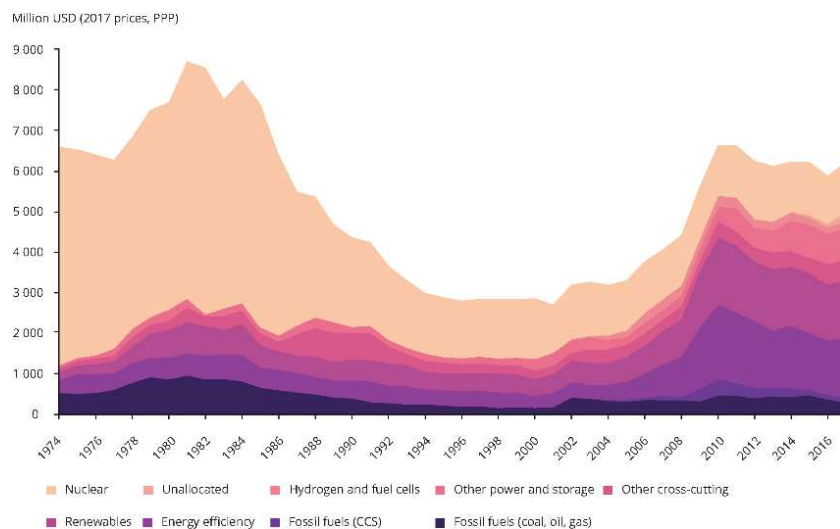
Figure 2. Evolution of total European energy RD&D spending by technology (USD-million, 2017 prices) (based on IEA estimates).[4]

The eSCALED project focuses on chemical storage using an electrochemical cell. Indeed, unlike in fossil fuel where the chemical energy comes from an intermediate combustion or thermal energy, electrochemical cells convert the energy that is stored in the form of chemical bonds straight into electricity. This is possible by means of the commonly used batteries (Lead cell, Li-ion batteries) and the development of fuel cells for the hydrogen storage for example. Despite the flammability and explosive aspects of hydrogen if poorly stored, it is one of the most environmentally friendly and powerful energy sources. Hydrogen is a stable easy to produce compound (*via* electrolysis) and its production feedstock that are water and photons are abundant on the surface of the earth.

1.2. Hydrogen production, storage, and usage

1.2.1. Hydrogen production

Hydrogen can be produced using energy sources that are: fossil energy, nuclear energy, and renewable energy. As of today, 95% of the hydrogen production comes from fossil fuels. The most developed methods for its production are partial oxidation, autothermal reforming, and steam reforming. Steam reforming of hydrocarbons is the most efficient method. It is important to mention that although this technique allows the production of high amounts of hydrogen and does not require oxygen or high temperatures during operation, it is also a very polluting technique. Indeed, significant quantities of CO and CO_2 gases are emitted in the atmosphere from this technique. [5]

The steam reforming process consists of cracking hydrocarbons under pressure (up to 25 bar) and using heat (~1000°C) following the chemical reaction below. A catalyst is often used for the reaction. Nickel containing catalysts are of choice mainly due to their low cost. Among the available fuels, oxygenated hydrocarbons such as methanol, dimethyl ether, or natural gases such as methane are used to produce hydrogen.

$$C_mH_n + m\ H_2O = m\ CO + (m + \tfrac{1}{2}\ n)\ H_2$$

$$CH_4 + H_2O \rightarrow CO + 3\ H_2$$
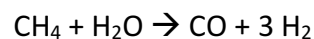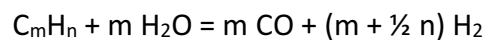
Before reforming, the fuel needs purification. Indeed, most of the fuels contain some sulphur. The desulfurization of the fuel can be done by a chemical reaction approach or by adsorption. With the chemical approach, the catalysts used to produce hydrogen are also capable of hydrogenating sulphur to make H_2S. In the adsorption approach, the molecules containing sulphur can be adsorbed on activated carbon, modified zeolites or nickel metal. [6] After reforming, the water-gas shift reaction is made.

This step consists of reacting the CO produced during reforming with steam once again to make more hydrogen, **Figure 3**, but also produces CO_2.

$$CO + H_2O \rightarrow CO_2 + H_2$$
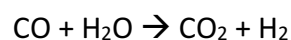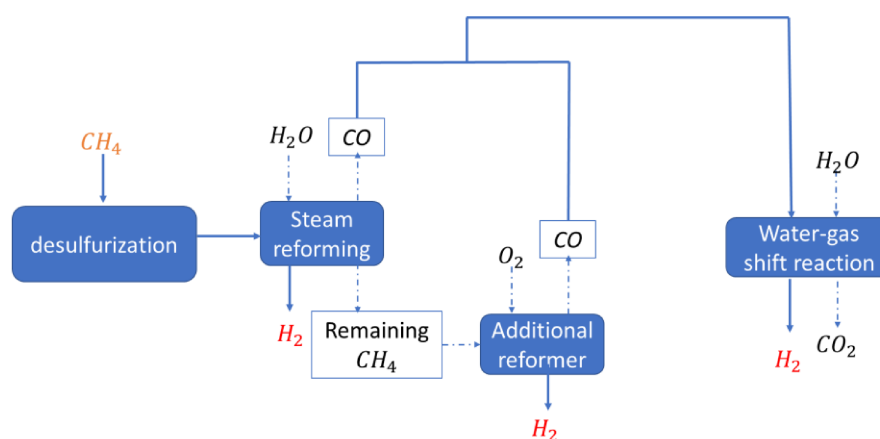
Figure 3. Steam reforming process of hydrocarbons for hydrogen production.

Hydrogen can also be produced from renewable energy. Usually by biological processes, using biomass or water electrolysis. The water electrolysis process will be described in depth in another section of this report (section 1.3.). Hydrogen from biomass has grown interest because of its sustainable aspect. In fact, on top of being abundant on the planet, plants used to make biomass consume CO_2 during their life cycle. Hence, it can be considered that the CO_2 emitted while producing bio-hydrogen is equivalent to the CO_2 consumed by the plants. Which puts the environmental balance of this process at zero.

The most mature technologies of hydrogen production are biomass gasification, and pyrolysis. When doing pyrolysis, it is very important to dry the biomass to avoid additional production of carbon oxides. Indeed, no oxygen or water are needed for the decomposition of biomass. Pyrolysis can also be used to produce hydrogen from hydrocarbons.[7] Biomass pyrolysis is a complex process to understand chemically as the results of the pyrolysis are the obtention of bio-oil, coke, and pyrolytic gases. Among the emitted gases are CO_2, CO, CH_4, H_2, ethane, propane.[8] Due to the competing processes occurring and the production of several gases, the yields of hydrogen produced are low. However, they can be improved by playing on parameters such as the operating temperature or the particle sizes. It was proven that pyrolysis temperature has a linear behaviour to the yield of volume of hydrogen produced. Although these yields are relatively low due to concurring reactions, it is possible for example to yield up to 54% of H_2 from hazelnut shell when operating at temperatures above 700 °C.[9] Moreover by using smaller particle sizes of biomass, the heating rate in the

reactor is increased and the formation of gases is favoured to the formation of coke, leading to higher yields of hydrogen.[10]

Biomass gasification on the other hand can be described as a combination of pyrolysis and steam reforming. It is important for the gasification that the biomass is deprived of its moisture. Unlike for pyrolysis, biomass gasification uses steam and oxygen to make hydrogen alongside CO and CO_2. At this stage, another reactor can be used to make hydrocarbons, or the water-gas shift reaction can be implemented to produce more hydrogen. An extra step is needed to separate hydrogen from the other gases generated to obtain pure hydrogen and to remove the other by-products of pyrolysis. Catalysts can also be used for the process.[6]

Hydrogen produced by biological processes also referred to as bio-hydrogen comes from living microorganisms such as microalgae or cyanobacteria. Indeed, using water and light those organisms can split water into hydrogen ions and oxygen. Those ions can then be combined to produce hydrogen using hydrogenase enzymes. This process will not be described in this report as there is still a lot of progress to be made and the rate and yield of production of hydrogen using this path are very low still. One of the challenges to overcome is the presence of oxygen. Indeed, oxygen inhibits the performance of the enzymes and anaerobic conditions are needed.[11, 12]

Three denominations exist for hydrogen. They depend on the nature of the feedstock used to produce it and how polluting the production is. Grey hydrogen and blue hydrogen are produced by the reforming process. The difference between both is that the process of capturing CO_2 can be implemented in the making of blue hydrogen. Green hydrogen on the other hand refers to a non-polluting production of the fuel.

1.2.2. Hydrogen storage

Three main approaches exist for hydrogen storage. Hydrogen can be stored in its gaseous state, in its liquid state or, as protons in solids.[5] The advantage of storing hydrogen in a gaseous state is that a bigger amount of hydrogen can be stored compared to storing its liquid counterpart. In the gaseous state, hydrogen is stored in high pressure tanks.

Nevertheless, due to the dangerous character of the chemical one should be cautious of the volume proportions to the pressure, and the thermal environment where the tank should be stored. Liquid hydrogen is obtained by cooling of gaseous hydrogen. They are typically stored in thermally insulated containers. The major drawback of liquefying hydrogen is the amount of energy consumed by the process (30 to 40% of the final energy content of hydrogen). Finally, hydrogen can be stored in its protonic form (H^+). By being very small by nature, hydrogen protons can easily be inserted in available spaces in metal alloy compounds such as $LaNi_5$ or FeTi. The hydrogenated metal materials are called metal hydrides. The drawbacks of this technique are the small amount of hydrogen storage in the metals, the cost and availability of the metals used, and the weight of such materials in applications such as cars. Other hydrogen storage techniques are in works and they consists of storing negatively charged hydrogen, store it into ammonia or using reversible organic liquids such as benzene or toluene.[5]

1.2.3. Hydrogen usage

Hydrogen produced from the non-renewable energy sources (grey and blue hydrogen), **Figure 4**, can be used as feedstock for fuel cells. A fuel cell is an electrochemical cell that generates electricity by converting chemical energy and oxidizing compounds using redox processes. The first hydrogen fuel cell was exhibited in 1839 by William Grove. It consisted of electrolysing water by use of an electric current and using two platinum electrodes immersed in an acid electrolyte. The electrolysis process is reversible and produces an electric current. Electrons formed at the anode flow around an external circuit while the protons pass through the liquid electrolyte (acid solution) to reach the cathode. This process only produced low amount of current. To improve its production, a new design was implemented which consisted of improving the contact area between the gas, the electrodes, and the electrolyte, and reducing the distance between electrodes. In this sense, the electrodes were made porous and the use of polymers having mobile H^+ was implemented. Those are ionomers and mostly known as proton-exchange membrane or polymer electrolyte membrane (PEM). Stacked to the electrodes, the distance problem was solved.[13] PEMs have been widely used in fuel cell processes.

Several types of fuel cells exist and may be distinguished by the temperature at which they operate. From lowest to highest temperatures there are: Alkaline Fuel Cell (AFC), Polymer Electrolyte Membrane Fuel Cell (PEMFC), Direct Methanol Fuel Cell (DMFC), Phosphoric Acid Fuel Cell (PAFC), Molten Carbonate Fuel Cell (MCFC), and Solid Oxide Fuel Cell (SOFC). Although further research is being made on their improvement especially concerning the materials, the table below summarizes the characteristics of each fuel cells (**Table 1**).

Table 1. Summary table of the operating conditions and materials for the different types of fuel cells, adapted from reference. [13]

Type of Fuel Cell	Operating temperature (°C)	Anode composition	Cathode composition	Electrolyte
AFC	60 - 90	Carbon/Platinum catalyst	Carbon/Platinum catalyst	Aqueous KOH
PEMFC	30 - 180	Carbon/Platinum catalyst	Carbon/Platinum catalyst	Acidic polymer
DMFC	60 - 90	Carbon/Platinum catalyst	Carbon/Platinum catalyst	Acidic polymer
PAFC	180 - 220	Carbon/Platinum catalyst	Carbon/Platinum catalyst	Phosphoric acid in SiC matrix
MCFC	550 - 650	Porous Ni	Porous NiO	Metal carbonates
SOFC	800 - 1000	Porous cermet of Ni and yttria/zirconia	Strontia-doped lanthanum	Ion conducting ceramics

Green hydrogen produced from renewable sources, by water electrolysis for example is a promising alternative to cleaner energies. Water electrolysis devices are inspired to some extent from the original fuel cells designs in terms of choice of materials. Electrical energy produced from hydrogen is used in various fields such as the industry, buildings, or transportation. A great example of the usage of green hydrogen that I have personally experienced in my daily life is the Fébus in the city of Pau, **Figure 4**. Fébus is the result of a 74 million euros mobility project funded by regional and European partners for the city of Pau. It is the first 18 metres green hydrogen-powered bus in the world with a capacity of 125 people. Fébus runs through Pau North to South on a 6 km trajectory, it's first ride was in 2019. On top of running a full day of service without the need to refuel, Fébus is a comfortable and silent transportation method. The hydrogen used to fuel the bus is

produced locally in a hydrogen plant, using solar energy in the future, and water as its main feedstock.

Figure 4. Hydrogen production classification and usage from article Hidrogen blau: frau o esperança contra l'emergència climàtica? Vilaweb journal, published on the 19/09/2021; Zero emission bus "Fébus", in the city of Pau-France, https://www.idelis.fr/se-deplacer/le-reseau-de-bus/febus-le-bus-zero-emission.

1.3. Water electrolysis

As mentioned in the previous section of this chapter, it is possible to produce hydrogen by water electrolysis. The water electrolysis process uses an electrical current to split water into oxygen and hydrogen. It has the advantage that it uses water which is a very abundant molecule on earth (water occupies over 70% of earth's surface). This results in less emission when the electricity source doesn't emit CO_2 (nuclear, photovoltaic, wind power, hydroelectricity).

An electrolyser cell is composed of two electrodes immersed in an electrolyte and parted by a physical separator to prevent recombination of hydrogen and oxygen. For the process to be effective, the separator needs to be electrochemically and physically stable. At the anode takes place the oxidation reaction (Oxygen Evolution Reaction - OER) and at the cathode the reduction reaction (Hydrogen Evolution Reaction - HER).

OER: $2\ H_2O_{(l)} \rightarrow O_{2\ (g)} + 4\ H^+_{(aq)} + 4\ e^-$

HER: $2\ H_2O_{(l)} + 2\ e^- \rightarrow H_{2\ (g)} + 2\ OH^-_{(aq)}$
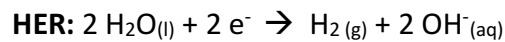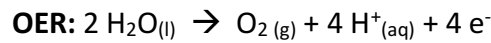
To understand the process, it is important to comprehend what is happening from the electrochemical and thermodynamic point of view. The overall performance of water electrolysers is determined by the efficiency at a determined current. Looking at the electrochemical reactions, the efficiency can be described by assessing the ratio between the electric potential required for water splitting and the potential applied to the electrochemical cell.

$$\eta = \frac{E^0}{E_{cell}} * 100 = \frac{(E^0_{anode} - E^0_{cathode})}{E_{cell}} * 100$$

With E^0, E^0_{anode}, and $E^0_{cathode}$ as the standard cell, anode, and cathode potentials respectively, and E_{cell} as the potential applied to the electrochemical cell. The E_{cell} parameter is an addition of the reversible cell voltage and all the voltage losses that are implicated in the electrochemical process. Those losses include the electrolyser current, the ohmic resistance of all components, the kinetic overpotentials at the anode and cathode, and the mass transport phenomena.

In terms of the electrolysis reaction, the theoretical minimum energy required to split water can be explained by the following equation:

$$E^0_{rev} = \left| \frac{-\Delta G^0}{nF} \right| = 1.23\ V$$

With E^0_{rev} the reversible cell voltage, ΔG^0 the Gibbs free energy (237 kJ/mol at 298 K and 1 bar), n the number of electrons transferred during the reaction, and F the Faraday constant (96 485 C/mol).

In terms of thermal balance, the potential studied is called the thermo neutral potential (E_{tn}^0) and it is the potential required for an isothermal operation of the electrochemical cell.

$$E_{tn}^0 = \left| \frac{-\Delta H^0}{nF} \right| = 1.48 \text{ V}$$

With ΔH^0 the reaction enthalpy at standard conditions (286 kJ/mol).

The hydrogen produced can be used chemically or as energy in fuel cells for example. Depending on the nature of the hydrogen used, the voltage efficiency is calculated using the Higher Heating Value (HHV) of H_2 or its the Lower Heating Value (LHV). HHV is chosen when H_2 is being used chemically (ΔH_{vap}^0 = 44 kJ.mol^{-1}) and LHV in the other case.[14, 15, 16]

Finally, among the parameters to include in the cell voltage calculation are the overpotentials at the electrodes. Indeed, the efficiency of the reaction is directly linked to the reaction rate at the electrodes. Hence, to the materials used for the cell. The overpotential assesses the amount of energy necessary to drive the reaction. If the overpotential value is high, it means that more energy is needed than what was expected thermodynamically. The overpotential at each electrode is measured by the Tafel equation.

$$\eta_{cathode} = 2.3 \frac{RT}{\alpha_c F} \times - \log \frac{i}{i_0}$$

$$\eta_{anode} = 2.3 \frac{RT}{(1 - \alpha_a) F} \log \frac{i}{i_0}$$

$$\eta = 2.3 \frac{RT}{\alpha F} \log \frac{i}{i_0} - 2.3 \frac{RT}{(1-\alpha)F} \log \frac{i}{i_0}$$

With η the overpotential, i_0 the exchange current density, i the current density, F the Faraday constant, α the transfer coefficient, and T the temperature. [14]

OER is known to have a higher overpotential than HER and it is usually the limiting part of the electrolyser. To resolve the overpotential problem, it is important to choose wisely the materials used at the electrodes.

Three types of electrolysers exist. They are alkaline electrolyser (AEC), proton exchange membrane electrolyser (PEM electrolyser) and solid oxide electrolysis cell (SOE). The following paragraphs will summarize the components commonly used for the efficient

water electrolysis of each cell. As membranes for PEM electrolysis is part of my research studies, a separate section will be dedicated for the state of the art on the material used for PEM in water electrolysers.

1.3.1. Alkaline Electrolysis

Alkaline electrolyser is the most developed and commercialized technology for water splitting. A direct current when applied will allow the transfer of electrons at the electrodes (from the anode to the cathode). At the cathode, those electrons will react with water to form hydrogen gas. Meanwhile, hydroxide ions will travel from the cathode to the anode. This transfer is accompanied by release of electrons, there oxygen is formed at the anode. The gases created at each electrode are then collected by gas receivers, dried, and purified before storage, **Figure 5**.

The chemical reactions occurring can be summarized as followed:

At the cathode: $2H_2O_{(l)} + 2e^- \rightarrow H_{2\,(g)} + 2OH^-_{(aq.)}$

At the anode: $4OH^-_{(aq.)} \rightarrow O_{2\,(g)} + 2H_2O + 4e^-$

Overall reaction: $2H_2O \rightarrow 2H2 + O_2$
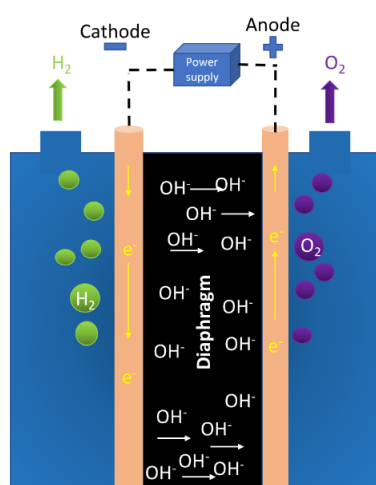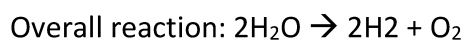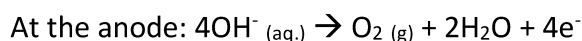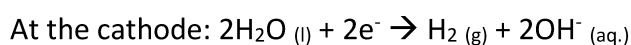
Figure 5. Representation of an alkaline electrolysis cell (AEC).

Metals are the common electrodes materials for alkaline electrolysis. Nickel is the material of interest for the electrodes due to its performance, availability, and low cost. Indeed, it results in a good electrochemical performance of the electrodes while being resistant to the alkali media of the electrolyte. In comparison, transition metals are good in terms of electrochemical activity but are not as resistant to the electrolyser. And Nobel

metals whilst being performant electrochemically and resistant to the media are too expensive.[14]

Although Nickel is praised as an electrode material it can also contribute to a less efficient water electrolysis process due to its ability to deactivate. At high concentrations of hydrogen and at high current densities, hydrogen in the media reacts with Ni at the cathode to form Nickel hydride, resulting in its deactivation overtime. [17] Deactivation also happens with other metals typically used at the cathode – Co, Pt, Fe. Studies have been made to prevent the deactivation from happening. The solutions include but are not limited to the coating or doping of electrodes with metals, the addition of electrocatalysts, or the modification of the electrodes.

Concerning the anode, the high overpotential values cause the electrode to be covered by oxide layers, which were found to increase the OER activity.[18] Thus, oxide compounds are mostly used for the OER. RuO_2, RhO_2, PtO_2, and especially IrO_2 are the best for OER. But, as it is the case for the HER, the goal is to use materials that perform well, that are made from abundant elements and that are not too expensive. All those conditions lead to the extensive studies of transition metals for OER. Indeed, the studies of Ni, Co and Fe oxides showed that Ni oxides performed better than the others metal oxides, with Fe oxide performing the worst.[19] To continue with the metals studies, having Ni based metal alloys gave better OER activity than pure Ni, spinel type oxide using Ni also demonstrated good results towards OER.[20]

KOH or NaOH solutions are used for the electrolyte in alkaline electrolysis cells. Comparing the two solutions, KOH gave better conductivity at a concentration of 30 wt%.[16] It has not been mentioned yet in this report, but the gas bubble formation can become an issue during electrolysis if not well managed. In fact, the gas forming at the electrodes/electrolyte interface can cause resistance to the process. Once again, the choice of materials is very important. With liquid electrolytes, the main issues are the risk of leakage, the corrosiveness of the alkali solution at high temperatures, and the carbonation process that takes place if hydroxide ions react with carbon dioxide ($2OH^- + CO_2 \rightarrow CO_3^{2-} + H_2O$). Furthermore, the risk of short circuit is higher if both electrodes share the same electrolyte solution. For that reason, the use of a solid separator is needed.

Therefore, diaphragms were developed as solid separators. On top of being OH^- ions conductors, diaphragms must be porous to allow the electrolyte to flow through. They must be stable in the electrolyte at the operating conditions of the cell and must prevent the recombination of the formed gases. The first separators for alkaline water electrolysis were asbestos (**$Mg_3Si_2O_5(OH)_4$**) cloth. With time due to its proven toxicity and the need for more resistant materials, they have been replaced. Inorganic oxide-ceramic materials, ceramic/polymers composite materials or hydrophilic/hydrophobic polymer blends gave interesting results as separators for alkaline electrolysers. Indeed, Zirfon® became very popular and commercialized. This separator is a polysulphone (15 wt%) mixed with inorganic zirconium oxide (85 wt%). More recently non-porous anionic membranes have been studied to act as the electrolyte instead of the diaphragm/alkali solution couple (leading to the same configuration as a PEM electrolyser). They are mechanically and thermally stable, they act as insulators, they are not costly, and they only require the use of deionized water instead of a high pH solution. One other major advantage is that by assembling the electrodes directly on the membrane, the distance between electrodes is significantly reduced which improves the electron conduction. Anion exchange membranes are usually made of polymers functionalized with cationic groups such as guanidinium, ammonium or pyridinium, **Figure 6**. The hydroxide transport is then done by some hopping or diffusion mechanisms that will be detailed further in this chapter (section 1.4.1.). Commonly used polymers are poly(tetrafluoroethylene) (PTFE), poly(ether ether ketone) (PEEK), or polyethylene (PE).[21, 22]
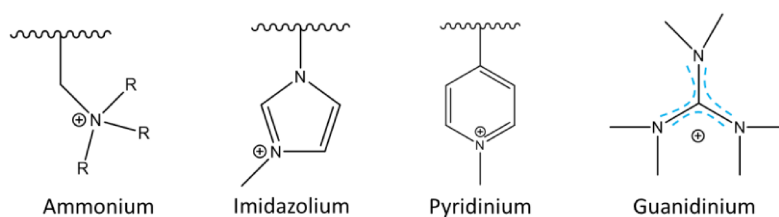
Figure 6. Common cationic groups used for anion exchange membranes.

1.3.2. Solid Oxide Electrolyser (SOE)

In Solid Oxide electrolyser, the water splitting process takes place at high temperatures (600 – 1000 °C). The operating process is the following, steam is fed at the cathode. At the cathode, water is reduced into hydrogen gas and oxide ions. Finally, the ions are transferred to the anode via a solid ion conducting ceramic electrolyte, where it will recombine to form oxygen, **Figure 7**. Few of the advantages of a SOE is that it is a solid-state system and a considerable part of energy needed to operate the cell comes from steam, which is cheaper than other electricity sources.
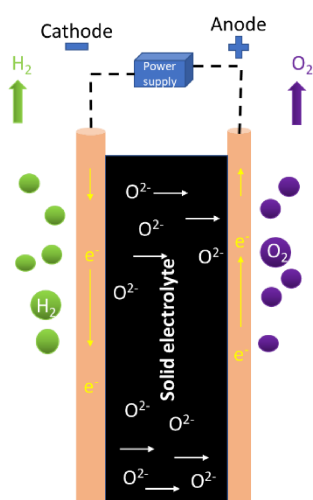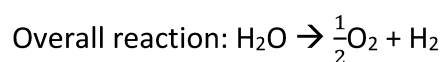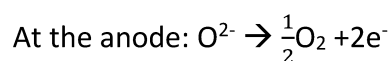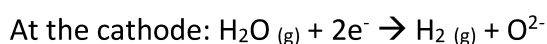
Figure 7. Representation of a solid oxide electrolyser (SOE).

The chemical reactions occurring can be summarized as followed:

At the cathode: $H_2O_{(g)} + 2e^- \rightarrow H_{2\,(g)} + O^{2-}$

At the anode: $O^{2-} \rightarrow \frac{1}{2}O_2 + 2e^-$

Overall reaction: $H_2O \rightarrow \frac{1}{2}O_2 + H_2$

The materials used for a SOE are usually the same used for solid oxide fuel cells (SOFC). Indeed, a lot of research has already been made for the development of SOFC. Although noble metals are amazing choices as electrode materials, their cost leads to look for more affordable materials with good performances. For SOE, the cathode is generally made of Ni or Co catalysed porous cermet (ceramic and metal mixture) on yttria-stabilized zirconia (YSZ). Zirconia prevents the sintering of metal particles and has good thermal properties. The porosity of the electrode is needed to allow the gases to efficiently pass through. Ideally, they should be 20 to 40% porous. The stability of the electrode is also determined by the particle size of its components, typically ~1μm. The anode is also porous and made of a composite of YSZ and strontium doped lanthanum manganite (LSM) *p*-type

semiconductor, p-type conducting perovskite can also be used. The solid electrolyte is an YSZ , typically 8 to 10 mol% of Y_2O_3 on ZrO_2. [23, 13]

The cells can be tubular or planar in design. No gas-tight seals are needed for the tubular design whereas the fabrication cost of the planar design is lower. Glasses of high transition temperature are used as sealer to provide gas tightness in the SOE. Although operating at high temperatures can increase the performance of the electrolyser, the stability of the materials is an issue to be fixed. Indeed, the degradation of the Ni/YSZ cathode is the main problem for SOE.[24]

1.3.3. Polymer Electrolyte Membrane (PEM) electrolysis

Within the framework of the eSCALED project, the ambition is to create a device capable of receiving solar energy and storing it under chemical form such as hydrogen or carbon molecules - artificial photosynthesis. To make it happen, the idea is to have a PEM water electrolyser device linked to a solar cell, **Figure 8**. Hence, for the means of the project, the focus on this chapter will be made on PEM electrolysers.
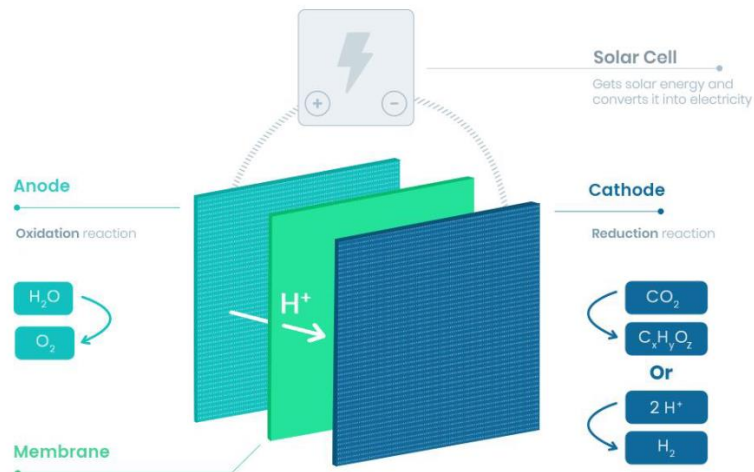
Figure 8. Prototype of the eSCALED PEM electrolyser.

In principle, a PEM electrolyser works the same way as an alkaline electrolyser. The major differences are that a PEM electrolyser is operated in acidic media and that the electrolyser is a thin polymer proton-conducting membrane. In a typical PEM electrolysis

system, the electrodes are directly assembled on the membrane, this assembly is called membrane electrode assembly (MEA), **Figure 9**. [25]

The chemical reactions occurring can be summarized as followed:

At the cathode: $4H^+ + 4e^- \rightarrow 2H_{2 (g)}$

At the anode: $2H_2O \rightarrow 4H^+ + O_2 + 4e^-$

Overall reaction: $2H_2O \rightarrow 2H2 + O_2$
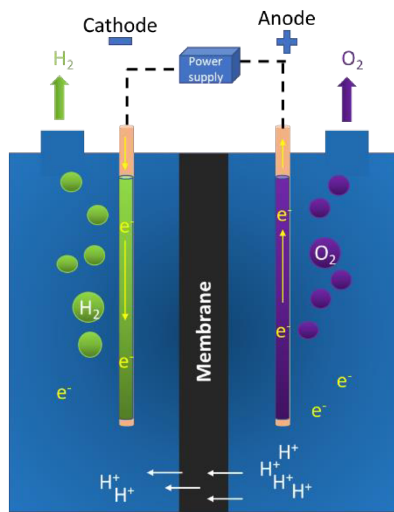
Figure 9. Representation of an PEM electrolyser.
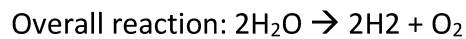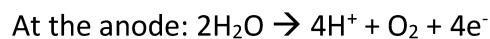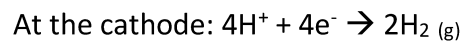
Most of the cathode materials for PEM electrolysers are platinum based. Indeed, Pt has the best HER activity and is very stable in acidic media. Research focuses a lot on reducing the Pt loading while displaying good activity of the electrode. Lowering the quantity of catalyst used is a way to reduce the overall cost of the cell. To reach this goal, studies were made on the loading of Pt on carbon black or on carbon nanotubes (CNTs).[26] Nowadays, the loading ranges from 0.5 to 1 mg.cm^{-2} for the cathode. In addition, other types of catalysts have been studied such as sulphides, phosphides, carbides, and nitrides. They have the advantage of being earth abundant. The most promising replacement material in this category are molybdenum sulphides (MoS_2) or MoS_2 on carbon-based supports such as graphene or reduced graphene oxides (RGO).[27] Metallic alloys and perovskites can also be considered as cathode materials.[28]

Similarly, to alkaline electrolysis the most promising materials for OER are metal oxides. RuO_2 and IrO_2 have demonstrated the best catalytic activity for OER in acidic media due to their high electronic conductivity. Studies have also been made on the use of mixed oxides as anode electrocatalysts. Indeed, although the Ru shows the best activity towards OER, it is prone to corrosion, leading to its instability. In that sense, $Ir_xRu_{1-x}O_2$ type oxides

were investigated with $Ir_{0.6}Ru_{0.4}O_2$ being the optimal type.[29] Moreover, since the electrode activity is not only controlled by the electronic conduction but also by the size of the particles and the loading of catalyst, research has also been dedicated to find suitable catalyst supports. Increasing the surface area of the support has been linked to an increase of catalytic activity. Thus, carbon-based materials such as activated multiwall carbon nanotubes (MWCNTs) were used, with the additional step of coating them with metals like Ti to prevent them from corroding. Having core-shell type metal oxides has also been reported in the literature as potential materials.[28, 30]

In PEM electrolysers, the electrolyte is a proton-conducting polymer material. Nafion® has been the material of choice but, its high cost raised the interest on finding cheaper materials with similar or higher performance. Section 1.1.4. of this chapter will discuss more in depth about the membranes used in PEM electrolysers.

To summarize, water electrolysis is a powerful method for hydrogen production in terms of cleanliness of the process. Indeed, renewable energy is used to split water and the production of clean gases (H_2 and O_2) reduces the emission factor of the process. Alkaline, PEM and SOE electrolysers are the three main technologies. PEM electrolysers and SOE are still in development, but the research is promising, **Table 2**. Currently, the need for the full development of those technologies is focused on the search for optimal materials. Whether new or improved, those materials must show good activity towards the water splitting process while being resistant to the operating conditions of each cell and being low in cost.

Table 2: Summary table of the different types of water electrolysers.

Technology	Best performing components Cathode / Electrolyte / Anode	Efficiency	Maturity
Alkaline electrolyser	Ni catalyst / Zirfon® + KOH / IrO_2	59-70%	Commercialized
PEM electrolyser	Pt catalyst / Nafion® / RuO_2	65-82%	Near term
Solid Oxide electrolysis	Ni-YSZ / YSZ / YSZ-LSM	40-60%	Still in development

1.4. Membranes for PEM electrolysis

In PEM electrolysers, the proton-conducting membrane is a key component of the device. Other than conducting protons from the anode to the cathode, the membrane prevents electron transport and the mixing of components coming from both electrodes. Moreover, the membranes are thin, which allows a better transfer of protons between both electrodes. In other to be effective, the membrane must be durable. Meaning that it should have a good chemical, and mechanical stability; a thermal and hydrolytic stability; a high proton conductivity and be compatible with the electrode's materials. The plus will be to have a membrane that is low cost. For this purpose, several polymer membranes have been synthetized and characterized throughout the years for the development of fuel cells and can be applied as well for electrolysis cells. In the literature, they are often classified in different categories, **Figure 10**. [31] An overview of some membranes of each category will be presented in the following sections. [31, 32, 33, 34, 35, 36]
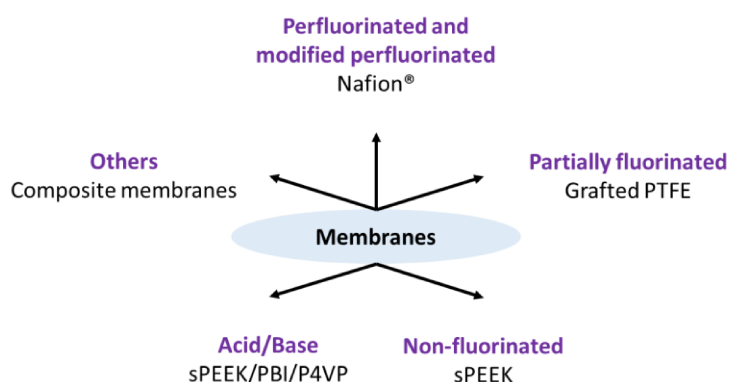
Figure 10. Categories of the different type of proton-conducting membranes.

1.4.1. Perfluorinated membranes

Perfluorinated polymers have grown over the years to be the most used materials for commercially available fuel cell membranes. They are Nafion® (Dupont, USA), Flemion® (Asahi Glass, Japan), Aciplex-S® (Asahi Kasei, Japan), Gore-select® (W.L. Gore, USA), **Figure 11**. Indeed, their high proton-conductivity, good mechanical properties and chemical stability make them a more than suitable candidate for proton-exchange membranes.

Nafion® is the best perfluorinated material for PEMFC. Chemically, they are composed of a linear fluorocarbon polymer chain with long or short chains of pendant acid functions. Those groups are mainly of sulfonic or carboxylic nature. The backbone chain is hydrophobic, and the acidic functions are hydrophilic.
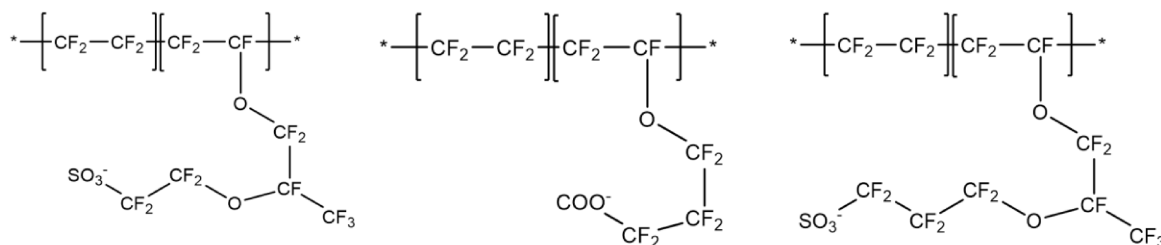
Figure 11. Commercially available perfluorinated membranes, Nafion®, Flemion® and Aciplex®.

The proton-conductivity mechanism of Nafion® has already been studied thoroughly. The particularity of Nafion® is the nano-separation that appears when the hydrophilic acidic function moieties are combined with the hydrophobic fluorocarbon chain. Indeed, from that association results the creation of hydrophilic channels where the proton-conductivity occurs. Under hydration, the protons in the membrane follow the water dynamics for conductivity. [37] For that reason, it is important to determine the correlation between the transport mechanisms of the protons and water in the membrane to understand the proton conduction process. A first description of this transports was made by Gierke and Hsu.[38] Their study consisted of understanding the organization of the material at the very low scale. They proposed a nano-separation of the hydrophilic and hydrophobic moieties as a cluster-network. In this model the separation is defined as "spherical clusters connected by short narrow channels", **Figure 12**. When, in presence of water, the clusters go into a swollen state where their diameter increases from 1.8 to 4 nm and the number of sulfonic groups from 26 to 70 (average values). [38, 39] In another model, the nano structure of Nafion® was not shown as an organized system but rather as a random placement of the hydrated parts in the matrix. It is called the "random network model".[40]
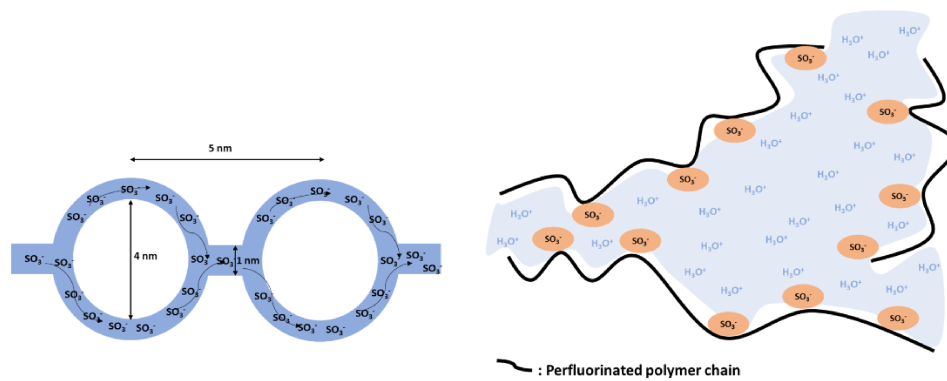
Figure 12. Cluster-network model in PFSA membranes, reproduced from reference. [38]

Concerning the proton conductivity in the hydrated material, two mechanisms have been proposed. They are : the Grotthus mechanism (or hopping mechanism) [41, 34] and the vehicular mechanism.[42] The choice of one over the other depends on the level of hydration of the material. In the Grotthus mechanism, a proton formed by hydrogen oxidation clings to a water molecule to form a hydronium ion. From this ion a different proton hops to another water molecule and so on and so forth. In this case, this hopping behaviour is made possible by the percolation of water when the material is swollen, **Figure 13**.
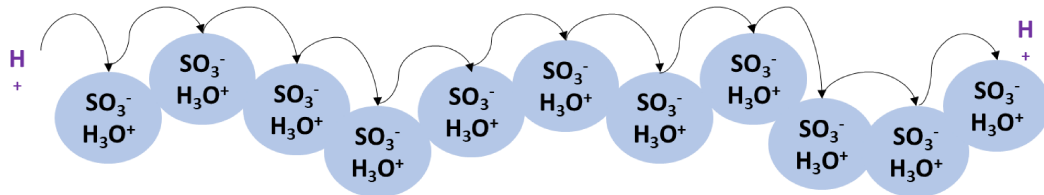
Figure 13. Proton-hopping mechanism, reproduced from reference. [32]

For the vehicular mechanism, hydrated protons are dragged from one part of the membrane to the other by the electroosmotic drag of water which is due to the electrochemical difference in the medium, **Figure 14**. The proton conductivity process has been also been explained theoretically by studying the proton-conduction mechanisms under high and low humidity but this is not the focus of our study.[41, 43]
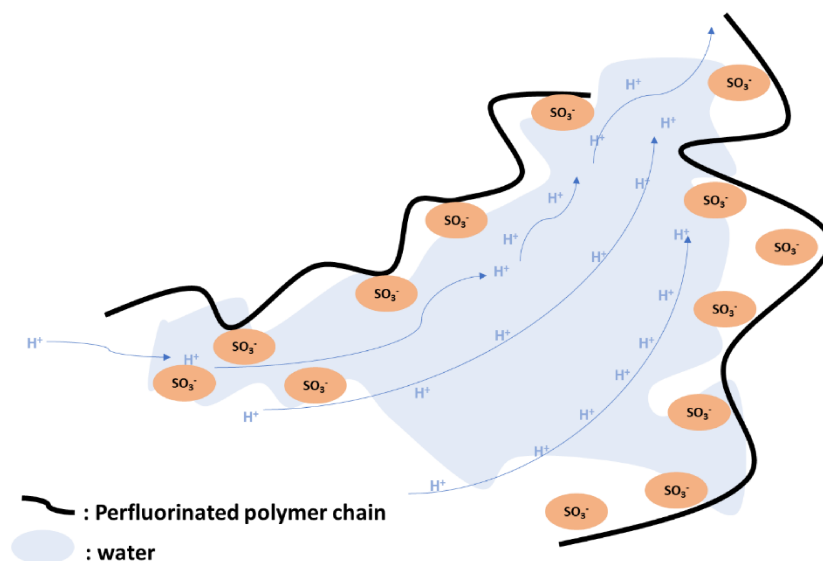
Figure 14. vehicular mechanism, interpreted from reference. [32]

There are two main advantages of Nafion®-like structures for proton-conductive membranes. The first advantage is that the PTFE polymer backbone gives a very good chemical stability to the polymer and the second one is that the hydration provides a good proton conductivity. Nevertheless, the synthesis process of the polymer is long, contains multiple steps and gives toxic reaction intermediates. All contributing to the high cost of manufacture of such membranes. Moreover, it has been shown that the membrane degrades at high operating temperatures. In other to improve the overall properties of Nafion® type membranes, studies have been made on their modification. Those modification involve reducing the membrane's thickness or making composites of PFSA membranes with solid inorganic compounds (eg. Nafion®/SiO_2) or heteropoly acids. [35, 44]

Although Nafion® is a great candidate for PEMFC, it might not be the best for PEM water electrolyser. Indeed, in PEM electrolysers, the membrane is constantly humidified because of its exposure to water needed for the process. Whereas, in PEMFC, the hydration of the membranes comes from the humidified gases. Since the proton-conductivity is dependent on the hydration state of the material, there are chances that this affects the performance of the membrane. Hence the need (in addition to the cost of Nafion®), to look for alternative polymer materials. They are to be described in the following sections.

1.4.2. Partially fluorinated membranes

Partially fluorinated membranes are made of polymers having a fluorinated or partially fluorinated backbone and side chains of non-fluorinated polymers bearing sulfonated groups. The particularity of such membranes is the synthesis of the polymer. Indeed, they are usually synthesized by radiation-induced grafting. The process consists of irradiating a polymer film of the backbone chains by using electron-beam, ɣ-ray, plasma, or UV light to create radicals in the polymer matrix. The film is then put in contact with non-fluorinated monomers which will swell the membrane and the radicals will initiate their polymerization to form grafted networks. Then the residual monomer is washed off and the membrane is sulfonated by immersion in an acid solution, **Figure 15**.
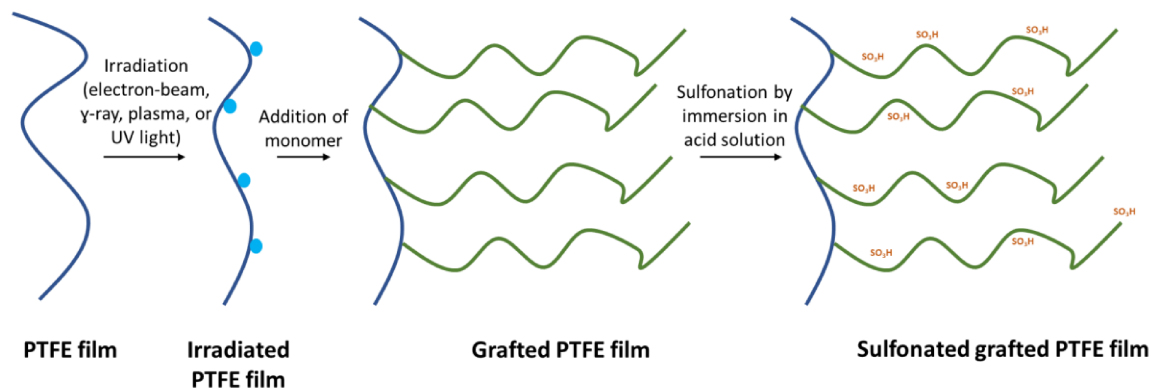
Figure 15. Grafting process of PTFE film by irradiation.

The starting polymer films are mainly poly(tetrafluoroethylene)-PTFE, poly(vinylidene fluoride)-PVDF, poly(ethylene-*alt*-tretrafluoroethylene)-ETFE, and, poly (tetrafluoroethylene-*co*-perfluorovinylether)-PFA. And as side chains poly(styrene), methyl or butyl styrene, divinylbenzene and their copolymers have been used.[45]

Radiation-grafted membranes for water electrolysers are a possible alternative to Nafion® membranes because they have lower hydrogen crossover and area resistance, superior mechanical qualities, and may be less expensive than perfluorinated membranes. But they present a major drawback which is the detachment of the grafted parts. At this weak interaction of the molecules and the polymer backbone, the detachment can be of

different nature. It can be due to swelling and high temperatures of the hydrophilic grafted groups, to the scission weak bonds at the grafting location (-O-O- peroxide bond for example), or to an oxygen-induced type of degradation if the work is not done under inert conditions.[46]

1.4.3. Non-fluorinated membranes

Non-fluorinated membranes are usually made from a hydrocarbon aliphatic and/or aromatic polymeric backbone. They are less expensive than perfluorinated polymers and they are easy to purchase. The thermal and chemical stability of hydrocarbon polymers is usually improved with the addition of aromatic groups. Indeed, the kinetics of fuel cells type devices are increased at higher temperature (100-200°C) thus, having a membrane that is thermally stable will allow to run the cell at optimal conditions. The most common and efficient polymers used in this category are sulfonated polystyrene, polyarylenes, polysulfones, polyimides, and poly(ether ketones). Those polymers at high molar masses can resist temperatures up to 300°C, **Figure 16**.[47]

Sulfonated poly(ether ether ketone) - sPEEK

Sulfonated poly(sulfone) - sPSU

Poly(benzimidazole) - PBI
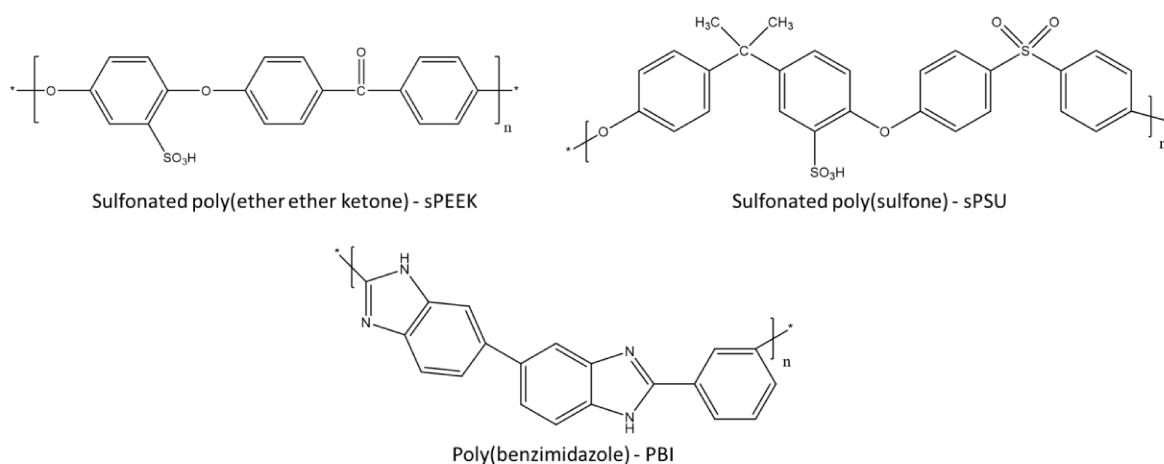
Figure 16. Examples of non-fluorinated sulfonated polymers for membranes application.

Like it has already be mentioned, water uptake and proton conductivity are very important parameters to consider when designing proton-conducting membranes. These parameters are conditioned by the presence and position of the sulfonic moieties in the polymer. Indeed, the sulfonic groups are hydrophilic and interact with water to provide the proton transport. Thus, the higher the degree of sulfonation, the higher amounts of water

the membrane will absorb and the higher the proton conductivity will be. Membranes such as sulfonated poly(oxy-1,4-phenyleneoxy-1,4-phenylenecarbonyl-1,4-pheneylene) (sPEEK) has shown similar behaviour with Nafion® in terms of water uptake. The membranes based on hydrocarbon polymers also perform well in terms of proton conductivities, with values in the order of 10^{-2} S/cm at relative humidity above 90%. And the conductivity was proven to be stable with the increase of temperature. [48]

1.4.4. Acid/Base blends membranes

Acid/Base polyelectrolyte complexes consist of an alkaline polymer (polybase) base doped with an acid component or blended with an acidic polymer (polyacid). The interactions between the polyacid and the polybase create ionic cross-linking or hydrogen bonds which help to reduce membrane swelling while preserving the flexibility of the membrane. Unlike in the case of Nafion® where the conductivity is highly dependent on the humidity rate, the conductivity in acid/base polyelectrolyte complexes is directed by the acid doping and the operating temperature.[32] The polyacid components are generally sPEEK or sPSU (*i.e.* sulfonic moieties) but sulfuric or phosphoric acids can also be used as dopants. The base components are then poly(4-vinylpyridine) P4VP or PBI. [35, 36] The most advanced systems are sPEEK/PBI - 90%/10% membranes that have very good thermal stability (>270°C) and good proton-conductivity (IEC >1.5 meq SO_3H/g).[49] Similarly, PBI doped with H_2SO_4 gave membranes that are also mechanically and thermally stable with conductivity in the order of 10^{-2} S/cm.[35]

Given the advantages and drawbacks of each category of membrane described in the sections above, other alternatives are to improve the performance of perfluorinated membranes while preserving their mechanical, thermal, and chemical stability. The idea is to blend the well-known polymer systems commonly used as membrane materials with other organic polymeric systems or inorganic compounds. In this sense a lot of research has been dedicated to blending or performing structural modification to the existing membrane materials.[44]

2. Copolymers and block-copolymers synthesis

Now that the different types of polymer membranes that are used in PEM fuel cells and water electrolysis have been covered, it is important to talk about their synthesis process. Most of the membranes are made of two components. Indeed, combining (co)polymers with different properties have proven to be beneficial in terms of targeting specific needs for the membranes. In fact, while one (co)polymer can be used to be the protons host, the other can support the mechanical properties of the membrane. Therefore, this section will discuss the synthesis techniques of (co)polymers and in particular block-copolymers which is the objective of this PhD work. Block-copolymers have appealing structural particularities, such as their self-assembly into film by percolating nano-phases, compared to random copolymers, those were proven to help the electrolyte transport and conduction mechanism.[50, 51]

2.1. Definition and properties of copolymers

By definition, a polymer is a macromolecule composed of several monomer units. The number of monomer units is characterized by the degree of polymerization (n or DP > 100 units). When the monomer units are of the same chemical nature, the polymer obtained is called a homopolymer. When two or more monomer units of different chemical nature are used, the macromolecule is then defined as a copolymer. Different types of copolymers exist and they depend on the micro-structure of the monomer units along the macromolecular chain, *i.e.* statistical, alternated, block and grafted copolymers, **Figure 17**.

Statistical copolymers

Alternated copolymers

Block-copolymers

Grafted copolymers
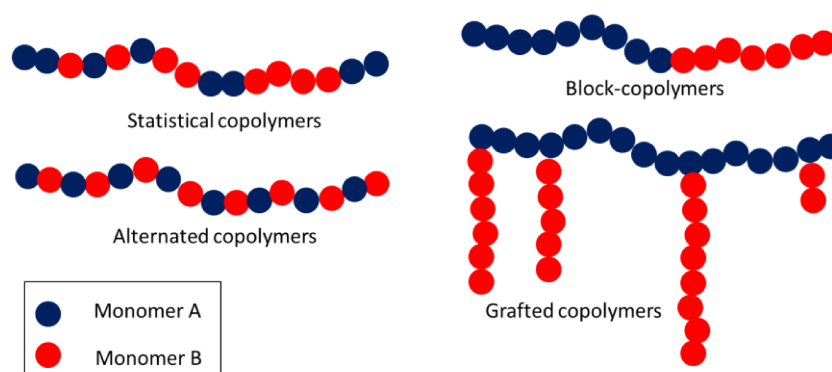
● Monomer A
● Monomer B

Figure 17. Copolymer categories.

Statistical copolymers are the result of a random polymerization of the different monomer units. In alternated copolymers, there is a regular distribution of each monomer unit one after the other in the macromolecular chain. In grafted copolymers, two different strategies can be used: either the second comonomer unit polymerizes from the main chain forming branches or as comomoner with a long sidechain, it is directly copolymerized. These branches can be distributed evenly or randomly along the polymer's main chain with same/different lengths. Usually, none of them can create some nano-phase segregation.

Block-copolymers represent a specific class of copolymers. Indeed, they can be synthesized following two strategies. The first one called "chain extension" is due to active end group which can be used to re-initiate a second monomer. Here we can mention the living process by anionic polymerization or the Controlled Radical Polymerization (NMP, ATRP or RAFT). [52] A second approach consist of a coupling reaction between two end-capped homopolymers with orthogonal functions (acid/alcohol, amino/acid, or azide/alkyne)[53]. Here, in the final form, the two blocks are covalently bonded and one of the main interests is then to combine antagonist properties in the global macromolecule, (*i.e.,* hydrophobic/hydrophilic, or elastomer/thermoplastic).

Moreover, on top of their ability to form different polymer architectures (*e.g.*: linear, star-like, comb-like polymers), block copolymers have the particularity to self-assemble at the nanometer scale. This allows for the synthesis of well-organized material at different level, with the ability of obtaining different properties for the material. Indeed, the macromolecule will have the properties of each of the polymers that makes its composition. Applications for block-copolymers are diverse. They include but are not limited to the medical filed with drug delivery and release [54, 55] or biomaterials [56], lithography for data storage [57], thermoplastic materials [58].

2.2. Synthesis of block-copolymers

Radical polymerization and especially free radical polymerization (FRP) has been the technique of choice for the preparation of synthetic polymers. Indeed, an average of 50% of commercial polymers are synthetized by this technique. It can be performed in homogeneous as well as heterogeneous medias (*e.g.*, emulsion polymerization). This chain polymerization technique has the advantage of being more tolerant to impurities such as water, oxygen, additives than ionic polymerization and is compatible with a broad range of functional vinylic monomers.

As it is the case for all chain polymerizations, three steps are involved in the free radical polymerization: initiation, propagation, and termination reactions. During initiation, the initiator decomposes to form free radicals which will react with the monomer to start a polymer chain. The newly created monomer radical will transfer its active centre by attacking another monomer. By repetition of this process, the chains are extended, and this is the propagation step. Finally, the termination is the end of growth of the polymer chain. It happens because radicals quickly react with each other as a bi-radical reaction. This step is an irreversible termination and can occur by combination of the chains or disproportionation, **Figure 18**. In free radical polymerizations, another type of reaction can occur, transfer reaction. It consists of the transfer of the active centre from one specie to another (solvent, monomer, initiator, polymer). Transfer and termination reactions are competing with the actual polymerization and can occur at any stage of the polymerization.

- **Initiation**
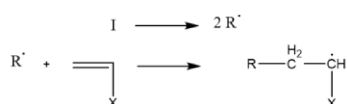
- **Propagation**
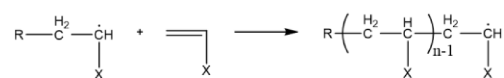
- **Termination**

Combination

Disproportionation
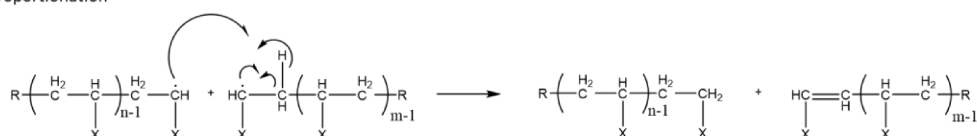
Figure 18. Free radical polymerization process.

Although free radical polymerization FRP is very efficient for polymers synthesis, it does not allow to synthetize polymers with a controlled architecture and molar mass such as block copolymers. Hence the need and development of living/controlled polymerization techniques.

2.3. Controlled radical polymerization

Controlled radical polymerization CRP is a pseudo-living polymerization technique. It is a radical polymerization technique inspired by the living anionic polymerization – first described by *Szwarc* in 1956. By analogy, CRP allows the synthesis of well-defined block-copolymers with low dispersity values (*Đ*). Indeed, CRP compared to FRP uses an additional reactant capable of drastically reducing the concentration of radicals in the medium by introducing a transfer or termination reaction rapidly reversible, creating an equilibrium between active and dormant species. This reversibility can be temperature, photochemical or chemical sensitive and decreases drastically the ratio of irreversible termination. Ideally in controlled radical polymerization, the concentration of active centre is constant throughout time and the degree of polymerization increases linearly with the conversion keeping the dispersity value as low as possible (*Đ* < 1.5).

Different techniques can be found to control the radical process. These techniques depend on the nature of the caping agent used to perform the reversible termination reaction. Among them are: nitroxide-mediated polymerization (NMP), atom transfer radical polymerization (ATRP) and reversible addition-fragmentation chain transfer (RAFT) radical polymerization.

NMP- NMP is the first controlled radical polymerization technique to be established.[59] In NMP an unimolecular alkoxyamine initiator is used for the polymerization. It decomposes upon heat in both initiator radicals and nitroxides. There is a reversibility of the termination step because of the activation/deactivation equilibrium existing between the macro-initiator and the nitroxide. The later acting as a control agent, to allow the control of the polymerization. Due to need of a constant rate of active centre throughout the reaction, there is an importance to tune the nitroxide/initiator ratio. In fact, having too much nitroxide in the media will shift the activation-deactivation equilibrium to dormant species leading to a decrease of polymerization rate. To prevent this from happening and simplify the process once more, unimolecular alkoxyamine initiators were synthetized leading to an even nitroxide/initiator ratio.[60] Quite a few nitroxides and alkoxyamines compounds were synthetized and are used for the NMP technique, **Figure 19**.[61]
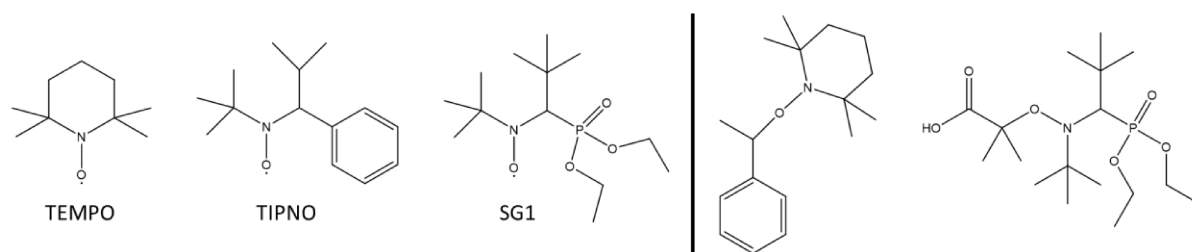
Figure 19. Some examples of typical NMP initiators.

As it is the case for living polymerization, controlled radical polymerization involves two steps: initiation and propagation. During the initiation step, alkoxyamines decomposes into radicals and nitroxide compound. The radicals created react with the monomer to create new radical species. The newly created monomer radical will then react with the remaining monomer in the media to form the polymer chains during propagation. The nitroxide compound is not an initiator but a "controlling agent" that can react reversibly with the propagating species to put them in a dormant state, **Figure 20**. From this polymerization

technique is created a stable macro-initiator which can be used to initiate the polymerization of another monomer to make block-copolymers.
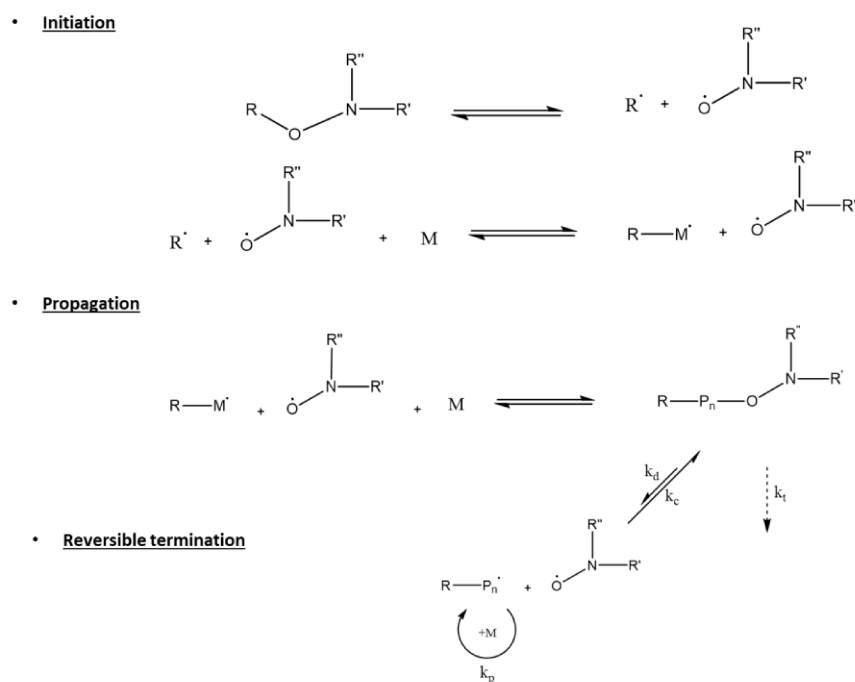
Figure 20. Nitroxide Mediated Polymerization (NMP) process.

The kinetic of polymerization by NMP is dependent on many factors such as the nature of alkoxyamines, the nature of the monomer, reaction temperature and radical concentration. Furthermore, by weakening the cleaving/forming (C-O-N) bond, the kinetic of polymerization can be increased.[61]

ATRP - In this technique, the initiator must carry a transferable halogen, a transition metal catalyst is needed, and some additives may be used for better control. The radicals are created by a reversible redox process catalysed by the metal catalyst complex. During the radical formation process, the transition metal of low oxidation degree collects the halogen of the initiator and creates a cleavage of the carbon-halogen bond. During propagation, the active chain reacts with the metal complex to create a dormant specie that carries a halogen. The equilibrium is shifted toward dormant species to keep the concentration in radicals low in the media. This will provide a better control of the polymerization, **Figure 21**.

- **Initiation**

$$R\text{---}X + M_t^nX/Lig \longrightarrow R^\cdot + M_t^{n+1}X_2/Lig$$

$$R^\cdot + M \longrightarrow RM^\cdot$$

$$RM^\cdot + M_t^{n+1}X_2/Lig \underset{k_{activation}}{\overset{k_{deactivation}}{\rightleftarrows}} RM\text{---}X + M_t^nX/Lig$$

- **Propagation**

$$RM^\cdot + M \longrightarrow P_n^\cdot$$

- **Reversible termination**

$$P_n^\cdot + M + M_t^{n+1}X_2/Lig \underset{k_{activation}}{\overset{k_{deactivation}}{\rightleftarrows}} P_n\text{---}X + M_t^nX/Lig$$

- **Irreversible termination**

$$P_n^\cdot + P_m^\cdot \longrightarrow P_{n+m}$$
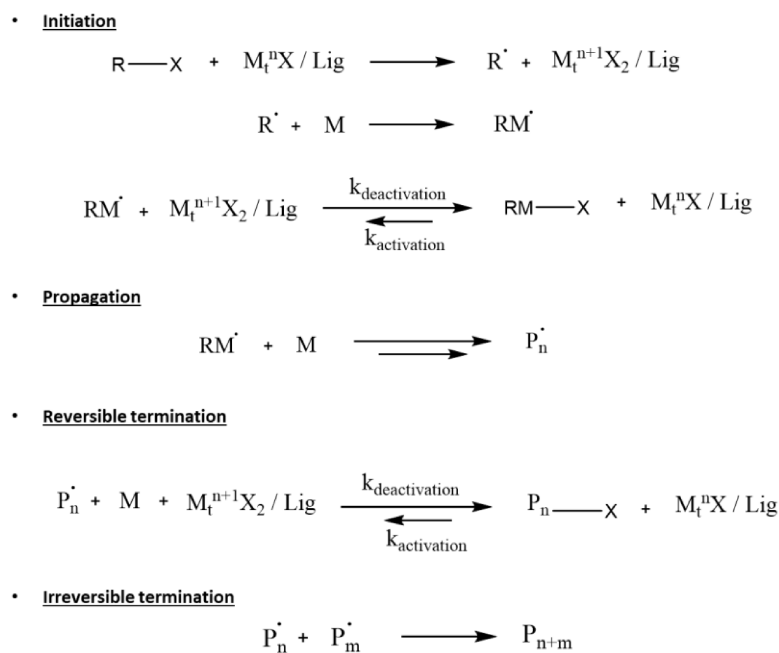
Figure 21. Atom Transfer Radical Polymerization (ATRP) process.

The choice of initiator is mainly determined by the nature of the halide group used. Indeed, the halide must rapidly travel between the growing chain and metal complex. Meaning that the carbon-halogen bond must be weak enough to allow this transition. Bromine or chlorine halides are usually preferred. The catalyst/ligand material dictates the equilibrium between active and dormant species. Copper catalyst is usually chosen both for its performance and low cost. Additionally, the role of the ligand is to help solubilize and stabilize the complex in the media and help for the removal and recycling of the catalyst after reaction. The most efficient ligands for copper catalysts are nitrogen based (*e.g.*, DBU, bipyridine, PMDETA).[62]

RAFT- Reversible addition-fragmentation chain transfer radical polymerization was discovered in 1998 by *Rizzardo* team.[63] The steps necessary to perform RAFT radical polymerization are the same as for the free radical polymerization. In the case of the RAFT, the control of polymerization and the decrease of the radical concentration is dictated by the addition of a transfer agent that reversibly deactivate the growing chains. Indeed, shortly after initiation, the monomer radical reacts with the transfer agent to form the corresponding radical. This step is reversible. This specie will then undergo fragmentation to

create an initiator and a new radical able of initiating polymerization. Termination reactions are drastically reduced with this technique, **Figure 22**.
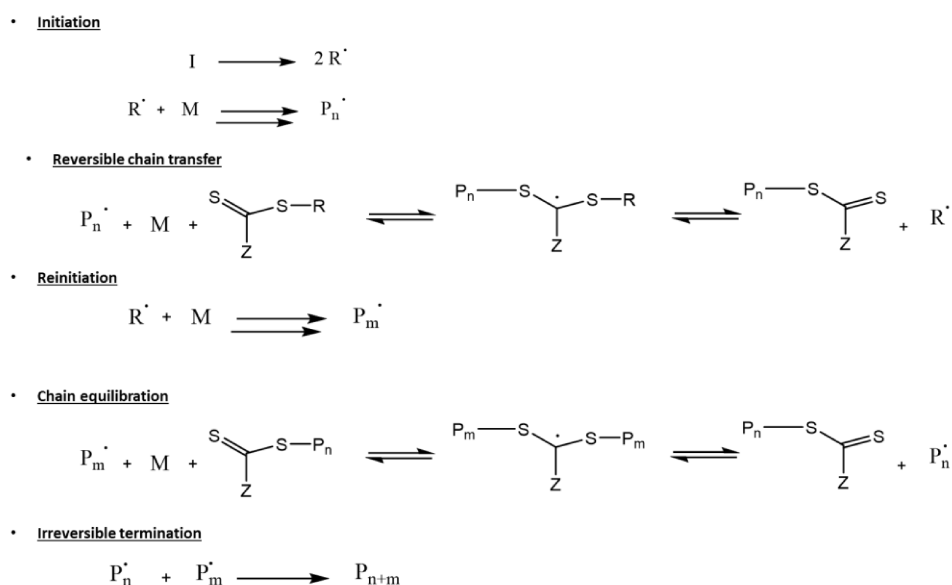
Figure 22. reversible addition-fragmentation chain transfer (RAFT) process.

The RAFT agents used belong to the thiocarbonylthio compounds (eg. Dithiocarbamates, trithiocarbonates, xynthates). The exact choice of compound depends on the nature of the monomer to polymerize. The choice of this compound as well as its concentration influence the efficiency of the polymerization. Conventional free radical polymerization initiators are used for RAFT (*e.g.*, AIBN, $K_2S_2O_8$).[63, 64]

To summarize, block-copolymers can be synthetized by living-ionic polymerization or controlled radical polymerization. Each polymerization techniques requires specific conditions and comes with its drawbacks and advantages. Regardless of the method used to synthetize them, block-copolymers have outstanding structural properties. In fact, they can self-assemble to yield a material that is organized at the nanometre scale.

2.4. Self-assembly of block-copolymers

Block-copolymers self-assembly (BCPs) allows for the obtention of well-structured materials, hence the still growing interest for them. Diblock-copolymers are macromolecules made from two blocks of homopolymers of different chemical nature covalently bonded together. Depending on their nature and properties, both polymers can be miscible or immiscible. They are miscible when their chemical structure and properties are very similar as their solubility parameters, especially. In that case, the BCP will present properties that are intermediate to both blocks and behaves as statistical copolymers.

But now, if immiscible, the BCP system will aim to minimize its interaction in other to achieve a thermodynamic equilibrium. This will result in a decrease of contact at the interface of both blocks. When this happens, the minor block in composition will disperse in the major one, leading to a phase separation. Due to the strong interaction of the covalent bond linking the block, the phase separation can only occur at the very small scale of the macromolecule, meaning at the nanometer scale and not at the macroscopic one. This phase separation is called micro-phase segregation. The parameters dictating the phase separation are the degree of polymerization DP_n, the volume fraction of both blocks in the BCP Φ and most importantly the Flory-Huggins parameter (χ_{AB}). This parameter represents the degree of incompatibility between both blocks and is dictated by the difference of the solubility parameters δ of each monomer units. Moreover, the degree of phase separation is determined by the χN segregation product.[65]

$$\chi_{AB} = \left(\frac{Z}{k_B T} \right) \left[\varepsilon_{AB} - \frac{(\varepsilon_{AA} + \varepsilon_{BB})}{2} \right]$$

With Z is the number of nearest neighbours per monomer unit, $k_B T$ is the thermal energy (with k_B = 1.281 * 10^{-23} J/K, Boltzmann constant), and ε the interaction energy per monomer between A-A, B-B, and A-B.

Depending on the χN segregation product and the temperature, it can be predicted if the regime will tend to be in an ordered state (phase separation) or otherwise a disordered state (mixing of polymer chains). In the case of a symmetric BCP (volume fraction of both

blocks = 0.5), the system is in a miscible state if χN < 10.5. This means that no phase segregation occurs, and the system is in a non-ordered state. With χN = 10.5, the state is at the weak segregation limit (WSL). The segregation strength is weak, the chains incompatibility generates the formation of a microphase separation of the phases. Finally, when χN > 10.5, there is a strong segregation limit (SSL) the system becomes ordered, and the phase separation is clearly noticeable, **Figure 23**.[66]
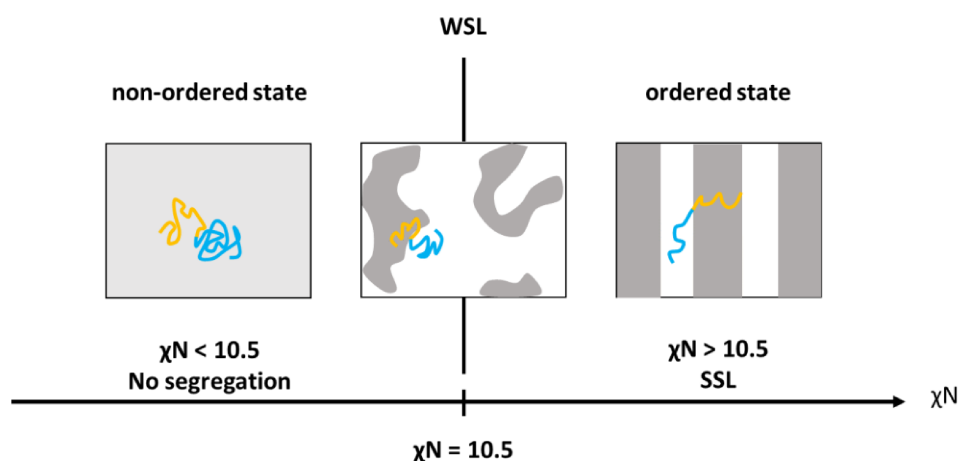
Figure 23. Representation of the order / disorder states of the BCPs depending on the χN parameter.

In addition to the χN value which determines the order to disorder transition of BCPs, the volume fraction of the blocks influences the phase behaviour after segregation. Indeed, the domains' structure is dictated by the volume fraction of one block into the BCP. Microphase separation is induced by the stretching of the BCP chains with the desire of lowering interfacial energy in the BCP. Depending on the volume fraction, the chains will stretch differently leading to different morphologies. Different nanostructures can be obtained with the nano-domains represented by the block with the lowest volume fraction. Those structures are closely packed spheres (CPS), body centered cubic spheres (S), hexagonally packed cylinders (C), bicontinuous gyroids (G) and lamellae (L). From the plotting of both parameters the phase behaviour of the BCP can be illustrated by a block-copolymer phase diagram, **Figure 24**.[65]
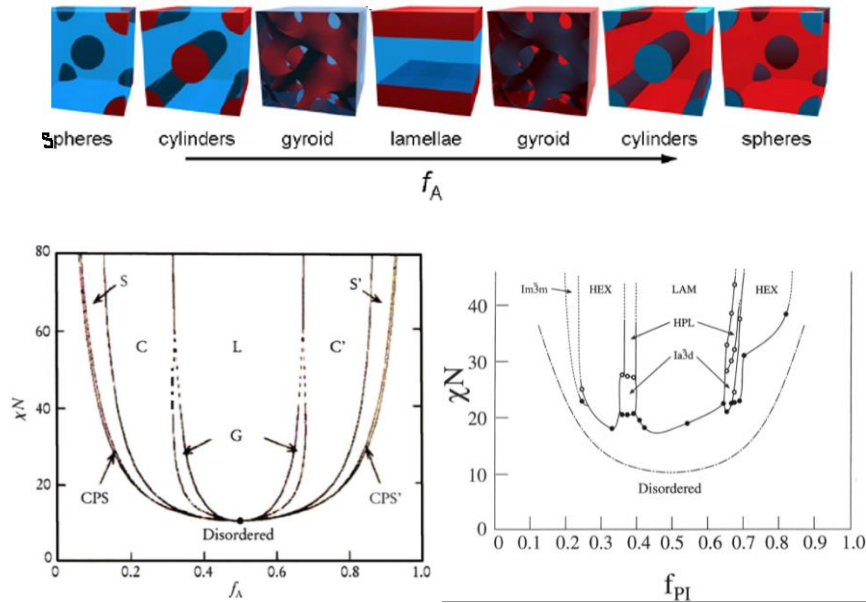
Figure 24. Morphologies after phase separation and Block-copolymer theoretical phase diagram of a linear AB deblock copolymer predicted by the self- consistent mean-field theory (left) Experimental phase diagram of polyisoprene-*b*-polystyrene copolymer, in which f_{PI} represents the volume fraction of polyisoprene (right).[65]

2.5. Block-copolymers for PEM water electrolysis

Due to their easy synthetic methods, statistical copolymers are the most developed materials for proton-conducting membranes.[67] However, in the recent years, an interest was put towards the synthesis of proton-conducting block-copolymers for membrane elaboration. Indeed, the importance of structuration in Nafion® has already been demonstrated to have an influence on the behaviour of proton transportation.[37] Thus, having organised materials such as multi block-copolymers for the proton-conducting membranes should be beneficial to control and drive the proton transport. [68]

As explained in the previous section (2.4.), block-copolymers of two or more blocks of different chemical properties can self-segregate at the nanometre scale. This segregation leading to domains of block A (blue) in the matrix of the block B (red) depending on their volume fraction among other parameters. In this sense, sulfonated block-copolymers will display several advantages such as the existence of proton-conductive channels resulting from the sulfonated domains (blue), **Figure 25**, or, the reduced-swelling properties and

mechanical stability coming from the matrix composed of the non-sulfonated block (red).[69, 70]
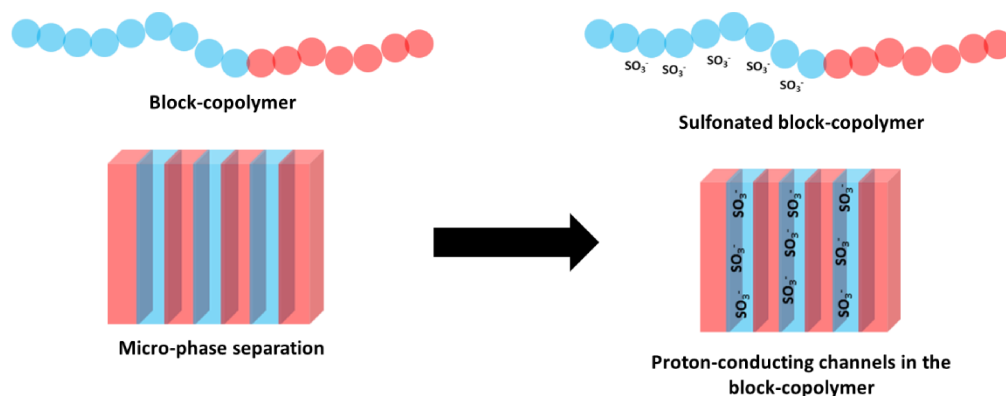
Figure 25. Representation of the BCP self-assembly and sulfonated conductive channels in the BCPs after sulfonation.

In the literature block-copolymers that are mainly used as conducting membranes are sulfonated. The sulfonation is either made post-synthesis of the block copolymers or by using sulfonated monomers for the polymerization. Those sulfonated block-copolymers can be divided into two categories, fluorinated and non-fluorinated block-copolymers. The morphological segregation is expected to be of higher importance in fluorinated BPCs due to the added hydrophobicity fluorine provides.[71, 72, 73]

Early examples of sulfonated amphiphilic BCPs used as proton-conducting membranes are sulfonated poly(sulfone-*b*-vinylidene fluoride), and sulfonated poly(styrene-*b*-isobutylene-*b*-styrene) (s-SIBS). Both gave excellent proton conductivities compared to Nafion®.[74, 75] It was proven for the same category of copolymer that having block-copolymers positively impacted the transport kinetics in the membrane. This observation is the result of the presence of well-defined and connected ionic channels in the BCPs. [51] Additionally, it was found that the conditions in which the membranes are prepared also have an impact on the overall properties of the conduction. Furthermore, the ion content and the interactions between the blocks can impact the properties of the membranes as well. In fact, having high quantities of ions swelling one block can lead to the modification of the morphology of the membrane, even leading to a disruption of the structural morphology. On the other hand, interactions between the blocks can have an impact on the

solubility of the sulfonated BCPs in water. In the case of s-SIBS, poly(isobutylene) acts as physical cross-linker, reducing the solubility of the BCP in water at high sulfonation degrees.[75]

Some sulfonated block-copolymers used don't always display the typical expected morphologies that are on the theoretical BCP phase diagram. But they create interconnected conductive networks architecture in the membrane that also help with the conduction properties. An example is the sulfonated aromatic ABA type triblock copolymer. With the A block as sulfonated poly(2,6-diphenyl-1,4-phenylene oxide) and the B block as poly(arylene ether sulfone). The studies also demonstrated that due to this unique architecture, the membranes were able to compete with Nafion® in term of conductive properties at low IEC (IEC < 1) and lower relative humidity (RH~40%).[76] Similar observations were made for the poly(styrene) (A block)/poly(vinylidene fluoride) (B block) system.[50]

On top of the morphological asset of the BCPs, it was also demonstrated that membrane dehydration that can occur when operating at high temperatures can be minimized by tuning the domains size (< 5 nm). Indeed, at this size, water condensates in the nanochannels due to capillary forces, preventing full evaporation of water.[77, 78] Furthermore, it is known that membrane annealing impacts the morphology adopted by the BCPs. But although some studies state that the conductivity is enhanced when the membranes have gyroids or lamellas morphologies,[77] to the best of our knowledge, no exhaustive work has been reported on the effect of the morphology of the BCPs on the conductivity of the membranes.[79]

3. Bulk sulfonation of polymers

Polymer's sulfonation follows the same functionalization principles as small molecules. Usually, they are made by substitution of atoms or functional groups in the backbones or pendant groups of the polymers. They result in a chemical modification of the material bringing to it new properties. This section will discuss the different ways used for polymers sulfonation in bulk for membrane applications.

In the polymers, the sulfonated parts can be found in the form of free acids (-SO$_3$H), salts (-SO$_3^-$Na$^+$) or esters (-SO$_3$R). To undergo sulfonation, the polymers must have aromatic rings or have double bonds in their structure. Indeed, the process of sulfonation is an electrophilic substitution where the protons of the aromatic ring are substituted by sulfonic acid when in presence of a sulfonation agent. The sulfonation agents can be categorized in two groups, which are strong and mild agents. The strong agents include but are not limited to sulfuric acid and chlorosulfonic acid and the mild group acetyl sulfate, sulfur trioxide complexes and trimethylsilyl chlorosulfonate.

The difference between both groups is that in the case of the strong agent there are risks of degradation of the polymer because of how reactive they are whereas with the mild agent a control of the sulfonation is more feasible (by considering the concentration of sulfonation agent, reaction time and temperature) with less side reactions occurring. In both cases, if the degree of sulfonation is too high, the polymer becomes water soluble.[80] The choice of the sulfonating agent to perform the functionalization resides on the compatibility it has with the polymer. Sulfuric acid, chlorosulfonic acid and acetyl sulfate can be used to sulfonate polysulfones, polystyrene, poly(phenylene oxide), polycarbonates and poly(hydrocarbons). Usually the experimental conditions involve a solvent, mild conditions and multiple separation and cleaning steps. [81]

Sulfonation can also be performed on the monomers before polymerization to avoid polymer chain degradation. It is also a way to introduce sulfonic groups into polymer backbones. Furthermore, with this method the degree of sulfonation is easily targetable. The drawbacks of this approach are that commercially available sulfonated monomers are not many and that the reactivity of the monomers can be lowered due to steric hindrance, making high molecular weight polymers difficult to obtain.[82] Sulfonated dihalo, bisphenol and diamine monomers are the most used. They are used to make polyarylene, poly(ether ether ketone), poly(arylene ether ketone) or poly(arylene ether sulfone), **Figure 26**.[80]
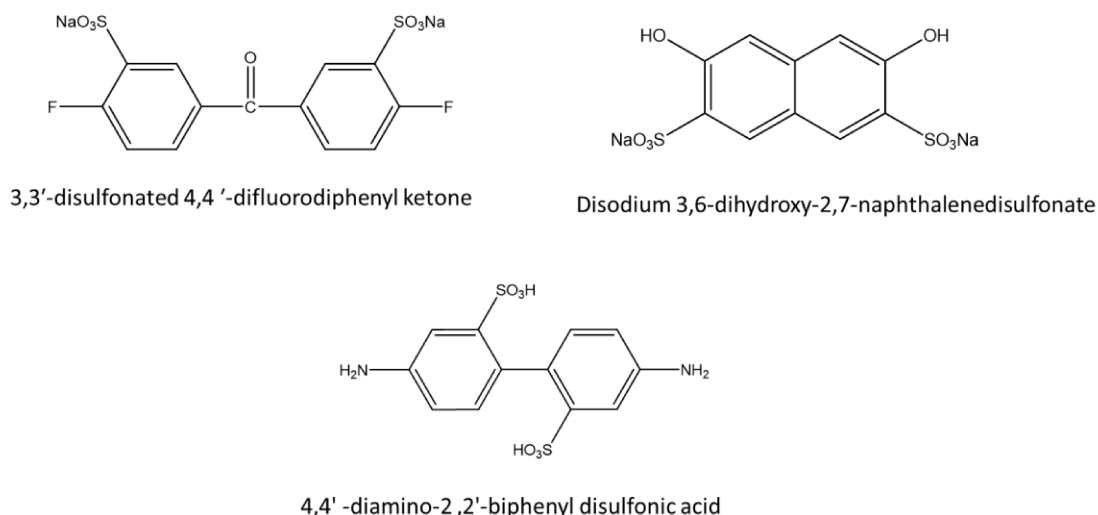
Figure 26. Example of sulfonated monomers.

Another approach for sulfonation of polymers is the grafting of the sulfonic moieties as side chains. This approach will give membranes that have added flexibility and the membranes that are phase separated with the hydrophobic backbone and hydrophilic grafted side chains. Grafting and can be performed on both non fluorinated or perfluorinated polymers.[83, 84] Famous reactions like click-chemistry [85] and *para*-thiol modification of fluorine in *para* position of an aromatic ring are also employed to make proton-conducting membranes [86, 87, 88].

4. Summary and objective of the PhD project

My PhD research is dedicated to the development of proton-conducting membranes. The aim of this literature chapter has been focused on that specific component of the PEM electrolyser. To date, the commercially available PEM displaying the best performance is Nafion®. However, Nafion® fabrication is a complex multistep process and this factor is contributing to the high cost of the membranes. In the objective of reducing the cost of PEM while improving the conductivity, mechanical and thermal properties of the membranes, other type of polymers were developed. They usually consist of perfluorinated and partially fluorinated polymers, as well as non-perfluorinated and polymer blends. The modification of already existing membranes has also been studied. Indeed, mixing of Nafion® with inorganic compounds or polymers from the other categories has proven to enhance the overall properties of the membranes. Moreover, by using hydrocarbon-based polymers, the cost of the membranes is significantly lowered. Plus, those polymers are widely commercially available.

The membranes are sulfonated for the proton-conduction. The sulfonation is provided to the membranes either by grafting of a sulfonated compound or by chemical modification the polymers end groups. The sulfonation can be done after the synthesis of the polymer by post-modification of the latter or by using a sulfonated monomer for the polymerization. The second option is less common due to the difficulty to find commercially available sulfonated monomers. Nevertheless, post-modification is a mature process. It can be done in the bulk by dissolving the polymer in an adequate solvent and using the adequate sulfonating agent. Post-modification is also possible at the surface of the membrane. By doing so the mechanical structure of the membrane is not impacted.

The factors influencing the proton conduction are also discussed in the chapters. This study was principally made on Nafion®. It was shown that the proton conduction in Nafion® is influenced by the separation of the hydrophilic sulfonated group from the hydrophobic polymer backbone. This separation plus the water dynamics creates interconnected conducting clusters providing the membrane with efficient proton-transport. Knowing that, studies were made to develop similar conduction properties with the other alternatives to Nafion®. Block-copolymers have emerged as potential candidates. Indeed, amphiphilic block

copolymers can phase separate and for different morphologies, leading to structures at the nanometer scale. In this way, water will preferably go to the hydrophilic block, optimizing the proton transport. Moreover, their mechanical properties are a combination of the properties of all the blocks. So, while the hydrophilic block drives the proton transport, the other block act helps with the overall mechanical properties of the membranes. Due to these great properties, membranes made from sulfonated block-copolymers displayed better conduction performances than their statistical counterparts. The synthesis of block-copolymers by controlled radical polymerization has also been discussed in this chapter.

The main objective of the present PhD thesis is to make sulfonated partially fluorinated block-copolymers membranes for the eSCALED water electrolysis device. The hydrophilic block is sulfonated poly(pentafluorostyrene) and the hydrophobic block is poly(butylacrylate). A section has been dedicated to the synthesis of the diblock-copolymer and its phase separation behaviour. Another section focused on the sulfonation and crosslinking of the block-copolymer and statistical copolymers by post-modification and the membranes elaboration and characterization. All the research was made with keeping in mind the requirements of PEM which are: good chemical, and mechanical stability; thermal and hydrolytic stability; high proton conductivity and compatibility with the electrode's materials. The challenges of the membrane electrode assembly (MEA) printing and upscaling were also discussed. Finally, the last chapter of this thesis is dedicated to life cycle assessment (LCA) of the membrane production. LCA will help assess the impact of the production of the membrane on the environment.
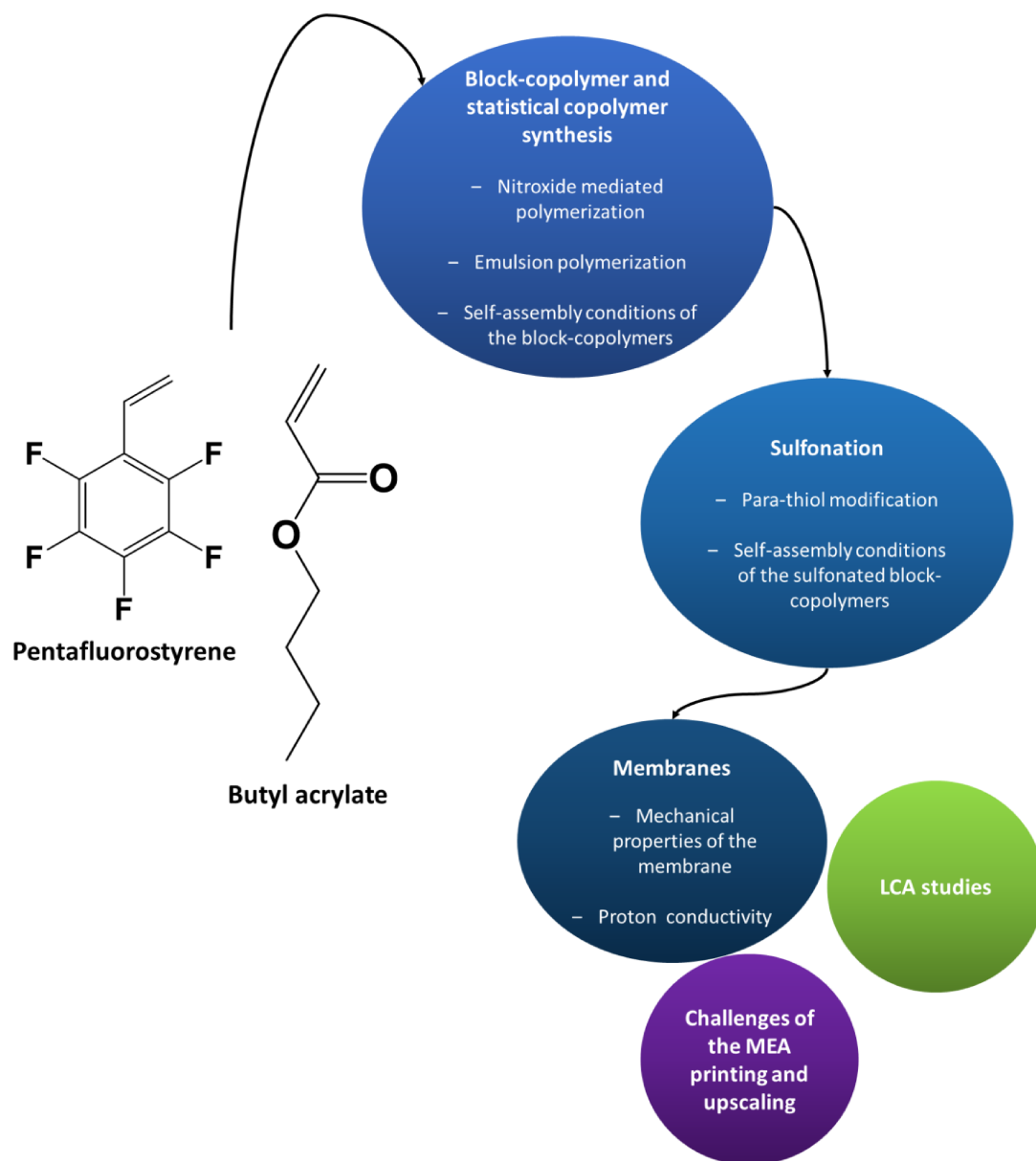
Figure 27. Scheme of the main objectives and challenges of the PhD.

5. References

1. Michaelides E. E. (Stathis), Alternative Energy Sources, Springer-Verlag Berlin Heidelberg, 2012. doi:10.2174/97816080528511120101.

2. Teichmann D., Arlt W., Wasserscheid P. & Freymann R., A future energy supply based on Liquid Organic Hydrogen Carriers (LOHC). *Energy Environ. Sci.* **4**, 2767–2773 (2011). https://doi.org/10.1039/C1EE01454D

3. International Energy Agency. Total final consumption (TFC) by sector, World 1990-2019.https://www.iea.org/data-and-statistics/data-browser?country=WORLD&fuel=Energyconsumption&indicator=TFCShareBySector, 2019 (accessed 24 February 2022).

4. European Environment Agency. Evolution of total European energy RD&D spending by technology (USD-million, 2017 prices) (based on IEA estimates). https://www.eea.europa.eu/data-and-maps/figures/evolution-of-total-european-energy, 2019 (accessed 25 August 2021).

5. Huggins R. A., Energy storage: Fundamentals, materials and applications, second ed., Springer International Publishing Switzerland 2010, 2016. doi:10.1007/978-3-319-21239-5.

6. Holladay, J. D., Hu, J., King, D. L. & Wang, Y., An overview of hydrogen production technologies. *Catal. today* **139**, 244–260 (2009). https://doi.org/10.1016/j.cattod.2008.08.039.

7. Muradov, N., Emission-free fuel reformers for mobile and portable fuel cell applications. *J. Power Sources* **118**, 320–324 (2003). https://doi.org/10.1016/S0378-7753(03)00078-8.

8. Hu, X. & Gholizadeh, M., Biomass pyrolysis: A review of the process development and challenges from initial researches up to the commercialisation stage. *J. Energy Chem.* **39**, 109–143 (2019). https://doi.org/10.1016/j.jechem.2019.01.024.

9. Demirbaş, A. & Arin, G., Hydrogen from biomass via pyrolysis: Relationships between yield of hydrogen and temperature. *Energy Sources* **26**, 1061–1069 (2004). https://doi.org/10.1080/00908310490494568.

10. Vigouroux, R. Z., PYROLYSIS OF BIOMASS • Rapid Pyrolysis at High Temperature • Slow Pyrolysis for Active Carbon Preparation. 113 (2001).

11. Kovács, K. L., Maróti, G. & Rákhely, G., A novel approach for biohydrogen production. *Int. J. Hydrogen Energy* **31**, 1460–1468 (2006). DOI: 10.1016/j.ijhydene.2006.06.011.

12. Kapdan, I. K. & Kargi, F., Bio-hydrogen production from waste materials. *Enzyme Microb. Technol.* **38**, 569–582 (2006). https://doi.org/10.1016/j.enzmictec.2005.09.015.

13. Winter, M. & Brodd, R. J., What are batteries, fuel cells, and supercapacitors? *Chem. Rev.* **104**, 4245–4269 (2004). https://doi.org/10.1021/cr020730k.

14. Zeng, K. & Zhang, D., Recent progress in alkaline water electrolysis for hydrogen production and applications. *Prog. Energy Combust. Sci.* **36**, 307–326 (2010). http://dx.doi.org/10.1016/j.pecs.2009.11.002.

15. Ursúa, A., Gandía, L. M. & Sanchis, P., Hydrogen production from water electrolysis: Current status and future trends. *Proc. IEEE* **100**, 410–426 (2012). DOI: 10.1109/JPROC.2011.2156750.

16. Guillet, N. & Millet, P., Alkaline Water Electrolysis. *Hydrog. Prod. By Electrolysis* 117–166 (2015). https://doi.org/10.1002/9783527676507.ch4.

17. Change in the Real Structure of Nickel due to the Ni $\leftrightarrow$ βNiH Phase Transformation. *Mater. Sci. Monogr.* **59**, 322–337 (1991). https://doi.org/10.1016/B978-0-444-98793-8.50017-3.

18. Godwin, I. J. & Lyons, M. E. G., Enhanced oxygen evolution at hydrous nickel oxide electrodes via electrochemical ageing in alkaline solution. *Electrochem. commun.* **32**, 39–42 (2013). http://dx.doi.org/10.1016/j.elecom.2013.03.040.

19. Lyons, M. E. G. & Brandon, M. P., A comparative study of the oxygen evolution reaction on oxidised nickel, cobalt and iron electrodes in base. *J. Electroanal. Chem.* **641**, 119–130 (2010). http://dx.doi.org/10.1016/j.jelechem.2009.11.024.

20. Mauer, A. E., Kirk, D. W. & Thorpe, S. J., The role of iron in the prevention of nickel electrode deactivation in alkaline electrolysis. *Electrochim. Acta* **52**, 3505–3509 (2007). https://doi.org/10.1016/j.electacta.2006.10.037.

21. Rosa, V. M., Santos, M. B. F. & Da Silva, E. P., New materials for water electrolysis diaphragm. **20**, 697–700 (1995). https://doi.org/10.1016/0360-3199(94)00119-K.

22. Pasquini, L., Knauth, P., Pelzer, K. & Di Vona, M. L., Anion-conducting sulfaminated aromatic polymers by acid functionalization. *RSC Adv.* **5**, 56636–56644 (2015).

https://doi.org/10.1039/C5RA03583J.

23.   Hauch, A., Ebbesen, S. D., Jensen, S. H. & Mogensen, M., Highly efficient high temperature electrolysis †. (2008) DOI:10.1039/B718822F.

24.   Larminie, J. & Dicks, A., Fuel Cell Systems Explained, Second ed., John Wiley & Sons LTD, England, 2003. DOI:10.1002/9781118878330.

25.   Marshall, A. Ã., Børresen, B., Hagen, G., Tsypkin, M. & Tunold, R., Hydrogen production by advanced proton exchange membrane (PEM) water electrolysers — Reduced energy consumption by improved electrocatalysis. *Energy* **32**, 431–436 (2007). https://doi.org/10.1016/j.energy.2006.07.014.

26.   Grigoriev, S. A., Millet, P. & Fateev, V. N., Evaluation of carbon-supported Pt and Pd nanoparticles for the hydrogen evolution reaction in PEM water electrolysers. *J. Power Sources* **177**, 281–285 (2008). https://doi.org/10.1016/j.jpowsour.2007.11.072.

27.   Corrales-Sánchez, T., Ampurdanés, J. & Urakawa, A., MoS2-based materials as alternative cathode catalyst for PEM electrolysis. *Int. J. Hydrogen Energy* **39**, 20837–20843 (2014). https://doi.org/10.1016/j.ijhydene.2014.08.078.

28.   Sapountzi, F. M., Gracia, J. M., Weststrate, C. J. (K. J.), Fredriksson, H. O. A. & Niemantsverdriet, J. W. (H.), Electrocatalysts for the generation of hydrogen, oxygen and synthesis gas. *Prog. Energy Combust. Sci.* **58**, 1–35 (2017). http://dx.doi.org/10.1016/j.pecs.2016.09.001.

29.   Marshall, A. T., Sunde, S., Tsypkin, M. & Tunold, R., Performance of a PEM water electrolysis cell using Irx Ruy Taz O2 electrocatalysts for the oxygen evolution electrode. *Int. J. Hydrogen Energy* **32**, 2320–2324 (2007). https://doi.org/10.1016/j.ijhydene.2007.02.013.

30.   Carmo, M., Fritz D. L., Mergel, J., Stolen, D., A comprehensive review on PEM water electrolysis. *Int. J. Hydrogen Energy* **8**, 4901-4934 (2013). https://doi.org/10.1016/j.ijhydene.2013.01.151.

31.   Maiyalagan, T. & Pasupathi, S., Components for PEM fuel cells: An overview. *Materials Science Forum* **657**, 143-189 (2010). https://doi.org/10.4028/www.scientific.net/MSF.657.143.

32.   Peighambardoust, S. J., Rowshanzamir, S. & Amjadi, M., Review of the proton exchange membranes for fuel cell applications. *International Journal of Hydrogen*

Energy **35**, 9349-9384 (2010). http://dx.doi.org/10.1016/j.ijhydene.2010.05.017.

33. Hamrock, S. J. & Yandrasits, M. A., Proton exchange membranes for fuel cell applications. *Polym. Rev.* **46**, 219–244 (2006). https://doi.org/10.1080/15583720600796474.

34. Mauritz, K. A. & Moore, R. B., State of understanding of Nafion. *Chem. Rev.* **104**, 4535–4585 (2004). https://doi.org/10.1021/cr0207123.

35. Smitha, B., Sridhar, S. & Khan, A. A., Solid polymer electrolyte membranes for fuel cell applications - A review. *J. Memb. Sci.* **259**, 10–26 (2005). https://doi.org/10.1016/j.memsci.2005.01.035.

36. Kerres, J. A., Development of ionomer membranes for fuel cells. *J. Memb. Sci.* **185**, 3–27 (2001). https://doi.org/10.1016/S0376-7388(00)00631-1.

37. Kreuer, K. D., On the development of proton conducting polymer membranes for hydrogen and methanol fuel cells. *J. Memb. Sci.* **185**, 29–39 (2001). https://doi.org/10.1016/S0376-7388(00)00632-3.

38. GIERKE, T. D. & HSU, W. Y., The Cluster—Network Model of Ion Clustering in Perfluorosulfonated Membranes. *A.C.S.*, 283–307 (1982). DOI:10.1021/bk-1982-0180.ch013.

39. Wang, Y., Chen, K. S., Mishler, J., Cho, S. C. & Adroher, X. C., A review of polymer electrolyte membrane fuel cells: Technology, applications, and needs on fundamental research. *Appl. Energy* **88**, 981–1007 (2011). http://dx.doi.org/10.1016/j.apenergy.2010.09.030.

40. Haubold, H. G., Vad, T., Jungbluth, H. & Hiller, P., Nano structure of NAFION: A SAXS study. *Electrochim. Acta* **46**, 1559–1563 (2001). https://doi.org/10.1016/S0013-4686(00)00753-2.

41. Kreuer, K. D., Proton conductivity: Materials and applications. *Chem. Mater.* **8**, 610–641 (1996). https://doi.org/10.1021/cm950192a.

42. Kreuer, K. -D, Rabenau, A. & Weppner, W., Vehicle Mechanism, A New Model for the Interpretation of the Conductivity of Fast Proton Conductors. *Angew. Chemie Int. Ed. English* **21**, 208–209 (1982). https://doi.org/10.1002/anie.198202082.

43. Dokmaisrijan, S. & Spohr, E., MD simulations of proton transport along a model Nafion surface decorated with sulfonate groups. *J. Mol. Liq.* **129**, 92–100 (2006).

https://doi.org/10.1016/j.molliq.2006.08.015.

44. Zhang, H. & Shen, P. K., Recent development of polymer electrolyte membranes for fuel cells. *Chem. Rev.* **112**, 2780–2832 (2012). https://doi.org/10.1021/cr200035s.

45. Chen, J., Asano, M., Yamaki, T. & Yoshida, M., Preparation and characterization of chemically stable polymer electrolyte membranes by radiation-induced graft copolymerization of four monomers into ETFE films. *J. Memb. Sci.* **269**, 194–204 (2006). https://doi.org/10.1016/j.memsci.2005.06.035.

46. Albert, A., Lochner, T., Schmidt, T. J. & Gubler, L., Stability and Degradation Mechanisms of Radiation-Grafted Polymer Electrolyte Membranes for Water Electrolysis. *ACS Appl. Mater. Interfaces* **8**, 15297–15306 (2016). https://doi.org/10.1021/acsami.6b03050.

47. Asensio, J. A., Borrós, S. & Gómez-Romero, P., Proton-conducting polymers based on benzimidazoles and sulfonated benzimidazoles. *J. Polym. Sci. Part A Polym. Chem.* **40**, 3703–3710 (2002). https://doi.org/10.1002/pola.10451.

48. Rikukawa, M. & Sanui, K., Proton-conducting polymer electrolyte membranes based on hydrocarbon polymers. *Prog. Polym. Sci.* **25**, 1463–1502 (2000). https://doi.org/10.1016/S0079-6700(00)00032-0.

49. Kerres, J., Ullrich, A., Meier, F. & Haring, T., Synthesis and characterization of novel acid–base polymer blends for application in membrane fuel cells. *Solid State Ionics* **125**, 243–249 (1999). https://doi.org/10.1016/S0167-2738(99)00181-2.

50. Xu, K., Li, K., Khanchaitit, P. & Wang, Q., Synthesis and characterization of self-assembled sulfonated poly (styrene-b-vinylidene fluoride-b-styrene) triblock copolymers for proton conductive membranes. *Chem. Mater.* **19**, 5937–5945 (2007). https://doi.org/10.1021/cm071626s.

51. Einsla, M. L., Kim, Y. S., Hawley, M., Lee, H.-S., McGrath, J. E., Liu, B., Guiver, M. D., Pivovar, B. S., Toward improved conductivity of sulfonated aromatic proton exchange membranes at low relative humidity. *Chem. Mater.* **20**, 5636–5642 (2008). https://doi.org/10.1021/cm801198d.

52. Braunecker, W. A., & Matyjaszewski, K., Controlled / living radical polymerization : Features , developments , and perspectives. *Prog. Polym. Sci*. **32**, 93–146 (2007). https://doi.org/10.1016/j.progpolymsci.2006.11.002.

53. Tsarevsky, N. V., Sumerlin, B. S. & Matyjaszewski, K., Step-growth 'click' coupling of telechelic polymers prepared by atom transfer radical polymerization. *Macromolecules* **38**, 3558–3561 (2005). https://doi.org/10.1021/ma050370d.

54. Rösler, A., Vandermeulen, G. W. M. & Klok, H. A., Advanced drug delivery devices via self-assembly of amphiphilic block copolymers. *Adv. Drug Deliv. Rev.* **64**, 270–279 (2012). http://dx.doi.org/10.1016/j.addr.2012.09.026.

55. Agrahari, V. & Agrahari, V., Advances and applications of block-copolymer-based nanoformulations. *Drug Discov. Today* **23**, 1139–1151 (2018). https://doi.org/10.1016/j.drudis.2018.03.004.

56. Lendlein, A. & Kelch, S., Shape-Memory Polymers. *Angew. Chem. Int. Ed. Engl.* **41**, 2034–2057 (2002). https://doi.org/10.1002/1521-3773(20020617)41:12<2034::AID-ANIE2034>3.0.CO;2-M.

57. Puglisi, R. A., Towards Ordered Silicon Nanostructures through Self-Assembling Mechanisms and Processes. *J. Nanomater.* **2015**, (2015). https://doi.org/10.1155/2015/586458.

58. Lu, W., Wang, Y., Wang, W., Cheng, S., Zhu, J., Xu, Y., Hong, K., Kang, N.-G., & Mays, J., All acrylic-based thermoplastic elastomers with high upper service temperature and superior mechanical properties. *Polym. Chem.* **8**, 5741–5748 (2017). https://doi.org/10.1039/C7PY01225J.

59. Solomon, D. H., Waverley, G., Rizzardo, E., Hill, W. & Cacioli, P., Polymerization process and polymers produced thereby. Patent number: 4,581,429 (1986).

60. Hawker, C. J., Barclay, G. G., Orellana, A., Dao, J. & Devonport, W., Initiating systems for nitroxide-mediated 'living' free radical polymerizations: synthesis and evaluation. *Macromolecules* **29**, 5245–5254 (1996). https://doi.org/10.1021/ma951905d.

61. Nicolas, J., Guillaneuf, Y., Lefay, C., Bertin, D., Gigmes, D., & Charleux, B., Nitroxide-mediated polymerization. *Prog. Polym. Sci.* **30**, 813 (2005). http://dx.doi.org/10.1016/j.progpolymsci.2012.06.002.

62. Matyjaszewski, K. & Xia, J., Atom transfer radical polymerization. *Chem. Rev.* **101**, 2921–2990 (2001). https://doi.org/10.1021/cr940534g.

63. Chiefari, J., Chong, Y. K. (B.), Ercole, F., Krstina, J., Jeffery, J., Le, T. P. T., Mayadunne, R.

T. A., Meijs, G. F., Moad, C. L., Moad, G., Rizzardo, E., & Thang, S. H., Living free-radical polymerization by reversible addition - Fragmentation chain transfer: The RAFT process. *Macromolecules* **31**, 5559–5562 (1998). https://doi.org/10.1021/ma9804951.

64. Moad, G., Rizzardo, E. & Thang, S. H., Living Radical Polymerization by the RAFT Process. *Aust. J. Chem.* **58**, 379–410 (2005). https://doi.org/10.1071/CH05072.

65. Mai, Y. & Eisenberg, A., Self-assembly of block copolymers. *Chem. Soc. Rev.* **41**, 5969–5985 (2012). https://doi.org/10.1039/C2CS35115C.

66. Matsen, M. W. & Bates, F. S., Unifying weak- and strong-segregation block copolymer theories. *Macromolecules* **29**, 1091–1098 (1996). https://doi.org/10.1021/ma951138i.

67. Peckham, T. J. & Holdcroft, S., Structure-morphology-property relationships of non-perfluorinated proton-conducting membranes. *Adv. Mater.* **22**, 4667–4690 (2010). DOI: 10.1002/adma.201001164.

68. Li, Y., Roy, A., Badami, A. S., Hill, M., Yang, J., Dunn, S., & McGrath, J. E., Synthesis and characterization of partially fluorinated hydrophobic-hydrophilic multiblock copolymers containing sulfonate groups for proton exchange membrane. *J. Power Sources* **172**, 30–38 (2007). https://doi.org/10.1016/j.jpowsour.2007.04.046.

69. Liu, Y. L., Developments of highly proton-conductive sulfonated polymers for proton exchange membrane fuel cells. *Polym. Chem.* **3**, 1373–1383 (2012). https://doi.org/10.1039/C2PY20106B.

70. Meier-Haack, J., Taeger, A., Vogel, C., Schlenstedt, K., Lenk, W., & Lehmann, D., Membranes from sulfonated block copolymers for use in fuel cells. *Sep. Purif. Technol.* **41**, 207–220 (2005). https://doi.org/10.1016/j.seppur.2004.07.018.

71. Roy, A., Yu, X., Dunn, S. & McGrath, J. E., Influence of microstructure and chemical composition on proton exchange membrane properties of sulfonated-fluorinated, hydrophilic-hydrophobic multiblock copolymers. *J. Memb. Sci.* **327**, 118–124 (2009). https://doi.org/10.1016/j.memsci.2008.11.016.

72. Bae, B., Miyatake, K. & Watanabe, M., Effect of the hydrophobic component on the properties of sulfonated poly(arylene ether sulfone)s. *Macromolecules* **42**, 1873–1880 (2009). https://doi.org/10.1021/ma8026518.

73. Li, X., Andruzzi, L., Chiellini, E., Galli, G., Ober, C. K., Hexemer, A., Kramer, E. J., &

Fischer, D. A., Semifluorinated aromatic side-group polystyrene-based block copolymers: Bulk structure and surface orientation studies. *Macromolecules* **35**, 8078–8087 (2002). https://doi.org/10.1021/ma020463k.

74. Shi, Z. & Holdcroft, S., Synthesis and proton conductivity of partially sulfonated poly([vinylidene difluoride-co-hexafluoropropylene]-b-styrene) block copolymers. *Macromolecules* **38**, 4193–4201 (2005). https://doi.org/10.1021/ma0477549.

75. Elabd, Y. A., Napadensky, E., Walker, C. W. & Winey, K. I., Transport properties of sulfonated poly(styrene-b-isobutylene-b-styrene) triblock copolymers at high ion-exchange capacities. *Macromolecules* **39**, 399–407 (2006). https://doi.org/10.1021/ma051958n.

76. Li, N., Lee, S. Y., Liu, Y. L., Lee, Y. M. & Guiver, M. D., A new class of highly-conducting polymer electrolyte membranes: Aromatic ABA triblock copolymers. *Energy Environ. Sci.* **5**, 5346–5355 (2012). https://doi.org/10.1039/C1EE02556B.

77. Park, M. J., Downing, K. H., Jackson, A., Gomez, E. D., Minor, A. M., Cookson, D., Weber, A. Z., & Balsara, N. P., Increased water retention in polymer electrolyte membranes at elevated temperatures assisted by capillary condensation. *Nano Lett.* **7**, 3547–3552 (2007). https://doi.org/10.1021/nl072617l.

78. Chen, L., Hallinan, D. T., Elabd, Y. A. & Hillmyer, M. A., Highly selective polymer electrolyte membranes from reactive block polymers. *Macromolecules* **42**, 6075–6085 (2009). https://doi.org/10.1021/ma901272s.

79. Elabd, Y. A. & Hickner, M. A., Block copolymers for fuel cells. *Macromolecules* **44**, 1–11 (2011). https://doi.org/10.1021/ma101247c.

80. Park, C. H., Lee, C. H., Guiver, M. D. & Lee, Y. M., Sulfonated hydrocarbon membranes for medium-temperature and low-humidity proton exchange membrane fuel cells (PEMFCs). *Prog. Polym. Sci.* **36**, 1443–1498 (2011). http://dx.doi.org/10.1016/j.progpolymsci.2011.06.001.

81. Smitha, B., Sridhar, S. & Khan, A. A., Synthesis and characterization of proton conducting polymer membranes for fuel cells. *J. Memb. Sci.* **225**, 63–76 (2003). https://doi.org/10.1016/S0376-7388(03)00343-0.

82. Hickner, M. A., Ghassemi, H., Kim, Y. S., Einsla, B. R. & McGrath, J. E., Alternative polymer systems for proton exchange membranes (PEMs). *Chem. Rev.* **104**, 4587–

4611 (2004). https://doi.org/10.1021/cr020711a.

83. Norsten, T. B., Guiver, M. D., Murphy, J., Astill, T., Navessin, T., Holdcroft, S., Frankamp, B. L., Rotello, V. M., & Ding, J., Highly fluorinated comb-shaped copolymers as Proton Exchange Membranes (PEMs): Improving PEM properties through rational design. *Adv. Funct. Mater.* **16**, 1814–1822 (2006). https://doi.org/10.1002/adfm.200500763.

84. Ding, J., Chuy, C. & Holdcroft, S., Solid polymer electrolytes based on ionic graft polymers: Effect of graft chain length on nano-structured, ionic networks. *Adv. Funct. Mater.* **12**, 389–394 (2002). https://doi.org/10.1002/1616-3028(20020517)12:5<389::AID-ADFM389>3.0.CO;2-5.

85. Norris, B. C., Li, W., Lee, E., Manthiram, A. & Bielawski, C. W., 'Click'-functionalization of poly(sulfone)s and a study of their utilities as proton conductive membranes in direct methanol fuel cells. *Polymer (Guildf).* **51**, 5352–5358 (2010). http://dx.doi.org/10.1016/j.polymer.2010.09.041.

86. Han, J., Kim, K., Kim, J., Kim, S., Choi, S.-W., Lee, H., Kim, J.-J., Kim, T.-H., Sung, Y.-E., & Lee, J.-C., Cross-linked highly sulfonated poly(arylene ether sulfone) membranes prepared by in-situ casting and thiol-ene click reaction for fuel cell application. *J. Memb. Sci.* **579**, 70–78 (2019). https://doi.org/10.1016/j.memsci.2019.02.048.

87. Li, Y., Wang, X., Xie, M., Liu, X. & Wang, C., Proton conducting electrolyte membranes derived from novel branched sulfonated poly(ether ether ketone)s with benzimidazole sulfonic acid pendants via thiol-ene click chemistry. *Int. J. Hydrogen Energy* **38**, 16276–16285 (2013). https://doi.org/10.1016/j.ijhydene.2013.10.036.

88. Kim, K., Heo, P., Han, J., Kim, J. & Lee, J. C., End-group cross-linked sulfonated poly(arylene ether sulfone) via thiol-ene click reaction for high-performance proton exchange membrane. *J. Power Sources* **401**, 20–28 (2018). https://doi.org/10.1016/j.jpowsour.2018.08.053.

Chapter 2. Printed electronics for the development of Membrane Electrode Assembly (MEA), studies towards membrane upscaling

Table of contents Chapter 2

During my PhD I performed a stay in Eurecat (Mataró) in the Functional Printing and Embedded Devices (FPED) Unit. There, I studied the use of printing techniques for membranes upscaling. The objectives of the stay were to test printing techniques to find the adequate ones for membrane printing and future upscaling. Preliminary work on a fully printed membrane electrode assembly (MEA) was done using commercial Nafion® as the membrane material, and graphite-composed paste as the electrode's material. This chapter includes an introduction on printed electronics, with an emphasis on two printing techniques (screen and inkjet printing). In addition, the early tests for the development of a printed MEA and preliminary work on PPFS will also be discussed.

1. Introduction

Printed electronics has been an emerging field since the past century as a low-cost replacement method to traditional electronics. They are based on the well-known mass production graphic techniques implemented for printing on paper. The use of these mass production techniques allows the rapid production of thin, lightweight, flexible, and low-cost electronic devices. Printed electronics are used to print conductive, semi-conductive or dielectric materials (inks, pastes, solutions). Those materials are printed on top of suitable substrates to create distinct multi-layered electrical structures such as displays, sensors, capacitors, or electronic circuits.[1] The substrates for printed electronics are various, ranging from flexible, bendable or stretchable substrates such as paper, PET or PU to rigid ones or even textiles. Hence, it can be considered as an easy way to implement mature technology that relies on simple additive processes, with the addition that less time and materials are consumed. Those advantages make printed electronics a highly versatile, and tailor-made technology for the creation of low-cost electronic components in large scale for diverse applications.[2]

In the field of printed electronics, two different printing approaches can be distinguished. They are analogue (conventional) and digital printing.[3] In analogue printing, the pattern printed on the substrate is based on a mask which carries the printing information. The printing is made through direct contact between the substrate and the

printing equipment. Digital printing on the other hand does not require a mask since the pattern is printed without physical contact between the substrate and the printing equipment. The choice of the printing technique should be made by taking into consideration the printing resolution, the desired thickness, homogeneity, printing speed and materials (inks and substrates). Analogue printing includes techniques such as screen-printing, gravure, lithography, flexography and offset. Digital printing includes non-impact inkjet printing, thermography, photography, or electrophotography.[3] A comparison between the most common printing techniques is presented in **Table 1** . As each printing technique presents advantages and drawbacks, it is usual to combine and/or modify them to improve printability and performance. Screen and inkjet printing are the most used techniques in printed electronics as they are the least expensive to implement at the first stages of research. Both techniques have been studied during my stay in FPED Unit of Eurecat for the printing of the MEA.

Table 1. Comparative table of common printing techniques.

	Flexography	Gravure	Offset	Screen	Inkjet
Printing form	Relief	Engraved	Flat	Stencil	Digital
Print Resolution (μm)	$30 - 75$	$20 - 75$	$20 - 50$	$50 - 100$	$20 - 50$
Print Speed (m.min^{-1})	$50 - 500$	$20 - 1000$	$15 - 1000$	$10 - 100$	$1 - 100$
Wet film thickness (μm)	$0.5 - 8$	$0.1 - 5$	$0.5 - 2$	$3 - 100$	$0.3 - 20$
Ink Viscosity (mPa.s)	$50 - 500$	$50 - 200$	$20000 - 100000$	$500 - 5e4$	$1 - 40$

Screen-printing is currently the most mature technology employed for the fabrication of printed electronics due to the wide range of substrates that can be used and its low-cost manufacturing aspect. Indeed, screen-printing can be performed on paper, cardboard, plastics, glass, metal, textiles, or ceramics. As in all printing techniques, the formulation of the material to be deposited is a crucial step in the printing process. High viscosities materials, paste-like viscosities (5 – 50 Pa.s) are needed for this technique. They prevent the spread of the material on the substrate after transfer. Moreover, with this technique, there is no obligation for a planar substrate. It can be performed in three different round-to-round

(R2R) assemblies that are: flat-to-flat (or flatbed), round-to-round (or rotary printing), and flat-to-round. The flat-to-flat method consists of transferring the paste through a screen with a movable squeegee (or blade) onto the substrate. The screen is the mask that supports a stencil which forms a negative image. In this case, both the screen and the substrate are flat. For the round-to-round method, the cylindrical printing screen contains the ink which is transferred on the substrate placed on impression cylinders. All the parts of the screen-printer are in rotation with this technique. The flat-to-round technique is a combination of the previous methods, with the use of a flat printing plate and the transfer of the ink on the substrate done by a rotating cylinder, **Figure 1**.[4]
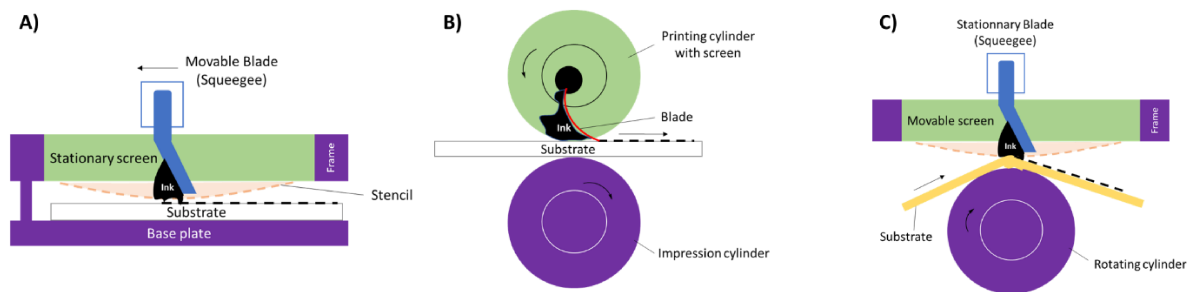
Figure 1. Schemes of the different screen-printing R2R assemblies, (A) flat-to-flat; (B) round-to-round; (C) flat-to-round. Reproduced from [4].

Inkjet is a non-impact and digital printing technology. With this technique, a printed film is obtained after picolitre volumes of ink is expelled from a cartridge through a certain number of micron-sized nozzles directly onto the substrate. As inkjet printing is a non-impact printing technique, there is no need for a screen. The printing is made after the creation of a digital pattern. Hence, the patterns are easily changeable and adjustable. Moreover, high printing resolution over a wide range of substrates is achievable. It is thus easier and cheaper to print different types of design and multiple layers using this technique. Additionally, with an inkjet printer, material consumption is lowered, only the needed quantities of ink for printing are used. Inks for inkjet printing must meet specific rheological requirements such as low viscosities (1 − 40 mPa.s), and surface tensions comprised between 24 − 40 mN/m.[5] Those specific conditions can be restrictive to the type of materials that can be printed by inkjet. Two main configurations of inkjet exist: continuous inkjet and drop-on-demand inkjet. In continuous inkjet there is a constant stream of selectively charged drops. The charged drops are diverted by an electric field, only the uncharged drops

will be printed on the substrate. In a drop-on-demand system, the drops are generated only when they are needed to form the printed film according to the predefined pattern, **Figure 2**. Drop-on-demand inkjet is characterized by smaller ink drop size and better placement accuracy. The ink drops are ejected by a pressure pulse created inside the ink filled. The pressure pulse can be created by three different stimuli: thermal pulse, electrostatic force, or a piezoelectric actuator. The thermal pulse creates a bubble, by vaporization of the liquid component of the ink, exerting pressure on the remaining ink and subsequently ejecting a drop. The electrostatic force is caused by an electric field between the ink and the substrate. When the piezoelectric actuator is used, the ink drops are ejected upon a volume change inside the ink chamber. The ejection is due to the deformation of the actuator caused by an applied electric field.[4, 6, 7, 8]
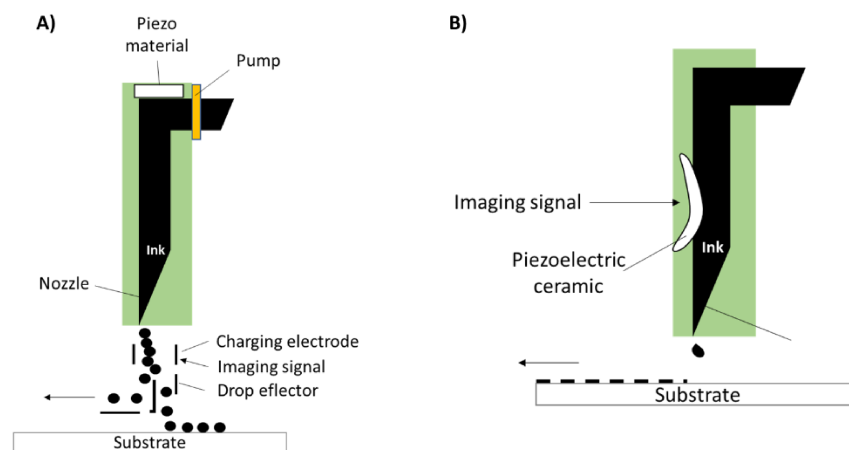
Figure 2. Schemes of the two main inkjet configurations (A) continuous; (B) piezoelectric drop-on-demand. Reproduced from[4].

A typical MEA is composed of a polymer membrane sandwiched between two electrodes. The electrodes are carbon-based materials loaded with catalysts. For that reason, the experiments were conducted using a graphite-composed paste for the electrodes and commercially available Nafion® for the membrane (Nafion® is the material of reference for our studies).

Two structure systems were studied. The idea was to make a supported device and an unsupported one. The difference between both is that with the supported device, the MEA is deposited on a substrate, **Figure 3**.
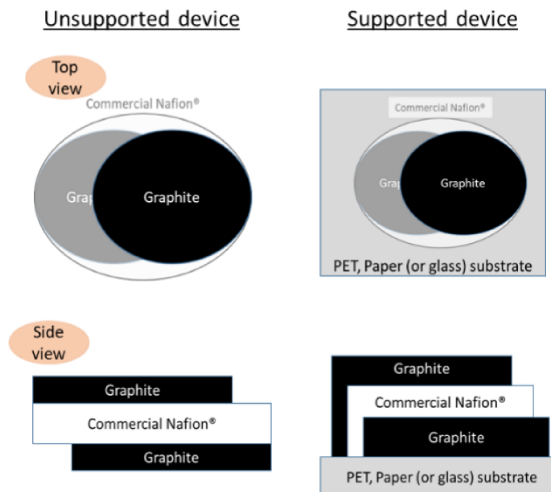
Figure 3. Top and side views of the unsupported and supported printed devices.

Before achieving the devices, experiments were made on the formulation of the Nafion® ink and graphite-based paste. Then, the properties of the printed materials were assessed (thickness, resistance). To do so, for the membrane, Nafion® was printed on PET and glass (microscope slides). This experiment allowed to test the printing of the membrane on two types of substrates. A flexible one that is 125 µm thick PET and a rigid one that is glass, the material's thickness is easily measured on the glass substrate using a profilometer. For the electrodes, the paste was printed on PET and paper. This time paper is a porous substrate that is convenient for paste-like formulas but not recommended for liquid formulas due to the absorption of the ink by paper. For the unsupported device, the electrodes ink was directly printed on a commercial Nafion® membrane 50 µm sheet. Both screen and inkjet printing were used to print a MEA. As we want to achieve the printing of a thin membrane, inkjet will be suitable to really control the thickness of the material and add layers accordingly.[9] The goal for the electrodes is to achieve thicker layers as the conductivity of the films improves with increasing the thickness of the material. However, to obtain this low resistance, the carbon loading in the material must be high. In this sense, screen-printing is the most suitable technique due to the deposition of thicker layers on the substrates. Indeed, in comparison to the other printing techniques, materials printed by screen-printing are the thickest. [3]

2. Experimental section

2.1. Materials.

Graphite powder (synthetic, <20 µm), p-xylene (≥99.0%), Nafion® perfluorinated resin solution (5 wt% in lower aliphatic alcohol and water, 15-20% of water), Nafion® 117 solution, 5% in a mixture of lower aliphatic alcohols and water, Nafion® perfluorinated membrane NRE-212 (50 µm) were purchased from Sigma-Aldrich. MBM (PMMA-*b*- PnBA-*b*-PMMA) polymer pellets were purchased from Kurarity.

2.2. Methods.

2.2.1. Graphite-based paste formulation for the electrodes.

The conductive paste used for the electrodes is composed of graphite, and a binder, dissolved in an adequate solvent. The solvent used for the formulation is p-xylene, and the binder is MBM (PMMA-*b*-PnBA-*b*-PMMA), **Figure 4**. Polymer binders are often added during formulation to increase the material's viscosity. The formulation of the paste was done in the framework of the PhD thesis of Bruno Branco during his stay in the FPED Unit of Eurecat (ESR14 of the eSCALED project). The formulation he used is reported in the first row of the table below, **Table 2**. A second formulation (second row of the table) was made to increase the viscosity of the mixture. Indeed, the paste is formulated for screen-printing so its viscosity must be high (500 – 5.10^4 mPa.s), paste 2 was used for the experiments. The procedure to make the paste consists of mixing MBM with p-xylene at a stirring rate of 750 rpm until complete dissolution (takes approximatively 1.5 hours). Finally, the graphite powder is added to the mixture, and all is stirred until homogeneous dispersion of the graphite powder. The container must be closed during stirring to prevent the solvent from evaporating.
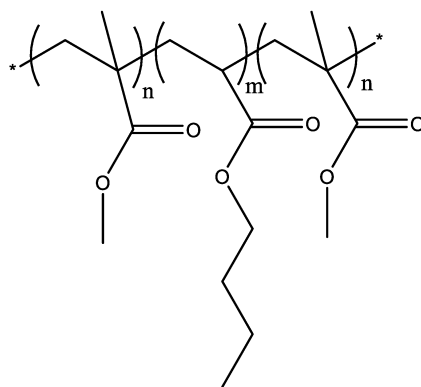
Figure 4. MBM (PMMA-*b*-PnBA-*b*-PMMA) binder.

Table 2. Composition of the Graphite-based paste for screen-printing the electrodes.

	Composition (wt%)		
	Graphite	MBM	p-xylene
Paste 1	23	10	67
Paste 2	25	15	60

2.2.2. Screen-printing. The electrodes were printed with a digital Electric Flat Screen Printer AT-60PD from ATMA topped with 43 mesh screen, (flat-to-flat assembly). The screens contained the designs used for screen-printing, **Figure 5**. The screen on the right has the design created for the eSCALED project the active area of the electrode has a diameter of 0.6 cm. The screen in the middle has a bigger electrode area, 2 cm diameter. The bigger electrode area was used for most of the tests as it is more suitable for the material's characterizations.
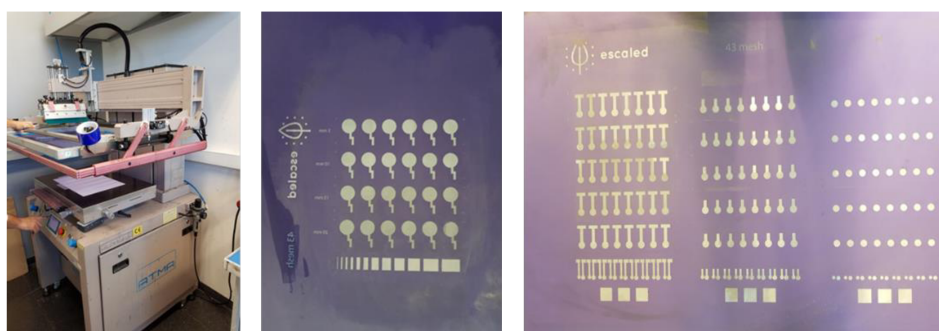
Figure 5. Screen-printer and screens used to print the electrodes.

The printing procedure of the individual electrodes for the supported device was the following:

1. The support materials (PET and Paper) were pre-treated in the oven at 120°C for 15 minutes.

2. Once the substrates are back to room temperature, one layer of the graphite-based paste was printed over the support material. For each layer, two passes with the squeegee were made. The newly printed layer was cured at 85°C for 5 minutes.

3. Step 2 is repeated until the desired number of layers is reached. Once the last layer was printed, the material was cured at 85°C for 10 minutes.

The screen and squeegee used to print the graphite-based paste were cleaned thoroughly with acetone between each layer printing to avoid clogging of the mesh. Indeed, the formulated paste dried quite fast, leading to clogging, and making the cleaning process more difficult. For the unsupported device the layers of graphite-based paste were directly printed on a Nafion® sheet with the same curing procedure as for the supported device. Curing the substrates allow to get rid of any humidity that is present on the surface that can interfere with the printing process.

2.2.3. Inkjet printing. The Inkjet used for the experiments is the Dimatix Materials Printer DMP-2800 Series. It is equipped with a FUJIFILM Dimatix piezoelectric drop-on-demand printhead. Compatible piezo-based jetting cartridge are used with the DMP. The single use cartridge is composed of 16 silicon nozzles aligned in a row. There are 21.5 µm in size and have a nozzle to nozzle spacing of 254 microns. The volume of ink deposited by a nozzle is 10 pL. The volume of ink that can be introduced in the cartridge is [0.2 - 1.5] mL. Nafion® solutions were inserted on the cartridge using a syringe, **Figure 6**. The patterns for the printing can either be drawn by a drawing software like for example CleWin or the Pattern Generator included in the user interface.

Figure 6. Screen-printer and cratridge used to print the membrane.

2.2.4. Dr. Blade. For Dr. Blade printing, Nafion® ink was printed on glass microscope slides and graphite-based electrodes using a ZAA 2300 Automatic Film applicator from Zehntner, always with a printing speed of 60

mm/s.

2.2.5. Profilometry. Profilometry was performed by Dektak 150 Surface Profiler from *Veeco*. The scans were done with a 2.5 μm stylus. The angle of the substrate was adjusted until it was less than 0.2˚. Subsequently, film thickness was obtained as the average step height – ASH. These measurements were repeated three times per sample.

2.2.6. Resistance measurements. Resistance measurements were done with 1906 High Resolution Computing multimeter from *TTi*. These measurements were repeated twice on the same place on the sample.

2.2.7. Viscosimeter. The viscosities of the inks were determined using the Anton Paar rheometer MCR 301. The viscosities of the solutions were measured at room temperature.

2.2.8. Contact angle. The contact angle experiments were performed using the Krüss drop shape analyser DSA100E.

3.   Results and discussion

3.1. Screen-printing the electrodes

Screen-printing is the technique used to print the electrodes. As a reminder, this technique is used for high viscosity materials and provides the layer with a high thickness. Details on the ink's formulation can be found in the experimental section. Up to three layers of ink were printed on each substrate to assess the electrical resistance of the material.

Indeed, by increasing the number of ink layers, the resistance of the material decreased. The electrodes were characterized by profilometry and resistance measurements. Profilometry measurements were made to determine the material's thickness. An increase in thickness was noticed when the number of layers increased. For two layers of ink on PET, the material has a thickness above 30 μm, **Figure 7**.
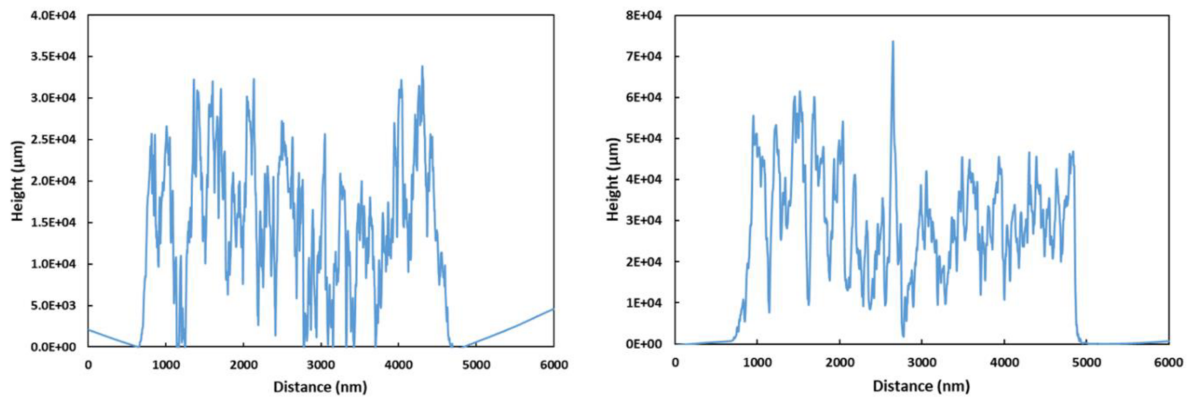
Figure 7. Profilometry measurements on PET: 1 layer of printed graphite-based paste (left); 2 layers of printed graphite-based paste (right).

Profilometry measurement as it was performed was not adequate for the paper substrate because the roughness of paper makes it difficult to measure the thickness of a single layer, **Figure 8**. Indeed, although the material has a paste consistency, paper can still absorb the solvent. PET appears to be the most fitting substrate for the graphite ink, mainly for characterization purposes.
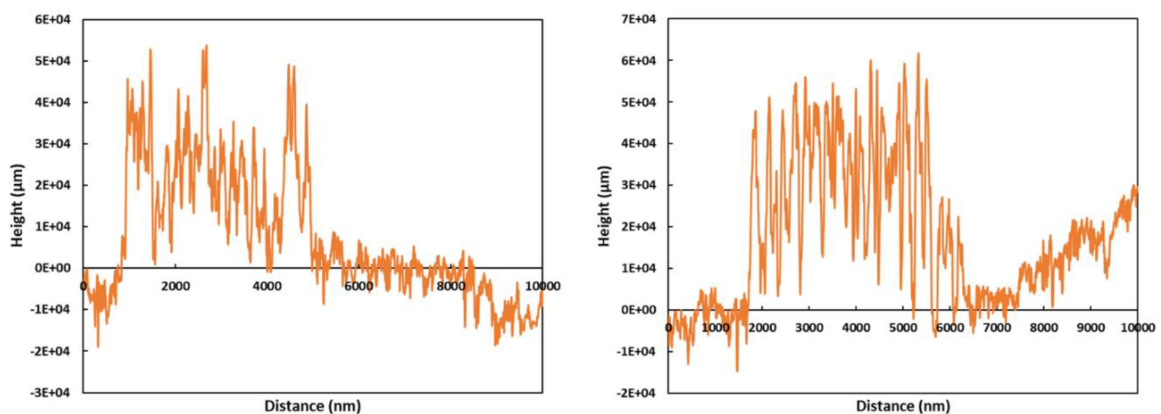
Figure 8. Profilometry measurements on paper: 1 layer of printed graphite-based paste (left); 2 layers of printed graphite-based paste (right).

Concerning the resistance, the graph below, (**Figure 9**), shows the evolution of the resistance in function of the number of printed layers. In fact, it was observed a lowering of the resistance with the increase of layers regardless of the substrate (paper or PET).
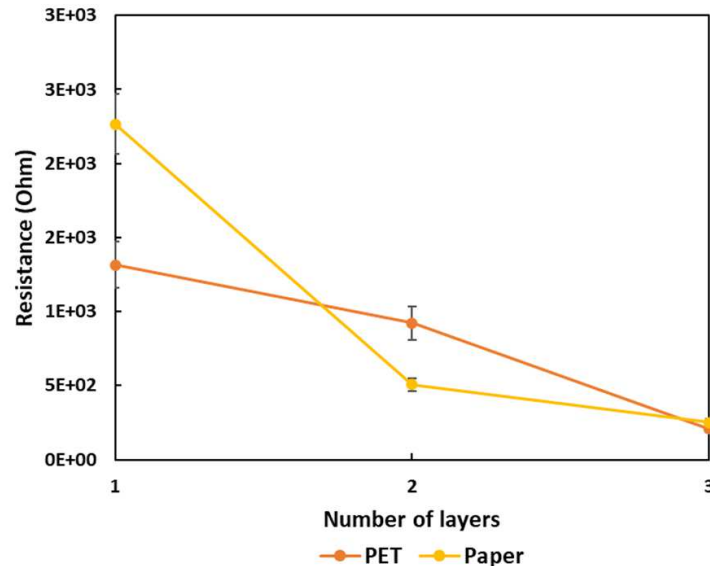
Figure 9. Resistance in function of number of printed graphite-based paste.

3.2. Inkjet printing of the Nafion® membrane

As mentioned in the objectives section, inkjet printing was studied by using commercial solutions of Nafion®. The first step of the study consisted of tuning the Inkjet parameters to achieve a printing of the solutions. Two commercial solutions were used: Nafion®117 and a Nafion® perfluorinated resin solution. They are both at 5% concentration and the Nafion® is in a mixture of water and alcohol. To the best of our knowledge, the difference between both solutions is that the amount of water in the perfluorinated solution is known (15-20 %). Both inks were tested for Inkjet printing. The end material on which the ink will be printed is the graphite-based electrode but to characterize the printed membrane, Nafion® was firstly printed on PET A3 sheets and glass. Designing a pattern is an important step for Inkjet printing. The patterns are easily scalable and can be designed using specific software. To perform the first printing trials, a design with diverse line patterns and with different drop spacing was used, **Figure 10**. The next step after designing the pattern, was the definition of the cartridge settings. Basically, the settings include the number of

layers that are to be printed, the cartridge cleaning cycles, and the number of nozzles used for printing. For the printing of Nafion®, a cleaning cycle of the nozzles was applied before printing and in between each printing cycles. It was noticed during printing that both Nafion® solutions were rapidly clogging the nozzles of the cartridge despite repetitive cleaning cycles. For this reason, the Nafion® solution was diluted to prevent the clogging from happening. In addition, continuous lines were obtained when using the perfluorinated resin solution as the ink. Hence, it was decided to use perfluorinated resin solution to perform the printing of the membrane.
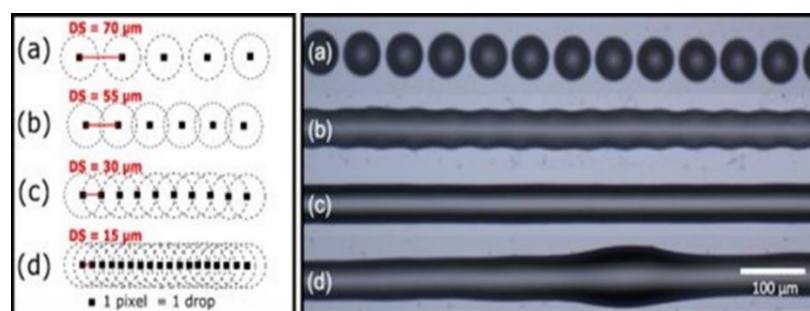
Figure 10. Pattern design specificities

Thus, a dilution of the solution to a 3% Nafion® concentration was performed following what was done in the literature. [2] 1-propanol was used to dilute the commercial perfluorinated resin solution. After dilution, the nozzles seemed to be less clogging. To characterize the thickness of the material, a new pattern was designed using the pattern design functionality included in the inkjet software. The pattern consists of an array of five rectangles – 8x1 mm^2 – where multiple layers (2, 4, 6, 8 and 10) were printed, **Figure 11**. The printing was made on PET sheets and glass microscope slides. Two layers of ink were printed per cycle.
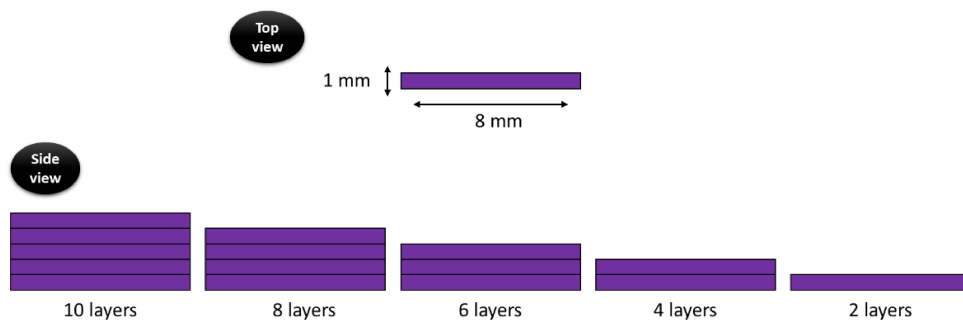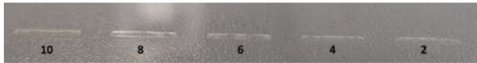
Figure 11. Representation of the pattern design to print layers of Nafion®.

It was noticed that for the printing of the same solution, changing some parameters can influence a lot the aspect of the film (number of nozzles, curing of Nafion®, substrate heating), **Table 3**. The first film printed on PET (PET 1) was smooth and some unevenness around the edges of the film was noticeable. For the second printing on PET (PET2), the substrate was pre-heated at 120°C for 15 mins prior the printing. Moreover, the printed film was cured in the oven at the same temperature and for the same amount of time. The pre-heating changed the energy surface of the substrate and not homogeneous layer was achieved. The last printing was made on glass because it is a rigid substrate which makes it better for profilometry analysis. Over glass the film was dried at room temperature to avoid the change of colour of the material. Indeed, due to its acidity, Nafion® can react with surrounding organic residues leading to its darker colouring. This effect does not impact the performance of the material. [10]

Table 3. characteristics of inkjet printed layers of Nafion®.

	Printing on PET 1	Printing on PET 2	Printing on glass
Photo of the printed Nafion®			
Zoom on one printed rectangle			

Printing parameters			
Number of nozzles	3	1	4
Temperature applied to the substrate	No	No	No
Jet voltage and firing frequency	35 V & 5 kHz	35 V & 5 kHz	35 V & 5 kHz
Curing of the Nafion®	90°C for 15 mins	120°C for 15 mins	Dried at room temperature
Pre-Heating of the substrate	No	120°C for 15 mins	/

The printed membranes were characterized by profilometry, **Figure 12** & **Figure 13**. What was immediately noticed was a profilometry pattern. Indeed, for all the films, there was a presence of more material on the edges of the films than in the middle, this is called coffee-ring effect. Nevertheless, the thickness values were taken where the height of the material was at the maximum. By doing this, an increase of thickness along with the increase of layers' number for PET1 and for the printing on the glass substrate could be observed. However, for PET1 and the glass substrate, a decrease of the thickness after addition of the 10th layer was noticed. This could be explained by the lack of drying time in between layer that could destroy the previously made layers when the material becomes too thick. A longer drying time might be necessary after the 8th printed layer.
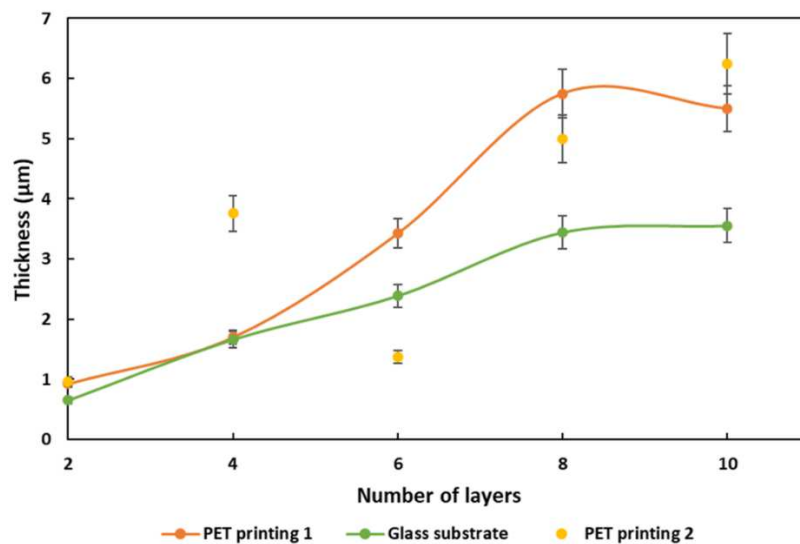
Figure 12. Thickness of membranes printed by inkjet on PET and glass in function of the number of printed layers.
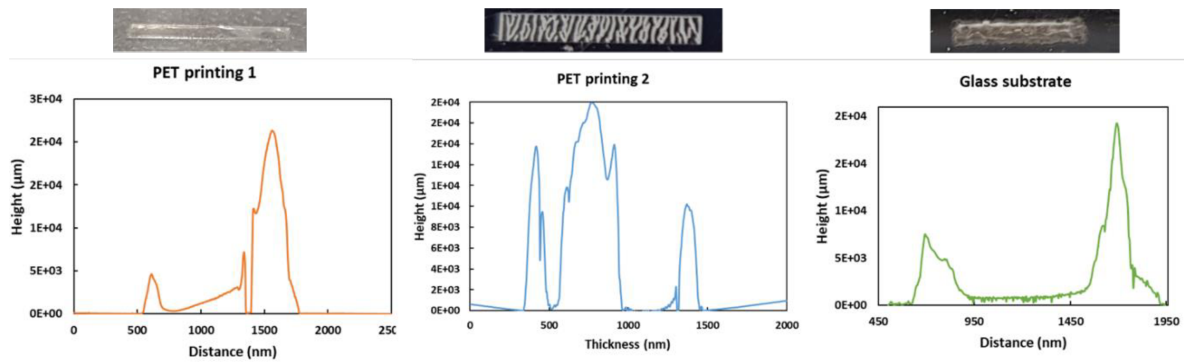
Figure 13. Profilometry measurements of 10 layers of inkjet printed Nafion® for each printing.

A reason for the presence of more material at the edges of the films is due to the evaporation process. The drying process follows the coffee-ring effect.[11] Films printed by Inkjet can have uneven drying resulting in the "coffee stain effect", mainly ascribed to low viscosity inks. This phenomenon is common to every printing technique, but it occurs more often in inkjet printing. The "coffee stain effect" arises from the outward capillary flow induced by the faster evaporation of the solvent at the edges of the films, resulting in printed films that contain more material at the edges, **Figure 14**. [12] This effect influences the printed film morphology and performance. This issue can be tackled by using a mixture of two or more solvents that have different vapor pressures and surface tensions, by increasing the viscosity after deposition or, by drying the droplets under an electric field.
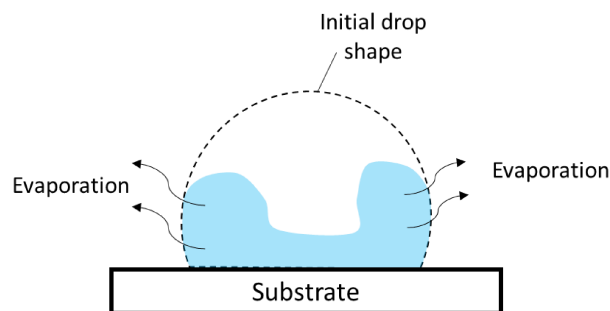
Figure 14. Representation of the drying process of a drop resulting in the coffee-stain effect.

3.3. MEA assembly, unsupported and supported devices

3.3.1. Unsupported device

Finally, MEA of the supported and unsupported devices were made. Printing the unsupported MEA was straightforward as the membrane was commercially purchased and consisted of a Nafion® sheet. On each side of the sheet were screen-printed 4 layers of the electrode ink, **Figure 15**.
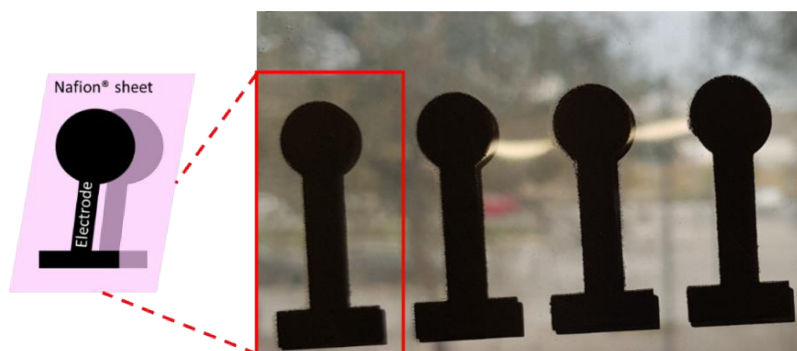
Figure 15. Printed unsupported device, 4 layers of graphite-based paste screen-printed on each side of a commercial Nafion® membrane.

3.3.2. Supported device

For the supported device, the diluted Nafion® solution was printed by inkjet on the electrodes. Those electrodes were printed on PET by screen-printing. The conclusions on printing the membrane on the electrode were that for our system, inkjet is not suitable for printing on large surfaces. Indeed, it took a lot of time to print on the 2 cm diameter electrode and the surface was not fully covered. However, on the smaller electrodes, the active area could be fully covered by Nafion® using Inkjet, **Figure 16**.
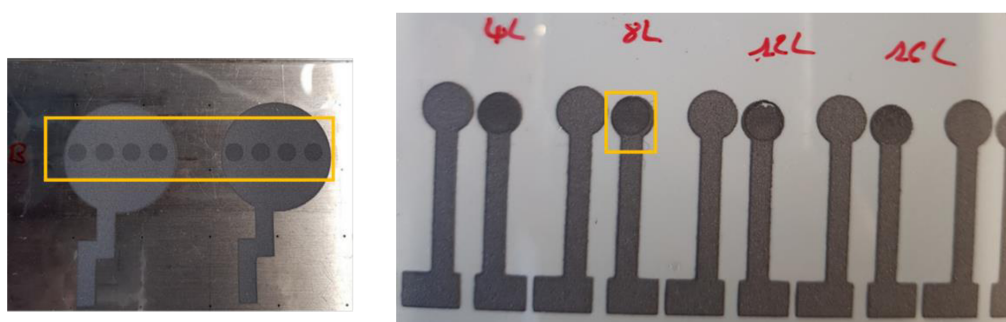
Figure 16. Inkjet printing of the membrane on the printed electrodes, (left) 2cm area electrodes, (right) 0.6 cm area electrodes.

Up to 16 layers of Nafion® were printed. Profilometry was performed on the layers of Nafion® printed on the graphite-based electrodes. At layer 0, the measured thickness is the one of the electrodes (~ 20 µm). There is a decrease of thickness upon addition of Nafion®. The thickness does not increase with the number of added layers [13 − 16] µm, **Figure 17**. This result may be due to the incompatibility between the electrode material and the polymer ink, the polymer solvent is dissolving the layers of the printed electrode paste.
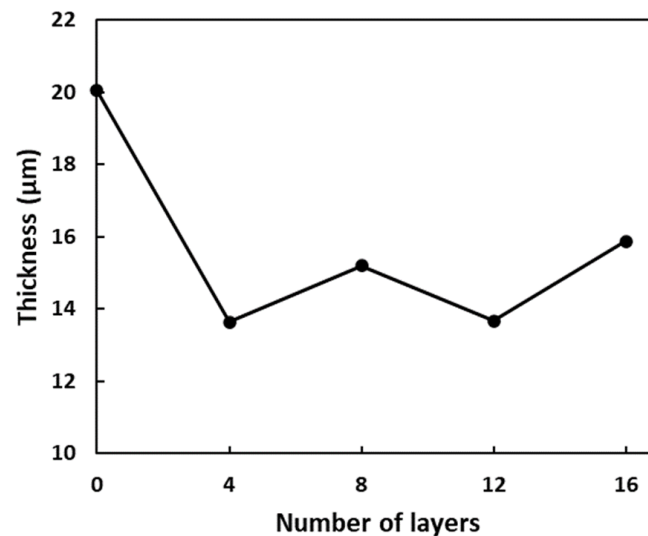
Figure 17. Thickness of inkjet printed Nafion® in function of the number of layers on the 0.6 cm area electrodes.

To cover the entire surface of the 2 cm diameter electrodes, increase the coverage of the number of samples at once, and avoid the high thickness at the edges of the membrane, Dr. Blade was performed. Dr. blade is an alternative thin layer deposition technique to printing, **Figure 18**. The issue observed while Nafion® solution was deposited by Dr. Blade was the spreading of the electrode ink. Because the quantity of membrane solution used with Dr. Blade is more important, the drying process of the layer was made in the oven at 85 °C for 5 minutes.
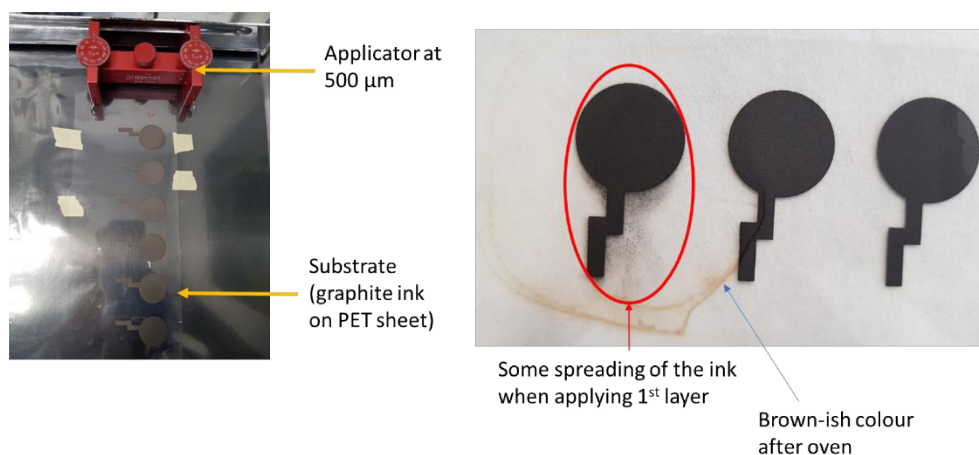
Figure 18. Dr. Blade deposition of Nafion® solution on the 2 cm area electrodes.

Contact angle measurement was performed by dropping the Nafion® solution on the printed electrode. The surface was wetted by the membrane solution with a contact angle of 25°. This observation indicated that the membrane solution is mixing with the electrode ink. Although this mixing is not desired, it should not be an issue if the electrodes are not in contact after final screen-printing of the electrode ink on top of the membranes. The final MEA was made by printing one layer of electrode paste on top of the membrane, **Figure 19**.
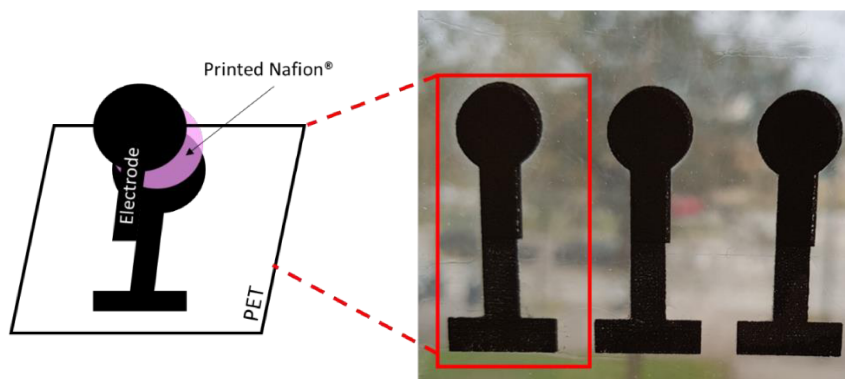
Figure 19. Printed supported device, Composed of: [PET substrate / 3 layers of graphite-based paste (screen-printing) / 1 to 3 layers of Nafion® (Dr. Blade) / 1 layer of graphite-based ink (screen-printing)].

3.4. Preliminary tests with poly(pentafluorostyrene)

Preliminary tests were performed with poly(pentafluorosytrene) (PPFS). The synthesis methods and characterizations are described in depth in the following chapters.

The final membrane consists of a copolymer of PPFS and poly(butyl acrylate) (PBuA). PPFS is the component of the membrane that is sulfonated to give the conductive properties to the material. Attempts at printing PPFS as a membrane were made.

As it was mentioned in this chapter's introduction, the parameters to consider when printing are the ink properties, the wettability of the ink by the substrate and the substrate properties. Hence, the first step consisted of making the PPFS polymer ink. PPFS (M_n = 105 kDa; M_w = 431 kDa; $Đ$ = 4.3) was synthetized during my stay at the Institut für Chemische Verfahrenstechnik (ICVT) group in Stuttgart. It was made my radical polymerization in emulsion. The ink was made by dissolving PPFS in THF. Two solutions were made, at 5 and 10 wt%. The viscosities of the inks were measured. For inkjet printing, PPFS 10% is on the high limits of the acceptable viscosity (1 – 40 mPa.s). The ink is not viscous enough for screen-printing. PPFS 5% on the other hand, has a similar viscosity than the commercial Nafion® solutions, **Figure 20**. Moreover, we notice a decrease in viscosity of the PPFS 10% ink before stabilization when applying shear strain. This behaviour is called shear thinning and in the case of polymers occurs when polymer chains are being disentangled. Indeed, applying the strain will break the interactions between polymer chains. The more the concentration of polymer is, the more this behaviour will be noticeable.
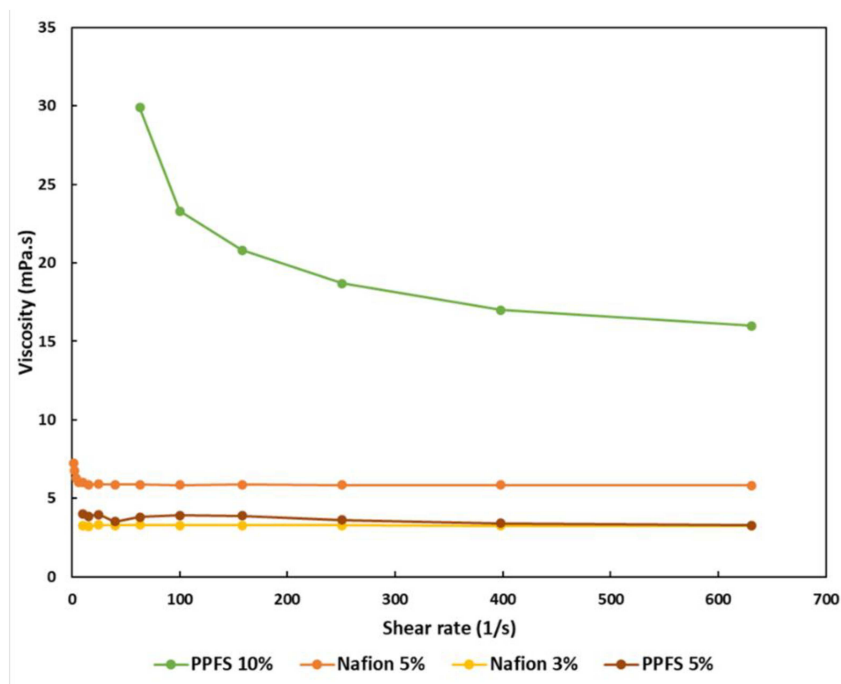
Figure 20. Viscosities of Nafion® and PPFS inks.

The second step in the process is to characterize the material/substrate interface. To do so, contact angle measurements were made with the electrode as a substrate. This technique allows to see the wettability of the substrate by the ink. The surface is considered hydrophilic and wettable if the contact angle is between 0 and 90°, and non-wettable and hydrophobic between 90 and 180°. Contact angles were measured using the commercial Nafion® solution (5%) and both PPFS solutions (5% and 10%). All three inks gave contact angles under 90°. The substrate can then be considered as hydrophilic. Additionally, the commercial Nafion® and PPFS 5% inks have similar contact angle values (~ 25°), **Table 4**.

Table 4. Contact angle measurements of membrane inks (Nafion® and PPFS) on the electrode material.

Ink	Commercial Nafion® 5%	PPFS 10%	PPFS 5%
Contact angle on graphite-based electrode	25.3°	83.4°	24.6°

As we demonstrated before when making the MEA with commercial Nafion®, the PPFS solution made using THF was not compatible with the printed electrode layers. This resulted in a mixing of the membrane solution with the graphite printed material. Considering that PPFS 5% is similarly wetting the electrode and that THF is not the best solvent to use for the development of the ink, further studies will be conducted to improve the printing conditions.

4. Conclusion and challenges to overcome

Supported and unsupported MEA were printed during my stay at FPED Unit of Eurecat. Although the studies shown represent a preliminary work, some challenges to overcome for a successful printing of the eSCALED MEA in the future could be highlighted. The important parameters to consider before printing are the ink properties, the wettability of the surface by the ink and the substrate properties (surface free energy of the substrate). Indeed, the viscosity of the ink will determine the adequate printing equipment to use. The wettability assessed by contact angle measurements allows to determine the compatibility between the substrate and the ink. Indeed, the MEA cannot be performed if the ink does not adhere to the substrate. The number of printed layers is also important. In fact, we saw that the more printed layers of electrode ink, the better the resistance was. The further needed characterizations such as the capacitance measurements and the mechanical properties of the MEA will determine if the printing is efficient and if the choice of the printing techniques are the correct ones. Additionally for the printing of polymers by Inkjet, the polymer characteristics such as its structure, the molecular weight, concentration, and solvent are important parameters to consider.

5. References

1. Keskinen, M., End-of-life options for printed electronics. *Waste Electr. Electron. Equip. Handb.* 352–364 (2012) doi:10.1533/9780857096333.3.352.

2. Graf, M., Gurlo, A., Bârsan, N., Weimar, U. & Hierlemann, A., Microfabricated gas sensor systems with sensitive nanocrystalline metal-oxide films. *J. Nanoparticle Res.* **8**, 823–839 (2006). DOI: 10.1007/s11051-005-9036-7.

3. Rosa, P. A. V. de J., Minimal Computation Structures for Visual Information Applications based on printed Electronics. 1–264 (2015).

4. Kipphan, H., Handbook of Print Media Technologies and production methods, Volume 1, Springer-Verlag Berlin Heidelberg (2001).

5. Aliqué, M., Simão, C. D., Murillo, G. & Moya, A., Fully-Printed Piezoelectric Devices for Flexible Electronics Applications. *Adv. Mater. Technol.* **6**, 1–17 (2021). https://doi.org/10.1002/admt.202001020.

6. Navarro, M. V., Inkjet printing : a flexible manufacturing of functional ceramic coatings by Chemical Solution Deposition. (2014). https://ddd.uab.cat/record/127644.

7. Derby, B., Inkjet Printing of Functional and Structural Materials: Fluid Property Requirements, Feature Stability, and Resolution. *Annu. Rev. Mater. Res.* **40**, 395–414 (2010). DOI: 10.1146/annurev-matsci-070909-104502.

8. Hue P. Le., Progress and Trends in Ink-jet Printing Technology. *J. Imaging Sci. Technol.* **42**, 49–62 (1998).

9. De Gans, B. J., Duineveld, P. C. & Schubert, U. S., Inkjet printing of polymers: State of the art and future developments. *Adv. Mater.* **16**, 203–213 (2004). https://doi.org/10.1002/adma.200300385.

10. PermaPure™. The Basic Physical and Chemical Properties of NafioN™ Polymer. https://www.permapure.com/environmental-scientific/nafion-tubing/nafion-physical-and-chemical-properties/, (accessed 5 December 2021).

11. Aleeva, Y. & Pignataro, B., Recent advances in upscalable wet methods and ink formulations for printed electronics. *J. Mater. Chem. C* **2**, 6436–6453 (2014). https://doi.org/10.1039/C4TC00618F.

12. Deegan, R. D., Bakajin, O., Dupont, T. F., Huber, G., Nagel, S. R., & Witten, T. A.,

Capillary flow as the cause of ring stains from dried liquid drops. *Nature* **389**, 827–829 (1997). https://doi.org/10.1038/39827.

Chapter 3. PentaFluoroStyrene-based Block Copolymers Controlled Self-Assembly Pattern: A platform paving the way to functional block-copolymers

Karell Bosson,[a,b,e] Pierre Marcasuzaa,[a,b] Antoine Bousquet,[b] Günter E.M. Tovar,[c,d] Vladimir Atanasov,[e] Laurent Billon[a,b]

[a] Bio-inspired Materials Group: Functionalities & Self-assembly, E2S UPPA, 64000 Pau, France

[b] Universite de Pau et Pays de l'Adour, E2S UPPA, CNRS, IPREM, UMR5254, 64000 Pau, France

[c] Institute for Interfacial Process Engineering and Plasma Technology IGVP, University of Stuttgart, Pfaffenwaldring 31, 70569 Stuttgart, Germany

[d] Fraunhofer Institute for Interfacial Engineering and Biotechnology IGB, Nobelstr. 12, 70569 Stuttgart, Germany

[e] Institute of Chemical Process Engineering, University of Stuttgart, Boeblingerstrasse 78, 70199 Stuttgart, Germany

Corresponding author: laurent.billon@univ-pau.fr

Table of contents Chapter 3

Review

PentaFluoroStyrene-based block copolymers controlled self-assembly pattern: A platform paving the way to functional block copolymers

Karell Bosson [a,b,e], Pierre Marcasuzaa [a,b], Antoine Bousquet [b], Günter E.M. Tovar [c,d], Vladimir Atanasov [e], Laurent Billon [a,b,*]

[a] *Bio-inspired Materials Group: Functionalities & Self-assembly, E2S UPPA, 64000 Pau, France*
[b] *Universite de Pau et Pays de l'Adour, E2S UPPA, CNRS, IPREM, UMR5254, 64000 Pau, France*
[c] *Institute for Interfacial Process Engineering and Plasma Technology IGVP, University of Stuttgart, Pfaffenwaldring 31, 70569 Stuttgart, Germany*
[d] *Fraunhofer Institute for Interfacial Engineering and Biotechnology IGB, Nobelstr. 12, 70569 Stuttgart, Germany*
[e] *Institute of Chemical Process Engineering, University of Stuttgart, Boeblingerstrasse 78, 70199 Stuttgart, Germany*

ABSTRACT

Diblock copolymers of 2,3,4,5,6-pentafluorostyrene (PFS) and butyl acrylate (BuA) were synthesized by nitroxide mediated polymerization (NMP). By varying the conversion and/or the BuA monomer to PPFS macro-initiator ratio, various molar compositions of the block copolymer BCP were obtained. Due to the immiscibility of both polymeric blocks, phase separation at the nanometre scale occurred. The variety of BCP synthesized gave rise to a large panel of morphologies by self-assembly. The structuration of the nanodomains of PPFS/PBuA BCPs were studied by AFM and SAXS. Nanodomain sizes ranging from 30 to 45 nm depending on the molar mass of the BCP were observed. Moreover, the lability of the fluorine atom in *para* position of the aromatic ring of the PFS units allows for the functionalization of the BCPs. Indeed, the *para* fluorine-thiol soft organo-catalysed substitution was performed with 1-hexanethiol as side group. The thermal properties and the self-assembly pattern of the BCP changes drastically by the incorporation of alkyl moiety, acting as an artificial increase of the volume fraction of the PPFS block and also matching the solubility parameter value of the PBA block, *i.e.* no more nano-pattern is observed by AFM and SAXS.

1. Introduction

Fluorinated polymers are well known for their thermal, chemical, and physical stability. For that reason, they can be used for sensors and cable insulation, membranes, packaging, sealing materials or chemical resistant components [1]. Among them, the most famous polymers are poly(vinylidene fluoride) (PVDF), poly(tetrafluoroethylene) (PTFE), or poly(vinyl fluoride) (PVF). Moreover, fluorinated polymers belong to the category of low surface energy materials, due to their relatively low attraction to other molecules. Therefore, their interfacial energy is low, leading to easy segregation [2]. All those properties make them suitable for the synthesis of block copolymers (BCPs) and their self-assembly. BCPs have gained interest throughout the years for the development of materials with novel properties. Indeed, BCP χ s with immiscible blocks, can microphase separate to form ordered structures. The parameters dictating the phase separation are the volume fraction Φ of both blocks in the BCP and the N segregation product, where χ is the

Flory-Huggins parameter (χ_{AB}) which represents the degree of incompatibility between both blocks and N represents the total degree of polymerization. Depending on the combination of both parameters, different morphologies can be targeted from the self-assembly of BCPs [3]. Properties of such final materials are a combination of the intrinsic properties of the individual polymers forming the blocks at the nanometer scale as well as at the micrometer scale. Thus, there is an interest in having custom-made BCPs for diverse applications such as: drug delivery and release [4,5], biomaterials [6], lithography for data storage [7], or thermoplastic materials [8].

Multiple techniques exist to synthesize BCPs, one of them is multi step living polymerization such as ionic (IP) or controlled radical polymerizations (CRP) [3]. These polymerization techniques allow for the synthesis of polymers with controlled degree of polymerization and low dispersity. Compared to the living ionic polymerization, CRP does not require strict synthetic conditions and a wide variety of functional monomers can be polymerized, which makes it an easier method for the

design of BCPs. Within CRP, different techniques were developed for almost a quarter of century [9,10,11]. The most used are: nitroxide-mediated polymerization (NMP) [12], atom transfer radical polymerization (ATRP) [13] and reversible addition-fragmentation chain transfer (RAFT) [14] radical polymerization. They are differentiated by the reversible termination reaction controlling of the chain growth. The NMP technique, uses an alkoxyamine compound that divides into a radical (initiator) and a nitroxide counter-radical (controlling agent) upon heat. It can react reversibly with the propagating species to put them in a dormant state, creating a macro-initiator that can be used to initiate the polymerization of another monomer to make BCPs. NMP was the chosen technique for the experiments as it is easy to implement with only one compound that gives both an initiator and a controlling agent. Furthermore, there is no need of the removal of the reagent after the reaction and the alkoxyamine could be used for a variety of monomers.

We report here on the efficient synthesis of poly(penta-fluorostyrene)-*block*-poly(butyl acrylate) PPFS-*b*-PBuA block co-polymers (Scheme 1).

We firstly discuss the synthesis of PPFS/PBuA by NMP using the BlocBuilder® initiator as an efficient controlled radical polymerization. Controlled radical polymerization of BCPs using poly(penta-fluorostyrene) have already been reported in the literature, but mainly by ATRP [15–20]. Few examples can also be found describing NMP [21–23] or RAFT [24] polymerizations methods. Additionally, PPFS can be easily modified due to the accessibility of the fluorine in *para*-position of the phenylene group, allowing for countless possibilities for polymer functionalization by nucleophilic substitution. Over the year's attractive post-modification techniques such as click-chemistry have been used for the ease they provide to functionalize polymers. Click-chemistry for *para* fluorine substitutions with azide [25] and thiol [26–28] have already been proposed for PPFS. In the second part of this manuscript, the successful *para* fluoro-thiol modification of the BCPs was performed with 1-hexanethiol (HT) to explore the impact of the alkyl chain on both the glass temperature transition *Tg* and the self-assembly properties of the derivatives BCP. Indeed, the *para*-addition of 1-hexanethiol gives some mobility to the polymer chains. Thus, a brittle to flexible transition is determined by DSC and macroscopically. Additionally, the self-assembly of the BCPs before and after modification with 1-hexanethiol was studied by AFM and SAXS.

2. Experimental section

2.1. Materials

Pentafluorostyrene (99 %, Sigma-Aldrich), butyl acrylate (99 %, Sigma-Aldrich), BlocBuilder® (Provided by Arkema), free-SG1 (83 %, Provided by Arkema), dimethylformamide (DMF, anhydrous, 99.8 %, Sigma-Aldrich), 1-hexanethiol (95 %, Sigma-Aldrich), 1,8-Diazabicyclo
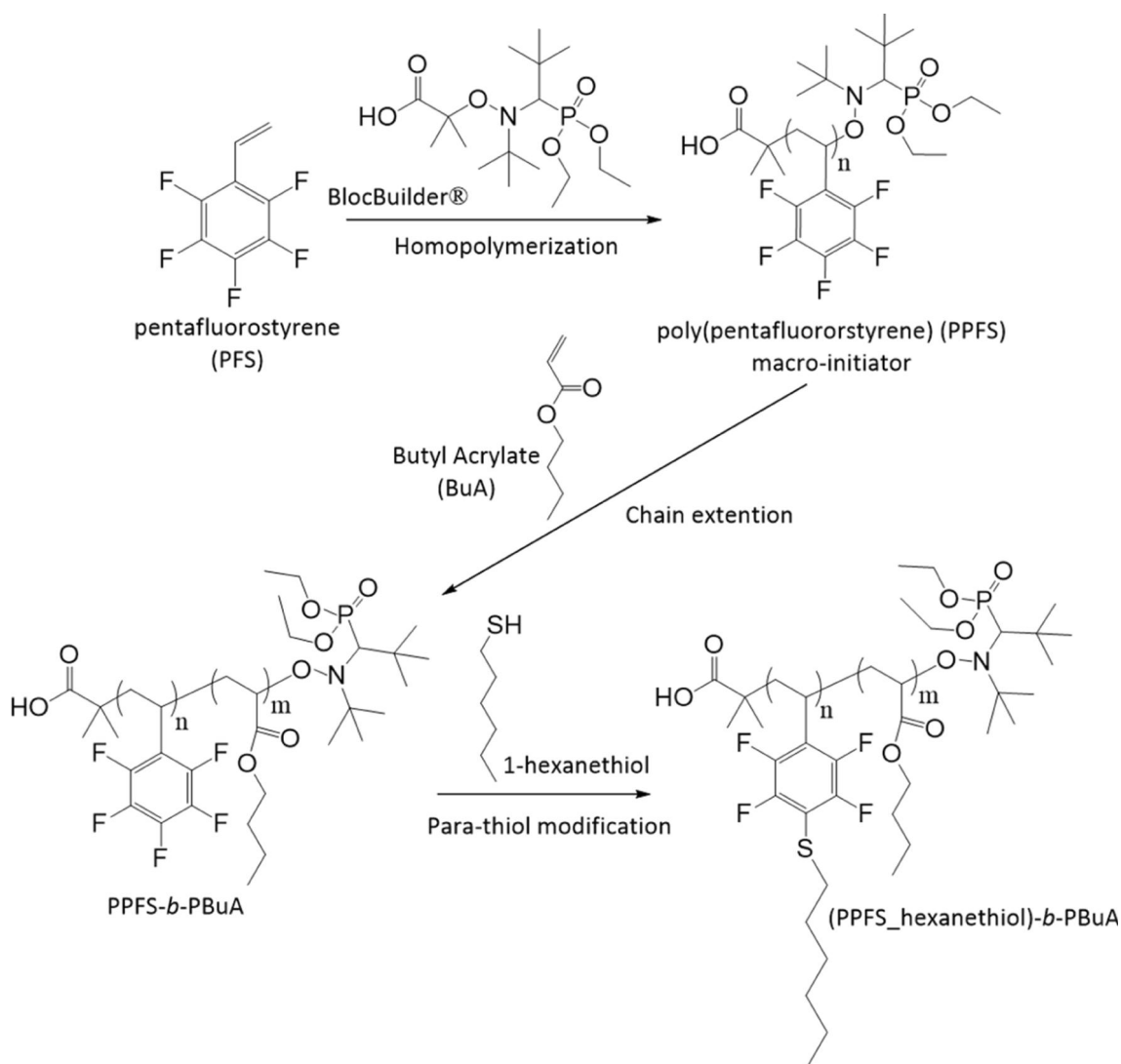
Scheme 1. Synthetic route of the PPFS-*b*-PBuA block copolymers and their 1-hexanethiol modified homologues.

[5.4.0]undec-7-ene (DBU, 99 %, Sigma, Aldrich), technical methanol (VWR), and THF (VWR), were used without further purification.

2.2. PPFS homopolymers and their block copolymers homologues

2.2.1. Homopolymerization of PFS.

The NMP of PFS was performed in bulk following a typical NMP procedure. Pentafluorostyrene (41.2 mmol), BlocBuilder® (0.10 mmol) and some free-SG1 (0.01 mmol) were added to a 25 mL round bottom flask equipped with rubber seals and a magnetic stirring bar. The mixture was placed into an ice bath and bubbled with nitrogen for 15 min and subsequently placed into an oil bath that was pre-heated at 115 °C. The mixture was left to stir for 5 h at 115 °C. The polymer was recovered by precipitation of the reaction mixture into methanol, after cooling down to room temperature. The precipitation was followed by filtration and drying of the polymer under vacuum oven at 60 °C overnight. Purification of the polymer was performed by dissolution in THF and subsequent precipitation in methanol. The purification step was repeated twice, PPFS was obtained (conversion: 60 %).

2.2.2. Chain extension of PPFS with BuA to yield PPFS-b-PBuA

The previously synthesized PPFS were used as a macro-initiator for the chain extension procedure with butyl acrylate (BuA) monomer. To do so, in a 25 mL round bottom flask was equipped with rubber seals and a magnetic stirring bar, the macro-NMP PPFS initiator (0.078 mmol) and some free-SG1 (0.0078 mmol) were dissolved into DMF (1.5 mL). Followed by the addition of BuA (35.7 mmol) in the mixture. Different ([BuA]/[PPFS]) ratios were calculated and used to target different self-assembly morphologies. The mixture was degassed with nitrogen at room temperature for 15 min before putting the flask in an oil bath pre-heated at 115 °C. The mixture was left to stir at 115 °C for 9 h. For the other BCP compositions, the monomers ratios and time of reaction were varied depending on the targeted monomer conversion. The BCP was recovered by precipitation of the mixture into methanol, after cooling down to room temperature. The precipitation was followed by filtration and drying of the polymer under vacuum oven at 60 °C overnight (conversion: 28 %).

2.2.3. para-thiol modification of the diblock copolymers

In an adequate round bottom flask, the block copolymer BCP3 (0.44 g, 0.74 mmol, 1 *eq*) was dissolved into DMF (5 mL). DBU (0.117 g, 0.78 mmol, 1.05 *eq*) was added to the mixture followed by the addition of 1-hexanethiol (0.092 g, 0.82 mmol, 1.1 *eq*). The mixture was left to stir at room temperature overnight to reach full modification. The reacted solution was precipitated into methanol twice to remove residual chemicals and dried under vacuum at 30 °C overnight.

3. Characterization methods

3.1. ^{1}H NMR, DOSY NMR & ^{19}F NMR

NMR spectra were recorded on a Bruker DPX-400 spectrometer using deuterated solvents obtained from Sigma-Aldrich (CDCl$_3$). The spectra were recorded at room temperature.

3.2. Size Exclusion Chromatography (SEC)

The molar mass of the polymers was determined by Size Exclusion Chromatography. The materials were dissolved in THF at a concentration of 3 g/L, Toluene was used as a flow marker. Prior to injection, the samples were filtered through 0.45 μm nylon filter. The analysis was performed at 30 °C at a flow rate of 1 mL/min. The set up consisted of a pump (LC-20A, Shimadzu), an autosampler (Sil- 20AHT), a differential refractometer (Optilab Rex, Wyatt), and three columns in series (Styragel HR2, HR4 and HR6 with pore sizes ranging from 102 to 106 Å).

3.3. Differential scanning calorimetry (DSC)

Between 1 and 10 mg of polymer was placed into aluminium capsules that were closed hermetically. The capsule was then placed into the DSC device (DSC Q100 from TA instruments) that was set to heating and cooling rates of 20 °C/min under nitrogen atmosphere at a flow of 50 mL/min. The characterization was performed at the temperature range of −80 °C to 180 °C.

3.4. Atomic force microscopy (AFM) & self-assembly process

AFM was performed on a Multimode 8 Atomic Force Microscope (Bruker) and recorded in PeakForce QNMmode. The solutions were obtained by dissolution of the polymers in a mixture of [Toluene: Propylene Glycol Methyl Ether Acetate (PGMEA)] [75: 25], (2 wt%). The polymer films were obtained by spin-coating of a diluted polymer solution onto a silicon wafer at 2 krpm for 60 s. The sample was first characterised by AFM directly after spin-coating and drying and then after annealing at 140 °C for 30 min and subsequent quenching at room temperature.

3.5. Small-angle X-ray scattering (SAXS)

SAXS experiments were performed with a high-resolution X-ray spectrometer Xeuss 2.0 from Xenox. The spectrometer operates with a radiation wavelength of $\lambda = 1.54$ Å (Copper K$_\alpha$ radiation). Scattering patterns were collected using a PILATUS 300 K Dectris detector with a sample-to-detector distance of 1637 mm. The collected data were analysed using Primus software. The film preparation for the SAXS experiment was done in a similar way as for the AFM characterization. The polymers were dissolved in a mixture of [Toluene: PGMEA] [75: 25], (2 wt%) and drop casted on a Kapton film. The films were annealed at 140 °C for 30 min before analysis.

4. Results and discussion

4.1. Block copolymer synthesis

Poly(pentafluorostyrene-*b*-butyl acrylate) (PPFS-*b*-PBuA) block copolymers were synthesized by NMP controlled radical polymerization. The reaction was carried out by first synthetizing PPFS that was further used as a macro-initiator for the chain extension with BuA. PPFS homopolymers were characterized by ^{1}H NMR, *SEC*, and DSC. The backbone of PPFS are found to be located between 1.7 and 3 ppm (**Fig. SI 1**). PPFS macro-initiators with molar masses ranging from 12 500 to 24 000 g/mol were obtained and their dispersity values *Đ* remained under 1.1 (Table 1). The glass transition temperature (*Tg*) of the PPFS homopolymer was determined to be around 100 °C (**Fig. SI 2**).

Acrylates were chosen for the BCP because they present properties such as flexibility, transparency, and toughness [29]. Moreover, poly (butyl acrylate) (PBuA) chemical atomic composition is different from poly(pentafluorostyrene)'s (PPFS), a suitable property to generate a nano-phase separation by self-assembly. Indeed, for a phase separation to occur, the two blocks in the BCP must be non-miscible, property driven by their solubility parameters δ. The Hansen solubility parameters of the homopolymers PPFS and PBuA were calculated using HSPiP software and were of 16.1 Mpa$^{1/2}$ and 17.3 Mpa$^{1/2}$, respectively. Other systems of phase separation with a difference of solubility parameters have already been described in the literature [30,31]. As an example, the PS/PBuA ($\delta_{PS} = 18.4$ Mpa$^{1/2}$) system is able to phase separate with a similar difference between solubility parameters than PPFS/PBuA system [32].

As described previously, the morphologies of the nano-phase separation are dictated by the volume fraction Φ of one block [33]. So, BCPs having different targeted molar ratios were synthesized to design different morphologies. To vary those molar ratios, different

Table 1
Summary table of block copolymer synthesis and characterizations.

BCPs	Polymer PPFS$_x$-b-PBuA$_y$ *	$\frac{[\text{monomer}]}{[\text{initiator}]}$	BuA Conv[b] (%)	M_n[a] (g/mol) Eq PS (M_n^{theo})	M_w[a] (g/mol) Eq PS	Đ[a]	Degree of Polymerization (DP$_n$)		f_v (PPFS)	f_v (PBuA)	T_g[c] (°C)	Structure by SAXS & AFM[d, e]	Pitch by SAXS[d] (nm)
							PPFS	PBuA					
BCP1[f]	PPFS$_{0.16}$-b-PBuA$_{0.84}$	414	69	31 000 (56 000)	38 800	1.26	65	340	0.18	0.82	−39	HCC	45
BCP2[g]	PPFS$_{0.33}$-b-PBuA$_{0.67}$	546	14	40 100 (34 000)	75 700	1.88	73	155	0.37	0.63	−40 / 104	HCC	45
BCP3[h]	PPFS$_{0.50}$-b-PBuA$_{0.50}$	483	12	34 000 (25 000)	42 000	1.2	79	79	0.54	0.46	−50 / 96	LAM	35
BCP4[f]	PPFS$_{0.54}$-b-PBuA$_{0.46}$	227	15	37 000 (19 000)	50 600	1.36	65	50	0.58	0.42	−39	HCC	46
BCP5[i]	PPFS$_{0.86}$-b-PBuA$_{0.14}$	195	15	30 600 (27 000)	34 400	1.12	125	19	0.88	0.12	103	HCC	28
BCP6[f]	PPFS$_{0.90}$-b-PBuA$_{0.10}$	97	2	17 400 (14 000)	19 100	1.09	65	8	0.91	0.09	–	Disorder	–

* With × = molar % of PPFS and y = molar % of PBuA.
[a] *Determined by SEC by equivalent PS,* [b] *Determined by* ^1H *NMR* (400 MHz, room temperature, CDCl$_3$), [c] *DSC,* [d] *SAXS &* [e] *AFM.* BCPs synthetized from macro-initiators: [f] (PPFS1) (Mn = 12 500 g/mol, Mw = 13 400 g/mol, Đ = 1.07), [g] (PPFS2) (Mn = 14 100 g/mol, Mw = 15 200 g/mol, Đ = 1.07), [h] (PPFS3) (Mn = 15 300 g/mol, Mw = 16 100 g/mol, Đ = 1.05), [i] (PPFS4) (Mn = 24 000 g/mol, Mw = 26 400 g/mol, Đ = 1.1).

experimental parameters can be used as the conversion of the monomers through reaction time and monomer to macro-initiator ratio (Table 1). The molar compositions were calculated by ^{1}H NMR after purification of the BCPs. A typical ^{1}H NMR spectrum of PPFS-b-PBuA copolymer, with chemical shifts of the backbone protons of the copolymer (–CH and –CH$_2$) located between 1.8 and 2.9 ppm is represented in Fig. 1. Protons of PBuA side chains, are located at 4 ppm (–OCH$_2$) and between 0.9 and 1.8 ppm for –CH$_3$ and –CH$_2$ ones. The final composition of each block in

the BCP can then be determined by dividing the integral value of protons corresponding to one of the blocks with the integral value of the protons corresponding to the other block. An example of calculation is given in the Supporting Information to illustrate the procedure with PPFS$_{0.50}$-b-PBuA$_{0.50}$ (Fig. 1, **Eq. SI 1**).

The efficiency of the re-initiation of the PPFS was observed by DOSY NMR and *SEC*. DOSY NMR is a powerful characterization technique to determine the number of species existing in a complex solution, each
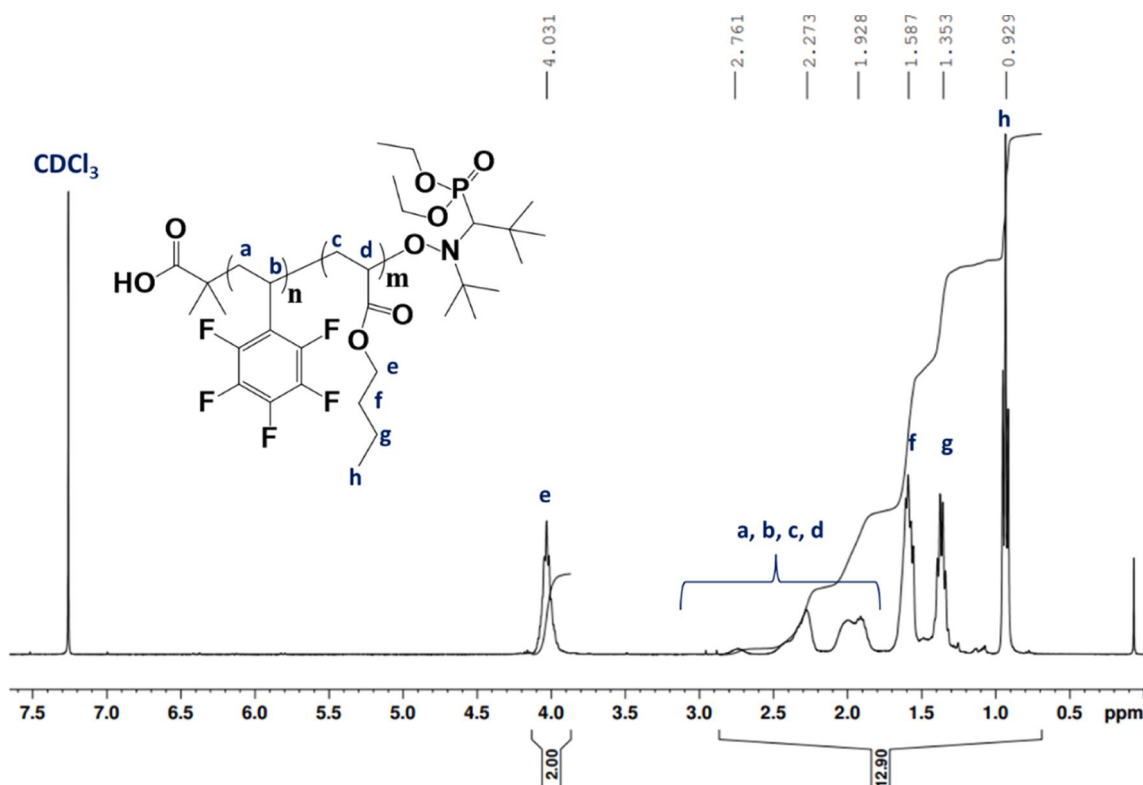

Fig. 1. Schematic structure and ^{1}H NMR spectrum (400 MHz, room temperature, CDCl$_3$) of purified (PPFS$_{0.50}$-b-PBuA$_{0.50}$)$_{34K}$ (BCP3).

being assessed by a diffusion coefficient [34]. Observing one diffusion coefficient means the presence of a unique species in the sample. For all PPFS-b-PBuA copolymers synthesized, only one diffusion coefficient is observed by DOSY NMR, which is characteristic of an efficient re-activation of the macro-initiator PPFS (**Fig. SI 3**). *SEC* characterizations corroborate the good control over the polymerization (Fig. 2 A). An increase in molar mass from homopolymers PPFS to PPFS-b-PBuA BCPs is attributed to the chain extension (Fig. 2). Dispersity values Đ between 1.09 and 1.88 are reported in Table 1. A dispersity value enhancement is noticed when the molar compositions of PBuA increases, with the apparition of a shoulder in the corresponding chromatograms corresponding to the highest molar mass of the macro-initiator PPFS (Fig. 2 A, **Fig. SI 4**). Such behaviour could be attributed to non-reversible termination reactions which would lead to dead chains when the polymerization of the first block is pushed towards high conversion (here 85 % for the PPFS macro-initiator).

4.2. Block copolymers self-assembly

As previously mentioned, when BCPs are immiscible, they present the intrinsic properties of both isolated blocks. Thus, two glass transition temperatures Tg, at −50 °C and 96 °C, are noticeable on the BCP DSC thermogram for a PPFS/PBuA molar composition of 50/50 (PPFS$_{0.50}$-b-PBuA$_{0.50}$)$_{34K}$ (here, the subscript 34 K represents the molar mass of the copolymer obtained by *SEC*, the same notation was used for all the copolymers throughout the manuscript) (Fig. 2 B). For the compositions with lower amount of PPFS, a different thermal pattern is observed with just the PBuA thermal transition. Indeed, the heat capacity Δ_{Cp} of PBuA is 3.8 times higher than the one of PPFS with values of −5.7 and −1.5 W/(kg.°C), respectively (**Fig. SI 5**). BCPs self-assembly allows to design well-structured materials, when composed of immiscible blocks. BCP systems will aim to minimize the interaction between blocks to reach a thermodynamic equilibrium. That microphase separation is induced by the stretching of the BCP chains with the desire of lowering interfacial energy in the BCP. The domains' structure is dictated by the volume fraction Φ of one block into the BCP. Depending on that volume fraction, the chains will stretch differently leading to different morphologies [33,35]. Typically, for the phase separation, the minor phase in volume will disperse in a matrix of the major one. Due to the strong interaction of the covalent bond linking the blocks, the phase separation can only occur at the macromolecular scale, meaning at the nanometre scale and not at the macroscopic one [3]. Moreover, domains size can be tuned by varying chains length N through the control of the molar mass.

Such nano-structured material based on the self-assembly behaviour of PPFS-b-PBuA BCPs can be observed at the scale length by Atomic Force Microscopy (AFM). To do so, solutions of each BCPs were prepared following the experimental section procedure. The solutions were then spin coated on silicon wafers. A thermal annealing of the films was done at 140 °C to reach the thermodynamic equilibrium (40° higher than the Tg of PPFS). Each sample was observed before and after annealing. The AFM results on thin films were correlated with bulk study by Small Angle X-rays Scattering SAXS. Indeed, the SAXS experiment will complement the information provided by AFM measurements and give detailed insight on the arrangement of the microstructures in the bulk (films of few hundred microns thick) and their domains size. If periodic structural structuration occurs, the SAXS pattern will reveal the presence of specific maxima of scattering intensities at different scattering vectors (q). Having a periodic structure, means having a repetition of planes in the different directions of the structure. The distance between the planes could be calculated knowing the Miller indices (h,k,l) of the structure. The mathematical determination of the scattering vector is given by the equation $q = [(4\pi \sin(\theta))/\lambda]$, where $\sin(\theta) = [(n\lambda)/(2d)]$ according to Bragg's law. The distance d between the planes in the atomic lattice can hence be determined using both formulas. Experimentally, the ratio between a given q and the maxima value of q in intensity (q^*) will provide information about the spacing between nanodomains, and the type of structuration in the material [36].

Taking (PPFS$_{0.50}$-b-PBuA$_{0.50}$)$_{34K}$ (BCP3) as an example, the molar composition of each block is 0.5, leading to a volume fraction Φ of 0.60 and 0.40 for PPFS and PBuA, respectively (ρ_{PFS} = 1.4 g/mL; ρ_{BuA} = 1.08 g/mL). According to the theoretical BCP phase diagram [33], the equilibrium morphology expected at this volume fraction is to be determined by lamellas (LAM), which was experimentally observed by AFM and SAXS (Fig. 3) with an average spacing between nanodomains of 35 nm. Indeed, the order peaks corresponding to the lamellar structuration are 1, 2, 3, 4 … The calculation of the spacing is provided in the Supporting Information (**Eq. SI 4**).

Similarly, for the other compositions the samples were annealed before AFM observation following the procedure described in the experimental section of this article. The volume fraction of each block was determined and the BCPs were observed by AFM and SAXS. Different morphologies were observed with distance between nanodomains ranging from 30 to 45 nm (Table 1). The results are shown in Fig. 4, where are presented for each composition the AFM images and corresponding SAXS results. As it was expected from the self-assembly theory, composition (PPFS$_{0.90}$-b-PBuA$_{0.10}$)$_{17K}$ (BCP6) gave no self-assembly both by AFM and SAXS, and the remaining BCPs were proven to self-assemble both by AFM and SAXS, giving a hexagonal
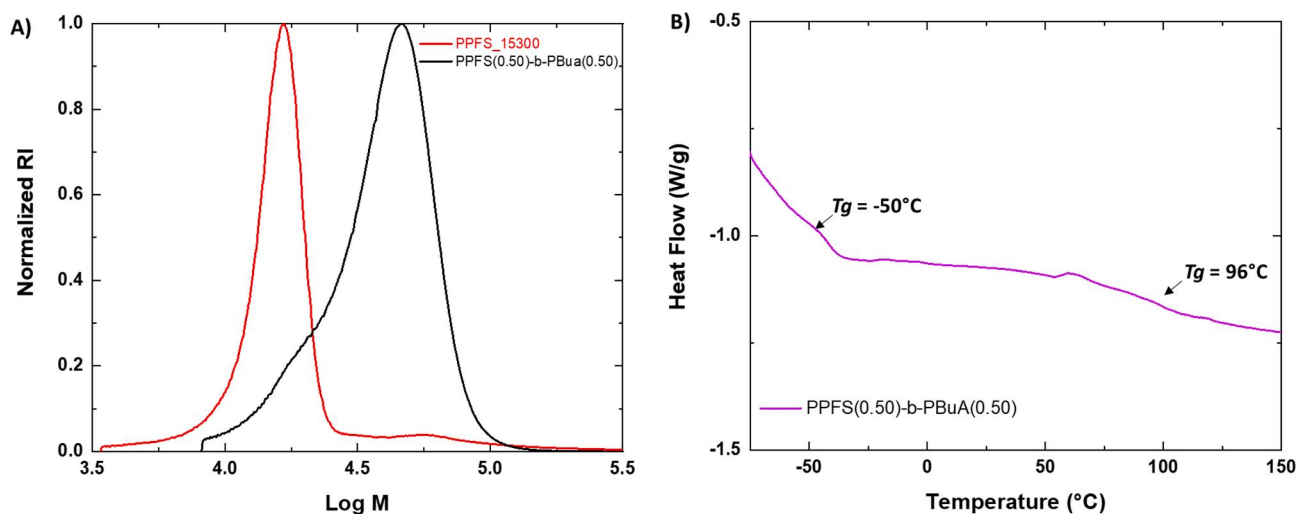
Fig. 2. (A) *SEC* traces of poly(pentafluorostyrene) macro-initiator (PPFS3) (Mn = 15 300 g/mol, Đ = 1.05) and the homologue (PPFS$_{0.50}$-b-PBuA$_{0.50}$)$_{34K}$ (BCP3) (Mn = 34 000 g/mol, Đ = 1.2). (B) DSC graph of BCP3 showing glass transition temperatures at −50 °C and 96 °C for PBuA and PPFS, respectively.
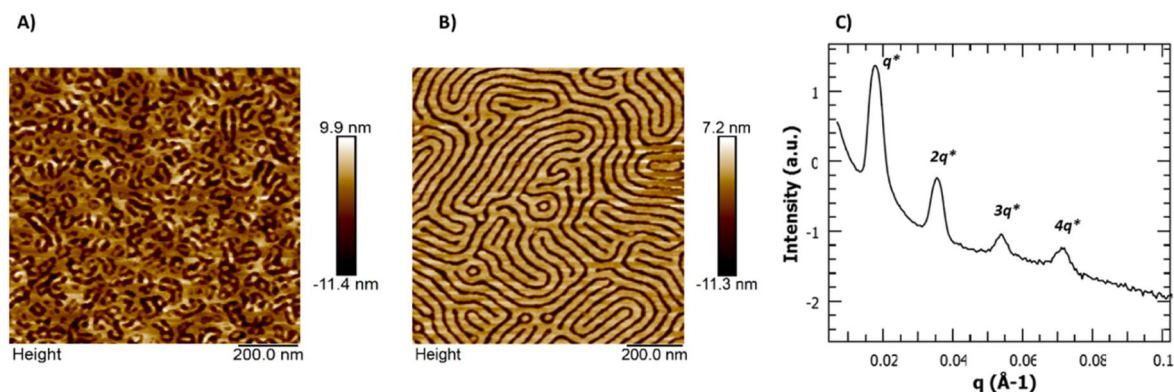
Fig. 3. (A) Peak Force mode AFM height images of PPFS$_{0.50}$-b-PBuA$_{0.50}$ (BCP3) film before annealing and (B) after annealing at 140 °C for 4 h; (C) Observation of the annealed film by SAXS.
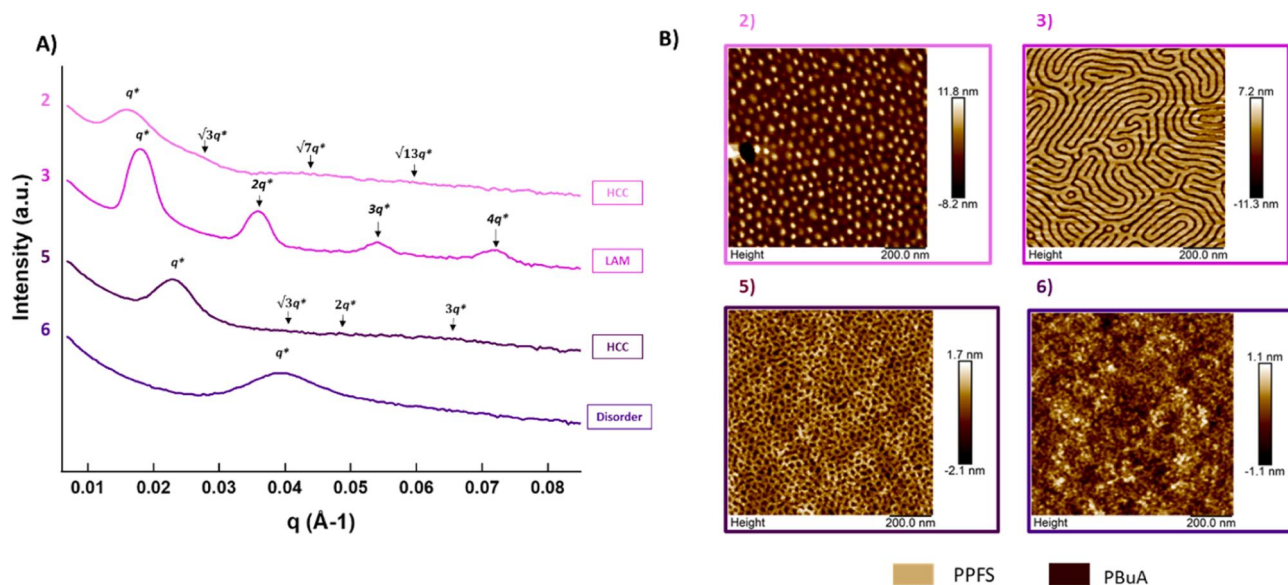
Fig. 4. (A) SAXS graph of the different block copolymers after annealing at 140 °C for 3 h. (B) Peak Force mode AFM height images of PPFS-b-PBuA BCPs after annealing at 140 °C for 4 h. (BCP2 ~ 2) (PPFS$_{0.33}$-b-PBuA$_{0.67}$)$_{40K}$; (BCP3 ~ 3) (PPFS$_{0.50}$-b-PBuA$_{0.50}$)$_{34K}$; (BCP5 ~ 5) (PPFS$_{0.86}$-b-PBuA$_{0.14}$)$_{31K}$; (BCP6 ~ 6) (PPFS$_{0.90}$-b-PBuA$_{0.10}$)$_{17K}$).

closed-packed cylinders HCC structuration. The HCC structuration was attributed to the presence of the HCC characteristic peaks at 1, $\sqrt{3}$, 2, $\sqrt{7}$, 3, $\sqrt{12}$, and $\sqrt{13}$.

4.3. Driven self-assembly of block copolymers

The morphology of the BCPs can be modified by addition of a defined amount of homopolymer in the blend. The idea is to mimic the presence of dead PPFS chains which could be present in the final block co-polymers and then perturb the self-assembly pattern. In order to check the impact of residual macro-nitiator, 10 wt% of PPFS1 homopolymer of a molar mass of 12 500 g/mol with Đ of 1.07 (DPn = 65) was added to BCP1 and BCP4, respectively (PPFS$_{0.16}$-b-PBuA$_{0.84}$)$_{31K}$ and (PPFS$_{0.54}$-b-PBuA$_{0.46}$)$_{37K}$. By doing so, the overall molar composition of PPFS is increased, leading to an enrichment of the PPFS phase, giving respectively PPFS$_{0.24}$-b-PBuA$_{0.76}$ (BCP1′) and PPFS$_{0.59}$-b-PBuA$_{0.41}$ (BCP4′). Hence a shift from the lower to higher volume fraction in PPFS in the BCP phase diagram is expected. On top of modifying the composition of the PPFS block, adding some homopolymer of PPFS in the blend has an influence on the self-assembly and nano-pattern of the material. In the case of BCP1 (PPFS$_{0.16}$-b-PBuA$_{0.84}$)$_{31K}$, enriching the PPFS phase

provided a better phase separation with well-defined nanodomains. Moreover, the SAXS analysis reveals a cubic structuration and a pitch distance decreasing from 45 to 38 nm. For BCP4 (PPFS$_{0.54}$-b-PBuA$_{0.46}$)$_{37K}$, two hypotheses could explain the contrast observed on the AFM images after addition of PPFS homopolymer (Fig. 5 **A & B** - BCP4 to BCP4′). Indeed, nanodomains of PBuA in a PPFS matrix are expected by AFM. However, this new composition displays the opposite result, *i.e.* nanodomains of PPFS in PBuA matrix (Fig. 5 **A** - BCP4′). The first explanation could be that the nanodomains of the initial composition (Fig. 5 **A** - BCP4) were mainly parallel to the surface of the film, *i.e. in-plane*, and they became perpendicular to it after addition of PPFS, *i.e. out-of-the plane*. The second explanation could be a metastable state of the copolymer, called HPL (Hexagonally Perforated Lamellae). Such structuration corresponds to lamellas of the minor PBuA polymer being covered by hexagonal arrangement of perforations [37]. This structure can be the result of the presence of chains of different length, *i.e.* dispersity value Đ of 1.36 plus free homopolymer PPFS [37,34]. Nevertheless, the pitch distance of 45 nm remained the same after addition of PPFS. Here, we demonstrated a way to drive the morphologies of PPFS-b-PBuA BCPs by adding a defined amount of homopolymer.

As mentioned previously, the substitution of the fluorine in *para*-
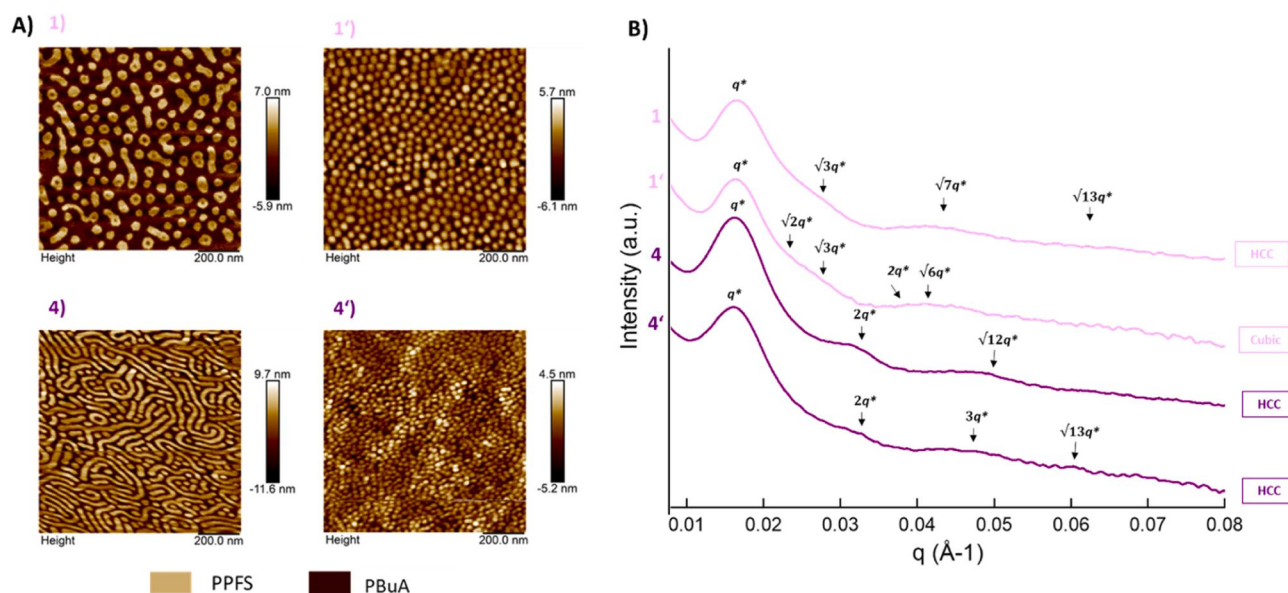
Fig. 5. (A) AFM of the original and tuned BCPs annealed at 140 °C for 4 h. Tunability of the morphology observed by adding 10 wt% of PPFS$_{12500}$ in BCP mixtures; shift of the molar composition of BCP1 ~ 1 (PPFS$_{0.16}$-b-PBuA$_{0.84}$) and BCP4 ~ 4 (PPFS$_{0.54}$-b-PBuA$_{0.46}$) after addition of PPFS1 to give BCP1′~1′ (PPFS$_{0.24}$-b-PBuA$_{0.76}$) and BCP4′~4′ (PPFS$_{0.59}$-b-PBuA$_{0.41}$) depending on the molar fraction of PPFS on a theoretical BCP phase diagram. (B) SAXS of the original and tuned BCPs annealed at 140 °C for 3 h.

position allows for many possibilities of functionalization permitting to tune either the volume fraction or the interaction parameter χ which is dependant of the difference of the solubility parameters δ of the two blocks of the modified BCP2 ((PPFS$_{0.33}$-b-PBuA$_{0.67}$)$_{40K}$). Here, the *para* fluorine-thiol modification was performed as an efficient soft substitution with a functional thiol, *i.e.* 1-hexanethiol compound, in a one-step organo-catalyzed procedure with 1,8-Diazabicyclo[5.4.0]undec-7-ene DBU. Indeed, mild conditions at room temperature and ambient atmosphere were used. Moreover, the versatility and the commercial availability of thiol compounds make them attractive for such reactions [38–40]. The reaction was performed in DMF overnight at room temperature. The modified BCP was characterized by ^{19}F NMR (Fig. 6). On the NMR spectrum, the full efficiency of the substitution is characterized by the complete disappearance of the chemical shift of the fluorine in *para* position (δ_{paraF} = -154 ppm). Moreover, the chemical up fields shift of the fluorine in *meta* positions is also observed from δ_{metaF} = -161 to 134 ppm, before and after modifications, respectively. This up field shift is due to the change from fluorine to sulphur neighbours.

After full modification of the BCP, the glass transition temperature *Tg* of the PPFS block is expected to be lowered due to the added side chain providing additional free volume and then mobility to the polymer

chains. Indeed, the *Tg* of the 1-hexanethiol modified PPFS drops down to 11 °C and the macroscopic aspect of the polymer changed from solid to viscous at room temperature after modification (**Figs. SI 6 & 7**). It is worth noting that similar behaviour is observed with the PPFS homopolymer. Indeed, the *Tg* decreases from 100 °C to 8 °C from before to full substitution by 1-hexanethiol, respectively (**Fig. SI 8**).

The AFM images of the modified BCP do not show a contrasted image after modification. This can be explained by the new solubility parameter of the 1-hexanethiol modified PPFS (17.4 Mpa$^{1/2}$), which is close to the one of PBuA (17.3 Mpa$^{1/2}$). This proximity of the solubility parameters strongly decreased the segregation ability along with similar thermal behaviours, *i.e.* both in an elastomeric state with *Tg* values below room temperature. Here, the modification with 1-hexanethiol did not preserve the nano-segregation of the initial self-assembled block copolymer (Fig. 7). This observation was confirmed by the SAXS experiment. Indeed, no other than the initial scattering vector *q** at 0.017 Å^{-1} were observed, characteristic of a liquid order.

5. Conclusion

In the present study, the synthesis and self-assembly behaviour of
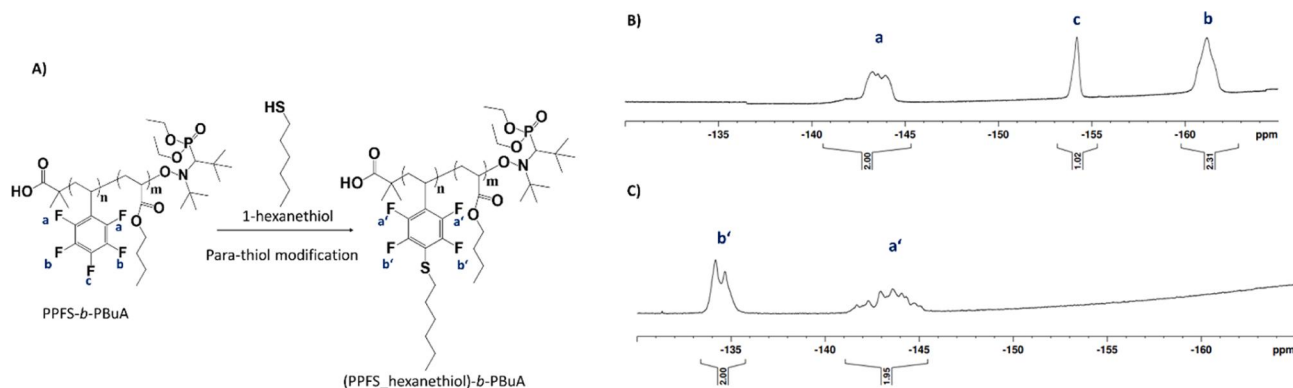
Fig. 6. (A) Polymer structure before and after modification, (B) ^{19}F NMR spectra of BCP2 (PPFS$_{0.33}$-b-PBuA$_{0.67}$)$_{40K}$ (300 MHz, room temperature, CDCl$_3$) and (C) BCP2 after modification with 1-hexanethiol (400 MHz, room temperature, CDCl$_3$).
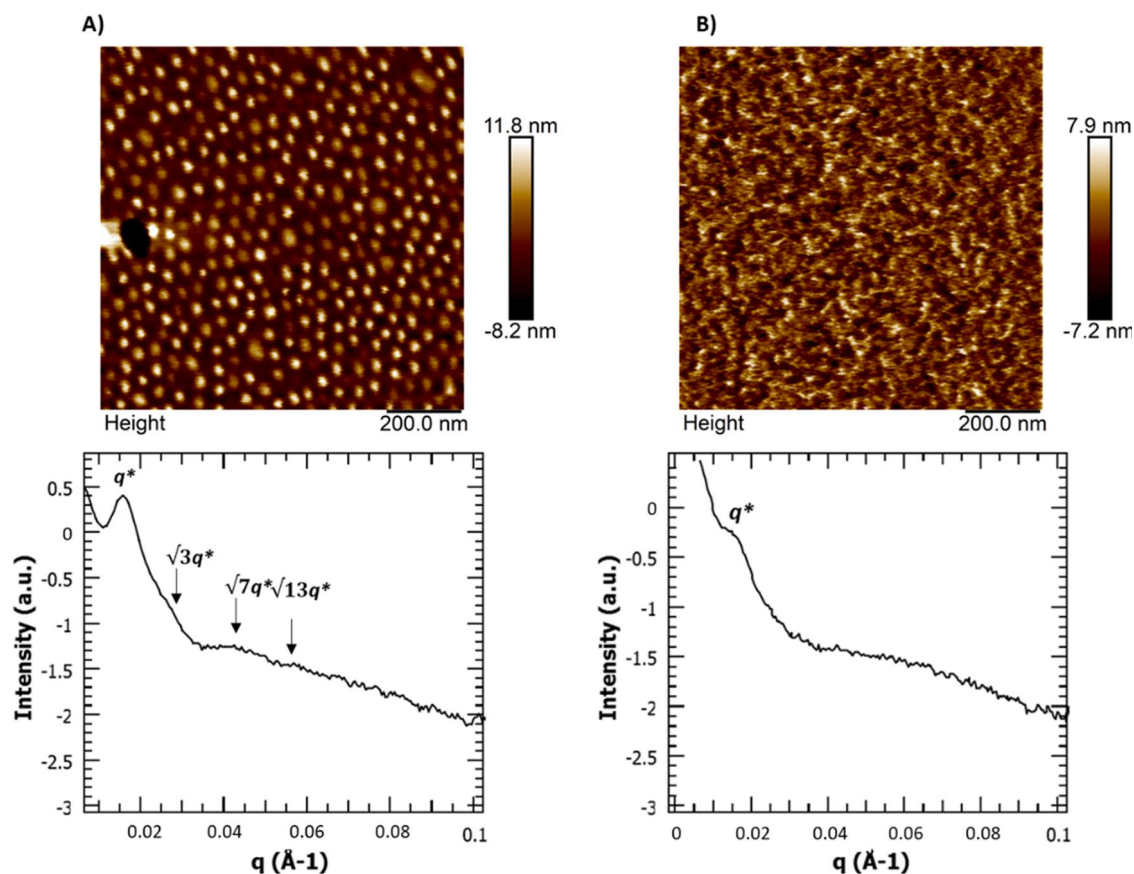
Fig. 7. (A) Peak Force mode AFM height images and corresponding SAXS characterizations of BCP2 (PPFS$_{0.33}$-*b*-PBuA$_{0.67}$)$_{40K}$, and (B) BCP2 modified with 1-hexanethiol after annealing.

PPFS-*b*-PBuA block copolymers were studied. The synthesis of the BCPs was performed by NMP controlled radical polymerization from PPFS macroinitiator by the chain extension with butyl acrylate BuA. BCPs of PPFS with molar fraction ranging from 0.16 to 0.90 were synthesized. The molar masses of the PPFS-*b*-PBuA BCPs were determined by *SEC* between 17 000 and 40 000 g/mol with dispersity values *Đ* between 1.07 and 1.88. The chromatograms showed an increase in molar mass due to the chain extension from the macro-initiator to the BCPs and a single diffusion coefficient by DOSY NMR.

Two glass transition temperatures *Tg* were observed by DSC for the block copolymers. The self-assembly behaviour of the PPFS-*b*-PBuA was brought to light by AFM observation on thin films correlated to SAXS analysis in bulk. Indeed, depending on the volume fraction of each block, the morphologies obtained were tuned from HCC to LAM. The size of the nanodomains was between 30 and 45 nm. Moreover, morphologies could also be varied by addition of 10 % of PPFS homopolymer to the BCP blend.

Finally, the BCPs were modified by *para* fluorine-thiol modification using 1-hexanethiol. The full modification of the PPFS block was determined by ^{19}F NMR and a change in thermal properties of the BCP was noticeable after modification with 1-hexanethiol.

The *para* fluorine-thiol modification can be finally considered as an easy mild and efficient organo-catalyzed method for the tailoring of functional block polymers microstructure in relationship with their physical or chemical properties due to the variety of available thiol functional side chains. Moreover, this method's added feature represents an important way to pave the development of nano-structured materials for different applications fields, as energy, especially. Indeed, by controlling the solubility parameter of the modified PPFS block and then maintaining it different enough of the second block one,

the degree nano-segregation can be tuned.

Declaration of Competing Interest

The authors declare that they have no known competing financial interests or personal relationships that could have appeared to influence the work reported in this paper.

Data availability

Data will be made available on request.

Appendix A. Supplementary data

Supplementary data to this article can be found online at https://doi.org/10.1016/j.eurpolymj.2022.111560.

References

[1] V.F. Cardoso, D.M. Correia, C. Ribeiro, M.M. Fernandes, S. Lanceros-Méndez, Fluorinated polymers as smart materials for advanced biomedical applications, Polymers 10 (2018) 1–26, https://doi.org/10.3390/polym10020161.

[2] D.R. Iyengar, S.M. Perutz, C.-A. Dai, C.K. Ober, E.J. Kramer, Surface segregation studies of fluorine-containing diblock copolymers, Macromolecules 29 (4) (1996) 1229–1234, https://doi.org/10.1021/ma950544z.

[3] Y. Mai, A. Eisenberg, Self-assembly of block copolymers, Chem. Soc. Rev. 41 (2012) 5969–5985, https://doi.org/10.1039/C2CS35115C.

[4] A. Rösler, G.W.M. Vandermeulen, H.A. Klok, Advanced drug delivery devices via self-assembly of amphiphilic block copolymers, Adv. Drug Deliv. Rev. 64 (2012) 270–279, https://doi.org/10.1016/j.addr.2012.09.026.

[5] V. Agrahari, V. Agrahari, Advances and applications of block-copolymer-based nanoformulations, Drug Discov. Today 23 (5) (2018) 1139–1151, https://doi.org/10.1016/j.drudis.2018.03.004.

[6] A. Lendlein, S. Kelch, Shape-Memory Polymers, *Angew. Chem. Int. Ed. Engl.* **41** (2002) 2034–2057.https://doi.org/10.1002/1521-3773(20020617)41:12%3C2034::AID-ANIE2034%3E3.0.CO;2-M.

[7] R.A. Puglisi, Towards Ordered Silicon Nanostructures through Self-Assembling Mechanisms and Processes, J. Nanomater. (2015) 1–20, https://doi.org/10.1155/2015/586458.

[8] W. Lu, Y. Wang, W. Wang, S. Cheng, J. Zhu, Y. Xu, K. Hong, N.-G. Kang, J. Mays, All Acrylic-based Thermoplastic Elastomers with High Upper Service Temperature and Superior Mechanical Properties, Polym. Chem. 8 (37) (2017) 5741–5748, https://doi.org/10.1039/C7PY01225J.

[9] D. Benoit, S. Grimaldi, J.P. Finet, P. Tordo, M. Fontanille, Y. Gnanou, Controlled/Living Free-Radical Polymerization of Styrene and n-Butyl Acrylate in the Presence of a Novel Asymmetric Nitroxyl Radical, ACS Symp. Ser. 685 (1998) 225–235, https://doi.org/10.1021/bk-1998-0685.ch014.

[10] J. Chiefari, Y.K. Chong, F. Ercole, J. Krstina, J. Jeffery, T.P.T. Le, R.T. A. Mayadunne, G.F. Meijs, C.L. Moad, G. Moad, E. Rizzardo, S.H. Thang, Living Free-Radical Polymerization by Reversible Addition - Fragmentation Chain Transfer : The RAFT Process, Macromolecules 31 (1998) 5559–5562, https://doi.org/10.1021/ma9804951.

[11] K. Matyjaszewski, Atom Transfer Radical Polymerization (ATRP): Current status and Future Perspectives, Macromolecules 45 (10) (2012) 4015–4039, https://doi.org/10.1021/ma3001719.

[12] J. Nicolas, Y. Guillaneuf, C. Lefay, D. Bertin, D. Gigmes, B. Charleux, Nitroxide-mediated polymerization, Prog. Polym. Sci. 38 (1) (2013) 63–235, https://doi.org/10.1016/j.progpolymsci.2012.06.002.

[13] K. Matyjaszewski, J. Xia, Atom Transfer Radical Polymerization, Chem. Rev. 101 (9) (2001) 2921–2990, https://doi.org/10.1021/cr940534g.

[14] G. Moad, E. Rizzardo, S.H. Thang, Living Radical Polymerization by the RAFT Process, Aust. J. Chem. 58 (2005) 379–410, https://doi.org/10.1071/CH05072.

[15] T.L. Bucholz, S.P. Li, Y.L. Loo, Ultra-low-κ materials derived from poly(D, L-lactide-b- pentafluorostyrene) diblock copolymers, J. Mater. Chem. 18 (2008) 530–536, https://doi.org/10.1039/B714941G.

[16] K. Jankova, P. Jannasch, S. Hvilsted, Ion conducting solid polymer electrolytes based on polypentafluorostyrene-*b*-polyether-*b*-polypentafluorostyrene prepared by atom transfer radical polymerization, J. Mater. Chem. 14 (2004) 2902–2908, https://doi.org/10.1039/B404097J.

[17] X. Li, L. Andruzzi, E. Chiellini, G. Galli, C.K. Ober, A. Hexemer, E.J. Kramer, D. A. Fischer, Semifluorinated Aromatic Side-Group Polystyrene-Based Block Copolymers: Bulk Structure and Surface Orientation Studies, Macromolecules 35 (2002) 8078–8087, https://doi.org/10.1021/ma020463k.

[18] S. Chen, A. Funtan, F. Gao, B. Cui, A. Meister, S.S.P. Parkin, W.H. Binder, Synthesis and Morphology of Semifluorinated Polymeric Ionic Liquids, Macromolecules 51 (21) (2018) 8620–8628, https://doi.org/10.1021/acs.macromol.1c00038.

[19] K.T. Powell, C. Cheng, K.L. Wooley, Complex Amphiphilic Hyperbranched Fluoropolymers by Atom Transfer Radical Self-Condensing Vinyl (Co) polymerization, Macromolecules 40 (13) (2007) 4509–4515, https://doi.org/10.1021/ma0628937.

[20] S. Borkar, K. Jankova, H.W. Siesler, S. Hvilsted, New Highly Fluorinated Styrene-Based Materials with Low Surface Energy Prepared by ATRP, Macromolecules 37 (3) (2004) 788–794, https://doi.org/10.1021/ma034952b.

[21] Q. Yin, A. Charlot, D. Portinha, E. Beyou, Nitroxide-mediated polymerization of pentafluorostyrene initiated by PS-DEPN through the surface of APTMS modified fumed silica: Towards functional nanohybrids, RSC Adv. 6 (63) (2016) 58260–58267, https://doi.org/10.1039/C6RA08973A.

[22] C.R. Becer, K. Babiuch, D. Pilz, S. Hornig, T. Heinze, M. Gottschaldt, U.S. Schubert, Clicking Pentafluorostyrene Copolymers: Synthesis, Nanoprecipitation, and Glycosylation, Macromolecules 42 (7) (2009) 2387–2394, https://doi.org/10.1021/ma9000176.

[23] C. Ott, R. Hoogenboom, U.S. Schubert, Post-modification of poly (pentafluorostyrene): a versatile "click" method to create well-defined multifunctional graft copolymers, Chem. Commun. (2008) 3516–3518, https://doi.org/10.1039/B807152G.

[24] C.S. Gudipati, M.B.H. Tan, H. Hussain, Y.e. Liu, C. He, T.P. Davis, Synthesis of Poly (glycidyl methacrylate)-*block*-Poly(pentafluorostyrene) by RAFT: Precursor to Novel Amphiphilic Poly(glyceryl methacrylate)-*block*-Poly(pentafluorostyrene), Macromol. Rapid Commun. 29 (23) (2008) 1902–1907, https://doi.org/10.1002/marc.200800515.

[25] J.-M. Noy, Y. Li, W. Smolan, P.J. Roth, Azide-*para*-Fluoro Substitution on Polymers: Multipurpose Precursors for Efficient Sequential Postpolymerization Modification, Macromolecules 52 (8) (2019) 3083–3091, https://doi.org/10.1021/acs.macromol.9b00109.

[26] L. Dumas, E. Fleury, D. Portinha, Wettability adjustment of PVDF surfaces by combining radiation-induced grafting of (2,3,4,5,6)-pentafluorostyrene and subsequent chemoselective "click-type" reaction, Polymer 55 (2014) 2628–2634, https://doi.org/10.1016/j.polymer.2014.04.002.

[27] Q. Yin, P. Alcouffe, E. Beyou, A. Charlot, D. Portinha, Controlled perfluorination of poly(2,3,4,5,6-pentafluorostyrene) (PPFS) and PPFS-functionalized fumed silica by thiol-*para*-fluoro coupling: Towards the design of self-cleaning (nano)composite films, Eur. Polym. J. 102 (2018) 120–129, https://doi.org/10.1016/j.eurpolymj.2018.03.016.

[28] M. Riedel, J. Stadermann, H. Komber, F. Simon, B. Voit, Synthesis, post-modification and self-assembled thin films of pentafluorostyrene containing block copolymers, Eur. Polym. J. 47 (4) (2011) 675–684, https://doi.org/10.1016/j.eurpolymj.2010.10.010.

[29] A. Serrano-Aroca, S. Deb, Acrylate Polym. Adv. Appl. (2019), https://doi.org/10.5772/intechopen.77563.

[30] P. Marcasuzaa, M. Save, P. Gérard, L. Billon, When a pH-triggered nanopatterned shape transition drives the wettability of a hierarchically self-organized film: A bio-inspired effect of "sea Anemone", J. Colloid Interface Sci. 581 (2021) 96–101, https://doi.org/10.1016/j.jcis.2020.07.130.

[31] P. Marcasuzaa, S. Pearson, K. Bosson, L. Pessoni, J.-C. Dupin, L. Billon, Reactive nano-patterns in triple structured bio-inspired honeycomb films as a clickable platform, Chem. Commun. 54 (93) (2018) 13068–13071, https://doi.org/10.1039/C8CC05333B.

[32] P. Escalé, M. Save, L. Billon, J. Ruokolainen, L. Rubatat, When block copolymer self-assembly in hierarchically ordered honeycomb films depicts the breath figure process, Soft Matter 12 (3) (2016) 790–797, https://doi.org/10.1039/C5SM01774B.

[33] M.W. Matsen, F.S. Bates, Unifying Weak- and Strong-Segregation Block copolymer Theories, Macromolecules 29 (4) (1996) 1091–1098, https://doi.org/10.1021/ma951138i.

[34] N. Cherifi, A. Khoukh, A. Benaboura, L. Billon, Diffusion-Ordered Spectroscopy NMR DOSY: An All-In-One Tool to Simultaneously Follow Side Seactions, Livingness and Molar Masses of PolyMethylMethacrylate by Nitroxide Mediated Polymerization, Polym. Chem. 7 (2016) 5249–5257, https://doi.org/10.1039/C6PY00927A.

[35] L. Leibler, Theory of Microphase Separation in Block copolymers, Macromolecules 13 (6) (1980) 1602–1617, https://doi.org/10.1021/ma60078a047.

[36] M. Zhang, R.B. Moore, T.E. Long, J.S. Riffle, Morphological Characterization and Analysis of Ion- Containing Polymers Using Small Angle X-ray Scattering Morphological Characterization and Analysis of Ion-Containing Polymers Using Small Angle X-ray Scattering, 2014.

[37] J. Listak, W. Jakubowski, L. Mueller, A. Plichta, K. Matyjaszewski, M. R. Bockstaller, Effect of Symmetry of Molecular Weight Distribution in Block Copolymers on Formation of "Metastable" Morphologies, Macromolecules 41 (15) (2008) 5919–5927, https://doi.org/10.1021/ma800816j.

[38] G. Delaittre, L. Barner, The: *para*-Fluoro-Thiol Reaction as an Efficient Tool in Polymer Chemistry, Polym. Chem. 9 (20) (2018) 2679–2684, https://doi.org/10.1039/C8PY00287H.

[39] D. Varadharajan, H. Turgut, J. Lahann, H. Yabu, G. Delaittre, Surface-Reactive Patchy Nanoparticles and Nanodiscs Prepared by Tandem Nanoprecipitation and Internal Phase Separation, Adv. Funct. Mater. 28 (39) (2018) 1800846, https://doi.org/10.1002/adfm.201800846.

[40] P. Mandal, P. Marcasuzaa, L. Billon, para-Fluoro/thiol click chemistry-driven pentafluorostyrene-based block copolymer self-assembly: to mimic or not to mimic the solubility parameter? Polym. Chem. 13 (33) (2022) 4757–4762, https://doi.org/10.1039/D2PY00784C.

6.   Supporting Information

PentaFluoroStyrene-based Block Copolymers Controlled Self-Assembly Pattern: A platform paving the way to functional block-copolymers

Karell Bosson,[a,b,e] Pierre Marcasuzaa,[a,b] Antoine Bousquet,[b] Günter E.M. Tovar,[c,d] Vladimir Atanasov,[e] Laurent Billon[a,b]

[a] Bio-inspired Materials Group: Functionalities & Self-assembly, E2S UPPA, 64000 Pau, France

[b] Universite de Pau et Pays de l'Adour, E2S UPPA, CNRS, IPREM, UMR5254, 64000 Pau, France

[c] Institute for Interfacial Process Engineering and Plasma Technology IGVP, University of Stuttgart, Pfaffenwaldring 31, 70569 Stuttgart, Germany

[d] Fraunhofer Institute for Interfacial Engineering and Biotechnology IGB, Nobelstr. 12, 70569 Stuttgart, Germany

[e] Institute of Chemical Process Engineering, University of Stuttgart, Boeblingerstrasse 78, 70199 Stuttgart, Germany

This supporting information contains:

-Total number of pages: **11 pages**

-Total number of figures: **7 figures**

> ^{1}H NMR, DOSY NMR, SEC, DSC of the block copolymers and modified block copolymer used in this work

-Total number of Equations: **4 Equations**

> Equations used to determine the molar compositions of the BCPs, the molar mass and volume fractions of the BCPs; and the pitch between nanodomains by SAXS

-Total number of Tables: **1 Table**

SAXS data of the copolymers described in this work

The supporting information of this article provides additional information on the synthesis and characterizations of the polymers. Here are presented the methodology for the calculations of polymer compositions, theoretical molar masses, distance between nanodomains for the SAXS analysis.
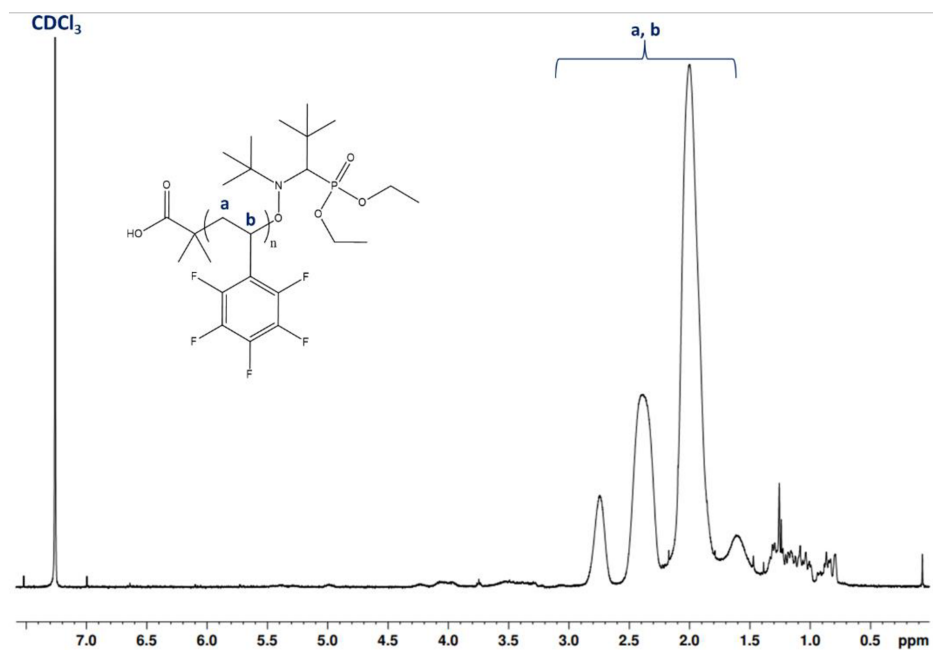
Figure SI 1. Structure and ^1H NMR spectrum (300 MHz, room temperature, CDCl$_3$) of poly(pentafluorostyrene) macro-initiator (PPFS2).
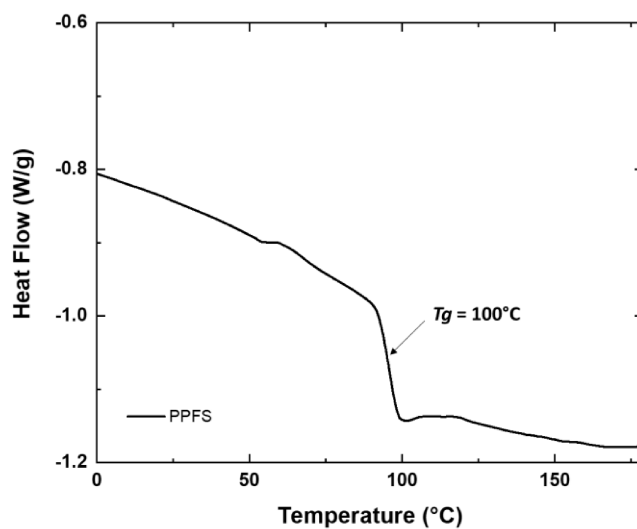
Figure SI 2. DSC of poly(pentafluorostyrene) macro-initiator (PPFS2), displaying a *Tg* of 100°C.

- Determining composition and volume fraction of PPFS and PBuA in the BCP

Like for the previous example, the attribution of the signals of each proton of the BCP was made, followed by the integration of those signals. The chemical shifts of the backbone protons of the copolymer (-CH and -CH$_2$) are located between 1.8 and 2.9 ppm (Integral$_{H\ PPFS}$ and Integral$_{H\ PBuA}$). Protons of PBuA side chains (-CH$_3$ and -CH$_2$) are located between 0.9 and 1.8 ppm and -OCH$_2$ protons of the PBuA side chain are situated at 4 ppm (Integral$_{H\ PBuA}$) (Figure 1). After calculation using the equation below, the molar composition of each block is of 0.50.

Equation SI 1. Molar composition of PPFS and PBuA in the BCP.

$$\%PBua = \frac{Integral_{1H\ PBua}}{Integral_{1H\ PPFS} + Integral_{1H\ PBua}} \times 100$$

$$\%PPFS = 100 - \%PBua$$

Equation SI 2. Volume fraction of PPFS and PBuA in the BCP.

$$\varnothing_{PBua} = \frac{\frac{MW_{PBua}}{\rho_{Bua}}}{\frac{MW_{PPFS}}{\rho_{PFS}} + \frac{MW_{PBua}}{\rho_{Bua}}}$$

$$\varnothing_{PPFS} = 1 - \varnothing_{PBua}$$

Where ρ_{PFS} = 1.4 g/mL and ρ_{BuA} = 1.08 g/mL

- Theoretical molar mass:

The theoretical molar mass (MW) of the block copolymers is determined using the conversion obtained by ^{1}H NMR. Considering PFS as monomer A and BuA as monomer B, the theoretical molar mass of the BCPs is:

Equation SI 3. Theoretical determination of the molar mass of the BCPs.

$$MW_{poly\,B_{theo.}} = MW_{BlocBuilder} + \left[\frac{molar\ composition_{monomer\,A} \times Conversion_A}{molar\ composition_{initiator}}\right] \times M_{monomer\,A}$$

$$+ \left[\frac{molar\ composition_{monomer\,B} \times Conversion_B}{molar\ composition_{initiator}}\right] \times M_{monomer\,B}$$
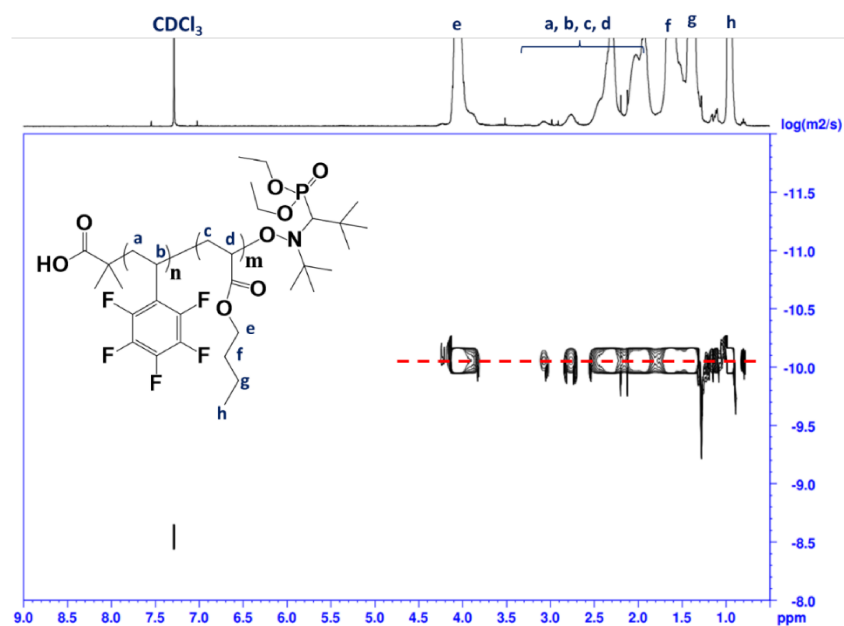
Figure SI 3. Structure and DOSY NMR spectrum (300 MHz, room temperature, CDCl$_3$) of purified (PPFS$_{0.54}$-b-PBuA$_{0.46}$)$_{37K}$ (BCP4).
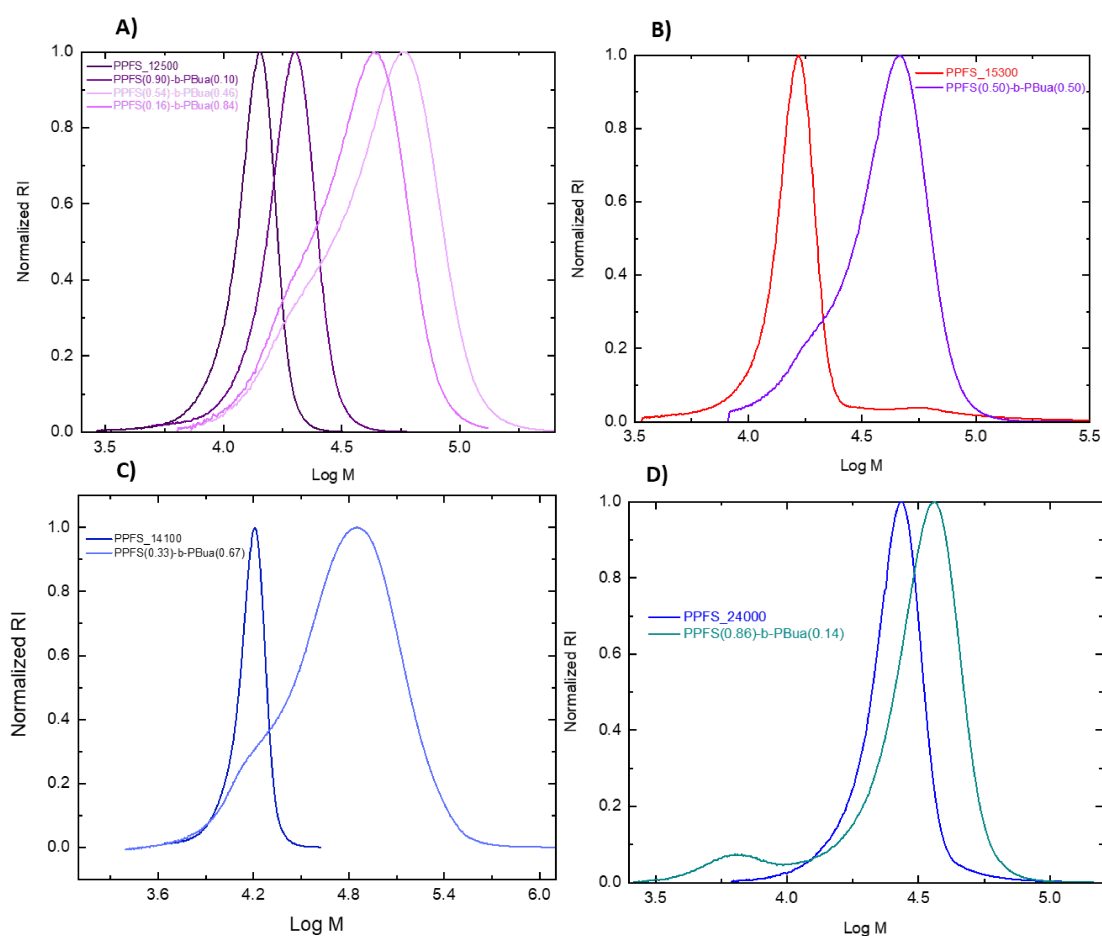
Figure SI 4. SEC chromatograms of (A) macro-initiator (PPFS1) (Mn = 12 500 g/mol, Mw = 13 400 g/mol, D = 1.07) and [(PPFS$_{0.90}$-b-PBuA$_{0.10}$)$_{17K}$ BCP6 (Mn = 17 400 g/mol, D = 1.09); (PPFS$_{0.54}$-b-PBuA$_{0.46}$)$_{37K}$ BCP4 (Mn = 37 000 g/mol, D = 1.36); (PPFS$_{0.16}$-b-PBuA$_{0.84}$)$_{31K}$ BCP1 (Mn = 31 000 g/mol, D = 1.26)] - chain extension from PPFS1.

(B) macro-initiator (PPFS3) (Mn = 15 300 g/mol, Mw = 16 100 g/mol, D = 1.05) and (PPFS$_{0.50}$-b-PBuA$_{0.50}$)$_{34K}$ BCP3 (Mn = 34 000 g/mol, D = 1.2) - chain extension from PPFS3.

(C) macro-initiator (PPFS2) (Mn = 14 100 g/mol, Mw = 15 200 g/mol, D = 1.07) and (PPFS$_{0.33}$-b-PBuA$_{0.67}$)$_{40K}$ BCP2 (Mn = 40 100 g/mol, D = 1.88) - chain extension from PPFS2.

(D) macro-initiator (PPFS4) (Mn = 24 000 g/mol, Mw = 26 400 g/mol, D = 1.1) and (PPFS$_{0.86}$-b-PBuA$_{0.14}$)$_{31K}$ BCP5 (Mn = 30 600 g/mol, D = 1.12) - chain extension from PPFS4.

- DSC of the block copolymers
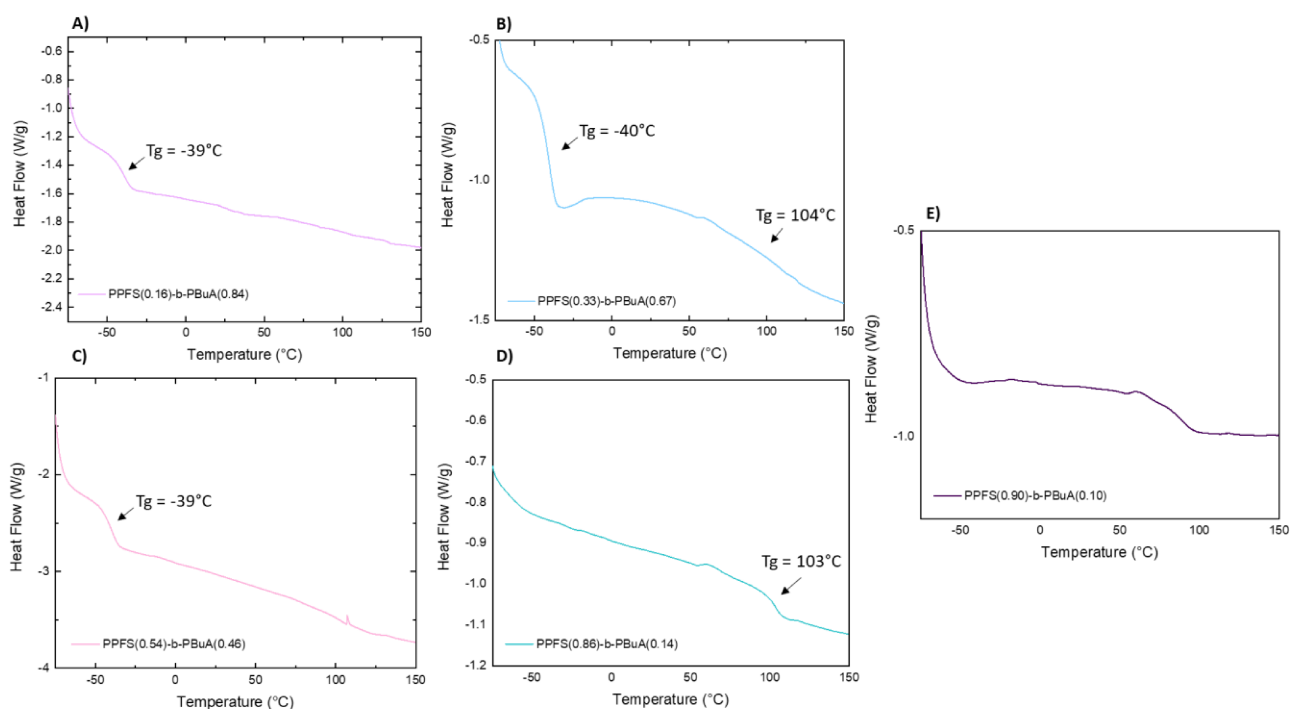
Figure SI 5. DSC of block copolymers ; (A) (PPFS$_{0.16}$-b-PBuA$_{0.84}$)$_{31K}$ BCP1, (B) (PPFS$_{0.33}$-b-PBuA$_{0.67}$)$_{40K}$ BCP2, (C) (PPFS$_{0.54}$-b-PBuA$_{0.46}$)$_{37K}$ BCP4, (D) (PPFS$_{0.86}$-b-PBuA$_{0.14}$)$_{31K}$ BCP5, (E) (PPFS$_{0.90}$-b-PBuA$_{0.10}$)$_{17K}$ BCP6.

- DSC of 1-hexanethiol modified PPFS$_{0.33}$-b-PBuA$_{0.67}$ (BCP2)
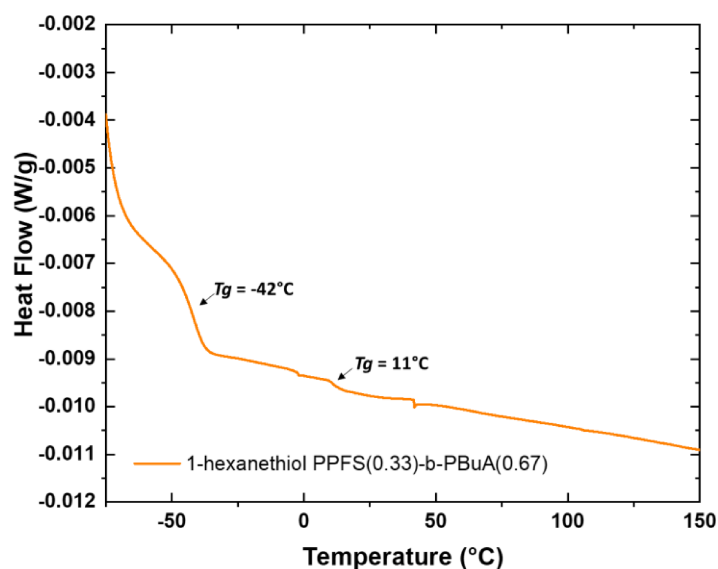
Figure SI 6. DSC of 1-hexanethiol modified PPFS$_{0.33}$-b-PBuA$_{0.67}$ BCP2.
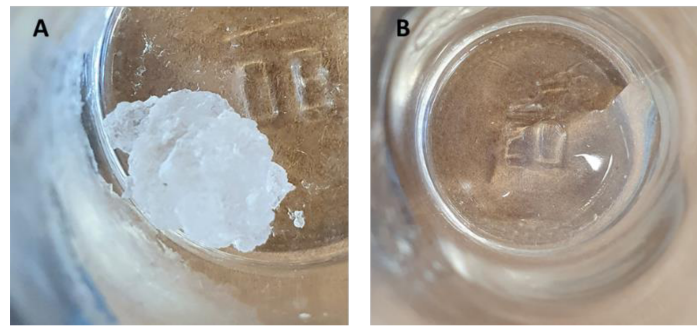
Figure SI 7. (A) BCP3 (PPFS$_{0.33}$-*b*-PBuA$_{0.67}$)$_{40K}$ polymer at room temperature, (B) BCP3 modified with 1-hexanethiol at room temperature.

- SAXS peaks attribution:

The attribution of the peaks was made using the Primus software an following the distance distribution placement of the peaks. Indeed, some peaks that were not as intense on the original graph were visible using this functionality of the software.
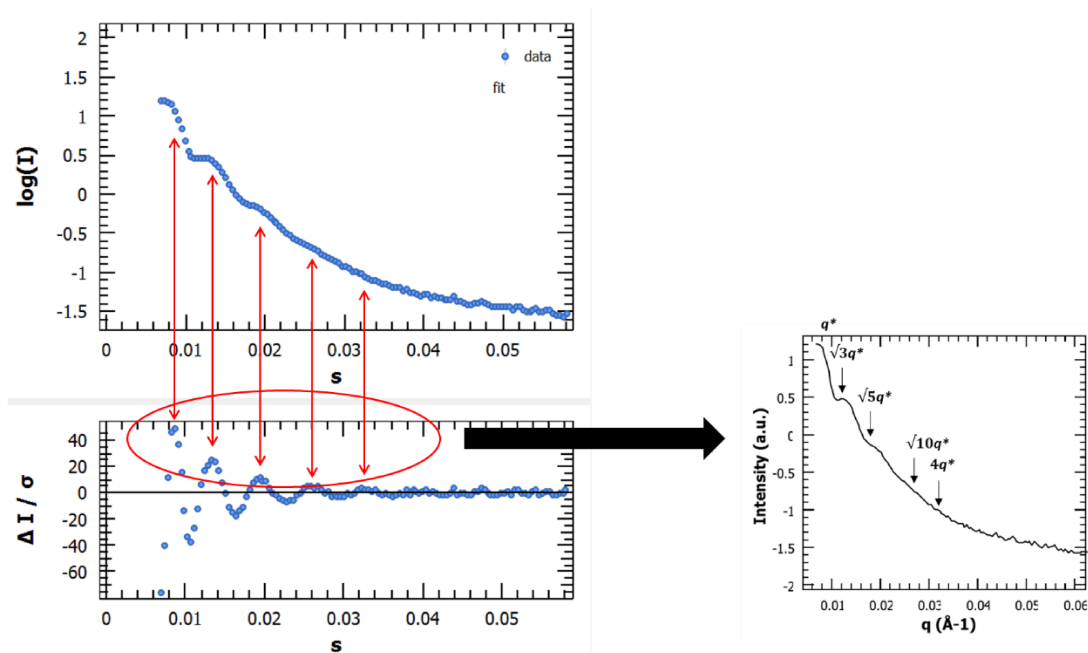
- Distance between nanodomains (SAXS):

Depending on the spacing between scattering vectors (q) and the structure of the material, the distance between nanodomains is calculated using different formulas. The choice of one over the other depends on the type of periodic structure and the number of dimensions involved. Indeed, for a one-dimensional periodic structure such as the lamellar (LAM) structure, equation (1) will be used; For a two-dimensional structure such as hexagonally

closed-packed cylinders (HCC), equation (2) will be used and finally; equation (3) is for a three-dimensional structure such as primitive cubic or body centered cubic (BCC). The dimensions in the equations are represented by the Miller indices: h, k, l. (36)

Equation SI 4. Determination of the distance between nanodomains.

$$q = \frac{4\,\pi\,\sin\theta}{\lambda}$$

$$(1) \qquad q_n = n\,\frac{2\pi}{d} \quad \longrightarrow \quad d = \frac{2\pi n}{q}$$

$$(2) \qquad q_n = \frac{4\pi}{\sqrt{3}\,d}\,\sqrt{h^2 + k^2 + hk} \quad \longrightarrow \quad d = \frac{4\pi}{\sqrt{3}\,q_n}\,\sqrt{h^2 + k^2 + hk}$$

$$(3) \qquad q_n = \frac{2\pi}{d}\,\sqrt{h^2 + k^2 + l^2} \quad \longrightarrow \quad d = \frac{2\pi}{q_n}\,\sqrt{h^2 + k^2 + l^2}$$

Experimentally for each block copolymer the peaks positions are:

Table SI 1. SAXS peak position of the block copolymers and the block copolymer modified with 1-hexanethiol.

Block copolymer	q (Å^{-1})	Peak position ratios	Pitch (nm)	Lattice structure
(PPFS$_{0.16}$-*b*-PBuA$_{0.84}$)$_{31K}$	0.0161	1	45	HCC
	0.0288	$\sqrt{3}$		
	0.0428	$\sqrt{7}$		
	0.058	$\sqrt{13}$		
(PPFS$_{0.33}$-*b*-PBuA$_{0.67}$)$_{40K}$	0.016	1	45	HCC
	0.0271	$\sqrt{3}$		
	0.0446	$\sqrt{7}$		
	0.0582	$\sqrt{13}$		
(PPFS$_{0.50}$-*b*-PBuA$_{0.50}$)$_{34K}$	0.018	1	35	LAM
	0.0361	2		
	0.0541	3		
	0.0718	4		

(PPFS$_{0.54}$-*b*-PBuA$_{0.46}$)$_{37K}$	0.0158	1		
	0.0329	2	45	HCC
	0.055	$\sqrt{12}$		
(PPFS$_{0.86}$-*b*-PBuA$_{0.14}$)$_{31K}$	0.0228	1		
	0.0409	$\sqrt{3}$	32	HCC
	0.048	2		
	0.0686	3		
(PPFS$_{0.90}$-*b*-PBuA$_{0.10}$)$_{17K}$	0.039	1	-	disorder
PPFS$_{0.24}$-*b*-PbuA$_{0.76}$ (Tuned from (PPFS$_{0.16}$-*b*-PBuA$_{0.84}$)$_{31K}$)	0.0167	1		
	0.024	$\sqrt{2}$		
	0.0285	$\sqrt{3}$	38	Cubic
	0.0347	2		
	0.0403	$\sqrt{6}$		
PPFS$_{0.59}$-*b*-PbuA$_{0.41}$ (Tuned from (PPFS$_{0.54}$-*b*-PBuA$_{0.46}$)$_{37K}$)	0.0162	1		
	0.0317	2		
	0.0473	3	45	HCC
	0.0604	$\sqrt{13}$		
1-hexanethiol modified PPFS$_{0.33}$-*b*-PBuA$_{0.67}$	0.017	1	43	disorder

Declaration of my independent performance Chapter 3: PentaFluoroStyrene-based Block Copolymers Controlled Self-Assembly Pattern: A platform paving the way to functional block-copolymers

For the most part, I performed the majority of the practical work, this specifically included:

- The synthesis of all the PPFS-*b*-PBuA block-copolymers (BCP1 to BCP6) and their relative PPFS macro-initiators.

- The *para*-thiol modification of BCP3 with 1-hexanethiol.

- ^{1}H-NMR analysis to determine the monomer conversions and polymer compositions, and ^{19}F NMR to assess the *para*-thiol modification. The sample preparation for the DOSY NMR, the experiment and data analysis were performed with an experienced colleague.

- Size Exclusion Chromatography (SEC) to obtain information on the polymer's molar masses and dispersity.

- Differential Scanning Calorimetry (DSC) for the thermal properties of the materials

- Atomic force microscopy (AFM) to observe the self-assembly of the BCP and the driven self-assembly when adding PPFS homopolymer.

- The sample preparation for the Small-angle X-ray scattering (SAXS) analysis. The samples were characterized in another lab (*Centre de Recherche Paul Pascal* (CRPP) in Bordeaux) because the apparatus is not available in our lab.

All data collected, were analysed by me. The vast majority of the peer-reviewed technical article was written by me; specifically, I conceived and wrote the original draft of the manuscript and took the lead in harmonizing and incorporating suggested changes from my co-authors.

Chapter 4. *para* fluoro-thiol clicked diblock-copolymer self-assembly: Towards a new paradigm for highly proton-conductive membranes

Karell Bosson,[a,b,e] Pierre Marcasuzaa,[a,b] Antoine Bousquet,[b] Günter E.M. Tovar,[c,d] Vladimir Atanasov,[e] Laurent Billon[a,b]

[a] Bio-inspired Materials Group: Functionalities & Self-assembly, E2S UPPA, 64000 Pau, France

[b] Universite de Pau et Pays de l'Adour, E2S UPPA, CNRS, IPREM, UMR5254, 64000 Pau, France

[c] Institute for Interfacial Process Engineering and Plasma Technology IGVP, University of Stuttgart, Pfaffenwaldring 31, 70569 Stuttgart, Germany

[d] Fraunhofer Institute for Interfacial Engineering and Biotechnology IGB, Nobelstr. 12, 70569 Stuttgart, Germany

[e] Institute of Chemical Process Engineering, University of Stuttgart, Boeblingerstrasse 78, 70199 Stuttgart, Germany

Corresponding author:

laurent.billon@univ-pau.fr

Table of contents Chapter 4

para fluoro-thiol clicked diblock-copolymer self-assembly: Towards a new paradigm for highly proton-conductive membranes

Karell Bosson [a,b,e], Pierre Marcasuzaa [a,b], Antoine Bousquet [b], Günter E.M. Tovar [c,d], Vladimir Atanasov [e], Laurent Billon [a,b,*]

[a] *Bio-inspired Materials Group: Functionalities & Self-assembly, E2S UPPA, 64000, Pau, France*
[b] *Universite de Pau et Pays de l'Adour, IPREM, CNRS UMR5254, 64000, Pau, France*
[c] *Institute for Interfacial Process Engineering and Plasma Technology IGVP, University of Stuttgart, Pfaffenwaldring 31, 70569, Stuttgart, Germany*
[d] *Fraunhofer Institute for Interfacial Engineering and Biotechnology IGB, Nobelstr. 12, 70569, Stuttgart, Germany*
[e] *Institute of Chemical Process Engineering, University of Stuttgart, Boeblingerstrasse 78, 70199 Stuttgart, Germany*

ABSTRACT

Sulfonated sPPFS-*b*-PBuA diblock and statistical copolymers based on 2,3,4,5,6-pentafluorostyrene PFS and butyl acrylate BuA were elaborated for Proton Exchange Membrane Water Electrolyser (PEMWE) purposes. The block copolymers (BCP) were synthetized by Nitroxide Mediated Polymerization NMP, a controlled radical polymerization technique that yields a well-defined molar mass and a low dispersity material. These diblock-copolymers have the ability to self-assemble due to the immiscibility of the two macromolecular segments PPFS and PBuA. Statistical copolymers of the similar chemical composition were synthetized by both controlled radical polymerization NMP in solution and by free radical polymerization FRP in emulsion as waterborne dispersed polymer with highest molar mass. The copolymers were sulfonated by a mild click-reaction, namely an organo-catalyzed nucleophilic substitution reaction with sodium 3-mercapto-1-propanesulfonate (SMPS) at low temperature. The morphology of the sulfonated diblock-copolymer BCP was studied by SAXS and AFM, revealing a nano-phase-segregated sulfonated membrane. The mechanical properties of the membranes were improved by ionic cross-linking with polybenzimidazole (PBI-OO). Finally, the conductive properties of the sulfonated BCPs and statistical copolymers were investigated as a function of parameters such as the morphology of the BCP, the molar mass, and the sulfonation degree of the materials.

1. Introduction

Over time, water electrolysis has emerged as the technique of choice for carbon-free hydrogen production. By using water and energy coming from renewable sources as its main feedstocks, water electrolysers are expected to help reduce carbon dioxide emissions. Electrolysers are divided into three types: alkaline electrolysers (AEC) [1], proton exchange membrane (PEM) electrolysers [2], and solid oxide electrolysis (SOE) cells [3]. Although AEC represents the most developed electrolyser technology to date, PEM electrolysers are regarded as most certainly superior due to their better energy efficiency, higher production rates, and compact electrolyser design [4]. A PEM electrolyser is operated in acidic media, and the electrolyte is a thin proton-conducting polymer membrane. In a typical PEM electrolysis system, the electrodes are directly assembled on the membrane, also called Membrane Electrode Assembly (MEA) [2]. At the anode, to which water is supplied, the oxidation reaction (Oxygen Evolution Reaction - OER) takes place with the decomposition of water into oxygen, protons, and electrons. At the cathode, the reduction reaction (Hydrogen Evolution Reaction - HER) takes place, recombining the electrons and protons into gaseous hydrogen. Most cathode materials for PEM electrolysers are based on platinum, which has the best HER activity and is very stable in acidic media. Metal oxides such as RuO_2 and IrO_2 are usually used as anode materials [5].

The proton-conducting membrane is the core component of the device. The membrane not only conducts protons, but also prevents the gas products coming from both electrodes from mixing. The thinner the membranes, the higher the transfer rate of protons between both electrodes. To be effective, the membrane must have a good chemical and mechanical stability, thermal and hydrolytic stability, and high proton

conductivity [6]. Nafion® is currently the material of reference for these membranes. Nafion® membranes have been thoroughly investigated and shown to have very good proton-conducting properties as well as very good chemical and mechanical properties. However, the synthesis of Nafion® requires several production steps, resulting in high production costs. With the aim of developing less expensive membranes with similar performances as Nafion®, different types of polymeric materials have been developed [7]. They consist of sulfonated fluorinated, partially fluorinated [8] or hydrocarbon polymers [9]. Sulfonated poly (ether ether ketone) (sPEEK), or poly(ether sulfone ketone) (sPESK) with a high degree of sulfonation (IEC >2 meq/g) have approached the conductivity of Nafion® [10–13].

The mechanism of proton conduction in Nafion® has also been studied. Its good proton conductivity is attributed to the phase segregation that occurs when the hydrophilic acidic moieties are combined with the hydrophobic fluorocarbon chain. This results in the formation of hydrophilic channels in which the proton-conductivity occurs according to the water dynamics [10,14]. For this reason, there has been an increased interest in the synthesis of amphiphilic diblock-copolymers for the preparation of membranes. It has already been shown that the structural organization of diblock-copolymers positively affects the transport kinetics in the membrane. Examples such as sulfonated BCPs of poly(sulfone-*b*-vinylidene fluoride), and poly(styrene-*b*-isobutylene-*b*-styrene) (s-SIBS) have already been investigated. In these studies, it was found that the transport properties increased by an order of magnitude when diblock-copolymers were used compared to random copolymers, with the most influential parameter being the connections of the hydrophilic domains [15–17].

In the present study, we investigated the structural and conductivity properties of new sulfonated poly(pentafluorotyrene-*b*-butyl acrylate) (sPPFS-*b*-PBuA) diblock copolymers. These copolymers were obtained from PPFS-*b*-PBuA diblock copolymers synthesized by nitroxide

mediated polymerization (NMP) followed by a mild organo-catalyzed *para* fluoro-thiol modification technique to introduce the sulfonated group on the PPFS block [18]. In addition, for a comparative study, PPFS/PBuA statistical copolymers were synthesized by emulsion polymerization and also investigated. The initial and the sulfonated copolymers were characterized by ^{1}H NMR and ^{19}F NMR, DSC, AFM, SAXS, rheology and conductivity measurements (Scheme 1).

The final aim of this work is to use the diblock-copolymer self-assembly to pave the way to the design of proton-conducting nano-channels across the membranes.

2. Experimental section

2.1. Materials

Pentafluorostyrene (99%, Sigma-Aldrich), butyl acrylate (99%, Sigma-Aldrich), BlocBuilder® (provided by Arkema), free-SG1 (83%, provided by Arkema), dimethylformamide (DMF, anhydrous, 99.8%, Sigma-Aldrich), potassium persulfate/$K_2S_2O_8$ (99%, Sigma-Aldrich), sodium dodecyl sulfate/SDS (99%, Sigma-Aldrich), sodium phosphate/Na_2HPO_4 (Merck), Sodium chloride/NaCl (99.5%, Sigma-Aldrich), DMSO (VWR), sodium 3-mercapto-1-propanesulfonate (95%, Sigma-Aldrich), 1,8-Diazabicyclo[5.4.0]undec-7-ene (DBU, 99%, Sigma, Aldrich), 2,2-(ethylenedioxy)diethanethiol (95%, Sigma-Aldrich), PBI-OO (Fumatech), technical methanol (VWR), THF (VWR). Used without further purification.

2.2. Copolymers synthesis

2.2.1. Synthesis of PPFS/PBuA diblock-copolymer

The NMP of PFS was performed in bulk following a typical NMP procedure [19]. Pentafluorostyrene (41.2 mmol), BlocBuilder® (0.10
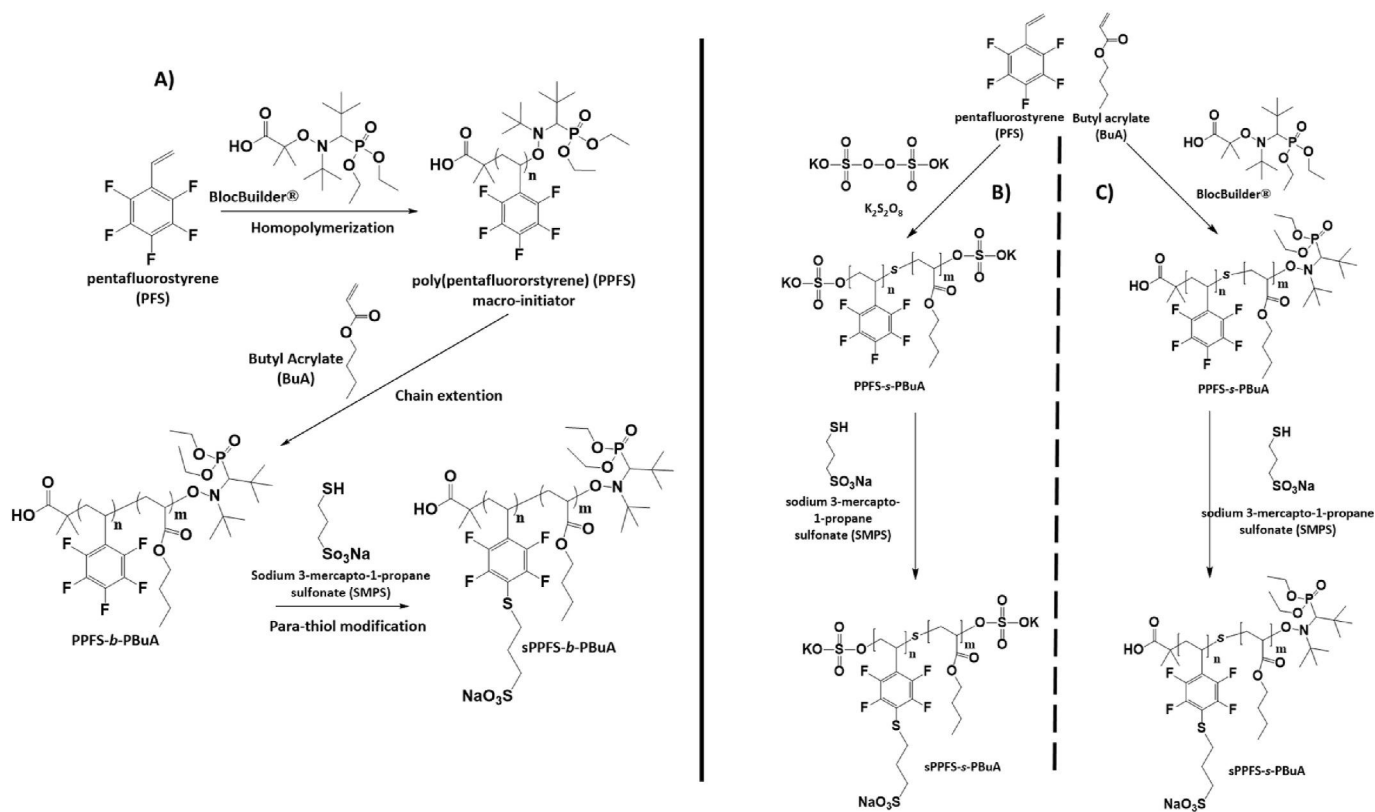
Scheme 1. Synthetic routes to sulfonated PPFS/PBuA diblock and statistical copolymers (sPPFS-*b*-PBuA and sPPFS-*stat*-PBuA). (A) BCP synthesized by NMP controlled radical polymerization; (B) Statistical copolymer synthetized by free radical polymerization in emulsion; (C) Statistical copolymer synthesized by NMP controlled radical polymerization.

mmol) and free-SG1 (0.01 mmol) were added to a 25 mL round bottom flask equipped with a septum and a magnetic stirring bar. The mixture was placed into an ice bath and bubbled with nitrogen for 15 min and subsequently placed into an oil bath that was pre-heated at 115 °C. The mixture was stirred for 5h at 115 °C. At the end of the reaction time, the mixture was cooled down to RT and the polymer was precipitated in methanol. The solid precipitants were collected by filtration and the polymer was dried under vacuum at 60 °C overnight. Purification of the polymer was performed by dissolution in THF and subsequent precipitation in methanol. The purification step was repeated twice and then the final macro-initiator PPFS was obtained. The so obtained PPFS macro-initiator was then used for the chain extension procedure with a butyl acrylate (BuA) monomer. To do so, the PPFS macro-initiator (0.049 mmol; Mn = 14 100 g/mol, Đ = 1.07 (Fig. SI 5)) and some free-SG1 (0.0049 mmol) were dissolved into DMF (1.5 mL) in a 25 mL round bottom flask equipped with rubber seals and a magnetic stirring bar. Subsequently, BuA (26.9 mmol) was added to the mixture. Different ([BuA]/[PPFS]) ratios were calculated and used to target different self-assembly morphologies. The mixture was degassed with nitrogen at room temperature for 15 min before putting the flask in an oil bath preheated at 115 °C. The mixture was stirred at 115 °C for 9h. The BCP was recovered by precipitation of the mixture into methanol after cooling down to room temperature. The precipitation was followed by filtration and drying of the polymer under a vacuum oven at 60 °C overnight (conversion: 91%). The synthesis was previously reported by our group [19].

2.2.2. Synthesis of statistical PFS/BuA copolymer by NMP

Statistical copolymerization of pentafluorostyrene (PFS) and butyl acrylate (BuA) was performed in DMF in similar way to the diblock-copolymer synthesis. PFS (33 mmol), BuA (21.5 mmol), BlocBuilder® (0.13 mmol) and some free-SG1 (0.013 mmol) were added to a 25 mL round bottom flask equipped with rubber seals and a magnetic stirring bar. The mixture was placed into an ice bath, purged with nitrogen for 15 min and subsequently placed into an oil bath that was pre-heated at 115 °C for 7 h. The copolymer was recovered by precipitation of the mixture into methanol after cooling down to room temperature. The precipitation was followed by filtration and drying of the polymer in a vacuum oven at 60 °C overnight. Purification of the polymer was performed by dissolution in THF and subsequent precipitation in methanol. The purification step was repeated twice. (Conversion BuA = 50%; conversion PFS = 66%)

2.2.3. Copolymerization PFS/BuA by free radical polymerization in emulsion

In a three-neck round bottom flask, water (200 g) was added and degassed with nitrogen for an hour at RT. Potassium persulfate (K$_2$S$_2$O$_8$, 1 mmol), sodium dodecyl sulfate (SDS, 6.9 mmol) and sodium phosphate (Na$_2$HPO$_4$, 0.84 mmol) were added under nitrogen flow. The mixture was stirred at room temperature (RT) until all components were dissolved (approximatively 30 min). The monomers PFS (151.5 mmol) and BuA (75.7 mmol) were pre-mixed by stirring and subsequently added to the flask under vigorous stirring. The temperature was raised as fast as possible with a preheated oil bath at 90 °C. When the desired temperature of 90°c was reached in the mixture, the temperature controller was adjusted to keep the temperature constant at 90 °C over time. The polymerization was stopped when the mixture became translucent, after 4 h in our case. After completion of the reaction, the mixture was cooled down to RT and sodium chloride (NaCl) was added until full aggregation of the polymer particles. The polymer was then rinsed with water to remove the excess of salt and dried at 100 °C under vacuum for 24 h (conversion = 100%)

2.2.4. Sulfonation by para fluoro-thiol modification of the copolymers

The copolymer (containing 41.2 mmol PPFS units) was dissolved into DMF (5 mL) ina round bottom flask. 1,8-Diazabicyclo[5.4.0]undec-

7-ene (DBU, 43.3 mmol) was added to the mixture followed by the addition of sodium-3-mecapto-1-propanesulfonate (SMPS, 45.1 mmol). The mixture was stirred at room temperature overnight. After completion of the reaction, the solution was dialysed to remove the excess of the water-soluble components. For that, the polymer was mixed with distilled water (30 mL), poured into an adequate dialysis tube (MWCO 3 kDa), and dialysed in distilled water for 3 days. After dialysis, the solution in the tube was lyophilised for 2 days. (conversion = 100%)

2.3. Polymer crosslinking and membranes preparation

The crosslinking of the membranes was performed by both covalent and ionic crosslinking. To perform the covalent crosslinking, the polymers must be partially sulfonated to contain unsubstituted penta-fluorostyrene units. The difunctional 2,2-(ethylenedioxy)diethanethiol molecule was used as a crosslinker agent. Different crosslinking ratios were studied. Here as an example is given the preparation of a membrane containing 12 mol% crosslinker. In a separate flask, 0.26 mmol of 2,2-(ethylenedioxy)diethanethiol was mixed with 0.26 mmol DBU in 3 ml DMSO. In another flask, a 10 wt% solution of copolymer was formed by dissolving the partially sulfonated copolymer in DMSO. Both solutions were then mixed and casted in a silicon mold. The mold was placed in the convection oven at 80 °C for 2 h followed by an increase of temperature to 120 °C overnight.

The ionic crosslinking was performed using Polybenzimidazole (PBI-OO). In a separate flask, PBI-OO was dissolved in DMSO (2 wt%). In another flask, a 10 wt% solution of copolymer was made by dissolving the sulfonated copolymer in DMSO. Both solutions were then mixed and casted in a silicon mold. The mold was placed in the convection oven at 80 °C for 2 h followed by an increase of temperature to 120 °C overnight. The dried membranes were then immersed into a 5% HCl solution overnight, rinsed several times with deionised water and dried at 50 °C under vacuum [20].

For the preparation of a membrane without crosslinking, the procedure was repeated without addition of 2,2-(ethylenedioxy)dieth-anethiol or PBI-OO/DBU mixture.

2.4. Characterization techniques

2.4.1. Nuclear magnetic resonance ^{1}H NMR & ^{19}F NMR

NMR spectra were recorded on a Bruker DPX-400 spectrometer using deuterated solvents obtained from Sigma-Aldrich (CDCl$_3$ and DMSO-d_6). The spectra were recorded at room temperature.

2.4.2. Size exclusion chromatography (SEC)

The molar mass of the copolymers was determined by SEC. The set up consisted of a pump (LC-20A, Shimadzu), an autosampler (Sil-20AHT), a differential refractometer (Optilab Rex, Wyatt), a light scattering detector (Dawn Heleos II, Wyatt), a viscosimeter (Viscoton, Wyatt), and three columns in series (Styragel HR2, HR4 and HR6 with pore sizes ranging from 102 to 106 Å). The polymers were dissolved in THF at a concentration of 3 g/L. Prior to injection, the samples were filtered through 0.45 μm nylon filter. The chromatography was performed at 30 °C at a flow rate of 1 ml/min.

2.4.3. Differential scanning calorimetry DSC

Polymer sample (1–10 mg) was placed into aluminium capsules that are closed hermetically. The capsule was then placed into the DSC device (DSC Q100 from TA instruments) that was set to heating and cooling rates of 20 °C/min under nitrogen atmosphere at a flow of 50 mL/min. The characterization was performed at the temperature range of −80 °C–180 °C.

2.4.4. Atomic force microscopy AFM

AFM was performed on a Multimode 8 Atomic Force Microscope (Bruker) and recorded in PeakForce QNMmode. For the BCPs, the

polymer film was obtained by spin-coating of a diluted polymer solution on a silicon wafer. The solution was obtained by dissolution of the polymers in a mixture of toluene: propylene glycol methyl ether acetate (PGMEA) = 75 : 25, (2 wt%). The sample was first characterized by AFM directly after spin-coating and drying and then after annealing at 140 °C for 30 min and subsequent quenching at RT. As the sulfonated BCPs were no longer soluble in the toluene/PGMEA mixture, they were solubilized in DMSO (2 wt%). The polymer solution was then drop casted on the silicon wafer and dried in the oven at 50 °C overnight.

2.4.5. Small-angle X-ray scattering SAXS

SAXS experiments were performed with a high-resolution X-ray Spectrometer Xeuss 2.0 from Xenox. The spectrometer operates with a radiation wavelength of λ = 1.54 Å (Copper K_α radiation). Scattering patterns were collected using a PILATUS 300K Dectris detector with a sample-to-detector distance of 1637 mm. The collected data were analysed using Primus software. The film preparation for the SAXS experiment was done in a similar way as for the AFM characterization. The polymers were solubilized in their adequate solvents (2 wt%) and drop casted on a Kapton film. The films were annealed prior to analysis. For the BCP, the annealing was done at 140 °C for 30 min, and for the sulfonated BCP at 50 °C overnight.

2.4.6. Rheology

Rheology was performed on an Anton Paar rheometer equipped with a SER (Sentmanat Elongational Rheometer) universal testing platform. The SER platform consisted of two counter rotating drums stretching the sample until the breaking point. The drums each had a diameter of 10.3 mm. A rectangular section was collected from the membranes and positioned on the drums. The films were stack to the drums at elevated temperature. The drums were set to a rotating speed of 0.1 $^{s-1}$, and the chosen rotational angle was 360°.

2.4.7. Ion exchange capacity

Ion Exchange Capacity (IEC) of the membranes were measured by titration method. A dry piece of membrane (in H-form) was immersed in 50 mL of saturated NaCl solution under stirring for 24 h. Solution was titrated with 0.1 N NaOH solution to the equivalence point of bromothymol blue indicator (pH = 7). The IEC was calculated according to the equation: [IEC (meq/g) = (V_{NaOH} × C_{NaOH})/W_d], where W_d is the dry weight (mg) of the sample and V_{NaOH} and C_{NaOH} are the volume (mL) and molar concentration of NaOH solution, respectively.

2.4.8. Water uptake measurement

Water uptake was determined by comparing the weight of the membrane in its dry state and in its hydrated state. To do so, the membrane was weighted in a dry state and immersed in deionised water for 24h at room temperature. The water uptake was calculated using the following formula:

2.4.9. Electrochemical Impedance Spectroscopy

The electric resistance of the membranes was determined via impedance spectroscopy (IM6 Impedance measurement system, Zahner elektrik) in a Teflon cell with gold-plated copper electrodes having the following electrode area: 0.25 cm^2. The impedance, where the phase angle between current and voltage was zero, was taken as the (ohmic) ion-exchange membrane resistance. The measurement was performed in 0.5 N H_2SO_4. The membrane was placed between two Nafion® 117 membranes and pressed in a stack between the two electrodes at T = 25 °C. By this method, the resistances at the interphase membrane/electrode are eliminated by first measuring all three membranes, followed by measurement of the two Nafion® membranes alone, and subtracting of the impedance of the Nafion® membranes from the impedance of all three membranes.

3. Results and discussion

3.1. Synthesis and characterization of diblock and statistical copolymers

Poly(pentafluorostyrene)-*b*-poly(butyl acrylate) (PPFS-*b*-PBuA) diblock-copolymer (BCP) was previously synthetized by NMP controlled radical polymerization. To summarize, the BCP was synthetized by NMP using the commercially available alkoxyamine BlocBuilder® as an initiator and control agent. By varying the monomer to initiator ratio and adjusting the reaction times, we were able to synthesize diblock-copolymers BCPs with different molar compositions. BCPs morphologies such as hexagonally closed-packed cylinders (HCC) or lamellas (LAM) were targeted by BCP self-assembly. Indeed, if the volume fraction of each block determines the morphology of the nano-segregation, the phase separation occurs only if the two blocks presents an interaction parameter X value high enough to force the non-miscibility. This last one is dependent on the difference of the solubility parameters δ between the blocks. Herein, the Hansen solubility parameters δ of the homopolymers PPFS and PBuA are calculated to be equal to 16.1 Mpa$^{1/2}$ and 17.3 Mpa$^{1/2}$ for PPFS and PBuA, respectively using HSPiP software [19].

It has been proven that favorable nano-structuration in the copolymer improves the proton-conduction in the membrane [21]. For that reason, we aimed to prepare proton-conducting membranes that self-organized into *out-of-the-plane cylinders* of PPFS in a PBuA matrix, *i.e.* perforating nano-channels through the film. Indeed, a polymer structured in such a way after sulfonation would result in a membrane that would dispose of sulfonated conductive channels with a diameter of a few dozens of nanometers. In order to achieve this goal, PPFS$_{0.33}$-*b*-PBuA$_{0.67}$ with a molar mass of 40 000 g/mol was used for the experiments. Its molar composition and molar mass were calculated from ^{1}H NMR and SEC characterizations, and its structure was observed by AFM and SAXS (Fig. 1). (PPFS$_{0.33}$-*b*-PBuA$_{0.67}$)$_{40K}$ (here, the subscript 40K represents the molar mass value of the copolymer by SEC and the same notation was used for all the copolymers) reveals to be composed of nano-domains of PPFS structured in hexagonally-closed-packed cylinders (HCC). Indeed, with a first order peak at q* = 1.6 10^{-2} nm^{-1} and a cylinder-to-cylinder distance of 45 nm (d = 4 π / $\sqrt{3}$ q*) and the following peaks at $\sqrt{3}$ q* and $\sqrt{7}$ q*, this pattern fits well with the HCC structure (Fig. 1 A). Hence, the BCP is able to self-assemble with PPFS cylinders nano-domains in a PBuA matrix. At the same time, PPFS$_{0.33}$-*b*-PBuA$_{0.67}$ displayed two glass transition temperatures at −40 °C and one at 104 °C corresponding to PBuA and PPFS *Tg*, respectively, and confirms the nano-phase separation between the two blocks (Fig. SI 1).

Statistical copolymers of PPFS/PBuA were synthesized by both NMP and free radical polymerization (FRP). NMP was performed in solution in DMF using the alkoxyamine BlocBuilder® as a control agent, and the FRP in emulsion using peroxodisulfate as the initiator. The copolymers were characterized by ^{1}H NMR, SEC, and DSC.

On a typical ^{1}H NMR spectrum of PPFS/PBuA copolymers, the chemical shifts of the backbone protons (-CH and –CH$_2$) are located between 1.8 and 2.9 ppm. Protons of PBuA side chains (-CH$_3$ and –CH$_2$) are located between 1 and 1.8 ppm and –OCH$_2$ protons of the PBuA side chain are located at 4 ppm (Fig. SI 2, Fig. SI 3, Fig. SI 4). From the attribution and integration of the proton signals, the molar composition of both PPFS and PBuA was determined (Table 1). The statistical copolymer (PPFS$_{0.87}$-*stat*-PBuA$_{0.13}$)$_{19K}$ obtained by NMP was composed of 87 mol% of PPFS in contrast to the 80 mol% of PPFS (PPFS$_{0.80}$-*stat*-PBuA$_{0.20}$)$_{140K}$ which were obtained by FRP. (PPFS$_{0.87}$-*stat*-PBuA$_{0.13}$)$_{19K}$ synthesized by NMP presents a dispersity *Đ* of 1.16, whereas the one made by the FRP method *Đ* = 15.2 (Fig. SI 5). The glass transition temperature *Tg* of the copolymers was determined by DSC giving a *Tg* around 64 and 89 °C for the copolymers by NMP and FRP, respectively. The increase in *Tg* could be explained by the high molar mass of the
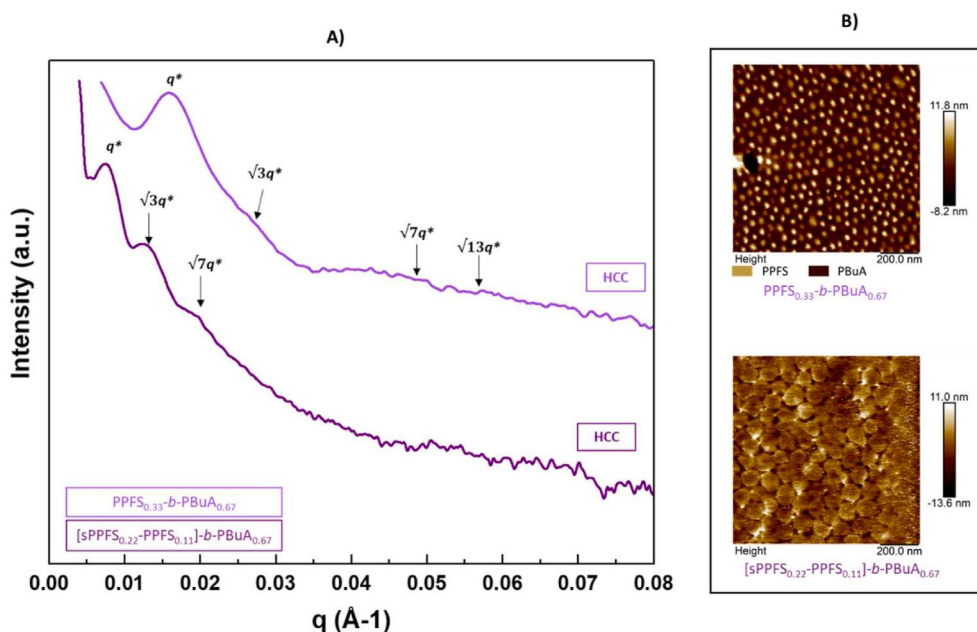
Fig. 1. (A) SAXS patterns of (PPFS$_{0.33}$-b-PBuA$_{0.67}$)$_{40K}$ BCP before and after partial sulfonation (DS = 68%, see Table 2); (B) Peak Force mode AFM height images showing morphology transition before and after sulfonation of the BCP.

Table 1
Summary of the experimental conditions and macromolecular characterizations of the PPFS/PBuA diblock and statistical copolymers.

Polymer (synthetic method)	Experimental conditions			Macromolecular features					
	[M]/[I]	Temp (°C)	Time (h)	M_n^a (kg/mol)	M_w^a (kg/mol)	$Đ^a$	Molar %PPFS^b (%)	Molar %PBuA^b (%)	T_g^c (°C)
PPFS$_{0.33}$-b-PBuA$_{0.67}$ (NMP/solution)	550*	115	22	40	76	1.88	33	67	−40/104
PPFS$_{0.87}$-stat-PMA$_{0.13}$ (NMP/solution)	370	115	7	19	22	1.16	87	13	64
PPFS$_{0.80}$-stat-PBuA$_{0.20}$ (FRP/emulsion)	230	90	6	140	2000	15.2	80	20	89

*[BuA]/[PPFS macro-initiator].
[a] Determined by SEC by equivalent PS.
[b] Determined by ^{1}H NMR (300 MHz, room temperature, CDCl$_3$).
[c] Determined by DSC.

Table 2
Summary of the *para* fluoro-thiol modification conditions and characterizations of the PPFS/PBuA diblock and statistical copolymers.

Polymer (synthesis method)	Thiol Sulfonate salt/PFS unit (eq)	Temp (°C)	Time^a (h)	DS^b (%)	T_g^c (°C)
(PPFS$_{0.33}$-b-PBuA$_{0.67}$)$_{40K}$ (NMP/solution)	≈0.70	25	24	68	- 42/60
	≈1	25	24	100	−40/15
(PPFS$_{0.87}$-s-PBuA$_{0.13}$)$_{19K}$ (NMP/solution)	≈0.5	25	48	57	32
(PPFS$_{0.80}$-s-PBuA$_{0.20}$)$_{140K}$ (FRP/emulsion)	≈1	50	24	100	61

[a] polymerization time.
[b] Degree of sulfonation (DS) determined by^{19}F NMR.
[c] Glass transition temperature (Tg) determined by DSC after sulfonation.

(PPFS$_{0.80}$-stat-PBuA$_{0.20}$)$_{140K}$ copolymer obtained by FRP method in emulsion process (Table 1).

3.2. Sulfonation by para fluoro-thiol modification of the copolymers

Here, the *para* fluoro-thiol modification was selected as an efficient

soft substitution of *para*-fluorine atom in perfluorinated phenyl ring. The substitution was performed with a functional thiol, *i.e.* sodium-3-mecapto-1-propanesulfonate (SMPS) in a one-step synthesis in the presence of a base 1,8-Diazabicyclo[5.4.0]undec-7-ene (DBU). The high capability of the *para*-F of the perfluorinated phenyl ring to thiols has features of a click-reaction: quick, and at mild conditions (RT). Moreover, the versatility and the commercial availability of thiol compounds make them attractive for such reactions [18].

Firstly, the kinetic of the *para* fluoro-thiol modification with the sulfonate compound was studied. To do so, the substitution reaction was performed on PPFS homopolymer and the reaction progress was controlled by ^{19}F NMR. In fact, the reaction mixture which consisted of PPFS homopolymer with a molar mass of 12 500 g/mol and dispersity Đ of 1.07, DMF, DBU (1.05 eq), and SMPS (1.1 eq) were introduced in an NMR tube and placed into the NMR rotor. ^{19}F NMR spectrum of the blend was recorded at room temperature over 24 h (Fig. 2). It turned out that the full substitution of the *para*-F of PPFS by SMPS was obtained after only 3.5 h of reaction. This experiment proved that in mild conditions, the *para* fluoro-thiol modification is very efficient and only few hours are needed for a full sulfonation.

Using the gathered information on the *para*-substitution with the sulfonate compound, the copolymers were fully or partially sulfonated according to the molar ratios of PFS monomer units and SMPS (Fig. 3 I). Even if the full conversion is reached at 3.5h, the reactions were left for
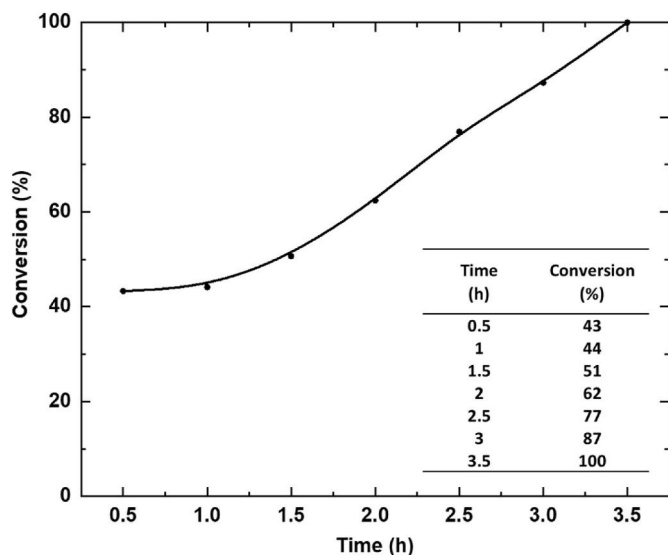
Fig. 2. *Para* fluoro-thiol modification of PPFS homopolymer by SMPS over time. The conversions were determined by ^{19}F NMR.

24 or 48h to make sure that all the polymer reacted with the thiol moiety. Because of its high molar mass, $(PPFS_{0.80}\text{-}s\text{-}PBuA_{0.20})_{140K}$ synthesized by FRP did not dissolve in DMF at room temperature. Therefore, the temperature was raised to 50 °C and the reaction proceeded for 24h. All the sulfonated copolymers were purified by dialysis in water. They were characterized by ^{19}F NMR and DSC (Table 2).

The ^{19}F NMR spectra of the non-modified polymers displays 3 signals for the fluorine at each position of the aromatic ring: δ $2F_{ortho} = -143$ ppm; δ $2F_{meta} = -161$ ppm; δ $1F_{para} = -154$ ppm (Fig. 3 II a). After full modification, there was no more fluorine in *para* position, and the signal of fluorine in *meta* positions is up-field shifted due to the presence of the sulphur in *para* position (δ $2F_{ortho} = -141$ ppm: δ $2F_{meta} = -134$ ppm) (Fig. 3 II c). The ^{19}F NMR spectra of the partially fluorinated copolymer displays the signals of all the fluorine of both the initial copolymer and

the sulfonated one (Fig. 3 II b).

3.3. Thermal properties of the diblock-copolymers

The diblock-copolymer was characterized by DSC before and after full and partial sulfonation (Table 2). A decrease in Tg is observed after sulfonation. Indeed, for the BCPs, the glass transition temperature of the sulfonated PPFS (sPPFS) moiety decreased from 100 °C to 60 °C (Fig. 4 a & b). It is worth noting that introducing a sulfonic group in the polymer chain has been reported in the literature to increase of the Tg of the polymer [22,23]. This increase has been attributed to the decrease of flexibility introduced in the chain by adding $-SO_3H$ groups, which is increasing the number of interacting species (e.g. h-bonding, ionic interactions). However, the compound used herein for sulfonation (sodium-3-mercapto-1-propanesulfonate, SMPS) presents a sulfonic moiety linked to a flexible alkane chain. The use of a short spacer ($-C_3H_6-$) between the backbone and the sulfonic acid functional group introduces some mobility to the polymer, and hence contributes to the decrease of the Tg.

Although it is clearly proven that the sulfonation of PPFS with SMPS is possible under mild conditions for both the homopolymer and the diblock copolymers. The fully sulfonated $(PPFS_{0.33}\text{-}b\text{-}PBuA_{0.67})_{40K}$ PPFS block displayed a Tg lower than the ambient temperature ($Tg = 15$ °C). This drastic decrease from the original Tg of PPFS ($Tg = 104$ °C) is not ideal for membrane purposes. For that reason, the partially sulfonated BCP ($Tg = 60$ °C) was used for further experiments.

3.4. Morphological studies of the sulfonated diblock-copolymer

As stated previously, having an organised sulfonated material was proven to be beneficial for the membrane conductivity. Using amphiphilic diblock-copolymers as membrane materials have increased the transport of protons [15]. Thus, continuous nano-domains of sPPFS through the membrane should provide an efficient transfer of protons from one side of the membrane to the other, *i.e.* nano-channels. In a previous study, it was proven both by AFM and SAXS that $(PPFS_{0.33}\text{-}b\text{-}PBuA_{0.67})_{40K}$ BCP displayed an HCC structuration of PPFS nano-domains in a PBuA matrix [19]. After sulfonation, the morphology
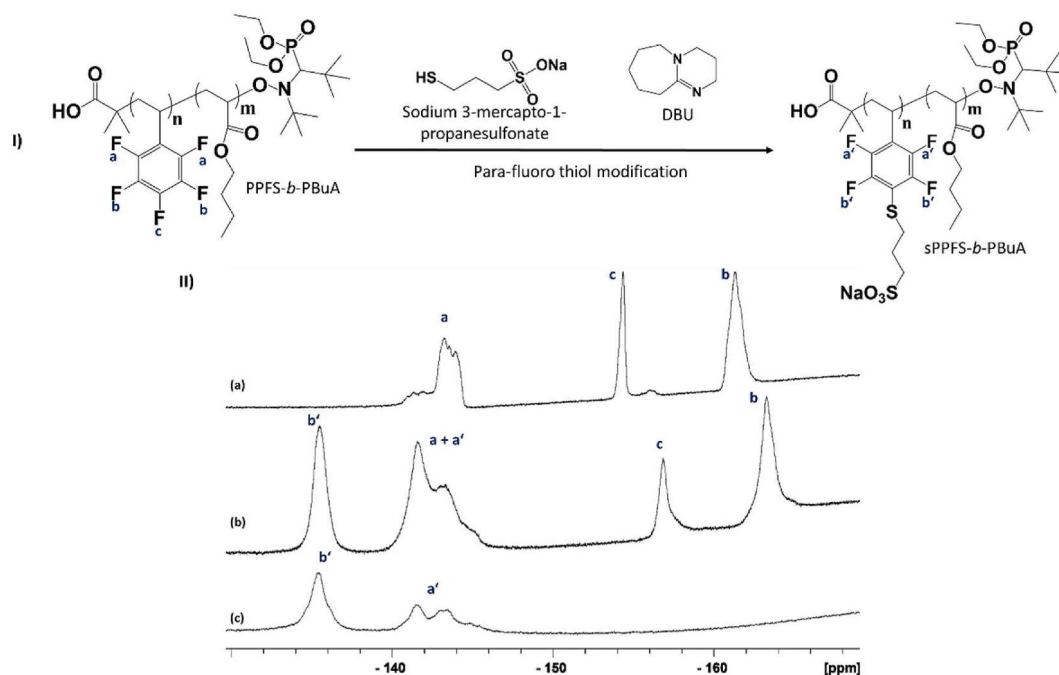
Fig. 3. (I) Sulfonation reaction of PPFS-*b*-PBuA with SMPS. (II) ^{19}F NMR spectra of (a) $(PPFS_{0.33}\text{-}b\text{-}PBuA_{0.67})_{40K}$ in CDCl$_3$; (b) Partially sulfonated $(PPFS_{0.33}\text{-}b\text{-}PBuA_{0.67})_{40K}$ in DMSO-d_6, DS = 68%; (c) Fully sulfonated $(PPFS_{0.33}\text{-}b\text{-}PBuA_{0.67})_{40K}$ in DMSO-d_6, DS = 100%.
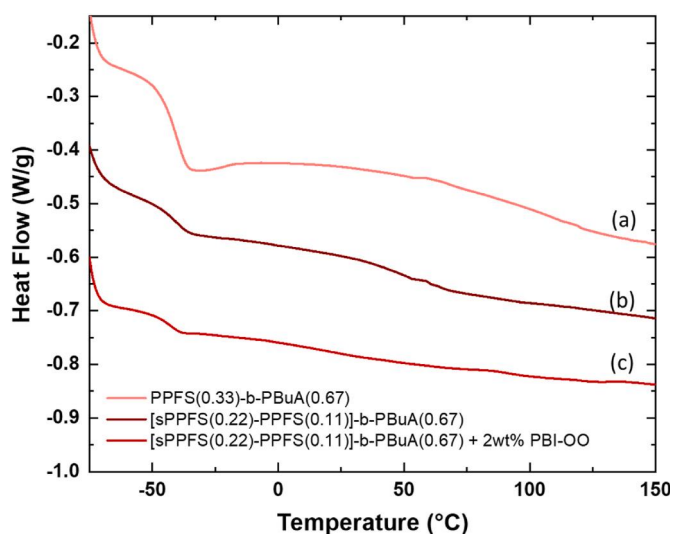
Fig. 4. DSC thermograms of: (a) $(PPFS_{0.33}\text{-}b\text{-}PBuA_{0.67})_{40K}$ with the glass transition temperatures Tg values at - 40 °C and 104 °C for PBuA and PPFS, respectively; (b) Partially sulfonated $(PPFS_{0.33}\text{-}b\text{-}PBuA_{0.67})_{40K}$ (DS = 68%) with Tg values of PBuA at - 40 °C and Tg of sPPFS at 60 °C; (c) Crosslinked sulfonated $(PPFS_{0.33}\text{-}b\text{-}PBuA_{0.67})_{40K}$ with 2 wt% PBI-OO with Tg of PBuA at - 43 °C and Tg of sPPFS(+2 wt% PBIOO) at 93 °C.

of the partially sulfonated BCP was studied by AFM and SAXS (Fig. 1). For this purpose, polymers were dissolved in DMSO (2 wt%) and drop casted on silicon wafer for AFM characterization and on Kapton film for the SAXS experiment. The films were then annealed in oven at 50 °C overnight.

AFM images showed an increase in size of nano-domains from 45 nm (PPFS) to 96 nm (sPPFS) after sulfonation. This may be due to a volume increase of the PPFS block caused by the addition of the sodium-3-mecapto-1-propanesulfonate moieties ($M_{PFS\ unit}$ = 194.1 g/mol; $M_{sPPFS\ unit}$ = 351.98 g/mol). Indeed, the morphological features of the self-assembled BCP are dictated by the volume fraction and specific chain/segment interactions of both blocks in the BCP among other factors. The SAXS measurements on the annealed film revealed an HCC structuration of the BCP after sulfonation, with a first order peak at q* = 7.5 10^{-2} nm^{-1} and a cylinder-to-cylinder distance of 96 nm (d = 4 π / $\sqrt{3}$ q*). The following peaks at $\sqrt{3}$ q* and $\sqrt{7}$ q* are representative of the HCC structure (Fig. 1). From those results, we can assume that the sulfonated BCP is able to self-assemble with nano-domains of *out-of-the-plane* cylinders of sPPFS in a PBuA matrix.

3.5. Membrane elaboration and properties

Membranes were prepared using the sulfonated copolymers and DMSO as a solvent. The challenge here is to define the conditions for achieving mechanically stable membranes. The choice of solvent was made considering the solubility of the sulfonated copolymers and their evaporation rate (bp_{DMSO} = 189 °C).

3.5.1. Membrane elaboration process without crosslinking

DMSO solutions (10 wt%, and 2 wt% in the case of $(PPFS_{0.80}\text{-}s\text{-}PBuA_{0.20})_{140K}$) of the fully or partially sulfonated copolymers were prepared. $(PPFS_{0.80}\text{-}s\text{-}PBuA_{0.20})_{140K}$ made by FRP in the emulsion was used at 2 wt% solution due to its high molar mass. For all the copolymers, the solutions were stirred until complete solubilization of the copolymers. They were then cast in a silicon mold and placed in the convection oven at 80 °C for 2 h and then at 120 °C overnight.

The partially sulfonated $(sPPFS_{0.33}\text{-}b\text{-}PBuA_{0.67})_{40K}$ BCP resulted in a very sticky membrane and was therefore difficult to unmold without tearing the membrane apart (Fig. 5 a). The sulfonated statistical

copolymers by NMP and FRP in emulsion, $(PPFS_{0.87}\text{-}s\text{-}PBuA_{0.13})_{19K}$ and $(PPFS_{0.80}\text{-}s\text{-}PBuA_{0.20})_{140K}$ respectively, resulted in free-standing membranes (Fig. 5 b & c). However, all the membranes swelled a lot and then solubilize when immersed in water, which is an issue for PEMWE applications (Fig. 5 d).

Crosslinking reactions were foreseen to enhance the mechanical properties of the membranes and decrease their swelling during subsequent use. Two different types of *in-situ* crosslinking were investigated. Either covalent crosslinking was performed *via para* fluoro-thiol modification on the PPFS units using the dithiol 2,2-(ethylenedioxy)diethanethiol, or ionic crosslinking by mixing the sulfonated anionic copolymers with polybenzimidazole (PBI-OO) [20]. Preliminary tests using the $(PPFS_{0.87}\text{-}s\text{-}PBuA_{0.13})_{19K}$ with a degree of sulfonation DS = 57%, *i.e.* $([sPPFS_{0.49}\text{-}PPFS_{0.38}]\text{-}s\text{-}PBuA_{0.13})$ were performed to optimise the amount of crosslinker. In fact, a subtle balance must be found to enhance the mechanical properties and reduce the swelling capacity of the membrane.

3.5.2. Covalent crosslinking

To crosslink the PPFS/PBuA copolymers, the *para* fluoro-thiol modification was performed as it has already proven to be an efficient reaction process for the sulfonation of the copolymers. A crosslinker, 2,2-(ethylenedioxy)diethanethiol with two reactive functional thiol groups was introduced to allow the creation of bridges between the polymer chains [24] using DBU in DMSO at room temperature (Fig. 6 A).

Different compositions were tested by calculating a molar ratio [2,2-(ethylenedioxy)diethanethiol]/[PFS units] of 3, 6 and 12 mol% with a polymer content of 10 wt% in DMSO. The crosslinked membranes were then characterized by DSC and elongational rheology. From the DSC thermograms, we notice a slight increase of Tg with the increase of the mol% of added crosslinker (Fig. 6 B). Indeed, as the mol% of the crosslinker increases, the more crosslinking occurs and the more energy the polymer needs to reach the rubbery state.

Elongational rheology experiments were performed on the covalently crosslinked membranes. To do so, a rectangular piece of the membrane was placed at 100 °C on two counter-rotating drums at 0.1 s^{-1} at a 360° angle rotation. The temperature was applied for the film to stick to the drums (Fig. SI 6) [25,26].

When looking at the rheology curves of all the samples, we noticed that the membranes without added covalent crosslinker and with 3 mol % of added covalent crosslinker behaved the same way to the stress applied. Indeed, the increase of viscosity is followed by a decrease of the extensional viscosity associated to the rupture of the film (Fig. 6 C). On the contrary, an upward deviation of the viscosity curves is observed for the copolymer with 6 mol% of added covalent crosslinker, this deviation is more noticeable with 12 mol%. This behaviour is called strain-hardening and is characteristic of the occurrence of a chemical crosslinking [26,27].

In fact, when the polymer is crosslinked, there is a creation of chemical intermolecular bonds between the polymer chains. This results in the creation of polymer nodes and in the change of the polymer's properties. Due to the presence of those nodes, the polymers' viscosity increases until the rupture of the chains when applying a strain to the material. From the rheology results, we notice that the covalent crosslinking of sulfonated $(PPFS_{0.87}\text{-}s\text{-}PBuA_{0.13})_{19K}$ was effective at 6 and 12 mol% of added covalent crosslinker. There is a correlation between the DSC and rheology results. They both show that to covalently crosslink the copolymers efficiently, the amount of 2,2-(ethylenedioxy)diethanethiol to be added to the mixture should be above 12 mol%.

3.5.3. Ionic crosslinking

Similarly, ionic crosslinking was performed on partially sulfonated $(PPFS_{0.87}\text{-}s\text{-}PBuA_{0.13})_{19K}$. To perform ionic crosslinking, one needs ionically charged crosslinker and polymer to create ion-pair interactions between them. Polybenzimidazole (PBI-OO) was used as a polymer base (Fig. 6 D). It presents good thermal and mechanical stabilities, with an
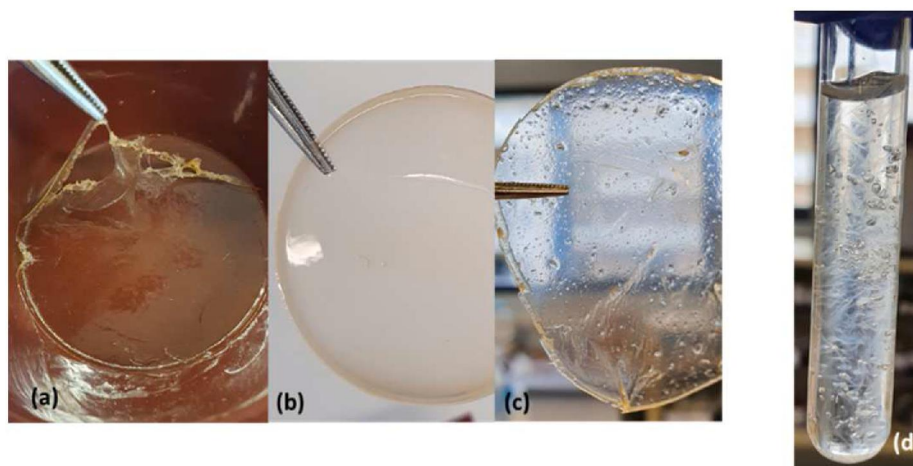
Fig. 5. (a) Pristine membranes from sulfonated $(PPFS_{0.33}\text{-}b\text{-}PBuA_{0.67})_{40K}$; (b) $(PPFS_{0.87}\text{-}s\text{-}PBuA_{0.13})_{19K}$; (c) $(PPFS_{0.80}\text{-}s\text{-}PBuA_{0.20})_{140K}$; (d) Swollen sulfonated $(PPFS_{0.87}\text{-}s\text{-}PBuA_{0.13})_{19K}$ membrane in water.

initial weight loss observed by TGA at temperatures above 600 °C [28].

Different PBI-OO crosslinking weight ratios were tested (2, 4 and 8 wt%). The membranes were made by solubilization in DMSO with a copolymer content of 10 wt%. The final dried membranes were immersed into an acid solution to promote the ionic crosslinking interactions. The Tg of the membrane was increased from 32 °C to 82 °C at the highest wt% of added crosslinker (8 wt%) (Fig. 6 E). An influence of the crosslinking with PBI-OO on the Tg is noticeable from 2 wt% of added crosslinker with a Tg increasing from 32 to 77 °C.

The rheology curves displayed a steady increase of the extensional viscosity of all the samples until rupture to strain regardless of the wt% of added ionic crosslinker (Fig. 6 F). This observation suggests the occurrence of strain-hardening of the membranes as it was the case for the covalent crosslinking. This behaviour occurs regardless of the added amounts of ionic crosslinker. In this sense, only 2 wt% of PBI-OO are necessary to ionically crosslink the partially sulfonated $(PPFS_{0.87}\text{-}s\text{-}PBuA_{0.13})_{19K}$ copolymer.

3.6. Water uptake, ion exchange capacity and conductivity of the membranes

3.6.1. Water uptake

Beside the proton-conductivity and ion exchange capacity, water uptake is a critical factor in determining the performance of a membrane. Indeed, the proton-conductivity is dictated by the water content and diffusion in the membrane. Nevertheless, too much absorbed water can negatively impact the mechanical properties of the membranes leading to a loss of their mechanical integrity. In fact, the water uptake parameter is dependent on the degree of sulfonation of the polymer as the presence of too many ion groups (IEC > 2–2.5 meq/g) causes an extreme swelling of the membranes. Water will act as a plasticizer and lower the Tg of the membranes [29]. Water uptake of the crosslinked partially sulfonated $(PPFS_{0.87}\text{-}s\text{-}PBuA_{0.13})_{19K}$ membranes was determined by comparing the weights of the dry and hydrated membranes. Following the detailed procedure in the experimental section, crosslinked membranes were placed in a vial containing deionised water for 24 h (Fig. SI 7 I & II). As already mentioned in the previous section, non-crosslinked membranes of PPFS/PBuA were excessively swollen and were disrupted after 24 h in water. Covalently crosslinked membranes having 3 and 6 mol% crosslinker behaved the same way as the pristine membranes. They swelled a lot and then were disrupted in water which rendered the water uptake determination impossible. In the case of 12 mol% of added crosslinker, the membranes were very swollen, with a water uptake exceeding 1000 wt%, and a hydration number of 563, they were losing their mechanical integrity. On the other hand, the

ionically crosslinked membranes were all stable in water with water uptake values around 45 wt%, and hydration number of 23–25 (Table 3), comparable to the Nafion®117 ones with a water uptake of ≈30 wt% and a hydration number of 18 [30].

All the copolymers ionically crosslinked with PBI-OO gave a similar water uptake around 45 wt%. The covalent crosslinking reaction of the partially sulfonated $([sPPFS_{0.49}\text{-}PPFS_{0.38}]\text{-}s\text{-}PBuA_{0.13})_{19K}$ copolymer was successfully demonstrated by rheology. However, the water uptake of these membranes was above 1000%, which is more than 30 times higher than Nafion®'s. On top of this, the covalently crosslinked membranes appeared to be too fragile as PEM for application in water electrolysis. On the contrary, ionic crosslinking with the PBI-OO performed better in terms of mechanical properties and stability in water, regardless of the added PBI-OO amounts. For that reason, ionic crosslinking by blending the copolymers with PBI-OO was selected as the most suitable crosslinking technique to finally tailor the membranes. As the percentage of added ionic crosslinker didn't have a severe impact on the properties of the membrane (2, 4 or 8 wt%), the chosen amount was 2 wt%. Indeed, using the lowest amount of crosslinker possible will allow to have more anionic groups available for the proton conduction. All the following characterizations were performed on the PBI-OO (2 wt%) crosslinked sulfonated membranes.

3.6.2. Proton conductivity

Factors influencing the conductivity are mainly the morphology (ion-channel structuring) of the membrane, the water uptake (content of water), and the degree of sulfonation (DS) of the polymers characterized by the IEC (Fig. SI 9). $([sPPFS_{0.49}\text{-}PPFS_{0.38}]\text{-}s\text{-}PBuA_{0.13})_{19K}$ showed IEC = 1.06 meq/g, higher than the reference that we are using Nafion®117 (IEC = 0.93 meq/g) (Table 4). A similar IEC was obtained for the other two copolymers $(sPPFS_{0.80}\text{-}s\text{-}PBuA_{0.20})_{140K}$ and $([sPPFS_{0.22}\text{-}PPFS_{0.11}]\text{-}b\text{-}PBuA_{0.67})_{40K}$, showing 0.3 meq/g and 0.35 meq/g, respectively. The lower IEC of the sulfonated $([sPPFS_{0.22}\text{-}PPFS_{0.11}]\text{-}b\text{-}PBuA_{0.67})_{40K}$ is explained by the low amounts of sPPFS that is 3 times less than $([sPPFS_{0.49}\text{-}PPFS_{0.38}]\text{-}s\text{-}PBuA_{0.13})_{19K}$. The low IEC of sulfonated $(sPPFS_{0.80}\text{-}s\text{-}PBuA_{0.20})_{140K}$ could be linked to high molar mass of the polymer making it difficult to access the sulfonated groups in the bulk of the 2 wt% crosslinked membrane during the 24h at room temperature. The difference between the experimental and theoretical IECs may be due to the environment making the sulfonate groups inaccessible. It could be the result of the polyelectrolyte effect of the BCP and/or hydrophobic environment in the case of statistical copolymers.

The conductivity of the membranes was determined by Electrochemical Impedance Spectroscopy (EIS). The membrane made with the BCP $([sPPFS_{0.22}\text{-}PPFS_{0.11}]\text{-}b\text{-}PBuA_{0.67})_{40K}$, gave the best proton-
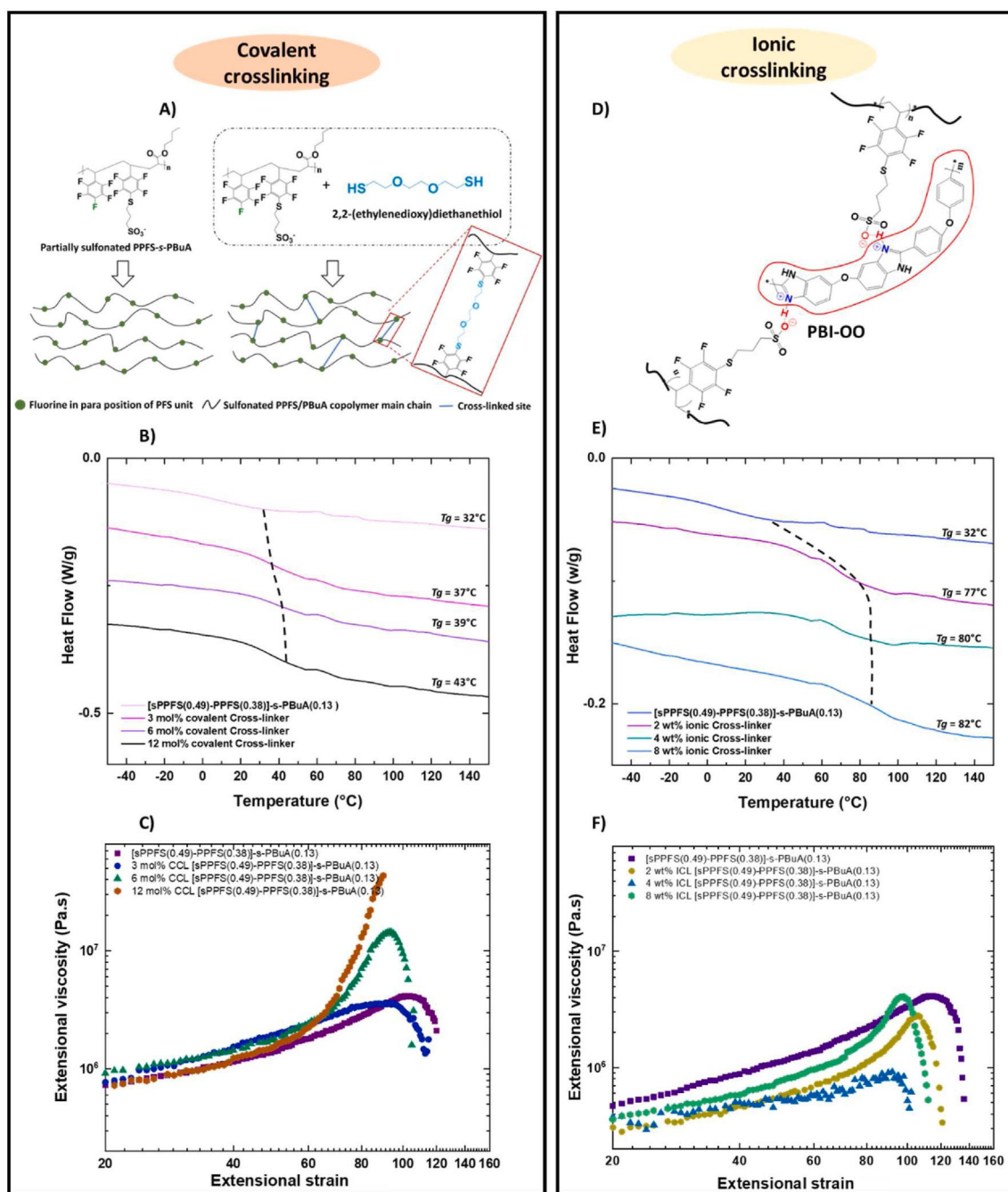
Fig. 6. (A) Molecular structures of partially sulfonated PPFS-*s*-PBuA membrane and its crosslinked homologue with 2,2-(ethylenedioxy)diethanethiol; (B) DSC thermograms of sulfonated (PPFS$_{0.87}$-*s*-PBuA$_{0.13}$)$_{19K}$ membrane and the membrane with added covalent crosslinkers; (C) Extensional viscosity *versus* extensional strain at 100 °C of partially sulfonated (PPFS$_{0.87}$-*s*-PBuA$_{0.13}$)$_{19K}$ ([sPPFS$_{0.49}$-PPFS$_{0.38}$]-*s*-PBuA$_{0.13}$) membrane with 0, 2, 6 & 12 mol% of 2,2-(ethylenedioxy)dieth-anethiol as covalent crosslinker (CCL); (D) Representation of the crosslinked site of the copolymer with PBI-OO; (E) DSC graphs of sulfonated (PPFS$_{0.87}$-*s*-PBuA$_{0.13}$)$_{19K}$ membrane and the membrane with added ionic crosslinkers; (F) Extensional viscosity *versus* strain of partially sulfonated (PPFS$_{0.87}$-*s*-PBuA$_{0.13}$)$_{19K}$ ([sPPFS$_{0.49}$-PPFS$_{0.38}$]-*s*-PBuA$_{0.13}$) with added of 0, 2, 4 & 8 wt% of PBI-OO ionic crosslinker (ICL).

conductivity from all studied membranes ($\sigma = 179$ mS/cm) (Table 4). The membrane made with ([sPPFS$_{0.49}$-PPFS$_{0.38}$]-*s*-PBuA$_{0.13}$)$_{19K}$ had a conductivity of 94 mS/cm and (sPPFS$_{0.80}$-*s*-PBuA$_{0.20}$)$_{140K}$ had the lowest conductivity of all three membranes, $\sigma = 16$ mS/cm. The BCP was ex-pected to conduct the best due to its higher IEC value, even if it has the lowest amount of sPPFS (22 mol%). This could be explained by the in-fluence of the morphology of the diblock-copolymer and then its self-assembly behaviour on the conductive performances of the materials. The low conductivity value of sulfonated (sPPFS$_{0.80}$-*s*-PBuA$_{0.20}$)$_{140K}$ compared to the other membranes could not be explained at this stage,

and further work is needed to improve the membrane formulation. Compared to the conductivity of the reference Nafion®117 with $\sigma = 12$ mS/cm, we were able to achieve a similar conductivity for (sPPFS$_{0.80}$-*s*-PBuA$_{0.20}$)$_{140K}$ and greater conductivities for ([sPPFS$_{0.49}$-PPFS$_{0.38}$]-*s*-PBuA$_{0.13}$)$_{19K}$ and ([sPPFS$_{0.22}$-PPFS$_{0.11}$]-*b*-PBuA$_{0.67}$)$_{40K}$ using the PPFS/PBuA copolymer system.

These results reveal the importance of the material nano-structuration in the proton conduction. Indeed, with the crosslinked sulfonated (PPFS$_{0.33}$-*b*-PBuA$_{0.67}$)$_{40K}$, AFM analysis also demonstrated the formation of *out-of-the-plane* cylinders with a pitch of 100 nm

Table 3

Water uptake values of crosslinked partially sulfonated ([sPPFS$_{0.49}$-PPFS$_{0.38}$]-*s*-PBuA$_{0.13}$)$_{19K}$.

Type of crosslinking	Crosslinker (%)	Water uptake (wt%)	λ^a [H$_2$O/SO$_3$H]
CCL	3 mol%	–	–
	6 mol%	–	–
	12 mol%	1076	563
ICL	2 wt%	44	23
	4 wt%	48	25.2
	8 wt%	45	23.6

[a] Hydration number: number of water molecules per sulfonic acid functional group, λ = Water uptake/(IEC$_{exp}$ × 100 × MW$_{water}$) [31].

(Scheme 2, Fig. SI 8). A similar morphology was observed without crosslinking (Fig. 1). Moreover, the DSC analysis reveals two distinct *Tg* domains characteristic of the phase separation of the BCP (Fig. 4 c). Interesting are the solubility parameters of sPPFS (23.6 Mpa$^{1/2}$), PBuA (17.3 Mpa$^{1/2}$) and the crosslinker PBI-OO (24.6 Mpa$^{1/2}$). They clearly predict an affinity and miscibility of PBI-OO into sPPFS due to electrostatic interactions and close solubility parameter values, respectively. Herein, the low amount of the ionic crosslinker PBI-OO (≈2 wt%) combines with its high difference of solubility parameter with the PBuA matrix, PBI-OO can neither disturb the self-assembly nor the nanosegregation morphology. If such nanostructures are percolating across the membrane, water will be attracted and conducted to the hydrophilic

sPPFS nano-domains structured in HCC. The protons will follow the water dynamic that in our case consists of following a straight path from one end of the membrane to the other, improving the overall transfer of protons compared to a random organization of the material (Scheme 2) [32]. It is worth noting that gyroid or lamellar phases could be suitable to increase the volume of the conductive moieties of the diblock copolymer self-assembly. However, those phases negatively impact the mechanical properties of the membranes. A solution to maintain both the good conductivity and the mechanical properties could be the use of a PBuA-*b*-sPPFS-*b*-PBuA triblock copolymer. This type of copolymer would allow the creation of bridges between the hydrophobic domains and then enhance the mechanical properties of the membranes.

4. Conclusion

The influence of the microstructure of PPFS/PBuA copolymers for proton-conducting membrane for PEMWE applications was investigated. For this purpose, a diblock-copolymer self-assembled in HCC structure was synthetized by NMP-controlled radical polymerization. In addition, statistical copolymers of PPFS/PBuA were synthetized in two ways: (i) NMP in solution (DMF) and (ii) free-radical polymerization in emulsion. The latter method resulted in an aqueous formulation with a higher molar mass copolymer. The copolymers were then fully or partially sulfonated by the efficient technique of soft *para* fluoro-thiol modification using sodium-3-mecapto-1-propanesulfonate according to a click-reaction. Partial sulfonation was carried out to achieve a high IEC

Table 4

IEC and conductivity of the sulfonated PPFS/PBuA crosslinked proton conductive membranes.

Polymer	DS (%)	sPPFS (mol%)	IEC Theoretical (meq/g)	IEC Experimental (meq/g)	Membrane thickness (μm)	Conductivity (mS/cm)
(PPFS$_{0.33}$-*b*-PBuA$_{0.67}$)$_{40K}$ (NMP/solution)	68	22	0.66	0.35	16	179
(PPFS$_{0.87}$-*s*-PBuA$_{0.13}$)$_{19K}$ (NMP/solution)	57	49	2.15	1.06	86	94
(PPFS$_{0.80}$-*s*-PBuA$_{0.20}$)$_{140K}$ (FRP/Emulsion)	100	80	2.76	0.3	6	16

Scheme 2. (A) Representation of sPPFS-*b*-PbuA BCP and its self-assembly at the nanometre scale in Hexagonally Compact Cylinders (HCC) of sPPFS in a PBuA matrix (top view); (B) Peak Force mode AFM height image of sulfonated (PPFS$_{0.33}$-*b*-PBuA$_{0.67}$)$_{40K}$ crosslinked with PBI-OO (2 wt%) on a large area of 25 μm^2 (5 × 5 μm); (C) Side view of the schematic sPPFS-*b*-PBuA crosslinked membrane with the representation of water dynamics; (D) Representation of the cluster network occurring in Nafion® for the proton-conduction.

and produce water-insoluble polymers and preserve some hydropho-bicity. Full sulfonation was performed on the copolymer with the higher molar mass, as it is the most mechanically stable. In addition, the membranes were ionically crosslinked using at least 2 wt% of PBI-OO. In this way, stable films were prepared, highlighting high IEC = 1.06 meq/g and conductivity σ = 179 mS/cm. The ionic crosslinking improved the mechanical stability of the membranes in water and reduced the water uptake to about 45%. The conductivity of the membranes was measured by EIS in 0.5 N H_2SO_4, with BCP showing the best conductivity with σ = 179 mS/cm, which is more than 10 times higher than the reference Nafion® 117 with the experimental conditions of the present study.

The use of amphiphilic diblock-copolymers modified by an elegant *para* fluoro-thiol reaction under mild conditions, allowing self-assembly in 100 nm diameter *out-of-the-plane* cylinders by AFM and SAXS characterizations, paves the way to design efficient proton-conducting nanochannels across the membranes. This new concept offers the opportunity to rethink the Nafion® paradigm for proton transport and water dynamic in the polymeric membrane but also be transposed to other thiol functional molecules for applied energy materials.

Declaration of competing interest

The authors declare the following financial interests/personal relationships which may be considered as potential competing interests:

Laurent Billon reports financial support was provided by Institute of Analytical Sciences and Physical Chemistry for the Environment and Materials. Laurent Billon reports a relationship with EU Framework Programme for Research and Innovation Science with and for Society that includes: funding grants.

Data availability

No data was used for the research described in the article.

Appendix A. Supplementary data

Supplementary data to this article can be found online at https://doi.org/10.1016/j.memsci.2022.120796.

References

[1] N. Guillet, P. Millet, Alkaline water electrolysis, Hydrog. Prod. Electrolysis (2015) 117–166, https://doi.org/10.1002/9783527676507.ch4.
[2] A.Ä. Marshall, B. Børresen, G. Hagen, M. Tsypkin, R. Tunold, Hydrogen production by advanced proton exchange membrane (PEM) water electrolysers — reduced energy consumption by improved electrocatalysis, Energy 32 (2007) 431–436, https://doi.org/10.1016/j.energy.2006.07.014.
[3] A. Hauch, S.D. Ebbesen, S.H. Jensen, M. Mogensen, Highly efficient high-temperature electrolysis, J. Mater. Chem. 18 (2008) 2332–2340, https://doi.org/10.1039/B718822F.
[4] A. Ursúa, L.M. Gandía, P. Sanchis, Hydrogen production from water electrolysis: current status and future trends, Proc. IEEE 100 (2012) 410–426, https://doi.org/10.1109/JPROC.2011.2156750.
[5] F.M. Sapountzi, J.M. Gracia, C. J. (Kee. J.) Weststrate, H.O.A. Fredriksson, Electrocatalysts for the generation of hydrogen, oxygen and synthesis gas, Prog. Energy Combust. Sci. 58 (2017) 1–35, https://doi.org/10.1016/j.pecs.2016.09.001. J. W. (Hans) Niemantsverdriet.
[6] T. Maiyalagan, S. Pasupathi, Components for PEM fuel cells: an overview, Mater. Sci. Forum 657 (2010) 143–189. www.scientific.net/MSF.657.143.

[7] B. Smitha, S. Sridhar, A.A. Khan, Solid polymer electrolyte membranes for fuel cell applications - a review, J. Membr. Sci. 259 (2005) 10–26, https://doi.org/10.1016/j.memsci.2005.01.035.
[8] J. Chen, M. Asano, T. Yamaki, M. Yoshida, Preparation and characterization of chemically stable polymer electrolyte membranes by radiation-induced graft copolymerization of four monomers into ETFE films, J. Membr. Sci. 269 (2006) 194–204, https://doi.org/10.1016/j.memsci.2005.06.035.
[9] M. Rikukawa, K. Sanui, Proton-conducting polymer electrolyte membranes based on hydrocarbon polymers, Prog. Polym. Sci. 25 (2000) 1463–1502, https://doi.org/10.1016/S0079-6700(00)00032-0.
[10] K.D. Kreuer, On the development of proton conducting polymer membranes for hydrogen and methanol fuel cells, J. Membr. Sci. 185 (2001) 29–39, https://doi.org/10.1016/S0376-7388(00)00632-3.
[11] C. Wang, B. Shen, H. Dong, W. Chen, C. Xu, J. Li, Q. Ren, Sulfonated poly(aryl sulfide sulfones) containing trisulfonated triphenylphosphine oxide moieties for proton exchange membrane, Electrochim. Acta 177 (2015) 145–150, https://doi.org/10.1016/j.electacta.2014.11.124.
[12] C. Wang, Y. Zhou, B. Shen, X. Zhao, J. Li, Q. Ren, Proton-conducting poly(ether sulfone ketone)s containing a high density of pendant sulfonic groups by a convenient and mild post-sulfonation, Polym. Chem. 9 (40) (2018) 4984–4993, https://doi.org/10.1039/C8PY00996A.
[13] C. Wang, S. Young Lee, D. Won Shin, N. Rae Kang, Y.M. Lee, M.D. Guiver, Proton-conducting membranes from poly(ether sulfone)s grafted with sulfoalkylamine, J. Membr. Sci. 427 (2013) 443–450, https://doi.org/10.1016/j.memsci.2012.09.040.
[14] H.G. Haubold, T. Vad, H. Jungbluth, P. Hiller, Nano structure of NAFION: a SAXS study, Electrochim. Acta 46 (2001), https://doi.org/10.1016/S0013-4686(00)00753-2, 1559–156.
[15] Y.A. Elabd, E. Napadensky, C.W. Walker, K.I. Winey, Transport properties of sulfonated poly(styrene-b-isobutylene-b-styrene) triblock copolymers at high ion-exchange capacities, Macromolecules 39 (2006) 399–407, https://doi.org/10.1021/ma051958n.
[16] M.L. Einsla, Y.S. Kim, M. Hawley, H.-S. Lee, J.E. McGrath, B. Liu, M.D. Guiver, B.S. Pivovar, Toward improved conductivity of sulfonated aromatic proton exchange membranes at low relative humidity, Chem. Mater. 20 (2008) 5636–5642, https://doi.org/10.1021/cm801198d.
[17] K. Xu, K. Li, P. Khanchaitit, Q. Wang, Synthesis and characterization of self-assembled sulfonated poly (styrene-b-vinylidene fluoride-b-styrene) triblock copolymers for proton conductive membranes, Chem. Mater. 19 (2007) 5937–5945, https://doi.org/10.1021/cm071626s.
[18] J.M. Noy, M. Koldevitz, P.J. Roth, Thiol-reactive functional poly(meth)acrylates: multicomponent monomer synthesis, RAFT (co)polymerization and highly efficient thiol-para-fluoro postpolymerization modification, Polym. Chem. 6 (2015) 436–447, https://doi.org/10.1039/C4PY01238K.
[19] K. Bosson, P. Marcasuzaa, A. Bousquet, V. Atanasov, G.E.M. Tovar, L. Billon, PentaFluoroStyrene-based Block Copolymers Controlled Self-Assembly Pattern, 2022. Submitted in.
[20] E. Bülbül, V. Atanasov, M. Mehlhorn, M. Bürger, A. Chromik, T. Häring, J. Kerres, Highly phosphonated polypentafluorostyrene blended with polybenzimidazole: application in vanadium redox flow battery, J. Membr. Sci. (2019) 570–571, https://doi.org/10.1016/j.memsci.2018.10.027, 194–203.
[21] Y. Li, A. Roy, A.S. Badami, M. Hill, J. Yang, S. Dunn, J.E. McGrath, Synthesis and characterization of partially fluorinated hydrophobic-hydrophilic multiblock copolymers containing sulfonate groups for proton exchange membrane, J. Power Sources 172 (2007) 30–38, https://doi.org/10.1016/j.jpowsour.2007.04.046.
[22] M. Hazarika, K. Malkappa, T. Jana, Particle-size-dependent properties of sulfonated polystyrene nanoparticles, Polym. Int. 61 (2012) 1425–1432, https://doi.org/10.1002/pi.4227.
[23] V. Atanasov, M. Bürger, S. Lyonnard, L. Porcar, J. Kerres, Sulfonated poly (pentafluorostyrene): synthesis & characterization, Solid State Ionics 252 (2013) 75–83, https://doi.org/10.1016/j.ssi.2013.06.010.
[24] J. Berger, M. Reist, J.M. Mayer, O. Felt, N.A. Peppas, R. Gurny, Structure and interactions in covalently and ionically crosslinked chitosan hydrogels for biomedical applications, Eur. J. Pharm. Biopharm. 57 (2004) 19–34, https://doi.org/10.1016/S0939-6411(03)00161-9.
[25] P. Filip, P. Svrcinova, Measurement of elongational viscosity of polymer melts using ser universal testing platform, Appl. Rheol. 22 (2012) 6–10, https://doi.org/10.3933/applrheol-22-14776.
[26] E. Dieuzy, S. Auguste, K. Chougrani, V. Alard, L. Billon, C. Derail, Microgel structure-driven linear and non-linear mechanical properties of self-assembled microgel films, Colloids Surf. A Physicochem. Eng. Asp. 613 (2021) 1–11, https://doi.org/10.1016/j.colsurfa.2020.126082.
[27] M. Yamaguchi, K.I. Suzuki, S. Maeda, Enhanced strain hardening in elongational viscosity for HDPE/crosslinked HDPE Blend. I. Characteristics of crosslinked HDPE, J. Appl. Polym. Sci. 86 (2002) 73–78, https://doi.org/10.1002/app.10914.
[28] J.A. Asensio, S. Borrós, P. Gómez-Romero, Proton-conducting polymers based on benzimidazoles and sulfonated benzimidazoles, J. Polym. Sci. Part A Polym. Chem. 40 (2002) 3703–3710, https://doi.org/10.1002/pola.10451.
[29] M.A. Hickner, H. Ghassemi, Y.S. Kim, B.R. Einsla, J.E. McGrath, Alternative polymer systems for proton exchange membranes (PEMs), Chem. Rev. 104 (2004) 4587–4611, https://doi.org/10.1021/cr020711a.

[30] R.F. Silva, M. De Francesco, A. Pozio, Solution-cast Nafion® ionomer membranes: preparation and characterization, Electrochim. Acta 49 (2004) 3211–3219, https://doi.org/10.1016/j.electacta.2004.02.035.

[31] P. Knauth, M.L. Di Vona, Hydration and proton conductivity of ionomers: the model case of sulfonated aromatic polymers, Front. Energy Res. 2 (2014) 1–6, https://doi.org/10.3389/fenrg.2014.00050.

[32] S.J. Peighambardoust, S. Rowshanzamir, M. Amjadi, Review of the proton exchange membranes for fuel cell applications, Int. J. Hydrogen Energy 35 (2010) 9349–9384, https://doi.org/10.1016/j.ijhydene.2010.05.017.

5. Supporting information

***Para* fluoro-thiol clicked diblock-copolymer self-assembly: Towards a new paradigm for highly proton-conductive membranes**

Karell Bosson,[a,b,e] Pierre Marcasuzaa,[a,b] Antoine Bousquet,[b] Günter E.M. Tovar,[c,d] Vladimir Atanasov,[e] Laurent Billon[a,b]

[a] Bio-inspired Materials Group: Functionalities & Self-assembly, E2S UPPA, 64000 Pau, France

[b] Universite de Pau et Pays de l'Adour, E2S UPPA, CNRS, IPREM, UMR5254, 64000 Pau, France

[c] Institute for Interfacial Process Engineering and Plasma Technology IGVP, University of Stuttgart, Pfaffenwaldring 31, 70569 Stuttgart, Germany

[d] Fraunhofer Institute for Interfacial Engineering and Biotechnology IGB, Nobelstr. 12, 70569 Stuttgart, Germany

[e] Institute of Chemical Process Engineering, University of Stuttgart, Boeblingerstrasse 78, 70199 Stuttgart, Germany

This supporting information contains

-Total number of pages: **6 pages**

-Total number of figures: **9 figures**

^{1}H NMR, SEC, AFM and DSC of the copolymers
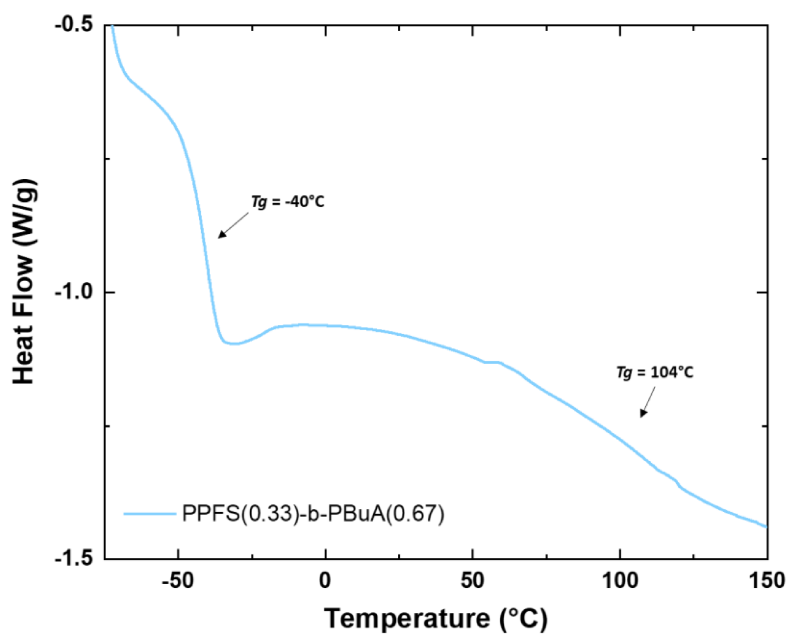
Figure SI 1. DSC of $(PPFS_{0.33}\text{-}b\text{-}PBuA_{0.67})_{40K}$ diblock-copolymer.
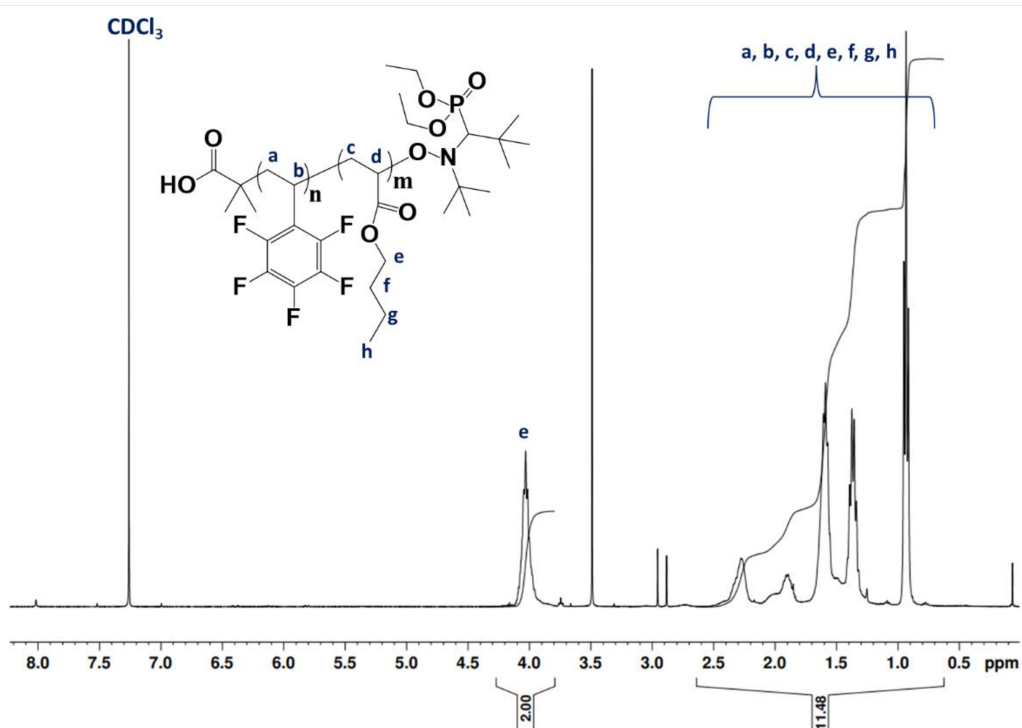
Figure SI 2. Structure and ^1H NMR spectrum (300 MHz, room temperature, $CDCl_3$) of $(PPFS_{0.33}\text{-}b\text{-}PBuA_{0.67})_{40K}$ synthetized by NMP controlled radical polymerization. The spectrum shows the absence of residual monomer.
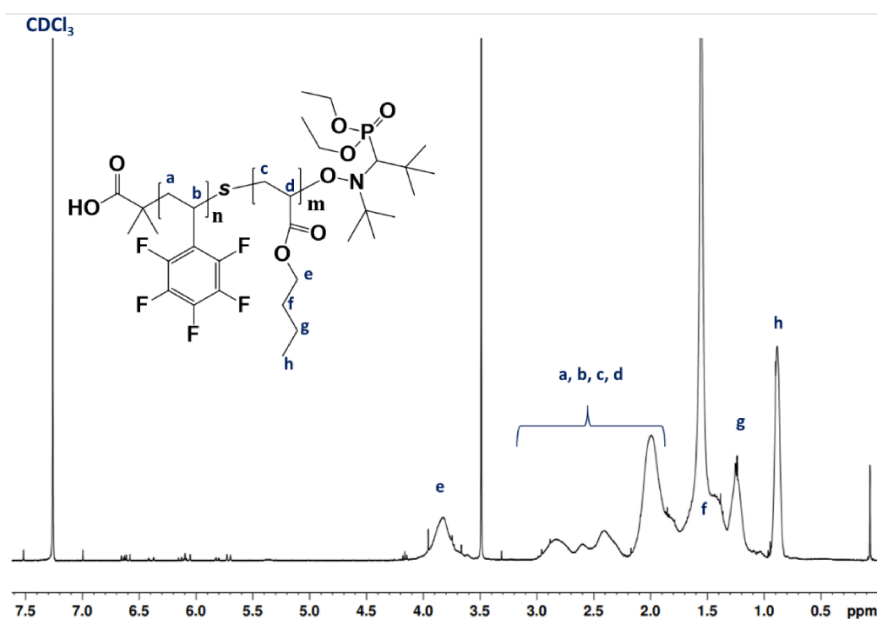
Figure SI 3. Structure and ^{1}H NMR spectrum (300 MHz, room temperature, CDCl$_3$) of (PPFS$_{0.87}$-s-PBuA$_{0.13}$)$_{19K}$ synthetized by NMP controlled radical polymerization. The spectrum shows the absence of residual monomer.
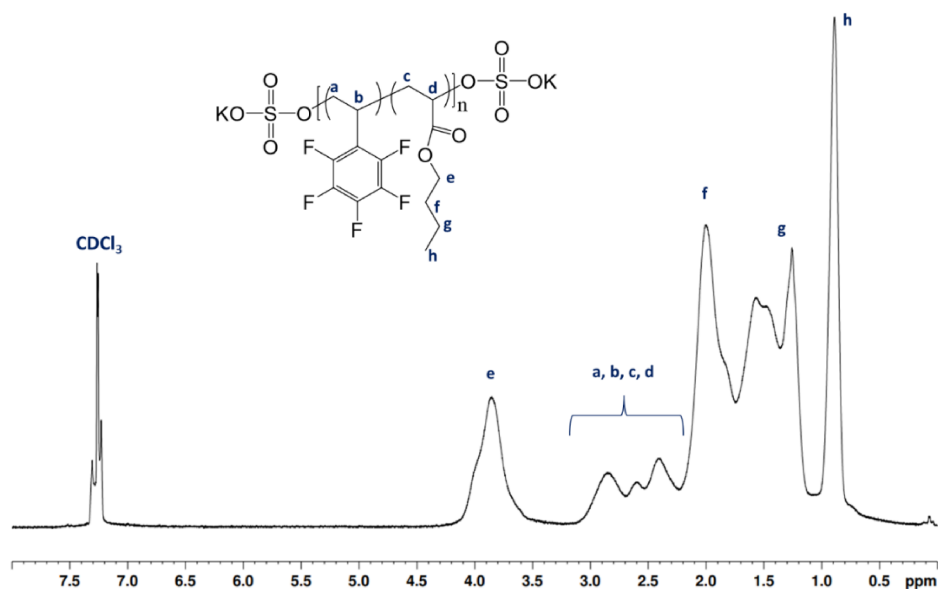
Figure SI 4. Structure and ^{1}H NMR spectrum (300 MHz, room temperature, CDCl$_3$) of purified (PPFS$_{0.80}$-s-PBuA$_{0.20}$)$_{140K}$ synthetized by free radical polymerization in emulsion. The spectrum shows the absence of residual monomer.
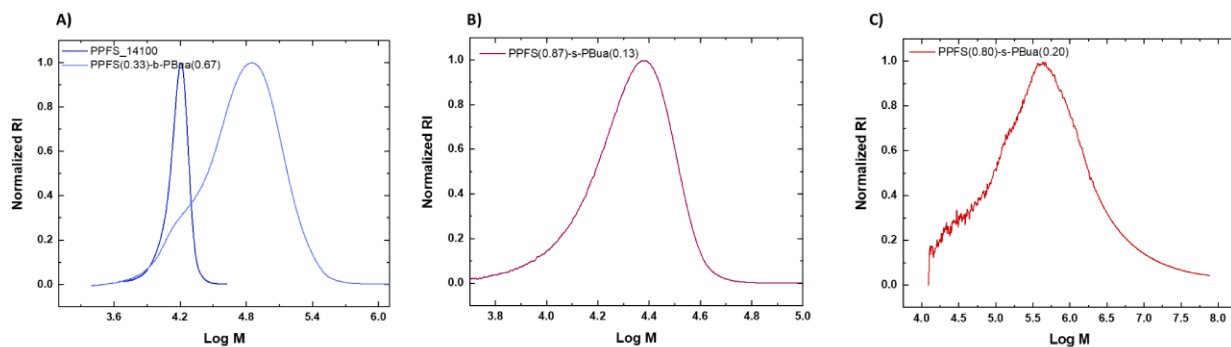
Figure SI 5. SEC chromatograms of macro-initiator ($PPFS_{14100}$) (Mn = 14 100 g/mol, D = 1.07) and ($PPFS_{0.33}$-*b*-$PBuA_{0.67}$)$_{40K}$ (Mn = 40 100 g/mol, D = 1.88) chain extension from $PPFS_{14100}$ (A); ($PPFS_{0.87}$-*s*-$PBuA_{0.13}$)$_{19K}$ (Mn = 19 100 g/mol, D = 1.16) (B); ($PPFS_{0.80}$-*s*-$PBuA_{0.20}$)$_{140K}$ (Mn = 140 200 g/mol, D = 15.2) (C).
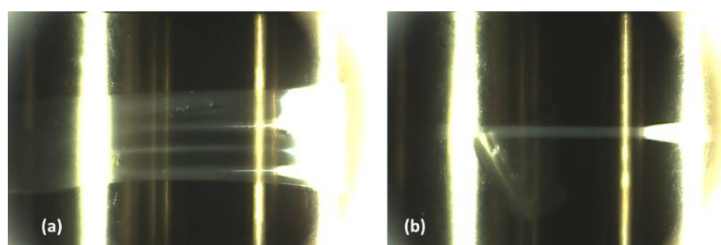
Figure SI 6. Film on the setup before test (a) and just before rupture (b).
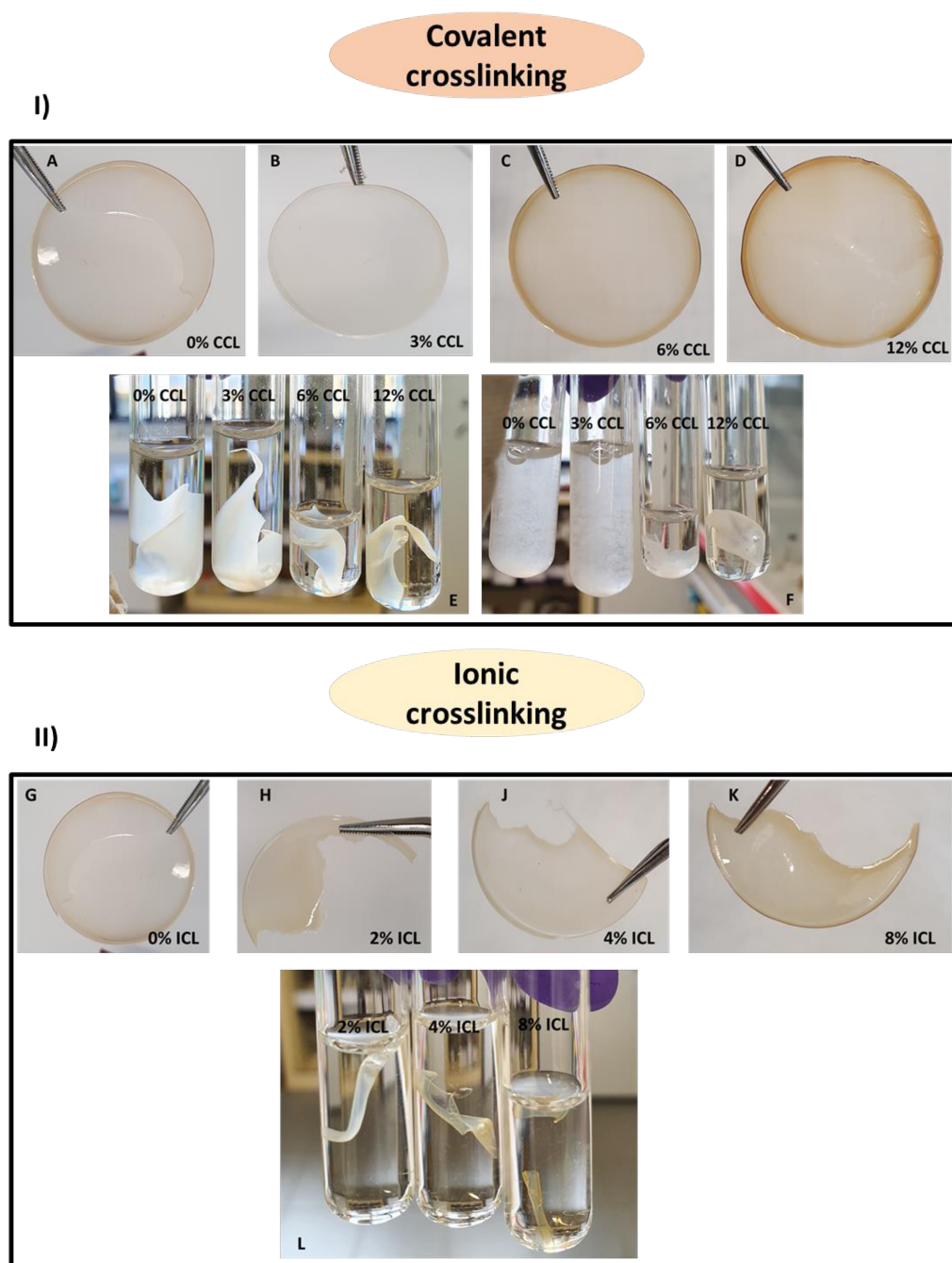
Figure SI 7. (I) Membranes of (A) partially sulfonated (PPFS$_{0.87}$-s-PBuA$_{0.13}$)$_{19K}$ ([sPPFS$_{0.49}$-PPFS$_{0.38}$]-s-PBuA$_{0.13}$) with 0 mol% of added covalent crosslinker (CCL);

(B) ([sPPFS$_{0.49}$-PPFS$_{0.38}$]-s-PBuA$_{0.13}$) with 3 mol% of added CCL;

(C) ([sPPFS$_{0.49}$-PPFS$_{0.38}$]-s-PBuA$_{0.13}$) with 6 mol% of added CCL;

(D) ([sPPFS$_{0.49}$-PPFS$_{0.38}$]-s-PBuA$_{0.13}$) with 12 mol% of added CCL;

Behaviour of the membranes in deionised water (E) at t = 0h and (F) at t = 24h

(II) Membranes of (G) partially sulfonated (PPFS$_{0.87}$-s-PBuA$_{0.13}$)$_{19K}$ ([sPPFS$_{0.49}$-PPFS$_{0.38}$]-s-PBuA$_{0.13}$) with 0 mol% of added ionic crosslinker (ICL);

(H) ([sPPFS$_{0.49}$-PPFS$_{0.38}$]-s-PBuA$_{0.13}$) with 2 wt% of added ICL;

(J) ([sPPFS$_{0.49}$-PPFS$_{0.38}$]-s-PBuA$_{0.13}$) with 4 wt% of added ICL;

(K) ([sPPFS$_{0.49}$-PPFS$_{0.38}$]-s-PBuA$_{0.13}$) with 8 mol% of added ICL;

(L) Behaviour of the membranes in deionised water at t =24h.
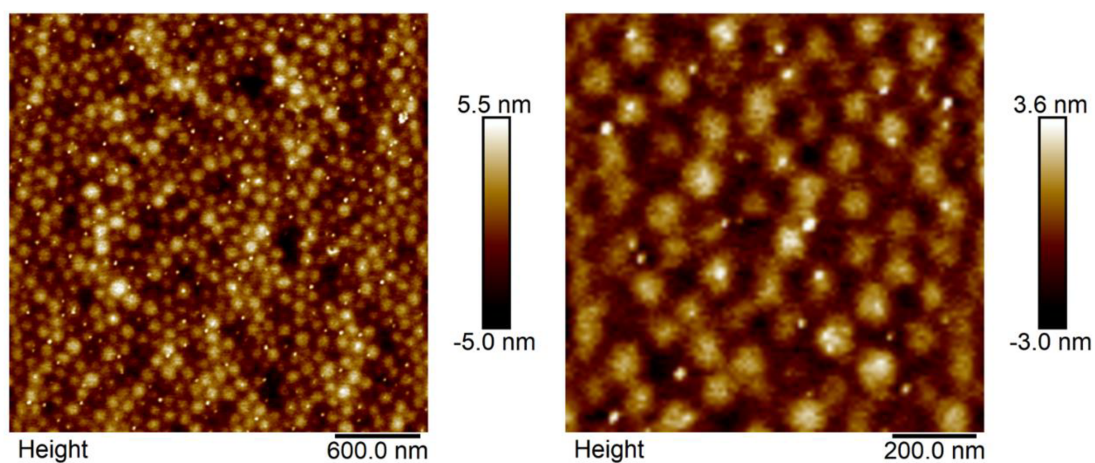
Figure SI 8. Peak Force mode AFM height images of sulfonated (PPFS$_{0.33}$-b-PBuA$_{0.67}$)$_{40K}$ crosslinked with PBI-OO (2wt%)
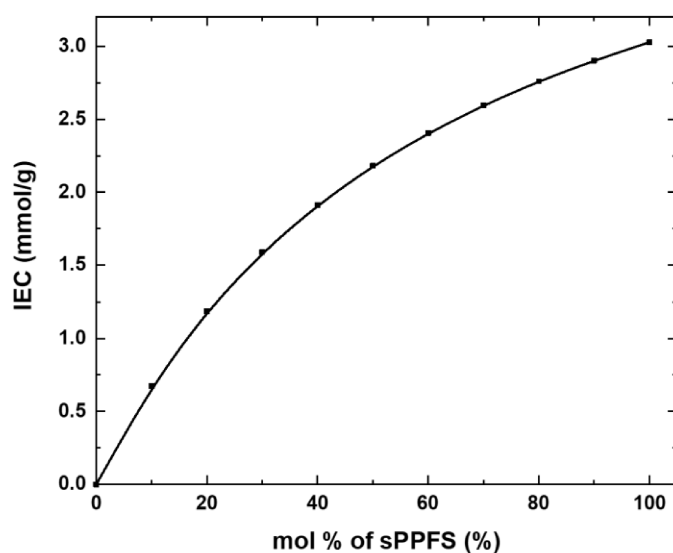
Figure SI 9. Theoretical IEC as function of the molar composition of sPPFS for a PPFS/PBuA copolymer system.

6. Future work perspective

In perspective to future work, membranes from copolymers of PFS and bio-sourced menthol acrylate to replace Butyl Acrylate were also developed during this PhD. The bio-sourced aspect of the chemicals provides an additional interest towards the use of greener chemicals to perform the same tasks of the already available petroleum-based chemicals. Although the synthesis process of the bio-sourced monomer doesn't use 100% bio-sourced compounds (around 75 %), it is already a first step paving the way to greener membranes. The monomer menthyl acrylate (MA) was synthesized using menthol with the monomer procedure followed a path already reported in literature.[41] Poly (menthyl acrylate) (PMA) has a higher glass transition temperature than PBuA but lower than PPFS (Tg PBuA = -40°C, Tg PMA = 69°C, Tg PPFS = 100°C). The initial goal of synthetizing copolymers was to give some flexibility to the brittle membrane made of PPFS. Poly(menthyl acrylate) might provide this flexibility to the membrane by having a higher Tg than PBuA.

6.1. Synthesis of menthyl acrylate monomer. In a three-neck 500 mL round-bottom flask equipped with rubber seals, a dropping funnel, and a magnetic stirrer, menthol (9.50 g, 0.06 mol), triethylamine (6.07 g, 0.06 mol), and dichloromethane (180 mL) were added. The mixture was placed in an ice bath and left to stir for 2 h. Subsequently, acryloyl chloride (8.14 g, 0.09 mol) was added dropwise via the dropping funnel. Upon complete addition, the mixture was left to stir for 30 min in the ice bath and for 24 h at ambient temperature. Then, the mixture was washed once with 1M HCl solution, then twice with 1M K_2CO_3 solution, and finally, it was washed several times with brine. The volatiles in the organic phase were removed by rotary evaporation to yield a transparent viscous liquid that is the monomer (Yield = 73%).

The signals of the ^{1}H NMR spectrum of the monomer were attributed (**Figure 7**). The chemical shifts of the vinylic protons (-CH and -CH₂) are located between 5.7 and 6.5 ppm. The -OCH proton of MA ring is located at 4.7 ppm and the remaining protons of the molecule (-CH, -CH₂ and -CH₃) are located between 0.7 and 2 ppm.
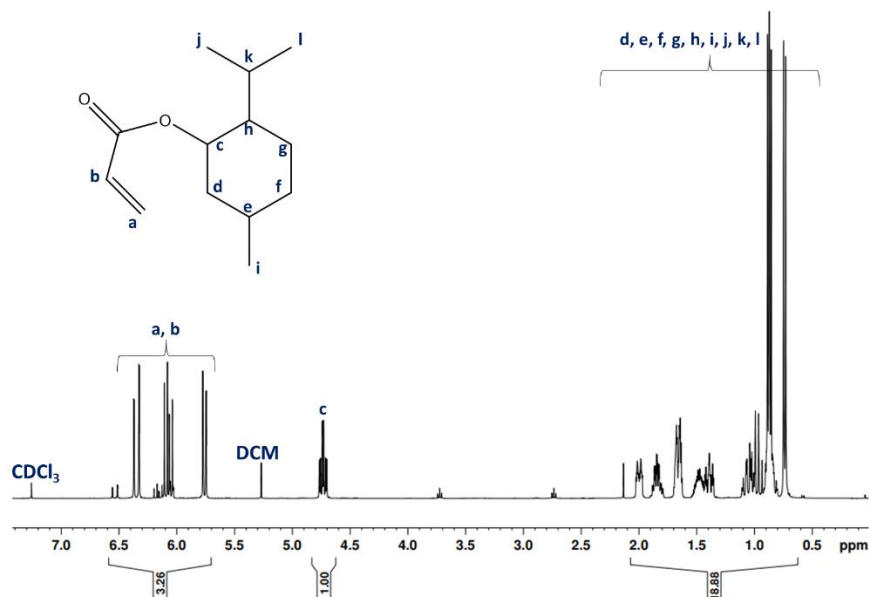
Figure 7. Structure and ^{1}H NMR spectrum (300 MHz, room temperature, CDCl$_3$) of the purified menthyl acrylate monomer.

6.2. Synthesis of PFS/menthyl acrylate statistical copolymer by NMP.

Similarly, to the copolymerization of PFS and BuA, the NMP radical copolymerization of pentafluorostyrene (PFS) and menthyl acrylate (MentA) was performed in DMF following a typical NMP procedure. PFS, MA, DMF, BlocBuilder® and slight excess of free-SG1 (10% of the molar quantity of BlocBuilder®) are added to a 25mL round bottom flask equipped with rubber seals and a magnetic stirring bar. The mixture is placed into an ice bath and bubbled with nitrogen for 15 minutes and subsequently placed into an oil bath that was pre-heated at 115°C.

The signals of the ^{1}H NMR spectrum of the copolymer were attributed (**Figure 8**). The chemical shifts of the -OCH proton of MA ring is located at 4.5 ppm. The polymer backbone protons (-CH and -CH$_2$) alongside the remaining protons of the macromolecule (-CH, -CH$_2$ and -CH$_3$) are located between 0.5 and 3.2 ppm. The composition of each polymer in the copolymer was also determined by ^{1}H NMR following the equations in the supporting information of chapter 3. The copolymer is composed of 77 mol% of PPFS and 23 mol% of PMA (PPFS$_{0.77}$-*s*-PMA$_{0.23}$).
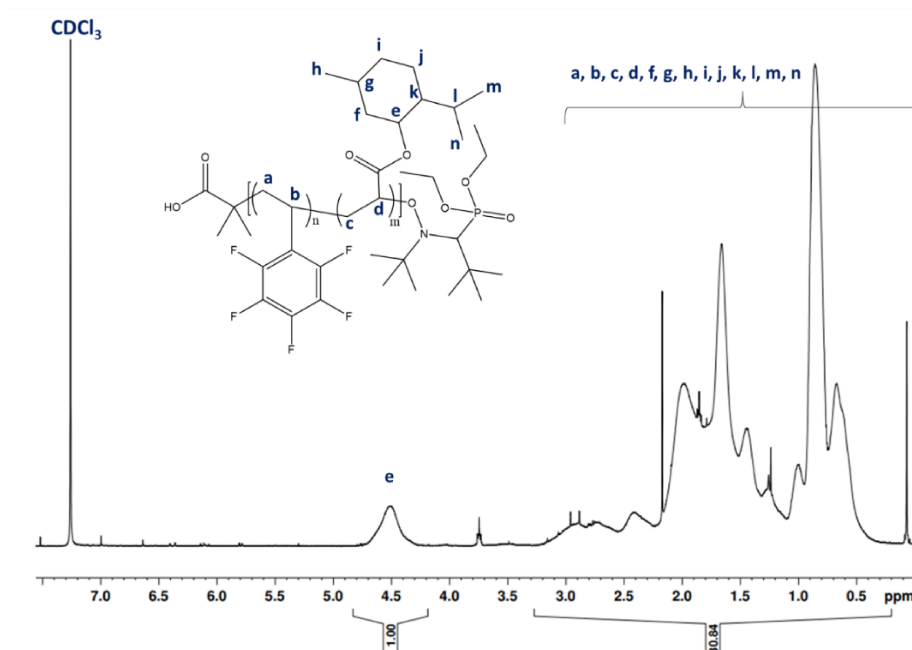
Figure 8. Structure and ^{1}H NMR spectrum (300 MHz, room temperature, CDCl$_3$) of the purified PPFS$_{0.77}$-s-PMA$_{0.23}$ copolymer.

The copolymer was fully sulfonated with sodium-3-mecapto-1-propanesulfonate (SMPS) following the para-fluoro thiol modification of the fluorine in *para* position of PFS units. The sulfonation and membrane elaboration procedures are the same as for the previous PPFS/PBuA polymer system. The characterization techniques and conditions are also the same as before. The ^{19}F spectra of the modified polymer displays two different fluorine environments. After full modification, there is no more fluorine in *para* position, and the signal of fluorine in *meta* positions is shifted due to the presence of the sulfur in *para* position (δ 2F$_{ortho}$ = -142 ppm: δ 2F$_{meta}$ = -135 ppm) (**Figure 9**). As a reminder, the chemical shifts of the fluorine of the non-modified copolymer are: δ 2F$_{ortho}$ = -143 ppm; δ 2F$_{meta}$ = -161 ppm; and δ 1F$_{para}$ = -154 ppm.
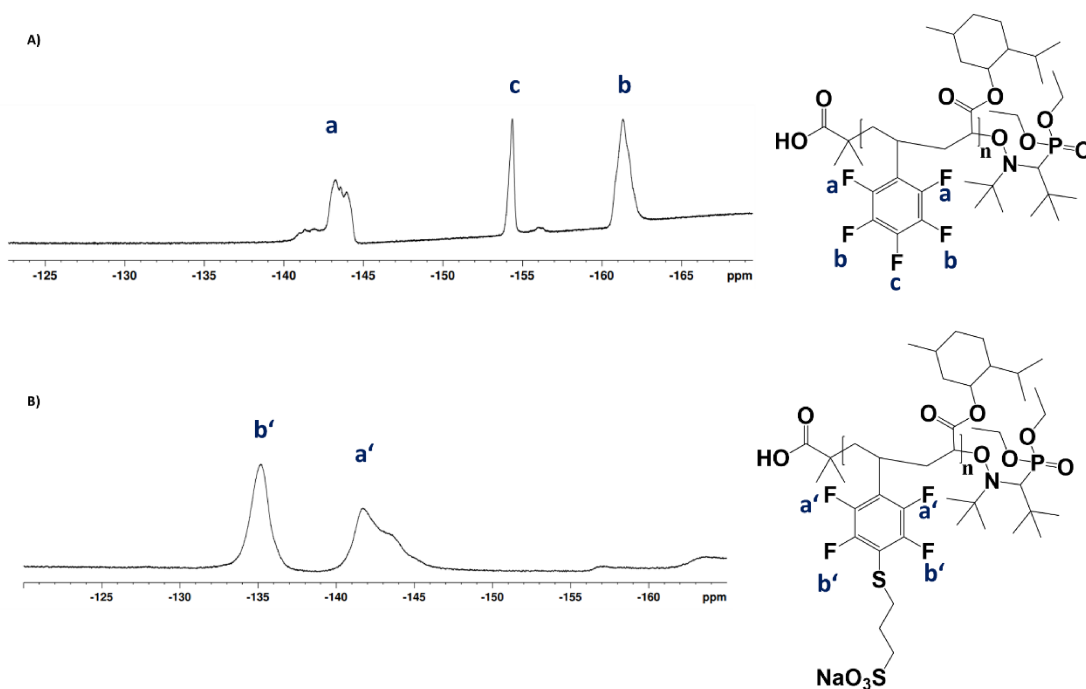
Figure 9. (A) Structure and ^{19}F NMR spectra of $PPFS_{0.77}$-*s*-$PMA_{0.23}$ (300 MHz, room temperature, $CDCl_3$) (B) Structure and ^{19}F NMR spectra of fully sulfonated $PPFS_{0.77}$-*s*-$PMA_{0.23}$ (300 MHz, room temperature, DMSO-d_6).

The copolymer was characterized by DSC (**Figure 10**). Before sulfonation, the material presents a glass transition temperature Tg = 95°C, which decreases to -3°C after sulfonation.
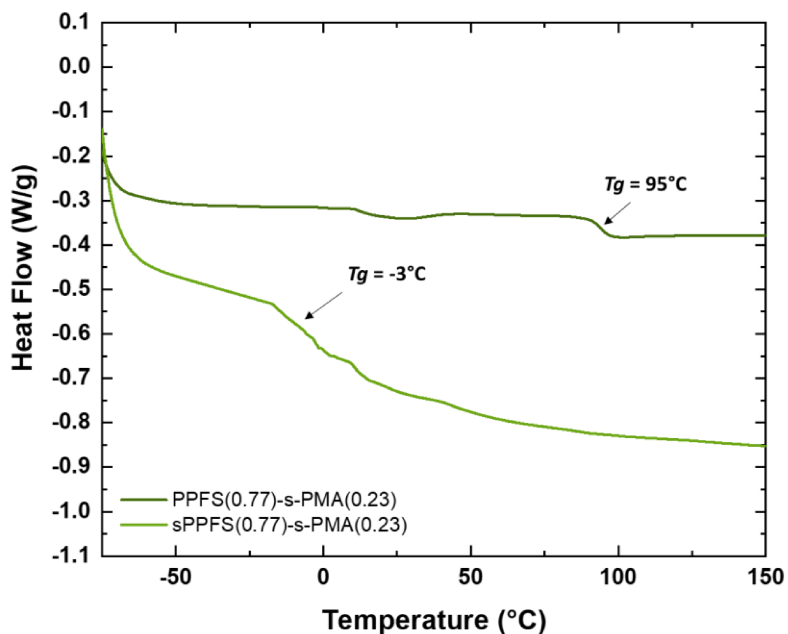
Figure 10. DSC graphs of $PPFS_{0.77}$-*s*-$PMA_{0.23}$ showing the glass transition temperatures of the copolymer before (Tg = 95°C) and after sulfonation (Tg = -3°C).

Membranes of the fully sulfonated PPFS$_{0.77}$-*s*-PMA$_{0.23}$ were made by performing ionic cross-linking with 2 wt% of PBI-OO (**Figure 11**).

Figure 11. Membrane of fully sulfonated PPFS$_{0.77}$-*s*-PMA$_{0.23}$ blended with 2 wt% of PBI.

The membrane made from PPFS/PMA has a water uptake of 42%, an experimental IEC value of 1.2 meq/g and an extraordinary conductivity in sulfuric acid of 690 mS/cm (**Table 5**) compared to Nafion®117 with a conductivity of 12 mS/cm, at similar hydration numbers (19.4 for PPFS$_{0.77}$-s-PMA$_{0.23}$ and 18 for Nafion®117). Such preliminary result could be related to the high hydrophobicity of the PMA units which can create favourite hydrophilic sPPFS pathways in the membrane as cluster network in Nafion®.

Table 5. IEC and conductivity of fully sulfonated PPFS$_{0.77}$-*s*-PMA$_{0.23}$ proton conducting

Polymer	DS (%)	IEC Theoretical (meq/g)	IEC Experimental (meq/g)	Water uptake (%)	λ [H$_2$O/SO$_3$H]	Membrane thickness (µm)	Conductivity (mS/cm)
PPFS$_{0.77}$-s-PMA$_{0.23}$	100	2.54	1.2	42	19.4	10	690

membrane.

In conclusion, we synthetized a very hydrophobic menthyl acrylate monomer made from bio-sourced cyclic C10 menthol. This monomer was copolymerized with PFS yielding a copolymer with the following composition: PPFS$_{0.77}$-*s*-PMA$_{0.23}$. Membranes of fully sulfonated PPFS$_{0.77}$-*s*-PMA$_{0.23}$ gave a conductivity of 690 mS/cm, higher than the one of

Nafion®117 and higher than the previously synthetized PPFS/PBuA copolymers. An explanation for these results could be the enhancement of the mechanical properties of the material due to both PMA and PPFS polymers having similar properties (Tg PMA = 69°C) and PPFS (Tg PPFS = 95°C). This might provide the material with more hydrophobic cohesive domain surrounded by preferential hydrophilic proton-conductive pathways as cluster network. It could be interesting to study as a future work the synthesis of sulfonated PPFS/PMA block-copolymers as well as the structural organization of both statistical and block copolymers by AFM and SAXS. Indeed, we have already seen the influence of the nano-patterned self-assembly on the conducting properties of PPFS/PBuA membranes.

[41]   S. Noppalit, A. Simula, N. Ballard, X. Callies, J. M. Asua, L. Billon, Renewable Terpene Derivative as a Biosourced Elastomeric Building Block in the Design of Functional Acrylic Copolymers, Biomacromolecules. 20 (2019) 2241-2251. https://doi.org/10.1021/acs.biomac.9b00185.

Declaration of my independent performance chapter 4: *Para* fluoro-thiol clicked diblock-copolymer self-assembly: Towards a new paradigm for highly proton-conductive membranes

For the most part, I performed the majority of the practical work, this specifically included:

- The synthesis of the PPFS/PBuA statistical and block-copolymers by controlled radical polymerization (CRP) and free radical polymerization in emulsion (FRP).

- The synthesis of the menthyl acrylate bio-sourced monomer. The purification of the monomer was performed with the guidance of and experienced colleague.

- The sulfonation of the all copolymers by *para*-thiol modification with sodium-3-mecapto-1-propanesulfonate.

- The membrane elaboration procedure from the formulation step using both covalent and ionic cross-linkers to the obtention of the final membrane.

- ^{1}H-NMR analysis to determine the monomer conversions and polymer compositions, and ^{19}F NMR to assess the *para*-thiol modification.

- Size Exclusion Chromatography (SEC) to obtain information on the polymer's molar masses and dispersity.

- Differential Scanning Calorimetry (DSC) for the thermal properties of the materials

- Atomic force microscopy (AFM) to observe the self-assembly of the BCP before and after sulfonation.

- Elongation rheology measurements to observe the behaviour of the membranes containing specific amounts of cross-linkers under strain.

- Water uptake of the membranes.

- The sample preparation for the Small-angle X-ray scattering (SAXS) analysis. The samples were characterized in another lab (*Centre de Recherche Paul Pascal* (CRPP) in Bordeaux) because the apparatus is not available in our lab.

- Ion Exchange Capacity. Ion Exchange Capacity (IEC) and Electrochemical Impedance Spectroscopy (EIS) were performed in the ICVT lab in Stuttgart. The sample preparation was made by me, the resulting data were given to me by the lab, and the interpretations of the results were made by me.

Unless specified otherwise, the data collected, were analysed by me. The vast majority of the peer-reviewed technical article was written by me; specifically, I conceived and wrote the original draft of the manuscript and took the lead in harmonizing and incorporating suggested changes from my co-authors.

Chapter 5. Life Cycle Assessment of the proton-conductive membrane

Table of contents Chapter 5

1. Introduction and state-of-the-art

Included in the United Nations (UN) sustainable goals, global warming is an active and urgent issue. Carbon dioxide emissions have increased of 50% in the past 30 years, leading to an increase in temperature above 1°C at the surface of the planet, severely impacting the world's climate. With the signature of the Paris agreement[1] (COP21-2015), countries agreed to aim to provide responses to the global warming issue by implementing financial and technological solutions to the problem. Life cycle assessment (LCA) is a way to support this initiative. LCA is defined as a tool to assess the environmental performance of a product. And can be considered in every stage of the manufacture of the product. Indeed, the LCA can cover the production of raw materials used to make the final product, the use, and finally the disposal or valorisation of a product or service. Hence, LCA is mainly performed with the aim for continuous improvement, as it provides a quantitative information of each stage involved in the whole life cycle of the product/service, **Figure 1**. The steps with the highest environmental impacts can be detected and opportunities for improving them could be associated. LCA can also be used to compare two or more products. Although the LCA is focused on the environmental impact, social and economic impacts can be included in the studies as well.
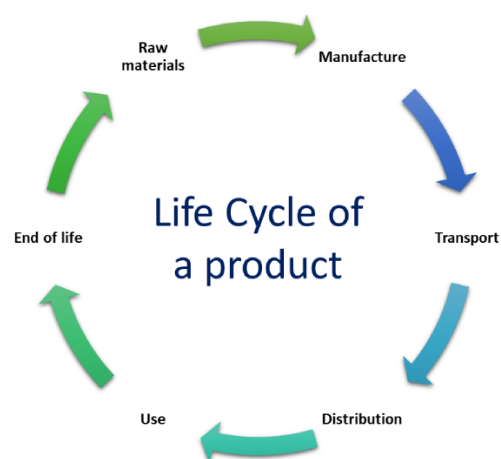
Figure 1. Life cycle of a product.

LCA and its derivatives are destined to everyone from undergraduate, to PhD, to industry professionals. Although LCA helps with the comprehension of environmental issues

as it covers a wide range of environmental impacts, the numerous processes involved and finite resources to perform the study often requires simplification. And by doing so this assessment includes uncertainties. Additionally, the results of a study do not necessary conclude whether a product is good enough to solve any specific environmental potential. Nevertheless, it can surely help improving the product's environmental profile and consequently, the linked negative effect on the environment.[2]

Literature on the life cycle assessment of hydrogen production is already very developed. The results of the studies show a very important impact on the emission of greenhouse gases for hydrogen production. That result is due to the energy input used that is most of the times partially fossil-based. Indeed, the original techniques to produce hydrogen such as steam reforming do not use renewable energies sources. Hydrogen production by electrolysis has demonstrated that using renewable energy had a positive impact in some of the impact categories such as acidification, photochemical ozone creation, or global warming potential. Concerning the actual components of the electrolyser, the electrodes and more specifically the anode, the bipolar plates, and the MEA (Membrane Electrodes Assembly) had the most impact on the global warming potential indicator. This is mainly due to the use of catalysts and their recyclability.[3] Nevertheless, the overall impact of hydrogen production can be lowered with the increasing use of renewable energy as energy source. This way, the balance between the energy used to produce hydrogen and the production of hydrogen to be used as a source of energy should be compensated.[4] Currently this is not really the case as the average European electricity mix is based on non-renewable sources.[5, 6]

Most of the research dedicated to membranes is focused on the environmental impact of the membranes before the use stage, and the inventory made consists of assessing the energy input for the manufacture of these materials. In general, what is lacking in the literature is a homogenisation of the studies on membranes LCA. When performed, the studies are independently made depending on everyone's angles, it is hence difficult to find comparisons points between the studies. However, some positive aspects such as the design of the membranes can be highlighted. On the negative side, the production of

membranes is not very environmentally friendly and sustainable due to the solvents used to fabricate them. They rate high in impact in specific environmental categories related to toxicity, as the associated waste management aspect is still something not resolved. Leading in a high impact of water bodies. Additionally, other categories are affected by the fact that the polymers used for the membranes are fossil-based.[7] However, the need for compacted devices has push to create thinner membranes which will lead to the consumption and use of less energy, and materials, resulting in the change of the current trends.[8] In some cases, tentative experiences focused on reusing and recycling the membrane materials are also considered with promising results. All of which participate to reduce the environmental impact of the membrane life cycle. For that reason, it is important to perform LCA studies primarily on the manufacturing stage of the membranes.[9, 10] This PhD and especially this chapter will propose a study of that preliminary stage.

2. Life cycle assessment (LCA) – Methodology

Life cycle assessment is the compilation and evaluation of potential inputs (*i.e.,* natural resources, products, or energy demand), outputs (*i.e.,* emissions, or solid waste) and potential environmental impacts of products, processes, or services, through its life cycle. A methodology to perform LCA is provided by the International Organization for Standardization (ISO): ISO 14040:2006(E)[11] and ISO 14044:2006(E)[12], **Figure 2**.

In order, the four phases of the LCA of a product are:

- – Goal and scope definition of the study
- – Life cycle inventory (LCI)
- – Life cycle impact assessment (LCIA)
- – Interpretation of the study
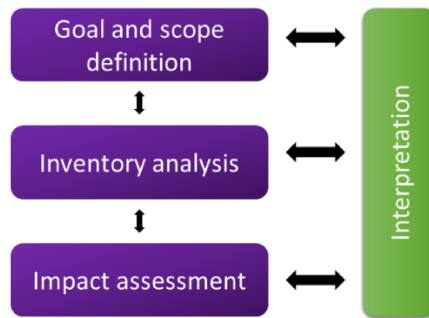
Figure 2. Life cycle assessment methodology.

In the **goal and scope** section are defined the aim of the study, the system boundaries, the functional unit of the study, the data and processes included in the study and the reasons for their inclusion. It is a guide to follow throughout the process to keep track on the study as well as the guide for the audience the study is intended for.

The **LCI** section gathers all the data necessary that are within the system boundaries to perform the LCA. The main system boundaries in LCA studies are cradle-to-grave, cradle-to-gate, cradle-to-cradle, and gate-to-gate. Once the boundaries set, the data can be categorized in background and foreground data. In the foreground data are the data that are directly linked to the product and the background data, the data that are involved in the production of generic material (*i.e.,* energy, transport). The collected data are interpreted to calculate the different impacts and acquire accurate results. At this stage, an emphasis should be put on the simplicity of what is reported for a better understanding of the audience. A flow chart is the typical format that is used to present the system.

In the **LCIA** section the data collected in the inventory are correlated to the environmental impacts using impacts categories. The later are chosen by the study maker in accordance with the relevance to the LCA study. This stage will provide necessary matter for the interpretation phase of the study. As much as this step facilitates the knowledge and understanding about the environmental impact of the inputs and outputs, it also allows improving the inventory analysis.

The last stage of **interpretation** has the aim to analyse the obtained results in correlation with the goal and scope definition. In this last stage, conclusions are reached, the

limitations of the results are presented, and recommendations are provided based on the full analysis of all the stages of the LCA study.

3. Goal and scope

The current LCA study was performed by Karell Bosson, Early-stage researcher of the eSCALED project. This chapter aims to give an overview of the LCA study of the membrane of the artificial photosynthesis eSCALED device. The goal is determined by the motivation of the study, the targeted audience and finally, the dissemination of the results to the public for comparison. The Scope considers the product system, the function of the product system, the functional unit, the system boundaries, limitations of the study, allocation procedures, methodology and interpretation methods to determine the impacts of the study, assumptions made, data requirements and limitations, and the type of report needed for the study.

3.1. Goal

The aim is to determine the feasibility and provide 'proof of concept' of using the membrane on a larger scale in a PEM water electrolyser. The purpose of the membrane is to allow the protons to travel from one electrode to the other, while acting as a barrier to prevent the mixing of chemicals from both side of the device. This study has allowed investigating and identifying the steps of membrane manufacturing that have the highest environmental impact to improve the processes in the future.

3.1.1. Purpose of the study

The principal objective of this LCA study is to evaluate the environmental impact and accumulated energy requirements related to the manufacturing of proton-conducting membrane.

3.1.2. Reasons to carry out LCA

This study was performed within the framework of the International Training Network (ITN) and European Joint Doctorate (EJD) of the eSCALED project. The project has

received funding from the European Union's Horizon 2020 research and innovation programme under the Marie Sklodowska-Curie grant agreement No 765376. The objective of the eSCALED project is so to mimic the natural photosynthesis process to transform solar energy, which is a renewable energy source, and store it in the form of hydrogen or solar fuels, to make an artificial leaf. This chapter will focus on the proton-conducting membrane of the device. By making this study we aim to pinpoint the aspect of the membrane manufacture that presents the most environmental impacts. Furthermore, a comparison of different membrane making scenarios was made, helping us decide the optimum one in terms of environmental performances.

3.1.3. Intended application and audience

As an intended application, the study aims to provide support on the future choices for a possible upscaling and commercialisation of membranes for proton-conductivity applications. The targeted audience is principally researchers involved in the eSCALED project, governmental and legislative bodies such as the European Commission (EC), academic partners and private commercial beneficiaries that are involved with the eSCALED consortium, the scientific community, actors of the energy field and in a broader way every interested parties. The results of the study are communicated in this report and in potential congress, scientific journals and any future considered publication of interest. As a matter of fact, an application to present the results of this study has been made for the SETAC conference happening in Copenhagen in May 2022. The application is still under revision but for information, SETAC is an organisation dedicated to the study, analysis, and solution of environmental issues.

3.1.4. Type of critical review

Standard ISO 14040:2006 states the need for critical review only in the case of a comparative assertion intended to be disclosed to the public. This includes some different comparative assessments for the environmental behaviour of a proton-conducting membrane. The study has been reviewed internally by LCA experts of the Eurecat technologic centre that are partners of the eSCALED project. Additionally, all the researchers

of the eSCALED consortium have been involved by approaching their vision and suggestions of improvement, in compliance with the iterative nature of the LCA methodology.

3.2. Scope

3.2.1. Functional unit

The functional unit describes the primary function to be fulfilled by a product system and indicates how much of this function must be considered in the intended LCA study. The choice of the functional unit can be difficult as a product can have multiple functions. Moreover, the functional unit must be chosen in a way that it is possible to compare the product of the study with similar ones. It is a parameter that can be changed throughout the study since the goal and scope could be under continuous revision and refinement.

In the case of membranes, most proton-conductive membranes fulfil the same function which is to conduct protons. The proton-conductivity is the most important property and is assessed by measuring the conductivity of the membrane, the unit is S/cm. The membranes are assembled with the electrodes (Membrane Electrode Assembly - MEA), for that reason the area of contact of the electrodes and the membrane also influence the conduction. The area is included in the conductivity equation, as well as the thickness of the membrane. Finally, the temperature and water content are parameters influencing the conductivity measurements that are not included in the conductivity equation. With all stated, the chosen functional unit for the LCA study of membranes has been selected as the manufacture of $1cm^2$ of membrane that has a proton-conductivity above 100 mS/cm at 80°C and an Ion Exchange Capacity (IEC) above 1meq H^+/g as technical requirements of the eSCALED project framework.

3.2.2. System boundaries

System boundaries are important to determine at the beginning of the study stages included on the study according to its goal. It is also important to make beforehand the inventory of the life cycle. The following LCA study has followed a cradle to gate approach, with the aim of providing a full picture of the environmental impact of the membrane, from

its raw material extraction and acquisition until its end of production, **Figure 3**. Studying the impact of the membrane in the use stage of the PEM electrolyser would have been too complicated to implement for the LCA studies at this stage. The final configuration including the inputs for all the parts of the eSCALED electrolyser for hydrogen production were not certain yet. Trying to implement them would have added greater uncertainties to the study. In other words, results could be altered by a lack of factual knowledge about the behaviour of the membrane during the use phase once installed in the artificial leaf. This will be limiting when it comes to meaningful information to the study. If we were to include the use phase in this studs, future decisions for upcoming developments would be with poor accuracy.
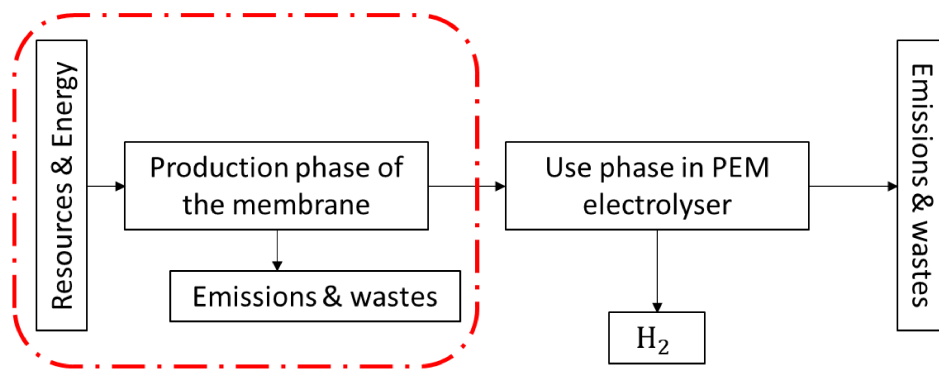
Figure 3. System boundaries of the membrane development.

3.2.3. Data sources and collection

The foreground and background data such as the lab data used to perform the study were primarily acquired by the PhD candidate. Project partners and technology providers as they are representative of the current manufacturing practices of the device also participated in the data collection. Although all partners of the eSCALED project contributed with their expertise, the primary partners involved in this study were the University of Pau and Adour countries, the University of Stuttgart, and the Eurecat Technological centre. The additional data that could not be found with the previous methods were recovered from the literature, patents, and the Ecoinvent v3.3 database included in the SimaPro software.

3.2.4. Data quality requirements

The data retrieved were analysed by giving special attention to the completeness of the processes at each stage as they needed to be modelled as accurately as possible; the reproducibility of the initial experiments, each source was clearly identified and referenced; finally, all gathered data used passed the quality limit for Europe. The data used to perform the study were clearly identified and referenced, making it reproducible. Therefore, anyone willing to perform the same study is fully capable of doing so. Furthermore, the data used were as updated as possible. When no data was available for some processes, public or private databases were used with using the most updated as possible version of the data.

3.2.5. Cut-off criteria

As stated in ISO 14040: 2006, the "cut-off" criteria specify the amount of material, energy flow, or the level of environmental significance associated with unit processes or product systems to be excluded from a study. This LCA study did not develop any cut-off based on mass or energy, or environmental relevance. Thus, all inputs of all the processes were considered in all stages.

3.2.6. Assumptions

Assumption can be made in the processes if specific data are not available. Those assumptions must be specified and are made to be as close as possible to the initial processes.

Patents and articles were used to model the processes that could not be found in the database. In respect to the laboratory scale of the present work, and regarding the energy inputs, assumptions were made that the equipment used to synthetize the materials were the ones from the lab. Hence, the hot plate and stirrer used are the ones from IKA, and the oven used to dry the chemicals is from the brand BINDER. Regarding the specific processes, assumptions were made according to the database information. BlocBuilder® and SG1 were both used for the controlled radical polymerization (CRP), SG1 was modelled based on a patent.[13] It was assumed that SG1 was equivalent to BlocBuilder® as they have similar

structure and an accurate BlocBuilder®'s synthesis was not found. 1,8-Diazabicyclo5.4.0undec-7-ene (DBU) was used as a base during the procedures. As its synthesis could not be found, it was replaced with triethylamine during modelling. Triethylamine is also a strong base that could be used in the lab as replacement to DBU. Finally, menthol was used to synthetize menthyl acrylate, as an inclusion of a bio-sourced option for the membrane development. During modelling, it was assumed that menthol is equivalent to mint.

4. Inventory analysis

The materials and energy requirements data were gathered and analysed in the inventory analysis step. Their impact was assessed in accordance with the functional unit previously defined in the Goal and Scope step.

4.1. Synthesis description

The synthesis of the proton-conducting membranes was detailed in chapters 3 and 4 of this PhD manuscript. A comparison of 4 proton-conducting membranes that differ from each other from their synthesis methods and choice of monomer was made. The membranes were synthetized using 2,3,4,5,6-pentafluorostyrene and (butyl or menthyl) acrylate-based sulfonated copolymers. The comparison was made between block and statistical copolymers of these systems that were synthetized by Nitroxide Mediated controlled radical polymerization (NMP) or free radical polymerization in emulsion. Additionally, the comparison was also made between the membranes made using butyl acrylate and membranes made using the use of the bio-sourced option.

4.2. Allocation procedures

The primary data were collected on a mass flow balance. Similarly, all the main products of the processes included in inventory analysis were allocated by mass. This approach followed the guideline of international standards.

4.3. Unitary process description

The Process of manufacturing the membrane related to this study can be described as: the synthesis of the copolymers and their purification (block or statistical), the sulfonation of the polymers, their blending with a cross-linker to increase the mechanical properties of the membranes and lastly, the membrane elaboration, **Figure 4**.
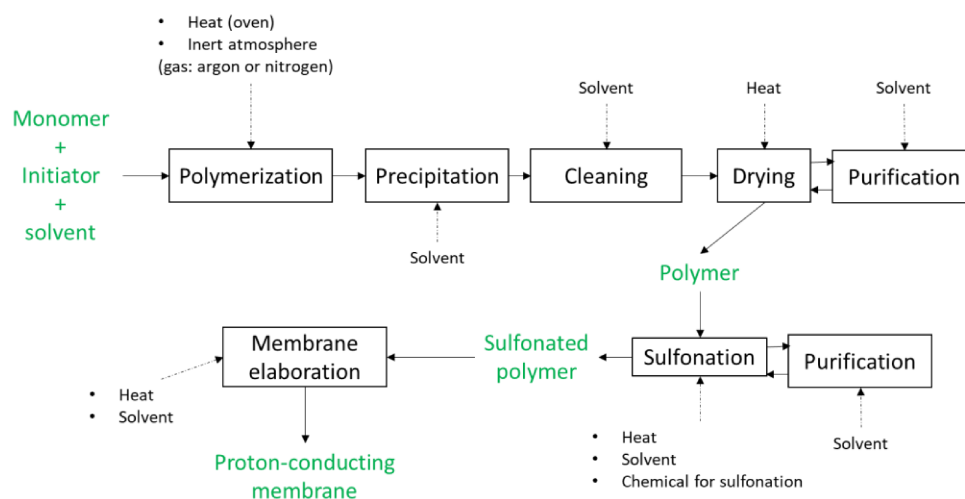
Figure 4. Process flow diagram of a membrane production.

4.4. Description of life cycle inventory data

Inventory data for the principal materials and processes are shown in **Table 1**, with values related to the functional units (FU), and their units. FRP stands for Free Radical Polymerization and CRP for Controlled Radical Polymerization. The monomers used were pentafluorostyrene (PFS), butyl acrylate (BuA), and menthyl acrylate (MA). The detailed experimental procedures are described in chapters 3 and 4 of this manuscript.

Table 1. Life cycle inventory data of the membrane processes.

Stage	Inputs	Value (per FU)	Unit	Comments
Synthesis of homopolymer of poly(pentafluorostyrene) (PPFS) by CRP and FRP				
CRP-PPFS	Monomer	1	g	Monomer is PFS; Initiator is SG1; Solvent is Methanol (polymer precipitation and purification).
	Initiator	0.0105	g	
	Solvent	40	g	
	Energy*	7.31	kW.h^{-1}	
FRP-PPFS	Monomer	1	g	Monomer is PFS; Initiator is sodium persulfate; The additional reagents are sodium dodecyl sulfate, and sodium phosphate (to make the emulsion), and sodium chloride (to obtain the polymer in solid form).
	Initiator	0.004	g	
	Additional reagents	3.105	g	
	water	10	g	
	Energy	9.59	kW.h^{-1}	
Synthesis of copolymers of PFS and BuA by CRP and FRP				
CRP-block-copolymer synthesis	Monomer	3.45	g	Monomer is BuA; Macro-initiator is CRP-PPFS; Solvents are DMF (synthesis) and Methanol (polymer precipitation and purification).
	Macro-initiator	0.7	g	
	Solvent	42	g	
	Energy	11.15	kW.h^{-1}	
CRP- statistical copolymer synthesis	Monomers	2.7	g	Monomers are PFS and BuA; Initiator is SG1; Solvent are DMF and Methanol.
	Initiator	0.054	g	
	Solvent	50	g	
	Energy	7.77	kW.h^{-1}	
FRP-statistical copolymer synthesis	Monomers	1.33	g	Monomers are PFS and BuA; Initiator is sodium persulfate; The additional reagents are sodium dodecyl sulfate, sodium phosphate, and sodium chloride (NaCl).
	Initiator	0.0092	g	
	Additional reagents	5.07	g	
	water	50	g	
	Energy	21.69	kW.h^{-1}	
Synthesis of menthyl acrylate (MA) monomer and PFS/MA copolymer by CRP				
Synthesis of MA	Reagents	2.79	g	Reagents are menthol, acryloyl chloride, and DBU; Solvents are Dichloromethane used for the reaction and NaCl brine solution use for the purification of the monomer.
	Solvents	3150	g	
	Energy	0.081	kW.h^{-1}	
CRP- statistical copolymer synthesis (With MA)	Monomers	1.56	g	Monomers are PFS and MA; Initiator is SG1; Solvents are DMF and Methanol.
	Initiator	0.027	g	
	Solvent	23.5	g	
	Energy	11.6	kW.h^{-1}	
Sulfonation processes of copolymers and membrane elaboration				
Sulfonation process	Copolymer	1	g	The sulfonating reagents are Sodium-3-mercapto-1-propanesulfonate and DBU; Solvents are DMF and water (used for the dialysis of the sulfonated polymer).
	Sulfonating reagents	0.9	g	
	solvent	3000	g	
	Energy	21	kW.h^{-1}	
Membrane elaboration	Sulfonated Copolymer	1	g	Polybenzimidazole (PBI) is used as a cross-linking agent in the

PBI	0.02	g	procedure; Solvents are DMSO
solvent	34	g	used to make the membranes, and
Energy	28	kW.h^{-1}	HCl solution used to cross-link the polymers.

For all the processes, Energy is a total of the energy inputs used for heating, drying, and stirring.

5. Life Cycle Impact Assessment (LCIA) and evaluation

In this section are presented the quantification and evaluation of environmental impacts associated with the proton-conducting membrane. The relevant systems are summarised based on the LCA performed with the help of the SimaPro software v9.1.0.8.

5.1. Impact characterization method selection

Following the ISO 14044:2006 standard, one of the mandatory elements on every life cycle assessment is the selection of impact categories, category indicators and characterisation models. Hence, the selection of the impact assessment method is crucial.

This study selected and implemented the impact assessment method ReCiPe Midpoint (H) for Europe v1.01 in the SimaPro software v9.1.0.8. This methodology integrates and harmonises two well-known Life Cycle Impact Assessment (LCIA) methods, CML and Ecoindicator 99, improving and updating the environmental science used.[14] The name, abbreviation and reference units for the sixteen mid-point categories implemented in the Recipe mid-point characterisation method are presented in **Table 2**.

Table 2. Impact categories.

Impact categories	Abbreviation	Units
Global warming Potential	GWP	kg CO_2 eq
Stratospheric Ozone Depletion	SOD	kg CFC-11 eq
Ionizing radiation	IR	kBq Co-60 eq
Ozone formation, human health	OF-HH	kg NO_x eq
Fine particulate matter formation	FP	kg PM2.5 eq
Ozone formation, terrestrial ecotoxicity	OF-TE	kg NO_x eq
Terrestrial acidification	TA	kg SO_2 eq
Freshwater eutrophication	FE	kg P eq
Marine eutrophication	ME	kg N eq
Freshwater ecotoxicity	FEco	kg 1,4-DCB* eq
Marine ecotoxicity	MEco	kg 1,4-DCB eq
Human toxicity[1]	HT	kg 1,4-DCB eq
Land use	LU	m^2a crop eq
Mineral resource scarcity	MRS	kg Cu eq
Fossil resource scarcity	FRS	kg oil eq
Water consumption	WC	m^3

DCB = dichlorobenzene

[1]*Including Human carcinogenic toxicity (HCT) and Human non-carcinogenic toxicity (HnCT)*

5.2. LCIA results

Multiple variables and impacts such as extraction of resources, emissions of certain compounds and land use are included in the LCA. A quantitative analysis is assessed when feasible; however, a qualitative analysis is done with the LCA to have a clear overview of all the involved variables and impacts.[11] Based on the work previously done, the study is centred on the membrane part of the eSCALED device.

To evaluate the environmental impact, accumulated energy requirements, and to determine the best synthesis materials related to the manufacture of the membranes, the focus was made on the most relevant steps of the work. Hence, here, the evaluation was made to identify the stages of the membrane elaboration that display the most environmentally friendly scenario.

The membrane elaboration stages that were considered are:

– The synthesis of the starting copolymer materials with a comparison between the chosen polymerization techniques (controlled or free radical polymerizations)

– The sulfonation of the copolymers

– The membrane elaboration including the blending with the polybenzimidazole (PBI) cross-linker

The information and results expected from the LCA work are:

The identification of the procedures and steps having the highest environmental costs;

The impact of the choices made during the experimental part of the work;

And, the identification of the best scenario for the proton-conducting membrane process.

A detailed overview of the results is described hereafter.

The quantitative impact of each impact categories is in the Appendix section (**Appendix 4** to **Appendix 17**)

5.3. Life cycle assessment interpretation and evaluation

In this final step are discussed the gathered information and obtained results of the inventory analysis and impact assessment steps. In this part of the study, conclusions are made according to the results in compliance with the initially defined goal and scope.

In the following LCIA results, a comparison between the obtained membranes is discussed. Furthermore, a comparison was made between:

– the synthesis method that was used to synthetise the copolymers (controlled radical polymerization -CRP, or free radical polymerization -FRP)

– their sulfonation processes

– the use of a bio-sourced monomer to make the membranes

– the synthetized membranes

5.3.1. LCIA polymerization technique

We can firstly have a look at the synthesis of poly(pentafluorostyrene) (PPFS). Indeed, PPFS is the main component of all the membranes. As mentioned before and described in the chapters 3 and 4 of this manuscript, the polymers were synthetized both by nitroxide mediated controlled radical polymerization in solution (CRP) and free radical polymerization in emulsion (FRP). As shown in **Figure 5**, of all the inputs, the most impact for the synthesis of PPFS by CRP comes from the monomer pentafluorostyrene (PFS). This result is the same for every impact category as the impact of PFS is over 90%. The second input with the highest impact is energy. This comes from the energy needed to heat and stir the reagents during polymerization and to dry the obtained product that is the polymer. The energy input of the drying step is the most impactful in terms of energy input.
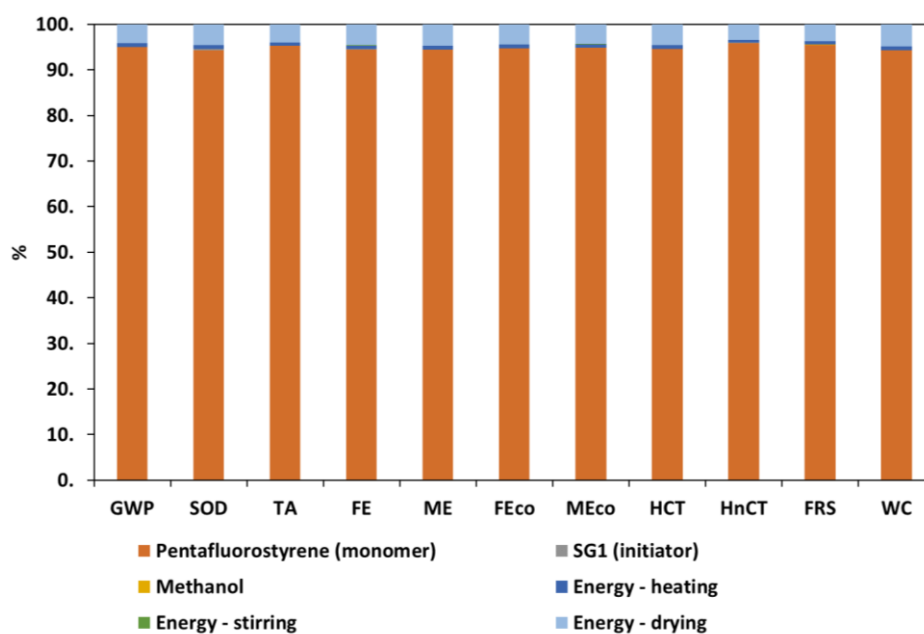
Figure 5. Impact analysis of the synthesis of 1g of PPFS by CRP.

A similar observation was made for the synthesis of PPFS by free radical polymerization as PFS has the most impact on the process, **Figure 6**. This result is not so surprising as the modelled synthesis process of PFS starts with the use of benzonitrile which is classified as dangerous for human health and for the ozone layer.

Its use contributes in making PFS not the most environmentally and health friendly compound.[15] Their impact is hence linked to this characteristic.
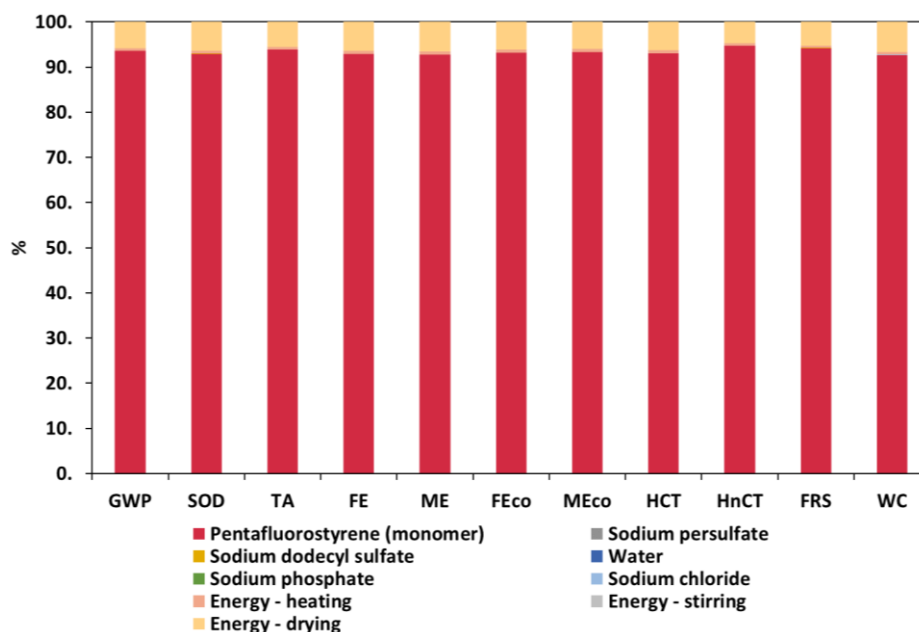
Figure 6. Impact analysis of the synthesis of 1g of PPFS by FRP.

When comparing both polymerization methods, for the same amount of material, PPFS synthetized by CRP (CRP-PPFS) has a slightly lower impact than the one made by FRP (FRP-PPFS), **Figure 7**. An explanation for this is the higher temperature needed to dry FRP-PPFS. In fact, as the reaction is made in water, the needed drying temperature is higher than the one of CRP-PPFS that uses methanol (MeOH) as the precipitation solvent ($T^{\circ}_{boiling\ MeOH}$ = 65°C; $T^{\circ}_{boiling\ water}$ = 100°C).
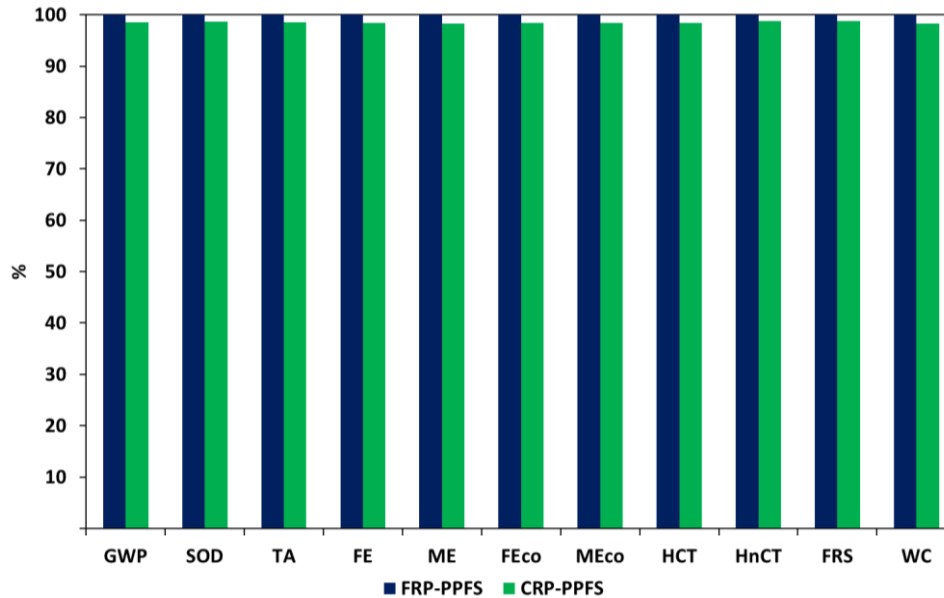
Figure 7. Impact comparison of 1g of CRP-PPFS and FRP-PPFS.

5.3.2. LCIA of PPFS/PBuA copolymers

The next step to obtain the membrane is the synthesis of the copolymers. As explained in chapter 4, butyl acrylate (BuA) was used to add some flexibility to the membrane. 3 copolymers were synthetized:

– A block copolymer made by CRP (CRP-PPFS-*b*-PBuA)

– A statistical copolymer made by CRP (CRP-PPFS-*stat*-PBuA)

– A statistical copolymer made by FRP (FRP-PPFS-*stat*-PBuA)

When comparing the 3 materials, we can see that the most impact for all the impact categories comes from FRP-PPFS-*stat*-PBuA and the material with the lowest impact is the block copolymer, CRP-PPFS-*b*-PBuA, **Figure 8**.
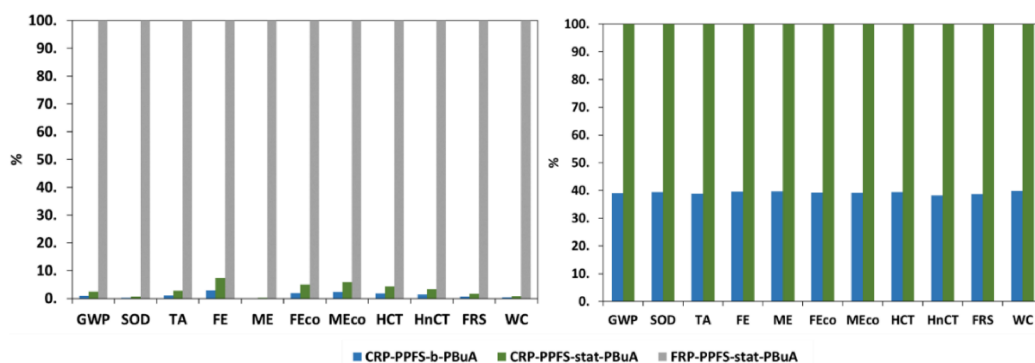
Figure 8. Impact comparison of 1g of CRP-PPFS-*b*-PBuA, CRP-PPFS-*stat*-PBuA, and FRP-PPFS-*stat*-PBuA.

Looking at each individual process, we can see that the most impact (close to 90%) comes from PPFS in the case of CRP-PPFS-*b*-PBuA (**Appendix 1**), and PFS in the other cases (**Appendix 2** & **Appendix 3**). Additionally, the impact of the electricity used to dry the polymer is more important in the case of FRP-PPFS-*stat*-PBuA (**Appendix 3**). This could explain the overall higher impact of FRP-PPFS-*stat*-PBuA when comparing the three processes. Furthermore, less PFS monomer is used for the synthesis of the block copolymer CRP-PPFS-*b*-PBuA, resulting in the lowest overall impact of CRP-PPFS-*b*-PBuA.

5.3.3. LCIA of sulfonated PPFS/PBuA copolymers

For the sulfonation, the copolymers were mixed with the sulfonating agent (sodium-3-mecrapto-1-propane sulfonate) in presence of a base, in DMF. The advantage of this technique is the mild conditions in which the reaction is made. Although no additional impact is brought from the energy inputs as the reaction is done at room temperature, we use large amounts of water for this procedure for the purification of the sulfonated copolymers that is done by dialysis. Nevertheless, the sulfonation step did not bring any change to the comparison of the impacts than what was obtained previously, as the sulfonation procedure is the same for all the copolymer systems. FRP-PPFS-*stat*-PBuA displayed the most impact of all the systems and CRP-PPFS-*b*-PBuA the lowest impact, **Figure 9**.
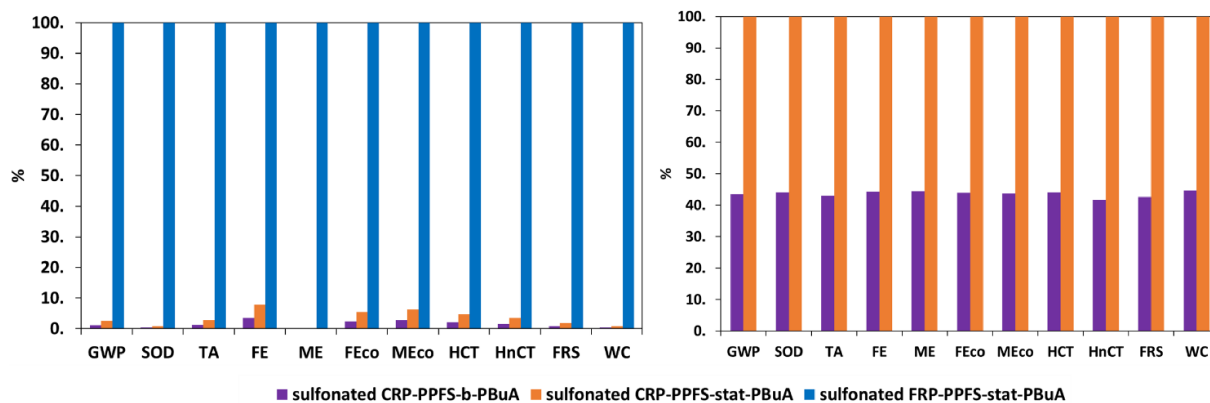
Figure 9. Impact comparison of 1g of sulfonated CRP-PPFS-*b*-PBuA, CRP-PPFS-*stat*-PBuA, and FRP-PPFS-*stat*-PBuA.

5.3.4. LCIA of sulfonated PPFS/PMA copolymer and comparison with the PPFS/PBuA system

The procedure to add a second monomer for the flexibility of the membrane was repeated but this time using menthyl acrylate. The monomer was synthetized using menthol, an organic compound derived from mint. On top of providing the flexibility property, menthol is bio-sourced as it is extracted from the natural mint. For this process, mint was assumed to be synthetized as menthol for the simulation. We can see from the obtained graphs that once again, the sulfonated FRP-PPFS-*stat*-PBuA has the most impact among all the sulfonated copolymers and CRP-PPFS-*b*-PBuA the lowest impact, **Figure 10**.
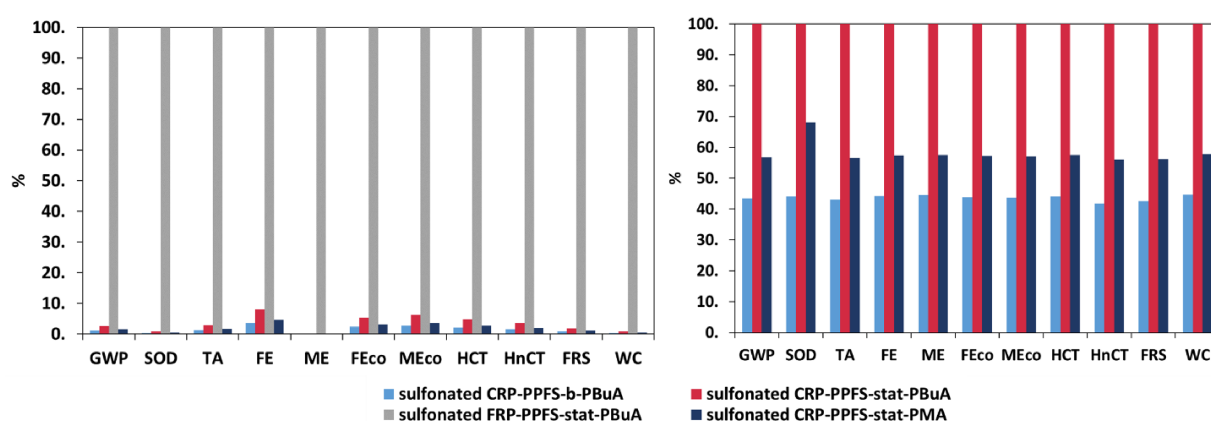
Figure 10. Impact comparison of 1g of sulfonated CRP-PPFS-*b*-PBuA, CRP-PPFS-*stat*-PBuA, FRP-PPFS-*stat*-PBuA, and CRP-PPFS-*stat*-PMA.

Expecting CRP-PPFS-*stat*-PMA to have the least impact due to the bio-sourced aspect, we took a closer look at the sulfonated copolymer on its own (**Figure 11 A**) and the menthyl acrylate monomer (**Figure 11 B**). Like it was the case for the other copolymers, PFS's impact is close to 90% on all the impact categories except the stratospheric ozone depletion impact where it is at 75%. On this specific impact category, the monomer menthyl acrylate has 15% impact, the highest for this compound in the process. By looking at the monomer's process in detail, the impact is mostly fed by acryloyl chloride, dichloromethane, and the brine solution used for washing during the experiment. The impact of mint that was used in replacement to menthol has close to no impact in comparison to the other inputs. The impact of the brine solution comes from the amount used (50 g for the functional unit) and the impact of acryloyl chloride and dichloromethane come from the fact that they are considered to be dangerous chemicals.[16, 17]
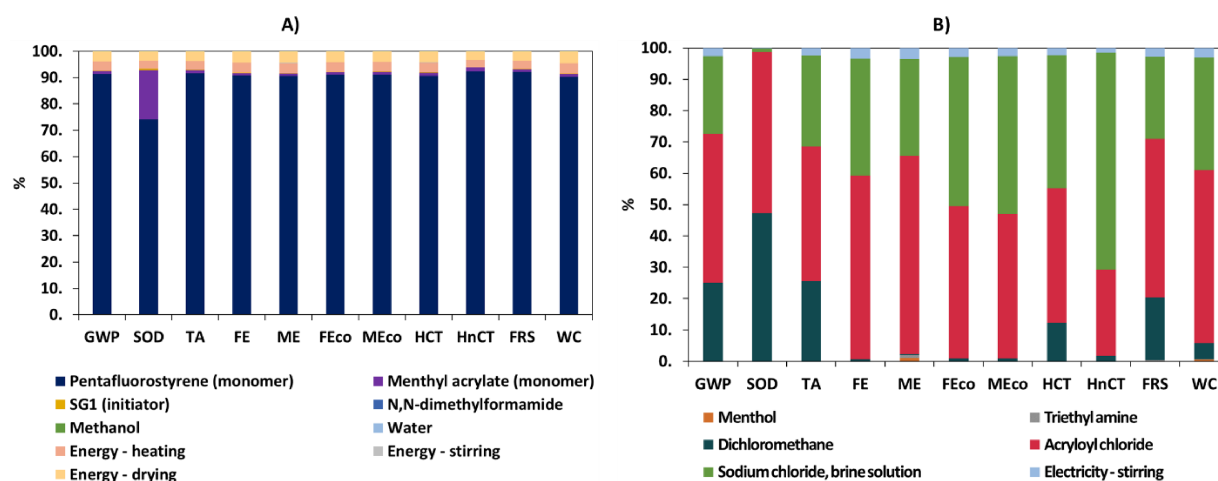
Figure 11. Impact analysis of the synthesis of 1g of CRP-PPFS-*stat*-PMA (A), Impact analysis of the synthesis of 1g of menthyl acrylate (B).

5.3.5. LCIA of the proton-conducting membranes

Finally, the membranes were made by blending the sulfonated copolymers with PBI in DMSO, with few dips in acid solution to provide the conductive properties (cf. chapter 4). The impacts of each membrane follow the same trend as the synthesis of the copolymers and their sulfonation. From highest to lowest impact, we have: FRP-PPFS-*stat*-PBuA, CRP-PPFS-*stat*-PBuA, CRP-PPFS-*stat*-PMA, and CRP-PPFS-*b*-PBuA, **Figure 12**. This result is also the effect of the equality of the procedure for each material.
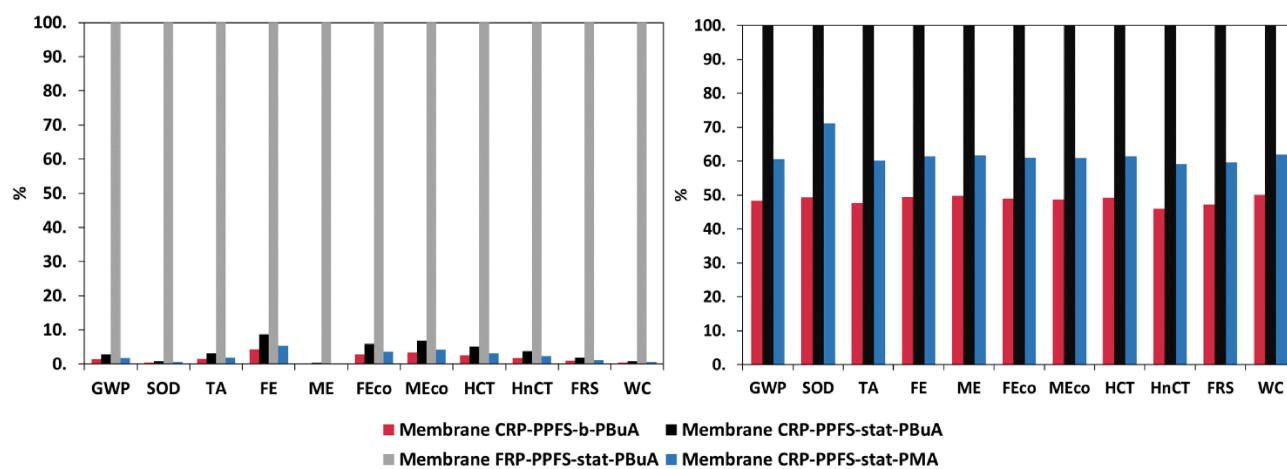
Figure 12. Impact comparison of the membranes of CRP-PPFS-*b*-PBuA, CRP-PPFS-*stat*-PBuA, FRP-PPFS-*stat*-PBuA, and CRP-PPFS-*stat*-PMA.

6. Conclusion

We conducted an LCA study on several proton-conducting membranes. The manufacturing process was broken down and evaluated. This has helped identifying hot spots within the processes that contribute to the environmental impact of the final membranes. The materials were made at the laboratory scale, and the highest impacts were proven to come from the use of pentafluorostyrene (PFS), the main component of the membranes. For proton-conduction properties, fluorinated materials are mostly used because of their proven stability (thermal, chemical, physical).[18] These quality help with their resistance to harsh acidic environments in the electrolysis cell. In this sense, the choice was made for the eSCALED membrane to use a fluorinated material. PFS, has on top of the fluorinated materials advantages, the fluorine in *para*-position of the phenyl group. This characteristic allows for countless possibilities of polymer functionalization by nucleophilic substitution. A benefit we used for the sulfonation of the copolymers.

Although PFS has all these structural advantages, we saw from the LCA point of view that it is not the best material to use. Indeed, for all the processes, the most impact came from PFS. The idea for a future work could be to choose another chemical that performs as good chemically but with a more balanced effect on the impact categories. Regarding the synthesis method of the copolymers with BuA, the most impact came from the copolymer synthetized by free radical polymerization (FRP-PPFS-*stat*-PBuA) and more particularly from the energy input for the drying step of the copolymer. Concerning the other PPFS/PBuA copolymers, we saw that the block-copolymer (CRP-PPFS-*b*-PBuA) had the lowest impact compared to the statistical one (CRP-PPFS-*stat*-PBuA). This is due to the lowest amount of PFS used during the procedure. Finally, we can say that using the bio-sourced compound did not have the positive impact expected due to the presence of PFS still and the synthesis method of the monomer that includes the use of acryloyl chloride and dichloromethane. Nevertheless, the membrane made with CRP-PPFS-*stat*-PMA had a better environmental result than the other membranes made from the statistical copolymers.

In correlation with the conductivity values obtained in chapter 4 (**Table 3**), for the PPFS/PBuA system, the membrane of CRP-PPFS-*b*-PBuA, has the least impact of the PPFS/PBuA system and performs better in terms of proton-conductivity. The membrane of CRP-PPFS-*stat*-PMA has the best conductivity of all the membranes and is placed second on the environment impact category. As explained in chapter 4, the incredible conductivity of the CRP-PPFS-*stat*-PMA comes from the cohesion of properties between PPFS and PMA.

Table 3. Conductivity values of the different membranes.

Polymer	Conductivity (mS/cm)
CRP-PPFS-*b*-PBuA	179
CRP-PPFS-*stat*-PBuA	94
FRP-PPFS-*stat*-PBuA	16
CRP-PPFS-*stat*-PMA	690

From this LCA study, we can conclude that controlling the copolymer synthesis is the best way to make a PPFS based proton-conducting membrane with improved environmental impact while achieving good proton-conductivities. This study aims to pave the way toward a more conscious and aware approach for developing proton-conducting membranes by giving suggestions and indications about the hotspots and the processes that need particular attention from the environmental point of view, which is a crucial point in nowadays research and innovation.

7. References

1. Delbeke, J., Runge-Metzger, A., Slingenberg, Y. & Werksman, J., The paris agreement. *Towar. a Clim. Eur. Curbing Trend* 24–45 (2019) doi:10.4324/9789276082569-2.

2. Hauschild, M. Z., Rozenbaum R. K., Olsen, S. I., Life Cycle Assessment: Theory and Practice, Springer International Publishing Switzerland, 2017. DOI: 10.1007/978-3-319-56475-3_6.

3. Mori, M., Stropnik, R., Sekavčnik, M. & Lotrič, A., Criticality and life-cycle assessment of materials used in fuel-cell and hydrogen technologies. *Sustain.* **13**, 3565 (2021). DOI: 10.3390/su13063565

4. Schropp, E., Naumann, G. & Gaderer, M., Life cycle assessment of a polymer electrolyte membrane water electrolysis. Sustainable Production, Life Cycle Engineering and Management (Springer International Publishing, 2021). doi:10.1007/978-3-030-50519-6_5.

5. Simons, A. & Bauer, C., Life cycle assessment of hydrogen production. Transition to Hydrogen: Pathways Toward Clean Transportation, Cambridge University Press (2011). doi:10.1017/CBO9781139018036.006.

6. Bhandari, R., Trudewind, C. A. & Zapp, P., Life cycle assessment of hydrogen production via electrolysis - A review. *J. Clean. Prod.* **85**, 151–163 (2014). http://dx.doi.org/10.1016/j.jclepro.2013.07.048.

7. Yadav, P., Ismail, N., Essalhi, M., Tysklind, M., Athanassiadis, D., & Tavajohi, N., Assessment of the environmental impact of polymeric membrane production. *J. Memb. Sci.* **622**, 118987 (2021). https://doi.org/10.1016/j.memsci.2020.118987.

8. Bareiß, K., de la Rua, C., Möckl, M. & Hamacher, T., Life cycle assessment of hydrogen from proton exchange membrane water electrolysis in future energy systems. *Appl. Energy* **237**, 862–872 (2019). https://doi.org/10.1016/j.apenergy.2019.01.001.

9. Monticelli, C. & Zanelli, A., Life Cycle Design and Efficiency Principles for Membrane Architecture: Towards a New Set of Eco-design Strategies. *Procedia Eng.* **155**, 416–425 (2016). http://dx.doi.org/10.1016/j.proeng.2016.08.045.

10. Prapainainar, P., Boonrod, B., Phetarporn, V., Saibautrong, W., Juntarungsee, S.,

Tiavirat, K., & Mungcharoen, T., Evaluating the environmental impacts of graft copolymer prepared by conventional emulsion polymerization, electron beam irradiation, and gamma ray irradiation through life cycle assessment. *J. Clean. Prod.* **167**, 1038–1047 (2017). http://dx.doi.org/10.1016/j.jclepro.2016.10.048.

11. Standard, I. INTERNATIONAL STANDARD Environmental management — Life cycle. **2006**, (2014).

12. The International Standards Organisation. INTERNATIONAL STANDARD assessment — Requirements and guilelines. *Int. J. Life Cycle Assess.* **2006**, 652–668 (2006).

13. Gillet, J.-P., Guerret, O. & Tordo, P., Method for preparing B phosphorous nitroxide radicals - US 6,624,322 B1. (2003).

14. Goedkoop, M., Heijungs, R., Huijbregts, M., De Schryver, A., Struijs, J., & Van Zelm, R., ReCiPe 2008, first ed., *Potentials* 1–44 (2009). http://www.pre-sustainability.com/download/misc/ReCiPe_main_report_final_27-02-2009_web.pdf.

15. Scientific, T. F. Safety Data Sheet - 2,3,4,5,6-Pentafluorostyrene. *Mater. Saf. Data Sheet* **4(2)**, 8–10 (2012).

16. Number, P. & Chesnes, L. I. D. A., Acryloyl Chloride. *Hawley's Condens. Chem. Dict.* 1–11 (2007) doi:10.1002/9780470114735.hawley00224.

17. Number, P. & Chesnes, L. I. D. A., Dichloromethane. (2021).

18. Cardoso, V. F., Correia, D. M., Ribeiro, C., Fernandes, M. M. & Lanceros-Méndez, S., Fluorinated polymers as smart materials for advanced biomedical applications. *Polymers (Basel).* **10**, 1–26 (2018). https://doi.org/10.3390/polym10020161.
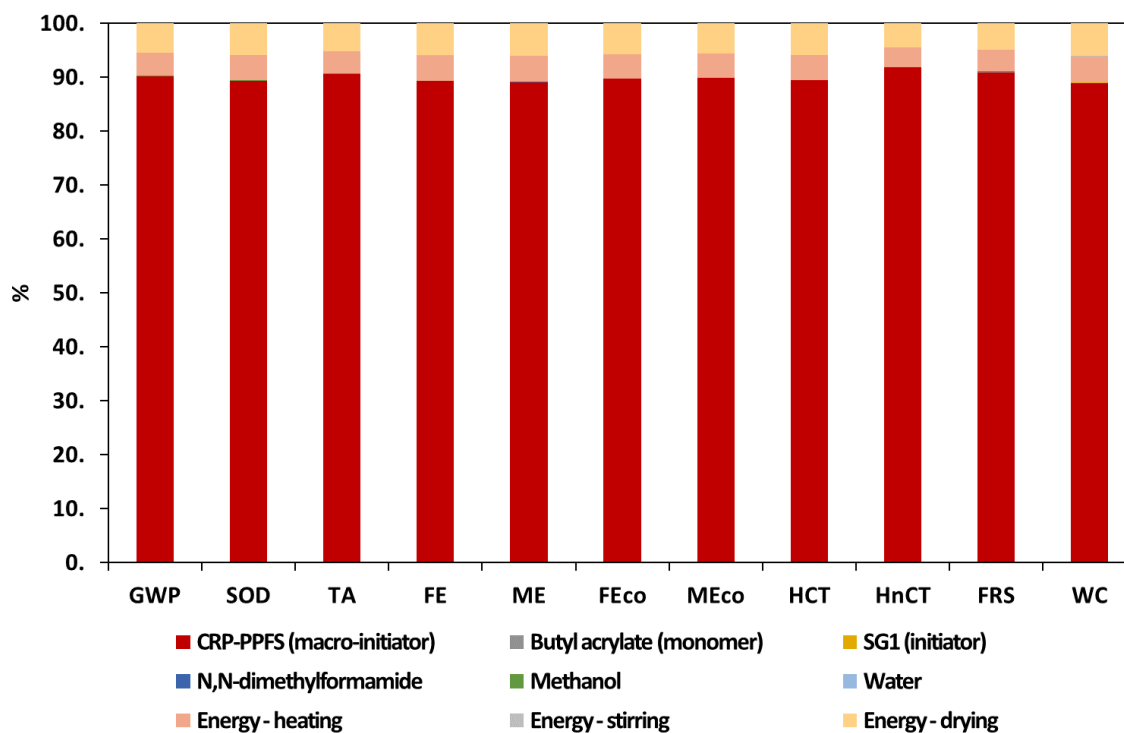
8. Appendix

Appendix 1. Impact analysis of the synthesis of 1g of CRP-PPFS-*b*-PBuA.
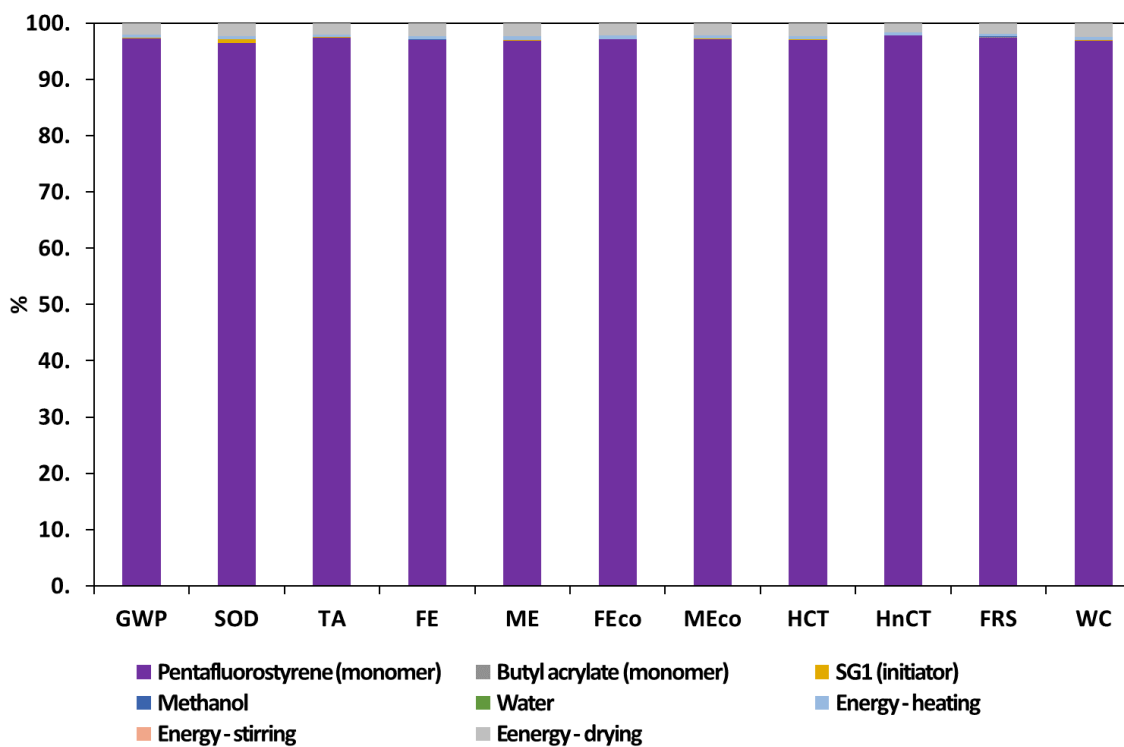
Appendix 2. Impact analysis of the synthesis of 1g of CRP-PPFS-*stat*-PBuA.
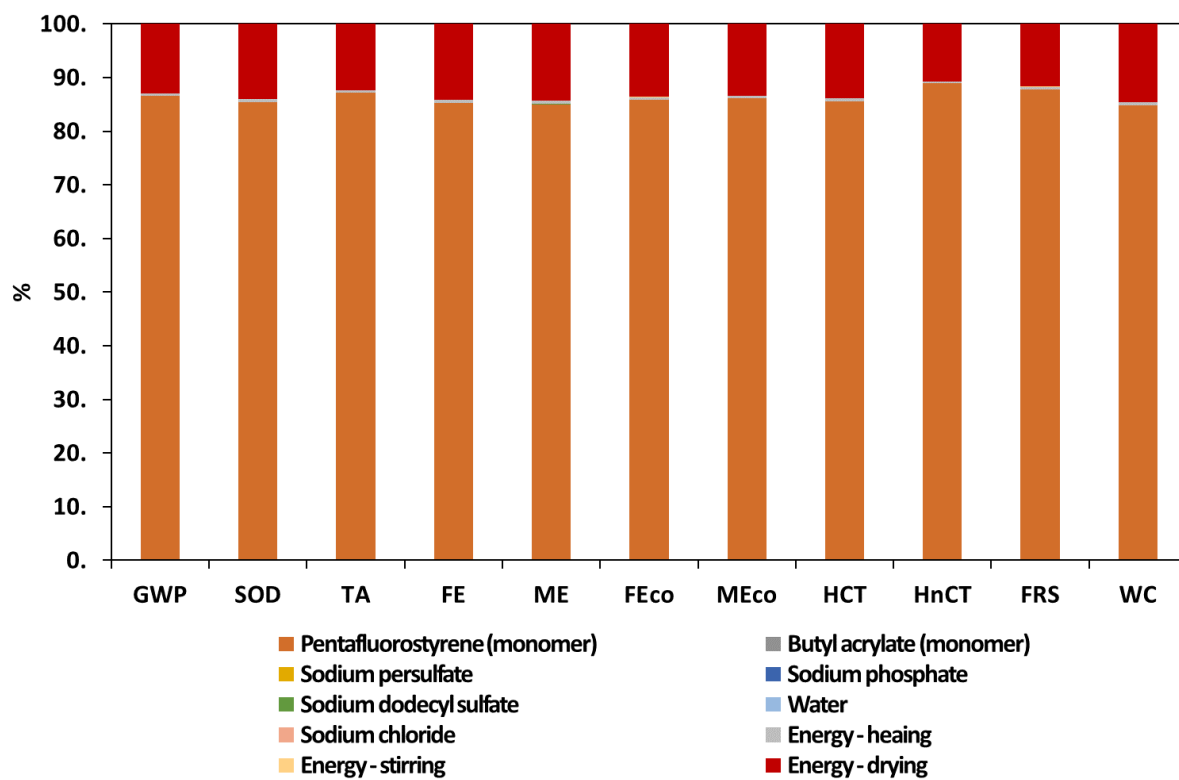
Appendix 3. Impact analysis of the synthesis of 1g of FRP-PPFS-*stat*-PBuA.

Appendix 4. Values of impact categories for the synthesis of 1 g of CRP-PPFS.

Impact category	Unit	Total	Pentafluorostyrene (monomer)	SG1 (initiator)	Methanol	Energy (heating)	Energy (stirring)	Energy (drying)
GWP	kg CO_2 eq	69.71	66.20	2.51E-02	2.74E-02	5.25E-01	7.09E-03	2.93
SOD	kg CFC-11 eq	3.08E-05	2.91E-05	8.15E-08	1.42E-08	2.54E-07	3.43E-09	1.42E-06
TA	kg SO_2 eq	3.32E-01	3.17E-01	1.12E-04	6.40E-05	2.38E-03	3.22E-05	1.33E-02
FE	kg P eq	6.11E-02	5.77E-02	1.89E-05	4.65E-06	5.09E-04	6.88E-06	2.84E-03
ME	kg N eq	4.21E-03	3.97E-03	2.56E-06	2.48E-07	3.56E-05	4.81E-07	1.98E-04
FEco	kg 1,4-DCB	5.29	5.01	1.56E-03	5.56E-04	4.23E-02	5.72E-04	2.36E-01
MEco	kg 1,4-DCB	6.92	6.56	1.98E-03	8.01E-04	5.41E-02	7.32E-04	3.02E-01
HCT	kg 1,4-DCB	3.91	3.70	1.35E-03	4.17E-04	3.19E-02	4.32E-04	1.78E-01
HnCT	kg 1,4-DCB	85.47	81.97	2.36E-02	1.78E-02	5.25E-01	7.09E-03	2.93
FRS	kg oil eq	19.29	18.39	6.17E-03	3.01E-02	1.30E-01	1.76E-03	7.27E-01
WC	m^3	9.60E-01	9.05E-01	3.71E-04	1.75E-04	8.27E-03	1.12E-04	4.61E-02

Appendix 5. Values of impact categories for the synthesis of 1 g of FRP-PPFS.

Impact category	Unit	Total	Pentafluorostyrene (monomer)	Sodium persulfate	Sodium dodecyl sulfate	Water	Sodium phosphate	Sodium chloride	Energy (heating)	Energy (stirring)	Energy (drying)
GWP	kg CO_2 eq	70.75	66.20	6.53E-06	8.62E-03	9.92E-06	1.55E-05	5.56E-04	4.12E-01	1.13E-02	4.11
SOD	kg CFC-11 eq	3.13E-05	2.91E-05	3.59E-12	1.32E-08	8.07E-12	4.00E-12	2.47E-10	1.99E-07	5.49E-09	1.99E-06
TA	kg SO_2 eq	3.37E-01	3.17E-01	4.16E-08	3.69E-05	4.44E-08	1.09E-07	2.96E-06	1.87E-03	5.15E-05	1.87E-02
FE	kg P eq	6.21E-02	5.77E-02	3.39E-09	2.40E-06	7.24E-09	1.22E-08	5.83E-07	4.00E-04	1.10E-05	3.99E-03
ME	kg N eq	4.28E-03	3.97E-03	2.73E-10	5.69E-06	5.60E-10	4.13E-10	1.20E-07	2.79E-05	7.69E-07	2.79E-04
FEco	kg 1,4-DCB	5.38	5.01	3.51E-07	3.09E-04	3.88E-07	9.99E-07	5.81E-05	3.32E-02	9.15E-04	3.32E-01
MEco	kg 1,4-DCB	7.03	6.56	4.98E-07	3.44E-04	5.43E-07	1.46E-06	8.29E-05	4.25E-02	1.17E-03	4.24E-01
HCT	kg 1,4-DCB	3.98	3.70	4.50E-07	2.64E-04	1.60E-06	5.59E-06	5.56E-05	2.51E-02	6.91E-04	2.50E-01
HnCT	kg 1,4-DCB	86.52	81.97	1.11E-05	7.57E-03	1.01E-05	2.65E-05	1.95E-03	4.12E-01	1.13E-02	4.11
FRS	kg oil eq	19.52	18.39	2.08E-06	3.45E-03	2.56E-06	3.61E-06	1.25E-04	1.02E-01	2.82E-03	1.02
WC	m^3	0.98	9.05E-01	2.37E-07	3.91E-04	1.04E-05	8.42E-07	1.32E-05	6.49E-03	1.79E-04	6.48E-02

Appendix 6. Values of impact categories for the synthesis of 1 g of CRP-PPFS-*b*-PBuA.

Impact category	Unit	Total	CRP-PPFS (macro-initiator)	Butyl acrylate (monomer)	SG1 (initiator)	N,N-dimethylfor mamide	Methanol	Water	Energy (heating)	Energy (stirring)	Energy (drying)
GWP	kg CO$_2$ eq	54.12	48.80	1.42E-02	3.58E-03	3.28E-03	2.74E-02	9.92E-06	2.32	3.12E-02	2.93
SOD	kg CFC-11 eq	2.42E-05	2.16E-05	3.04E-09	1.16E-08	1.55E-09	1.42E-08	8.07E-12	1.12E-06	1.51E-08	1.42E-06
TA	kg SO$_2$ eq	2.57E-01	2.33E-01	4.95E-05	1.60E-05	1.25E-05	6.40E-05	4.44E-08	1.05E-02	1.42E-04	1.33E-02
FE	kg P eq	4.79E-02	4.28E-02	2.99E-06	2.70E-06	1.19E-06	4.65E-06	7.24E-09	2.25E-03	3.03E-05	2.84E-03
ME	kg N eq	3.31E-03	2.94E-03	1.87E-07	3.65E-07	3.82E-06	2.48E-07	5.60E-10	1.57E-04	2.12E-06	1.98E-04
FEco	kg 1,4-DCB	4.13	3.71	2.25E-04	2.23E-04	9.86E-05	5.56E-04	3.88E-07	1.87E-01	2.52E-03	2.36E-01
MEco	kg 1,4-DCB	5.39	4.84	3.24E-04	2.83E-04	1.37E-04	8.01E-04	5.43E-07	2.39E-01	3.22E-03	3.02E-01
HCT	kg 1,4-DCB	3.06	2.74	3.22E-04	1.93E-04	1.03E-04	4.17E-04	1.60E-06	1.41E-01	1.90E-03	1.78E-01
HnCT	kg 1,4-DCB	65.13	59.83	7.11E-03	3.38E-03	2.94E-03	1.78E-02	1.01E-05	2.32	3.12E-02	2.93
FRS	kg oil eq	14.85	13.50	6.58E-03	8.81E-04	1.98E-03	3.01E-02	2.56E-06	5.76E-01	7.75E-03	7.27E-01
WC	m^3	7.56E-01	6.72E-01	5.39E-04	5.30E-05	5.22E-05	1.75E-04	1.04E-05	3.65E-02	4.92E-04	4.61E-02

Appendix 7. Values of impact categories for the synthesis of 1 g of CRP-PPFS-*stat*-PBuA.

Impact category	Unit	Total	Pentafluorostyrene	Butyl acrylate	SG1	Methanol	Water	Energy (heating)	Energy (stirring)	Energy (drying)
GWP	kg CO_2 eq	138.55	134.72	2.76E-03	1.29E-01	2.74E-02	9.92E-06	7.37E-01	9.92E-03	2.93
SOD	kg CFC-11 eq	6.13E-05	5.91E-05	5.92E-10	4.19E-07	1.42E-08	8.07E-12	3.57E-07	4.81E-09	1.42E-06
TA	kg SO_2 eq	6.61E-01	6.44E-01	9.64E-06	5.76E-04	6.40E-05	4.44E-08	3.35E-03	4.50E-05	1.33E-02
FE	kg P eq	1.21E-01	1.18E-01	5.82E-07	9.71E-05	4.65E-06	7.24E-09	7.16E-04	9.64E-06	2.84E-03
ME	kg N eq	8.34E-03	8.08E-03	3.64E-08	1.32E-05	2.48E-07	5.60E-10	5.00E-05	6.73E-07	1.98E-04
FEco	kg 1,4-DCB	10.51	10.20	4.39E-05	8.01E-03	5.56E-04	3.88E-07	5.95E-02	8.00E-04	2.36E-01
MEco	kg 1,4-DCB	13.73	13.34	6.32E-05	1.02E-02	8.01E-04	5.43E-07	7.61E-02	1.02E-03	3.02E-01
HCT	kg 1,4-DCB	7.76	7.53	6.26E-05	6.93E-03	4.17E-04	1.60E-06	4.49E-02	6.04E-04	1.78E-01
HnCT	kg 1,4-DCB	170.63	166.81	1.38E-03	1.22E-01	1.78E-02	1.01E-05	7.37E-01	9.93E-03	2.93
FRS	kg oil eq	38.40	37.43	1.28E-03	3.17E-02	3.01E-02	2.56E-06	1.83E-01	2.47E-03	7.27E-01
WC	m^3	1.90	1.84	1.05E-04	1.91E-03	1.75E-04	1.04E-05	1.16E-02	1.56E-04	4.61E-02

Appendix 8. Values of impact categories for the synthesis of 1 g of FRP-PPFS-*stat*-PBuA.

Impact category	Unit	Total	Pentafluorostyrene	Butyl acrylate	Sodium persulfate	Sodium phosphate	Sodium Dodecyl sulfate	Water	Sodium chloride	Energy (heating)	Energy (stirring)	Energy (drying)
GWP	kg CO_2 eq	76.46	66.20	1.35E-03	1.50E-05	1.23E-05	5.69E-03	4.96E-05	9.27E-04	3.66E-01	1.84E-02	9.87
SOD	kg CFC-11 eq	3.40E-05	2.91E-05	2.91E-10	8.25E-12	3.19E-12	8.73E-09	4.04E-11	4.12E-10	1.77E-07	8.92E-09	4.78E-06
TA	kg SO_2 eq	3.63E-01	3.17E-01	4.73E-06	9.57E-08	8.68E-08	2.43E-05	2.22E-07	4.94E-06	1.66E-03	8.36E-05	4.48E-02
FE	kg P eq	6.77E-02	5.77E-02	2.86E-07	7.79E-09	9.71E-09	1.58E-06	3.62E-08	9.72E-07	3.55E-04	1.79E-05	9.58E-03
ME	kg N eq	4.67E-03	3.97E-03	1.79E-08	6.29E-10	3.28E-10	3.76E-06	2.80E-09	1.99E-07	2.48E-05	1.25E-06	6.69E-04
FEco	kg 1,4-DCB	5.84	5.01	2.15E-05	8.07E-07	7.98E-07	2.04E-04	1.94E-06	9.68E-05	2.95E-02	1.49E-03	7.96E-01
MEco	kg 1,4-DCB	7.62	6.56	3.10E-05	1.15E-06	1.17E-06	2.27E-04	2.72E-06	1.38E-04	3.77E-02	1.90E-03	1.02
HCT	kg 1,4-DCB	4.32	3.70	3.08E-05	1.04E-06	4.47E-06	1.74E-04	7.98E-06	9.27E-05	2.23E-02	1.12E-03	6.01E-01
HnCT	kg 1,4-DCB	92.24	81.97	6.80E-04	2.55E-05	2.12E-05	4.99E-03	5.07E-05	3.25E-03	3.66E-01	1.84E-02	9.87
FRS	kg oil eq	20.94	18.39	6.29E-04	4.79E-06	2.88E-06	2.27E-03	1.28E-05	2.08E-04	9.09E-02	4.58E-03	2.45
WC	m^3	1.07	9.05E-01	5.16E-05	5.46E-07	6.75E-07	2.58E-04	5.19E-05	2.20E-05	5.76E-03	2.90E-04	1.56E-01

Appendix 9. Values of impact categories for the synthesis of 1 g of CRP-PPFS-*stat*-PMA.

Impact category	Unit	Total	Pentafluorostyrene	Menthyl acrylate	SG1	N,N-dimethyl-formamide	Methanol	Water	Energy (heating)	Energy (stirring)	Energy (drying)
GWP	kg CO_2 eq	73.76	67.39	8.05E-01	6.44E-02	1.31E-03	1.37E-02	2.98E-06	2.52	3.40E-02	2.92
SOD	kg CFC-11 eq	3.99E-05	2.96E-05	7.46E-06	2.10E-07	6.21E-10	7.10E-09	2.42E-12	1.22E-06	1.65E-08	1.42E-06
TA	kg SO_2 eq	3.51E-01	3.22E-01	3.91E-03	2.88E-04	5.00E-06	3.20E-05	1.33E-08	1.15E-02	1.54E-04	1.33E-02
FE	kg P eq	6.48E-02	5.88E-02	6.03E-04	4.86E-05	4.77E-07	2.32E-06	2.17E-09	2.45E-03	3.30E-05	2.84E-03
ME	kg N eq	4.46E-03	4.04E-03	4.04E-05	6.58E-06	1.53E-06	1.24E-07	1.68E-10	1.71E-04	2.31E-06	1.98E-04
FEco	kg 1,4-DCB	5.61	5.10	5.97E-02	4.01E-03	3.95E-05	2.78E-04	1.16E-07	2.04E-01	2.74E-03	2.36E-01
MEco	kg 1,4-DCB	7.33	6.68	8.11E-02	5.09E-03	5.49E-05	4.01E-04	1.63E-07	2.61E-01	3.51E-03	3.02E-01
HCT	kg 1,4-DCB	4.16	3.77	5.50E-02	3.47E-03	4.12E-05	2.09E-04	4.79E-07	1.54E-01	2.07E-03	1.78E-01
HnCT	kg 1,4-DCB	90.41	83.45	1.41	6.08E-02	1.18E-03	8.91E-03	3.04E-06	2.52	3.40E-02	2.92
FRS	kg oil eq	20.30	18.72	1.86E-01	1.59E-02	7.93E-04	1.51E-02	7.67E-07	6.28E-01	8.46E-03	7.27E-01
WC	m^3	1.02	9.21E-01	1.12E-02	9.54E-04	2.09E-05	8.73E-05	3.11E-06	3.98E-02	5.36E-04	4.61E-02

Appendix 10. Values of impact categories for the synthesis of 1 g of sulfonated CRP-PPFS-*b*-PBuA.

Impact category	Unit	Total	CRP-PPFS-b-PBuA	Sodium 3-mercapto propane sulfonate	Triethyl amine	N,N-dimethylformamide	Water	Energy (stirring)	Energy (drying)
GWP	kg CO_2 eq	64.71	54.12	6.88E-01	1.23E-03	3.72E-03	2.98E-03	3.06E-02	9.87
SOD	kg CFC-11 eq	2.93E-05	2.42E-05	3.32E-07	1.97E-10	1.76E-09	2.42E-09	1.48E-08	4.78E-06
TA	kg SO_2 eq	3.05E-01	2.57E-01	3.13E-03	3.52E-06	1.42E-05	1.33E-05	1.39E-04	4.48E-02
FE	kg P eq	5.82E-02	4.79E-02	6.61E-04	4.45E-07	1.35E-06	2.17E-06	2.97E-05	9.58E-03
ME	kg N eq	4.03E-03	3.31E-03	4.61E-05	4.05E-07	4.33E-06	1.68E-07	2.08E-06	6.69E-04
FEco	kg 1,4-DCB	4.98	4.13	5.48E-02	2.28E-05	1.12E-04	1.16E-04	2.47E-03	7.96E-01
MEco	kg 1,4-DCB	6.48	5.39	7.02E-02	3.34E-05	1.56E-04	1.63E-04	3.16E-03	1.02
HCT	kg 1,4-DCB	3.70	3.06	4.15E-02	2.92E-05	1.17E-04	4.79E-04	1.86E-03	6.01E-01
HnCT	kg 1,4-DCB	75.73	65.13	6.84E-01	7.50E-04	3.33E-03	3.04E-03	3.06E-02	9.87
FRS	kg oil eq	17.49	14.85	1.74E-01	7.05E-04	2.25E-03	7.67E-04	7.61E-03	2.45
WC	m^3	9.26E-01	7.56E-01	1.10E-02	1.58E-05	5.91E-05	3.11E-03	4.83E-04	1.56E-01

Appendix 11. Values of impact categories for the synthesis of 1 g of sulfonated CRP-PPFS-*stat*-PBuA.

Impact category	Unit	Total	CRP-PPFS-stat-PBuA	Sodium 3-mercapto propane sulfonate	Triethyl amine	N,N-dimethylformamide	Water	Energy (stirring)	Energy (drying)
GWP	kg CO_2 eq	149.15	138.55	6.88E-01	1.23E-03	3.72E-03	2.98E-03	3.06E-02	9.87
SOD	kg CFC-11 eq	6.65E-05	6.13E-05	3.32E-07	1.97E-10	1.76E-09	2.42E-09	1.48E-08	4.78E-06
TA	kg SO_2 eq	7.10E-01	6.61E-01	3.13E-03	3.52E-06	1.42E-05	1.33E-05	1.39E-04	4.48E-02
FE	kg P eq	1.31E-01	1.21E-01	6.61E-04	4.45E-07	1.35E-06	2.17E-06	2.97E-05	9.58E-03
ME	kg N eq	9.06E-03	8.34E-03	4.61E-05	4.05E-07	4.33E-06	1.68E-07	2.08E-06	6.69E-04
FEco	kg 1,4-DCB	11.36	10.51	5.48E-02	2.28E-05	1.12E-04	1.16E-04	2.47E-03	7.96E-01
MEco	kg 1,4-DCB	14.83	13.73	7.02E-02	3.34E-05	1.56E-04	1.63E-04	3.16E-03	1.02
HCT	kg 1,4-DCB	8.40	7.76	4.15E-02	2.92E-05	1.17E-04	4.79E-04	1.86E-03	6.01E-01
HnCT	kg 1,4-DCB	181.22	170.63	6.84E-01	7.50E-04	3.33E-03	3.04E-03	3.06E-02	9.87
FRS	kg oil eq	41.04	38.40	1.74E-01	7.05E-04	2.25E-03	7.67E-04	7.61E-03	2.45
WC	m^3	2.07	1.90	1.10E-02	1.58E-05	5.91E-05	3.11E-03	4.83E-04	1.56E-01

Appendix 12. Values of impact categories for the synthesis of 1 g of sulfonated FRP-PPFS-*stat*-PBuA.

Impact category	Unit	Total	FRP-PPFS-stat-PBuA	Sodium 3-mercapto propane sulfonate	Triethyl amine	N,N-dimethylformamide	Water	Energy (stirring)	Energy (drying)
GWP	kg CO_2 eq	87.54	76.46	1.16	2.07E-03	3.72E-03	2.98E-03	3.06E-02	9.87
SOD	kg CFC-11 eq	3.94E-05	3.40E-05	5.62E-07	3.33E-10	1.76E-09	2.42E-09	1.48E-08	4.78E-06
TA	kg SO_2 eq	4.13E-01	3.63E-01	5.29E-03	5.95E-06	1.42E-05	1.33E-05	1.39E-04	4.48E-02
FE	kg P eq	7.84E-02	6.77E-02	1.12E-03	7.52E-07	1.35E-06	2.17E-06	2.97E-05	9.58E-03
ME	kg N eq	5.42E-03	4.67E-03	7.82E-05	6.85E-07	4.33E-06	1.68E-07	2.08E-06	6.69E-04
FEco	kg 1,4-DCB	6.73	5.84	9.29E-02	3.86E-05	1.12E-04	1.16E-04	2.47E-03	7.96E-01
MEco	kg 1,4-DCB	8.76	7.62	1.19E-01	5.64E-05	1.56E-04	1.63E-04	3.16E-03	1.02
HCT	kg 1,4-DCB	5.00	4.32	7.04E-02	4.94E-05	1.17E-04	4.79E-04	1.86E-03	6.01E-01
HnCT	kg 1,4-DCB	103.30	92.24	1.16	1.27E-03	3.33E-03	3.04E-03	3.06E-02	9.87
FRS	kg oil eq	23.70	20.94	2.94E-01	1.19E-03	2.25E-03	7.67E-04	7.61E-03	2.45
WC	m^3	1.24	1.07	1.86E-02	2.67E-05	5.91E-05	3.11E-03	4.83E-04	1.56E-01

Appendix 13. Values of impact categories for the synthesis of 1 g of sulfonated CRP-PPFS-*stat*-PMA.

Impact category	Unit	Total	CRP-PPFS-stat-PMA	N,N-dimethylformamide	Triethyl amine	Sodium 3-mercapto propane sulfonate	Water	Energy (stirring)	Energy (drying)
GWP	kg CO$_2$ eq	84.83	73.76	3.72E-03	2.07E-03	1.16	2.98E-03	3.06E-02	9.87
SOD	kg CFC-11 eq	4.53E-05	3.99E-05	1.76E-09	3.33E-10	5.62E-07	2.42E-09	1.48E-08	4.78E-06
TA	kg SO$_2$ eq	4.02E-01	3.51E-01	1.42E-05	5.95E-06	5.29E-03	1.33E-05	1.39E-04	4.48E-02
FE	kg P eq	7.55E-02	6.48E-02	1.35E-06	7.52E-07	1.12E-03	2.17E-06	2.97E-05	9.58E-03
ME	kg N eq	5.22E-03	4.46E-03	4.33E-06	6.85E-07	7.82E-05	1.68E-07	2.08E-06	6.69E-04
FEco	kg 1,4-DCB	6.50	5.61	1.12E-04	3.86E-05	9.29E-02	1.16E-04	2.47E-03	7.96E-01
MEco	kg 1,4-DCB	8.47	7.33	1.56E-04	5.64E-05	1.19E-01	1.63E-04	3.16E-03	1.02
HCT	kg 1,4-DCB	4.83	4.16	1.17E-04	4.94E-05	7.04E-02	4.79E-04	1.86E-03	6.01E-01
HnCT	kg 1,4-DCB	101.48	90.41	3.33E-03	1.27E-03	1.16	3.04E-03	3.06E-02	9.87
FRS	kg oil eq	23.06	20.30	2.25E-03	1.19E-03	2.94E-01	7.67E-04	7.61E-03	2.45
WC	m^3	1.20	1.02	5.91E-05	2.67E-05	1.86E-02	3.11E-03	4.83E-04	1.56E-01

Appendix 14. Values of impact categories of a sulfonated CRP-PPFS-*b*-PBuA membrane.

Impact category	Unit	Total	sulfonated CRP-PPFS-b-PBuA	Polybenzimidazole (PBI)	Dimethyl sulfoxide	Hydrochloric acid	Water	Energy (stirring)	Energy (drying)
GWP	kg CO_2 eq	78.70	64.71	7.80E-01	1.45E-02	1.18E-03	1.98E-05	3.40E-02	13.16
SOD	kg CFC-11 eq	3.61E-05	2.93E-05	4.05E-07	6.69E-09	7.44E-10	1.61E-11	1.65E-08	6.37E-06
TA	kg SO_2 eq	3.68E-01	3.05E-01	3.53E-03	4.79E-05	3.97E-06	8.87E-08	1.54E-04	5.97E-02
FE	kg P eq	7.18E-02	5.82E-02	7.51E-04	4.90E-06	5.30E-07	1.45E-08	3.30E-05	1.28E-02
ME	kg N eq	4.98E-03	4.03E-03	5.96E-05	3.08E-07	4.64E-08	1.12E-09	2.31E-06	8.92E-04
FEco	kg 1,4-DCB	6.11	4.98	6.24E-02	4.67E-04	3.45E-05	7.77E-07	2.74E-03	1.06
MEco	kg 1,4-DCB	7.92	6.48	7.98E-02	6.71E-04	4.86E-05	1.09E-06	3.51E-03	1.36
HCT	kg 1,4-DCB	4.56	3.70	4.72E-02	4.63E-04	4.54E-05	3.19E-06	2.07E-03	8.01E-01
HnCT	kg 1,4-DCB	89.71	75.73	7.78E-01	1.49E-02	1.03E-03	2.03E-05	3.40E-02	13.16
FRS	kg oil eq	20.98	17.49	1.97E-01	1.23E-02	6.51E-04	5.11E-06	8.46E-03	3.27
WC	m^3	1.15	9.26E-01	1.23E-02	2.71E-04	2.40E-05	2.07E-05	5.36E-04	2.07E-01

Appendix 15. Values of impact categories of a sulfonated CRP-PPFS-*stat*-PBuA membrane.

Impact category	Unit	Total	sulfonated CRP-PPFS-stat-PBuA	Polybenzimidazole (PBI)	Dimethyl sulfoxide	Hydrochloric acid	Water	Energy (stirring)	Energy (drying)
GWP	kg CO$_2$ eq	163.14	149.15	7.80E-01	1.45E-02	1.18E-03	1.98E-05	3.40E-02	13.16
SOD	kg CFC-11 eq	7.33E-05	6.65E-05	4.05E-07	6.69E-09	7.44E-10	1.61E-11	1.65E-08	6.37E-06
TA	kg SO$_2$ eq	7.73E-01	7.10E-01	3.53E-03	4.79E-05	3.97E-06	8.87E-08	1.54E-04	5.97E-02
FE	kg P eq	1.45E-01	1.31E-01	7.51E-04	4.90E-06	5.30E-07	1.45E-08	3.30E-05	1.28E-02
ME	kg N eq	1.00E-02	9.06E-03	5.96E-05	3.08E-07	4.64E-08	1.12E-09	2.31E-06	8.92E-04
FEco	kg 1,4-DCB	12.49	11.36	6.24E-02	4.67E-04	3.45E-05	7.77E-07	2.74E-03	1.06
MEco	kg 1,4-DCB	16.27	14.83	7.98E-02	6.71E-04	4.86E-05	1.09E-06	3.51E-03	1.36
HCT	kg 1,4-DCB	9.25	8.40	4.72E-02	4.63E-04	4.54E-05	3.19E-06	2.07E-03	8.01E-01
HnCT	kg 1,4-DCB	195.21	181.22	7.78E-01	1.49E-02	1.03E-03	2.03E-05	3.40E-02	13.16
FRS	kg oil eq	44.53	41.04	1.97E-01	1.23E-02	6.51E-04	5.11E-06	8.46E-03	3.27
WC	m^3	2.29	2.07	1.23E-02	2.71E-04	2.40E-05	2.07E-05	5.36E-04	2.07E-01

Appendix 16. Values of impact categories of a sulfonated FRP-PPFS-*stat*-PBuA membrane.

Impact category	Unit	Total	sulfonated FRP-PPFS-stat-PBuA	Polybenzimidazole (PBI)	Dimethyl sulfoxide	Hydrochloric acid	Water	Energy (stirring)	Energy (drying)
GWP	kg CO_2 eq	100.90	87.54	1.56E-01	1.45E-02	1.21E-03	1.98E-05	3.40E-02	13.16
SOD	kg CFC-11 eq	4.59E-05	3.94E-05	8.10E-08	6.69E-09	7.68E-10	1.61E-11	1.65E-08	6.37E-06
TA	kg SO_2 eq	4.74E-01	4.13E-01	7.07E-04	4.79E-05	4.10E-06	8.87E-08	1.54E-04	5.97E-02
FE	kg P eq	9.14E-02	7.84E-02	1.50E-04	4.90E-06	5.47E-07	1.45E-08	3.30E-05	1.28E-02
ME	kg N eq	6.33E-03	5.42E-03	1.19E-05	3.08E-07	4.79E-08	1.12E-09	2.31E-06	8.92E-04
FEco	kg 1,4-DCB	7.81	6.73	1.25E-02	4.67E-04	3.56E-05	7.77E-07	2.74E-03	1.06
MEco	kg 1,4-DCB	10.13	8.76	1.60E-02	6.71E-04	5.02E-05	1.09E-06	3.51E-03	1.36
HCT	kg 1,4-DCB	5.81	5.00	9.44E-03	4.63E-04	4.69E-05	3.19E-06	2.07E-03	8.01E-01
HnCT	kg 1,4-DCB	116.67	103.30	1.56E-01	1.49E-02	1.07E-03	2.03E-05	3.40E-02	13.16
FRS	kg oil eq	27.03	23.70	3.94E-02	1.23E-02	6.72E-04	5.11E-06	8.46E-03	3.27
WC	m^3	1.45	1.24	2.46E-03	2.71E-04	2.48E-05	2.07E-05	5.36E-04	2.07E-01

Appendix 17. Values of impact categories of a sulfonated CRP-PPFS-*stat*-PMA membrane.

Impact category	Unit	Total	sulfonated CRP-PPFS-stat-PMA	Polybenzimidazole (PBI)	Dimethyl sulfoxide	Hydrochloric acid	Water	Energy (stirring)	Energy (drying)
GWP	kg CO$_2$ eq	98.82	84.83	7.80E-01	1.45E-02	1.18E-03	1.98E-05	3.40E-02	13.16
SOD	kg CFC-11 eq	5.21E-05	4.53E-05	4.05E-07	6.69E-09	7.44E-10	1.61E-11	1.65E-08	6.37E-06
TA	kg SO$_2$ eq	4.65E-01	4.02E-01	3.53E-03	4.79E-05	3.97E-06	8.87E-08	1.54E-04	5.97E-02
FE	kg P eq	8.91E-02	7.55E-02	7.51E-04	4.90E-06	5.30E-07	1.45E-08	3.30E-05	1.28E-02
ME	kg N eq	6.17E-03	5.22E-03	5.96E-05	3.08E-07	4.64E-08	1.12E-09	2.31E-06	8.92E-04
FEco	kg 1,4-DCB	7.63	6.50	6.24E-02	4.67E-04	3.45E-05	7.77E-07	2.74E-03	1.06
MEco	kg 1,4-DCB	9.91	8.47	7.98E-02	6.71E-04	4.86E-05	1.09E-06	3.51E-03	1.36
HCT	kg 1,4-DCB	5.68	4.83	4.72E-02	4.63E-04	4.54E-05	3.19E-06	2.07E-03	8.01E-01
HnCT	kg 1,4-DCB	115.46	101.48	7.78E-01	1.49E-02	1.03E-03	2.03E-05	3.40E-02	13.16
FRS	kg oil eq	26.55	23.06	1.97E-01	1.23E-02	6.51E-04	5.11E-06	8.46E-03	3.27
WC	m^3	1.42	1.20	1.23E-02	2.71E-04	2.40E-05	2.07E-05	5.36E-04	2.07E-01

Chapter 6. Final discussion of results and outlook

Table of contents Chapter 6

For the eSCALED project PEMWE, the choice was made on perfluorinated membranes[1] due to the proven excellent properties of fluorinated compounds. If the good conductivity of Nafion® (order of the 100 mS/cm) has been attributed to the organisation of the membrane into connected hydrophilic clusters for the conductivities, and PTFE hydrophobic moieties for its mechanical properties, the conductivity is also strongly dependent on the water dynamics in the membrane. Indeed, the level of hydration has a strong impact on the conductivity and mechanical properties of the membrane.[2, 3]

Having all this gathered information, the aim of the work was to manufacture sulfonated membranes that perform well in terms of conductivity as well as mechanical stability with improved synthesis processes. For these reasons, to structure the material differently than Nafion®, the self-assembly of functional diblock copolymers BCP was the aim of the scientific approach. Indeed, it would be of interest to tune the Nafion® paradigm for the conductivity properties of the membrane and water transportation. In fact, due to their self-assembly capability, BCPs are well-structured materials at the nanometer scale. They allow for the tailoring of domains segregation to the desired applications.[4]

Then we focused on the use of the flexible butyl acrylate (BuA) for the mechanical property and the 2,3,4,5,6-pentafluorostyrene (PFS), which has demonstrated to be full of potential for membranes application. It's sulfonation[5], phosphonation[6, 7], and grafting[8] have been studied for this purpose. Recent studies conducted by Atanasov *et al*. have shown an excellent membrane performance of partially phosphonated PPFS for fuel cell application as the membrane did not display any acid loss and showed to be durable at temperatures up to 200°C.[9] However, poly(pentafluorostyrene) (PPFS) membranes can be brittle due to their high glass transition temperature of 100°C.

1. Synthesis of poly(pentafluorostyrene)/poly(butyl acrylate) copolymers

1.1. Synthesis of poly(pentafluorostyrene)-*b*-poly(butyl acrylate), PPFS-*b*-PBuA

The first part of the work was devoted to the synthesis of PPFS-*b*-PBuA diblock-copolymers (BCPs) and their self-assembly (Chapter 3). BCPs were successfully synthesized

by NMP controlled radical polymerization, with PPFS used as a macroinitiator for the chain extension with butyl acrylate BuA. Compared to the other controlled radical polymerization techniques (ATRP and RAFT), NMP uses a single alkoxyamine that separates into a radical (initiator) and a nitroxide counter-radical (controlling agent) upon heat. Moreover, NMP can be used for a large variety of monomer and no reagent removal is needed (Chapter 1, section 2.3.).[10] In the literature, among the 75 documents referring to the search of PFS and the listed above controlled polymerization techniques (NMP, RAFT, and ATRP), 52% are related to the polymerization of PFS by ATRP, 37% for the RAFT technique and only 11% for the NMP. There is hence an interest in the development of the NMP synthesis technique for PFS (Scopus research made on the 25th of March 2022). The determination of the monomer's conversions and polymer's compositions was performed by ^{1}H NMR. Six BCPs with different molar compositions were synthesized.

On the ^{1}H NMR spectrum of the BCPs, the chemical shift of the polymer backbone is located between 1.8 and 2.9 ppm, protons of PBuA side chains are located at 4 ppm for -OCH$_2$, and between 0.9 and 1.8 ppm for the -CH$_3$ and -CH$_2$ protons. With this allocation settled, the composition of each block was determined by integral calculations (Chapter 3, Equation SI 1). BCP with PPFS molar compositions of 16, 33, 50, 54, 86 and 90% were synthesized. A single diffusion coefficient for the BCP was obtained by DOSY NMR. This means that the sample is pure and that the only specie in the media is the BCP (Chapter 3, Figure SI 3).

The dispersity values $Đ$ of the BCPs obtained by SEC ranged from 1.09 to 1.88 are for the most part in accordance with the literature.[11] Ideally in controlled radical polymerization, the low dispersity values ($Đ$ < 1.5) are due to the constant concentration of active sites throughout time and the linear increase of the degree of polymerization with the conversion. The highest $Đ$ value at 1.88 could be attributed to the high conversion of the macroinitiator (conversion of 85%) making the termination step of the polymerization non-reversible and giving polydisperse molar masses. The molar masses of the BCPs ranged from 17 400 to 40 100 g/mol. Two glass transition temperatures Tg, at -40°C and 100°C, for PBuA and PPFS respectively were noticeable on the BCP DSC thermogram. In fact, When BCPs are immiscible, they present the intrinsic properties of both isolated blocks. Nevertheless, for

the BCPs with higher compositions in PBuA, only a *Tg* at -40°C was observed due to the heat capacity Δ_{Cp} of PBuA that is 3.8 times higher than PPFS's.

Since PPFS and PBuA are chemically different and immiscible (solubility parameter δ of 16.1 Mpa$^{1/2}$ and 17.3 Mpa$^{1/2}$, respectively), they are potential candidates for nano-phase separation by self-assembly. In fact, the structure of the domains is dictated by the volume fraction Φ of the blocks in the BCP and their size by chains length N through the control of the molar mass, **Figure 1**.[12] The nano-phase separation of the BCPs was observed by AFM after spin coating of the polymer solutions and subsequent annealing. Their structure was determined by SAXS (Chapter 3, Figure 4). HCC and LAM morphologies were obtained having PPFS nanodomains in a BuA matrix, and vice versa, **Figure 1**. The sizes of the nanodomains ranges from 28 to 46 nm. This result represents the first systematic study of the PPFS-based diblock copolymers self-assembly.
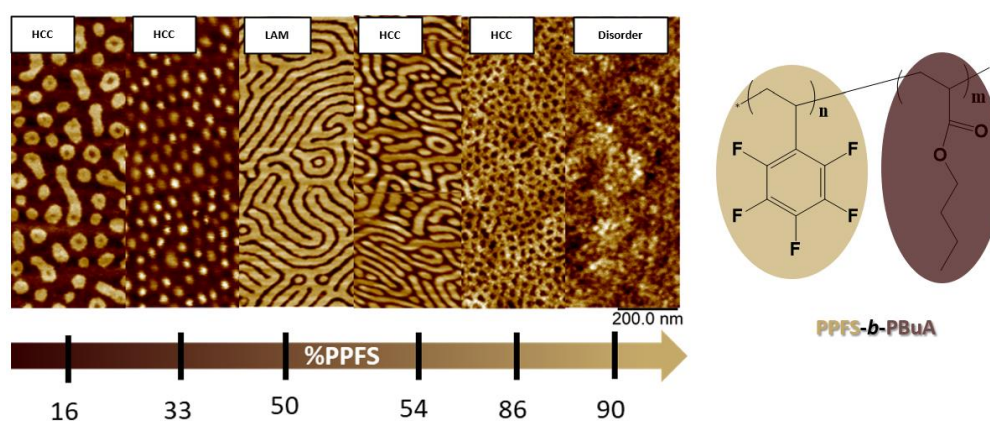
Figure 1. Self-assembly of PPFS-*b*-PBuA.

A study was conducted in parallel on the driven self-assembly of PPFS-*b*-PBuA. 10 wt% of PPFS homopolymer was added to the BCP blend (PPFS: MW= 12 500 g/mol, *Đ* = f 1.07, DPn = 130). By doing so, PPFS molar composition was increased, leading to an enrichment of the PPFS phase. Adding PPFS homopolymer to the blend shifted PPFS volume fraction higher in the BCP phase diagram. That shift influenced the self-assembly and nano-pattern of the material as the morphology observed by AFM differed form the initial one. In the case of BCP1 (PPFS$_{0.16}$-*b*-PBuA$_{0.84}$)$_{31K}$, a better phase separation was obtained with a decrease in the pitch distance from 45 to 38 nm for BCP1' (PPFS$_{0.24}$-*b*-PBuA$_{0.76}$). In the case of BCP4 (PPFS$_{0.54}$-*b*-PBuA$_{0.46}$)$_{37K}$, the pitch distance remained of 45 nm and the change in

morphology of BCP4' (PPFS$_{0.59}$-*b*-PBuA$_{0.41}$) was attributed to either a shift in the configuration of the nanodomains (from *in-plane* to *out-of-plane*, or a shift from the HCC morphology to the HPL (hexagonally perforated lamellae) state (Chapter 3, Figure 5).

1.2. Synthesis of poly(pentafluorostyrene)-*stat*-poly(butyl acrylate), PPFS-*stat*-PBuA

Additionally, statistical copolymers of the PPFS/PBuA system were synthesized by NMP controlled radical polymerization and free radical polymerization (FRP) in emulsion. Both statistical copolymers were used as comparative materials to the previous BCP but also to "mimic" the NAFION microstructure which is a copolymer with neutral and sulfonated units in the main chain. In this sense the influence on the membrane properties was discussed with the structuration of the BCPs, and the synthesis technique (NMP or FRP). The chemical shifts of the backbone protons (-CH and -CH$_2$) are located between 1.8 and 2.9 ppm on the ^{1}H NMR spectrum. Protons of PBuA side chains (-CH$_3$ and -CH$_2$) are located between 1 and 1.8 ppm and -OCH$_2$ protons of the PBuA side chain are located at 4 ppm. The molar composition of each copolymer was determined using the same equation as for the BCPs (Chapter 3, Equation SI 1) and their dispersity and molar mass was determined by SEC.

(PPFS$_{0.87}$-*stat*-PBuA$_{0.13}$)$_{19K}$ synthesized by NMP gave a low dispersity value *Đ* of 1.16 and (PPFS$_{0.80}$-*stat*-PBuA$_{0.20}$)$_{140K}$ synthesized by FRP 15.2. Indeed, with the FRP, all the polymerization steps occur simultaneously resulting in the polymer having a lack of structure and a molar masse that is not controlled. A single *Tg* for each statistical copolymer was observed at 64 and 89°C respectively.

Along with the two statistical copolymers, the previously synthesized (PPFS$_{0.33}$-*b*-PBuA$_{0.67}$)$_{40K}$ BCP was chosen for the study as it presents out-of-the-plane cylinders of PPFS in a PBuA matrix (AFM & SAXS characterization). The idea behind this choice was that if the self-assembly is preserved after sulfonation, those nano-cylinders will allow the flow of water and protons directly from one end of the membrane to the other, enhancing the proton conductivity of the membrane (Chapter 1, section 2.5.).

2. Sulfonation of the copolymers and morphological study of the sulfonated BCP

The following step of the membrane manufacture consisted of the sulfonation of the polymer materials. The sulfonation of PPFS has been performed into a two-step process that included a thiolation step before the sulfonation. Usually with this technique, temperatures of 42°C and 50°C were applied for each step respectively. Moreover, additional purification and drying stages are needed at the thiolation step.[4] For the first time, the *para*-fluoro thiol nucleophilic substitution was performed as an easy mild and efficient organo-catalysed method to sulfonate the PPFS. That can be easily applied to PFS as the molecule presents an accessible fluorine in *para* position of its phenylene ring. This simplified greatly the sulfonation step.[13] Indeed, the commercially available Sodium 3-mercapto propane sulfonate (SMPS) was used as the sulfonic thiol compound in presence of DBU and in DMF. A full sulfonation of the polymers was achievable in just 3.5 hours at room temperature (Chapter 4, Figure 2). The sulfonation process can be easily tuned by adjusting the reactants from fully to partially sulfonated copolymers, modification monitored by ^{19}F NMR (Chapter 4, Table 2).

On the ^{19}F NMR spectra, non-modified polymers have 3 signals for the fluorine at each position of the aromatic ring: δ $2F_{ortho}$ -143 ppm; δ $2F_{meta}$ -161 ppm; δ $1F_{para}$ -154 ppm. After full modification, there was no more fluorine in *para* position, and the signal of fluorine in *meta* positions was up-field shifted due to the presence of the sulphur in *para* position (δ $2F_{ortho}$ = -141 ppm: δ $2F_{meta}$ = -134 ppm). The ^{19}F NMR spectra of the partially fluorinated copolymer showed the signals of all the fluorine of both the initial copolymer and the sulfonated one (**Figure 2**).
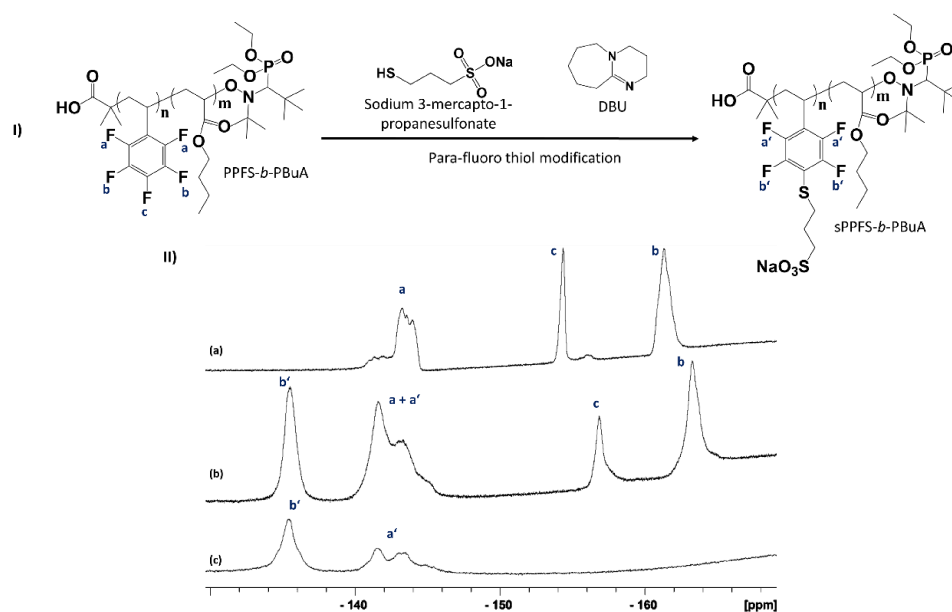
Figure 2. (I) Sulfonation reaction of PPFS-*b*-PBuA with SMPS. **(II)** ^{19}F NMR spectra of (a) (PPFS$_{0.33}$-*b*-PBuA$_{0.67}$)$_{40K}$ in CDCl$_3$, (b) Partially sulfonated (PPFS$_{0.33}$-*b*-PBuA$_{0.67}$)$_{40K}$ in DMSO-d$_6$, DS = 68% and (c) Fully sulfonated (PPFS$_{0.33}$-*b*-PBuA$_{0.67}$)$_{40K}$ in DMSO-d$_6$, DS = 100%. Figure 3 from Chapter 4.

The sulfonated copolymers were characterized by DSC. A decrease of *Tg* was observed and is due to the presence of the alkane chain of SMPS introducing some mobility and flexibility to the polymer. For the BCP the *Tg* of sPPFS block decreased from 104 to 60°C (Chapter 4, Figure 4), and from 64 to 32°C and 89 to 61°C for the statistical copolymers made by NMP and FRP respectively.

Self-assembly of the sulfonated (sPPFS$_{0.33}$-*b*-PBuA$_{0.67}$)$_{40K}$ BCP was successful with nanodomains size increased from the original BCP, from 45 to 100 nm, (**Figure 3**). This increase was attributed to the addition of the sulfonated compound, increasing the volume fraction of the block (M$_{PFS\ unit}$ = 194.1 g/mol; M$_{sPPFS\ unit}$ = 351.98 g/mol). With an HCC structuration, the membranes were organized into 100 nm wide *out-of-the-plane* cylinders efficient to attain the goal of having proton-conducting nano-channels across the membranes. Most of the work concerning block copolymers has been made with triblock or diblock copolymers. The diblock copolymers were usually made of a first block of sulfonated polystyrene and a second block of an alternating copolymer.[14, 15, 16] In these articles is also reported an increase in pitch of the nanodomains and in some cases a shift in morphology

after sulfonation of the copolymers following the BCP phase diagram. Lamellar morphologies were mostly studied. Similarly to our PPFS/PBuA system, sPS-*b*-PMMA diblock copolymer was reported in the literature, a series of morphologies were synthesized (HCC, HPL, LAM). For their system, an increase in conductivity was noticed when the degree of sulfonation was increase but also the volume fraction of the conductive domain.[9]
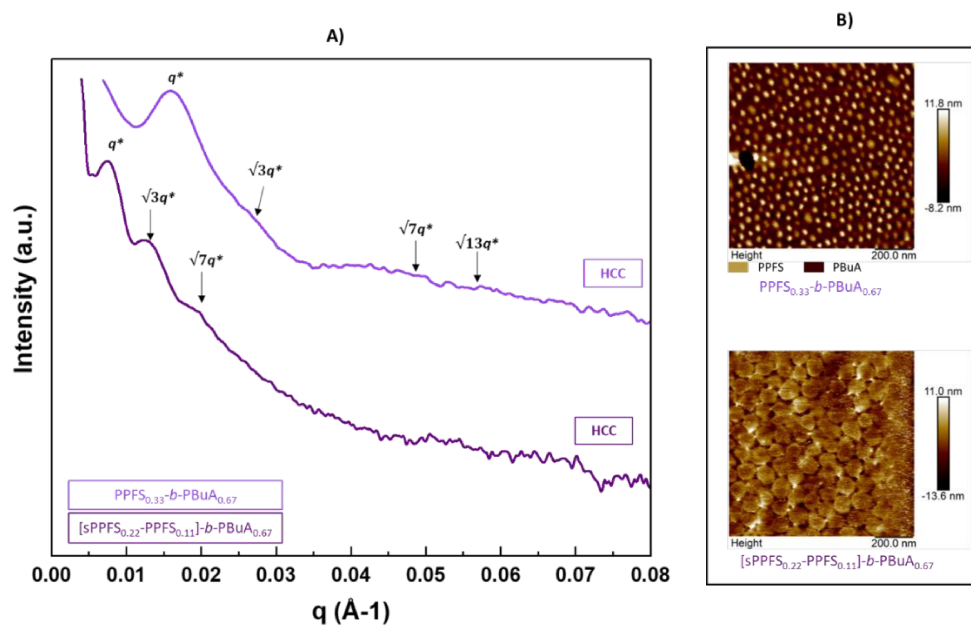
Figure 3. SAXS patterns of $(PPFS_{0.33}\text{-}b\text{-}PBuA_{0.67})_{40K}$ BCP before and after sulfonation (A); Peak Force mode AFM height images showing morphology transition before and after sulfonation of the BCP (B). Figure 1 from Chapter 4.

3. Membrane elaboration and properties

3.1. Membrane elaboration process

The membranes were prepared by dissolving the sulfonated copolymers in DMSO and subsequent oven drying (80°C for 2 hours and 120°C overnight). The challenge was the formulation of the membranes to obtain mechanically stable membranes with equivalent proton conductive properties as Nafion®. 10 wt% polymer content solutions were prepared of the sulfonated BCP ($[sPPFS_{0.22}\text{-}PPFS_{0.11}]\text{-}b\text{-}PBuA_{0.67}$) and statistical copolymer made by NMP ($[sPPFS_{0.49}\text{-}PPFS_{0.38}]\text{-}s\text{-}PBuA_{0.13}$). The solution of the sulfonated statistical copolymer made by FRP in emulsion ($sPPFS_{0.80}\text{-}s\text{-}PBuA_{0.20}$) was at 2 wt% polymer content to prevent

having a highly viscous media. The high viscosity is attributed to the higher molar mass of the copolymer.

Initially, the membranes of the sulfonated copolymers were not mechanically stable and disrupted when unmoulding and when put in water. Membranes being stable in water is a must as it is the media of the electrolysis cell (Chapter 1, section 1.3.3.). For that reason, preliminary crosslinking test were performed in two ways, covalent crosslinking (CCL) and ionic crosslinking (ICL), on ([sPPFS$_{0.49}$-PPFS$_{0.38}$]-s-PBuA$_{0.13}$). With the crosslinking, a creation of either chemical or electrostatic bridges are made between the polymer chains, resulting in the increase of their mechanical properties.

CCL was made by the efficient *para*-fluoro thiol modification using a difunctional thio 2,2-(ethylenedioxy)diethanethiol, using the same approach in presence of DBU in DMSO as described for sulfonation step. Molar ratios of 3, 6 and 12 mol% of crosslinker were added to the polymer solutions. After drying the membranes were characterized by DSC and elongational rheology. A slight increase in *Tg* with the increase of crosslinker mol% was noticed (from *Tg* of 32°C at 0 mol% CCL, to a *Tg* of 43°C at 12 mol% CCL – Chapter 4, Figure 6 B). With elongation rheology, a strain-hardening behaviour of the membranes was observed upon addition of mol% CCL and is characteristic of the occurrence of a chemical crosslinking (Chapter 4, Figure 6 C).[17] When a polymer is crosslinked, there is a creation of chemical intermolecular bonds between the polymer chains. This results in the creation of polymer nodes and in the change of the polymer's properties. Due to the presence of those nodes, under strain, the polymers' viscosity increases until rupture of the chains. The covalent crosslinking of ([sPPFS$_{0.49}$-PPFS$_{0.38}$]-s-PBuA$_{0.13}$) was effective at 6 and 12 mol% of added covalent crosslinker.

Similarly, ICL was performed with 2, 4 and 8 wt% of polybenzimidazole (PBI-OO) and 10 wt% polymer content in DMSO. After the drying step, the membranes were immersed into an acid solution to promote the ionic crosslinking interactions. PBI-OO is known for its very high thermal stability having a degradation temperature above 600°C. The increase of the *Tg* of the membranes by DSC upon addition of crosslinker also supported this observation (*Tg* from 32°C at 0 wt% CCI, to 82°C at 8 wt% of added PBI-OO) (Chapter 4, Figure 6 E). However, an influence of the crosslinking with PBI-OO on the *Tg* is noticeable

from 2 wt% of added crosslinker with a *Tg* increasing from 32 to 77°C. The crosslinking effectiveness was also shown by extensional rheology with the occurrence of a strain-hardening behaviour of the membranes (Chapter 4, Figure 6 F). However, this behaviour occurred for all the ionically crosslinked membranes. Hence, only 2 wt% of PBI-OO was necessary to ionically crosslink ([sPPFS$_{0.49}$-PPFS$_{0.38}$]-*s*-PBuA$_{0.13}$).

3.2. Behaviour of the crosslinked membranes in water

The proton-conductivity is dictated by the water content and diffusion in the membrane (Chapter 1, section 1.4.2.). Water uptake of the crosslinked membranes was conducted. That parameter is dependent on the degree of sulfonation of the polymer. In fact, water in presence of a highly sulfonated material will act as a plasticizer and cause extreme swelling of the membranes, lowering the *Tg* of the membranes. Water uptake is measured by comparing the weights of the dried and hydrated membranes (membranes soaked in water for 24h). After crosslinking, mechanically water-stable films were produced with an average water uptake of 45% and a hydration number λ of 23. Those values are in the same range as the reference Nafion$^{®}$ 117 with a 30% water uptake and hydration number of 18. In the case of the covalently crosslinked membranes, the membranes with 12 mol% of crosslinker kept its mechanical integrity after 24h in water, the other membranes were disrupted. Nevertheless, the membranes with 12 mol% crosslinker were very swollen, with a water uptake exceeding 1000 wt%, and a hydration number of 563. They were losing their mechanical integrity.

On the other hand, the ionically crosslinked membranes were all stable in water with water uptake values around 45 wt%, and hydration number around 23-25, (Chapter 4, Table 3) comparable to the Nafion$^{®}$117. These results have comforted the choice to perform the ICL with 2 wt% of PBI-OO for all the membranes.

3.3. Proton-conductivity of the membranes

Ion exchange capacity (IEC) and electrochemical impedance spectroscopy (EIS) were performed. IEC is a value directly linked to the sulfonation degree and gives an idea of the

number of sulfonic groups available for conduction. ([sPPFS$_{0.49}$-PPFS$_{0.38}$]-s-PBuA$_{0.13}$) showed an IEC = 1.06 meq/g, higher than the reference Nafion®117 (IEC = 0.93 meq/g). A similar IEC was obtained for (sPPFS$_{0.80}$-s-PBuA$_{0.20}$) and ([sPPFS$_{0.22}$-PPFS$_{0.11}$]-b-PBuA$_{0.67}$) of 0.3 meq/g and 0.35 meq/g, respectively. The lower IEC of ([sPPFS$_{0.22}$-PPFS$_{0.11}$]-b-PBuA$_{0.67}$) was explained by the low amounts of sPPFS (22 %). The IEC of (sPPFS$_{0.80}$-s-PBuA$_{0.20}$) was lower than expected and could be explained by the high molar mass of the polymer. This hindrance might make the access to the sulfonated groups in the bulk of the material difficult.

EIS was used to determine the conductivity of the membranes. The BCP ([sPPFS$_{0.22}$-PPFS$_{0.11}$]-b-PBuA$_{0.67}$) have demonstrated a very good conductivity. Compared to the statistical copolymers, a high conductivity in 0.5N H$_2$SO$_4$ of 179 mS/cm was achieved. This is more than 10 times higher than the reference Nafion® 117 (σ = 12 mS/cm). Moreover, the statistical copolymer made by NMP ([sPPFS$_{0.49}$-PPFS$_{0.38}$]-s-PBuA$_{0.13}$) had a better conductivity than the one made by FRP (sPPFS$_{0.80}$-s-PBuA$_{0.20}$) σ = 94 and 16 mS/cm, respectively, **Table 1**.

This proved that although the high molar mass of the copolymer made by FRP (sPPFS$_{0.80}$-s-PBuA$_{0.20}$) favoured the mechanical stability of the membrane, controlling the polymerization and having lower molar masses helped with the proton conduction and water flow in the membrane. Compared to the Nafion®'s hydrophilic cluster network with a diffusion of protons occurring by the hopping or vehicular mechanisms the self-assembly of sulfonated BCPs offers a new approach for the transport of protons in the membrane. The protons can be led from the sides of the membranes through well-defined 100 nm wide channels by following the water dynamics (**Scheme 1**).
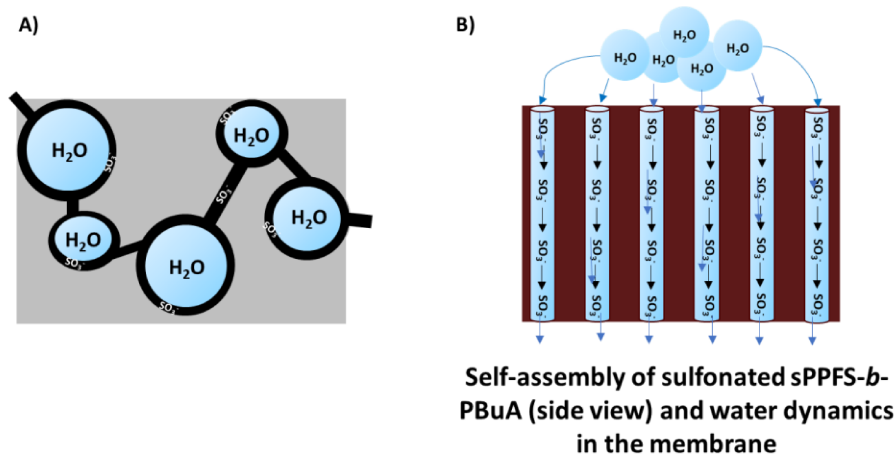
Scheme 1. Representation of the cluster network occurring in Nafion® for the proton-conduction (A); Representation of sPPFS-*b*-PbuA channels organised in Hexagonally Compacted Cylinders (HCC) of sPPFS in a PBuA matrix with the representation of water dynamics (B).

4. Life cycle assessment (LCA) of the membranes

Finally, a LCA study was performed to assess the environmental impact of the membrane manufacture (Chapter 5). LCA is defined as a tool to assess the environmental performance of a product. It is the compilation and evaluation of inputs, outputs, and potential environmental impacts of products through their life cycle. This study was made by following a very meticulous methodology provided by the International Organization for Standardization (ISO): ISO 14040:2006(E) and ISO 14044:2006(E). This methodology follows 4 steps: goal and scope definition of the study, life cycle inventory (LCI), life cycle impact assessment (LCIA) and interpretation of the study. In the goal and scope section, the aim of the study is defined and the boundaries of the study as well. The LCI step consists of gathering all the necessary data within the system boundaries to make the study. In the LCIA section, the data collected in the LCI step are correlated to the environmental impact using impact categories. The last interpretation stage is the presentation of the results and their discussion.

The work aimed to give an overview of the LCA study of the membrane of the artificial photosynthesis eSCALED device. The study is destined to the eSCALED project partners in a smaller scale, and the scientific community and the public in the bigger picture.

The system boundaries were set to a cradle-to-gate approach (from the extraction and acquisition of raw materials to the end of production of the membrane). Indeed, studying the impact of the membrane in the use stage of the PEMWE would have been too complicated to implement for the LCA studies at this stage. The chosen impact categories are presented in the Table 2 of Chapter 5 and include impacts such as global warming potential, human toxicity, water consumption, freshwater toxicity, or fossil resource scarcity. The necessary data for the study (input, output) was collected from the lab experiments and the literature (when the data could not be provided by the lab experiments). In the case of unavailability of data, assumptions were made and fully disclosed in Chapter 5, section 3.2.6. The study was performed with the SimaPro software.

The LCA study of the membranes highlighted the high impact of PFS as the main compound. Its impact was important for the free radical polymerization technique (FRP) applied to synthesize the copolymers. In fact, the impact came from the drying stage of the polymers, with the removal of water that is needed at high temperatures for a long duration (90°C overnight). The study also showed that the less impact came from the synthesis of the membrane made with the BCP as less PFS was used for the synthesis (only 33% molar composition of PPFS). This completed and emphasised the overall advantages of using BCPs and tailored structuration in materials for membrane purposes.

5. Outlook

As an outlook, a copolymer was synthesized using menthyl acrylate (MA) bio-sourced monomer in replacement of butyl acrylate BuA. The aim of the study is to propose alternative "greener" options to the development of proton-conductive membranes. Menthol was used as the primary compound for the synthesis of the acrylate monomer. MA monomer was characterized by ^{1}H NMR, a yield of 73% was obtained. On the ^{1}H NMR spectrum, the chemical shifts of the vinylic protons (-CH and -CH$_2$) of the monomer are located between 5.7 and 6.5 ppm. The -OCH proton of MA ring is located at 4.7 ppm and the remaining protons of the molecule (-CH, -CH$_2$ and -CH$_3$) are located between 0.7 and 2 ppm (Chapter 4, Figure 7).

PPFS-*stat*-PMA was synthesized by NMP controlled radical polymerization. On the ^{1}H NMR, the chemical shifts of the -OCH proton of MA ring is located at 4.5 ppm. The backbone protons of the polymer (-CH and -CH$_2$) alongside the remaining protons of the macromolecule (-CH, -CH$_2$ and -CH$_3$) are located between 0.5 and 3.2 ppm. The copolymer is composed of 77 mol% of PPFS and 23 mol% of PMA (PPFS$_{0.77}$-*s*-PMA$_{0.23}$) and has a *Tg* of 95°C.

The copolymer was fully sulfonated following the previous *para*-fluoro thiol modification with SMPS (Chapter 4, Figure 9). After sulfonation, a decrease in *Tg* to -3 °C was obtained. Following the study made with the PPFS/PBuA system, (sPPFS$_{0.77}$-*s*-PMA$_{0.23}$) was ionically crosslinked with 2 wt% PBI-OO. The water uptake and hydration number of the membranes was of 42% and 19.4 respectively (30% and 18 for reference Nafion®117), and its IEC of 1.2 meq/g.

The membrane gave an astonishing conductivity of 690 mS/cm (σ Nafion® 117 = 12 mS/cm). Both PMA and PPFS polymers having similar properties (*Tg* PMA = 69°C) and PPFS (*Tg* PPFS = 95°C), an explanation of this result could be the cohesiveness of the hydrophobic domain surrounding the hydrophilic proton-conductive cluster. It could be interesting to study as a future work the synthesis of sulfonated PPFS/PMA block-copolymers as well. As a matter of fact, the structural organization of the membranes could greatly improve the conductivity, similarly to the work on the PPFS/PBuA membranes, **Table 1**.

Furthermore, the environmental impact of the BCP using PMA should be significantly lowered compared to BuA. A LCA study would provide a full circle work on the developed proton-conducting membranes.

Table 1. Summary table of the study on membranes conduction properties

Polymer	DS (%)	sPPFS (mol%)	IEC Theo (meq/g)	IEC Exp (meq/g)	Membrane thickness (μm)	Conductivity (mS/cm)
$(PPFS_{0.33}\text{-}b\text{-}PBuA_{0.67})_{40K}$ (NMP / solution)	68	22	0.66	0.35	16	179
$(PPFS_{0.87}\text{-}s\text{-}PBuA_{0.13})_{19K}$ (NMP / solution)	57	49	2.15	1.06	86	94
$(PPFS_{0.80}\text{-}s\text{-}PBuA_{0.20})_{140K}$ (FRP / Emulsion)	100	80	2.76	0.3	6	16
$PPFS_{0.77}\text{-}s\text{-}PMA_{0.23}$ (NMP / solution)	100	77	2.54	1.2	10	690

Additionally, the upscaling of the membranes could be performed by printing. The main requirements for its feasibility were brought up in this manuscript (Chapter 2). A preliminary work was made on the use of Inkjet printing and screen-printing for the development of membrane electrode assembly (MEA). In this study the importance of ink and paste formulations as well as the choice of the printing substrate was found to be determining printing parameters. A cohesion between the ink and substrate properties (wettability of the surface by the ink and surface free energy of the substrate) is in fact needed for a successful printing.

6. References

1. Maiyalagan, T. & Pasupathi, S. *Components for PEM fuel cells: An overview*. *Materials Science Forum* vol. 657 (2010).

2. GIERKE, T. D. & HSU, W. Y. The Cluster—Network Model of Ion Clustering in Perfluorosulfonated Membranes. 283–307 (1982) doi:10.1021/bk-1982-0180.ch013.

3. Kreuer, K. D. Proton conductivity: Materials and applications. *Chem. Mater.* **8**, 610–641 (1996).

4. Rubatat, L., Li, C., Nyka, A. & Ruokolainen, J. Structure - Properties Relationship in Proton Conductive Sulfonated Polystyrene - Polymethyl Methacrylate Block Copolymers (sPS - PMMA). 8130–8137 (2008).

5. Atanasov, V., Bürger, M., Lyonnard, S., Porcar, L. & Kerres, J. Sulfonated poly(pentafluorostyrene): Synthesis & characterization. *Solid State Ionics* **252**, 75–83 (2013).

6. Atanasov, V., Oleynikov, A., Xia, J., Lyonnard, S. & Kerres, J. Phosphonic acid functionalized poly(pentafluorostyrene) as polyelectrolyte membrane for fuel cell application. *J. Power Sources* **343**, 364–372 (2017).

7. Bülbül, E. *et al.* Highly phosphonated polypentafluorostyrene blended with polybenzimidazole: Application in vanadium redox flow battery. *J. Memb. Sci.* **570–571**, 194–203 (2019).

8. Atanasov, V. & Kerres, J. ETFE-g-pentafluorostyrene: Functionalization and proton conductivity. *Eur. Polym. J.* **63**, 168–176 (2015).

9. Atanasov, V. *et al.* Synergistically integrated phosphonated poly(pentafluorostyrene) for fuel cells. *Nat. Mater.* **20**, 370–377 (2021).

10. Nicolas, Julien; Guillaneuf, Yohann; Lefay, Catherine; Bertin, Denis; Gigmes, Didier; Charleux, B. Nitroxide-mediated polymerization. *Prog. Polym. Sci.* **30**, 813 (2005).

11. Braunecker, W. A., & Matyjaszewski, K., Controlled / living radical polymerization : Features , developments , and perspectives. **32**, 93–146 (2007).

12. Mai, Y. & Eisenberg, A. Self-assembly of block copolymers. *Chem. Soc. Rev.* **41**, 5969–5985 (2012).

13. Delaittre, G. & Barner, L. The: Para -fluoro-thiol reaction as an efficient tool in polymer chemistry. *Polym. Chem.* **9**, 2679–2684 (2018).

14. Mani, S., Weiss, R. A., Williams, C. E. & Hahn, S. F. Microstructure of ionomers based on sulfonated block copolymers of polystyrene and poly(ethylene-alt-propylene). *Macromolecules* **32**, 3663–3670 (1999).

15. Gromadzki, D. *et al.* Morphological studies and ionic transport properties of partially sulfonated diblock copolymers. *Eur. Polym. J.* **42**, 2486–2496 (2006).

16.	Rubatat, L., Shi, Z., Diat, O., Holdcroft, S. & Frisken, B. J. Structural study of proton-conducting fluorous block copolymer membranes. *Macromolecules* **39**, 720–730 (2006).

17.	Dieuzy, E. *et al.* Microgel structure-driven linear and non-linear mechanical properties of self-assembled microgel films. *Colloids Surfaces A Physicochem. Eng. Asp.* **613**, 1–11 (2021).